# CARBONATE DIAGENESIS AND POROSITY EVOLUTION IN THE GUELPH FORMATION, SOUTHWESTERN ONTARIO

by

Qing Zheng

A thesis

presented to the University of Waterloo

in fulfilment of the

thesis requirement for the degree of

Doctor of Philosophy

in

Earth Sciences

Waterloo, Ontario, Canada, 1999

© Qing Zheng 1999

National Library of Canada
Acquisitions and Bibliographic Services
395 Wellington Street
Ottawa ON K1A 0N4
Canada

Bibliothèque nationale du Canada
Acquisitions et services bibliographiques
395, rue Wellington
Ottawa ON K1A 0N4
Canada

*Your file Votre référence*

*Our file Notre référence*

The author has granted a non-exclusive licence allowing the National Library of Canada to reproduce, loan, distribute or sell copies of this thesis in microform, paper or electronic formats.

The author retains ownership of the copyright in this thesis. Neither the thesis nor substantial extracts from it may be printed or otherwise reproduced without the author's permission.

L'auteur a accordé une licence non exclusive permettant à la Bibliothèque nationale du Canada de reproduire, prêter, distribuer ou vendre des copies de cette thèse sous la forme de microfiche/film, de reproduction sur papier ou sur format électronique.

L'auteur conserve la propriété du droit d'auteur qui protège cette thèse. Ni la thèse ni des extraits substantiels de celle-ci ne doivent être imprimés ou autrement reproduits sans son autorisation.

0-612-51245-2

Canada

The University of Waterloo requires the signatures of all persons using or photocopying this thesis. Please sign below, and give address and date.

# CARBONATE DIAGENESIS AND POROSITY EVOLUTION IN THE GUELPH FORMATION, SOUTHWESTERN ONTARIO

## ABSTRACT

The Middle Silurian Guelph Formation in southwestern Ontario is composed of shelfward patch reefs, basinward pinnacle reefs, and interreef facies developed on a gently-sloping carbonate ramp. Core and petrographic studies indicate that the Guelph Formation has undergone a complicated diagenetic history including pre-dolomitization diagenesis, pervasive dolomitization and post-dolomitization diagenesis. Guelph dolomite mainly consists of three types of replacive dolomites, including microcrystalline (20-50 μm) anhedral dolomite (Type 1), finely crystalline (50-150 μm) euhedral to subhedral dolomite (Type 2), and medium to coarsely crystalline (150-400 μm) euhedral to anhedral dolomite (Type 3).

Type 1 dolomite has the best preserved limestone textures, identical $^{87}Sr/^{86}Sr$ ratios to both limestone and Middle Silurian seawater, and similar low Fe and Mn contents to limestone. This dolomite is interpreted to represent the 'least-altered' dolomite phase that is geochemically the closest to the initial dolomite. The general basinward dolomite-decreasing trend in the Guelph Formation indicates that dolomitizing fluids were derived from shelfward sources. Combined stratigraphic, petrographic and geochemical data suggest that this initial dolomitization probably resulted from regional subsurface (< 300 m) reflux of normal to near-normal seawater that was induced by evaporative drawdown during the Late Silurian. Depleted $\delta^{18}O$ values in Type 1 dolomites may have resulted from early recrystallization in a fluid similar to that for initial dolomitization but at deeper burial (320-1200 m).

The coexistence of three dolomite fabrics with relict textures and their crosscutting relationships indicate that Type 1 dolomite was altered to Type 2 and Type 3 dolomite. The systematic covariance between increasing crystal size with increasing $^{87}Sr/^{86}Sr$ ratios and increasing Fe and Mn contents reflects an advanced alteration of early-formed dolomite in pore fluids with increasing $^{87}Sr$, Fe and Mn input from associated siliciclastics during burial.

Several altered intervals containing variable amounts of Type 2 dolomite and finer crystalline (20-50 μm) dedolomite are observed in eight cores from five pinnacle reefs on the lower ramp. Common replacement fabrics such as numerous corroded dolomite relicts, poikilotopic fabrics, rhombic calcite pseudomorphs, and micrometer-sized dolomite inclusions indicate that Guelph dedolomite resulted from the replacement of preexisting Type 2 dolomite. Guelph dedolomite shows depleted Sr, enriched Fe, Mn and $^{87}Sr/^{86}Sr$ values relative to limestone, but similar elemental and isotopic values to Type 2 dolomite. Dedolomitization is interpreted to have resulted from subsurface circulation of modified seawaters in the same conduit system as that for Type 2 dolomite formation, but extra Ca was acquired from the dissolution of remaining limestone under similar burial depth and temperature conditions to those for earlier Type 2 dolomite formation.

Low-porosity primary limestone resulted from early calcite cementation and porous limestone intervals resulted from extensive dissolution. Type 1 dolomite commonly shows similar low porosity to associated low-porosity limestone due to fabric-preserving dolomitization and early recrystallization. Most Type 2 and Type 3 dolomite intervals are porous due to fracturing, dissolution, and dolomite alteration. Dedolomite exhibits low porosity relative to Type 2 dolomite, suggesting that dedolomitization is a porosity-reducing process. Other post-dolomitization diagenesis, especially halite cementation, also played important roles in controlling the final porosity in Guelph carbonate.

# Acknowledgements

I would like to thank my supervisor, Dr. Mario Coniglio, for his continued encouragement through all stages of this project. He has guided me through the world of carbonate diagenesis with high research standards and critical thinking. The exhaustive reviews of the drafts by Dr. Mario Coniglio have greatly improved this thesis. His patience and generosity are greatly appreciated.

I gratefully acknowledge the great efforts of my advisory committee members Dr. D.E. Lawson, Dr. S.K. Frape and Dr. E.J. Reardon for their enthusiastic support through this program and critical review and examination of this thesis. I would also like to thank external examiners Dr. I.S. Al-Aasm from University of Windsor and Dr. M.A. Ioannidis from Chemical Engineering for their valuable comments.

This research was funded by a research grant from Canada's Natural Sciences and Engineering Research Council (NSERC) awarded to Dr. Mario Coniglio. Union Gas provided additional funding for strontium isotopic analysis that was done at the University of Alberta. I wish to thank T.R. Carter at the Ontario Ministry of Natural Resources (OMNR) for his logistical support during core description. Elemental and stable isotopic analyses were carried out at the Environmental Isotope Laboratory at the University of Waterloo under the guidance of Ling Zhang, Rick Heemskerk and Bob Drimmie. Special thanks go to Dr. D. E. Lawson for providing financial support through Graduate Scholarship and Teaching Assistantships. Many thanks are given also to Syed Mohammed Kaleem, Tim Hagan, Mike Kunert and John Grimwood, who have been coworkers and friends through the years. Many ideas in this thesis were obtained through discussions with them. I acknowledge the assistance of Jie He and Alexander Blyth in examining fluid inclusions and Rob Frizzell in formatting the references and appendices.

Finally, I wish to thank my parents and my wife, Shizhen. This thesis could have not been completed without their continued encouragement and support.

# TABLE OF CONTENTS


| | | |
|---|---|---|
| Abstract | | iv |
| Acknowledgments | | vi |
| List of figures | | xi |
| List of tables | | xiii |
| **Chapter 1** | **Introduction** | 1 |
| 1.1 | Study area | 1 |
| 1.2 | Hydrocarbon occurrence | 4 |
| 1.3 | Previous studies | 5 |
| 1.4 | Study objectives | 10 |
| 1.5 | Methodology | 12 |
| 1.6 | Organization of the thesis | 17 |
| **Chapter 2** | **Geological Setting** | 20 |
| 2.1 | Regional geology | 20 |
| 2.2 | Paleoclimate | 26 |
| 2.3 | Stratigraphy | 27 |
| 2.4 | Depositional setting of the Guelph Formation | 37 |
| 2.5 | Burial and thermal history | 42 |
| 2.6 | Formation water composition | 46 |
| **Chapter 3** | **Reefal facies and pre-dolomitization diagenesis** | 50 |
| 3.1 | Abstract | 50 |
| 3.2 | Reefal facies | 51 |
| | 3.2.1 Basal crinoidal mud mound facies | 51 |
| | 3.2.2 Coral-stromatoporoid reef core facies | 51 |
| | 3.2.3 Crinoidal-bryozoan flank facies | 54 |
| | 3.2.4 Stromatolitic cap facies | 54 |
| | 3.2.5 Interreef mud facies | 55 |
| 3.3 | Reef growth history | 55 |
| 3.4 | Reef-evaporite relationship | 57 |
| 3.5 | Paragenetic sequence | 60 |
| 3.6 | Pre-dolomitization diagenesis | 62 |
| | 3.6.1 Fibrous calcite cement | 63 |
| | 3.6.2 Equant calcite cement | 63 |
| | 3.6.3 Internal sediments | 65 |
| | 3.6.4 Neomorphosed calcite | 65 |
| | 3.6.5 Limestone dissolution | 65 |

3.7 Interpretation of pre-dolomitization diagenesis 66
3.8 Conclusions 68

**Chapter 4 Dolomite and dolomite origin** 70
4.1 Abstract 70
4.2 Introduction 72
4.3 Terminology 74
4.4 Dolomite distribution 76
4.5 Dolomite petrography 79
4.5.1 Dolomite fabrics 79
4.5.1.1 Type 1. Microcrystalline dolomite with preserved fabric 80
4.5.1.2 Type 2. Finely crystalline dolomite with partially preserved fabric 83
4.5.1.3 Type 3. Medium to coarsely crystalline dolomite without preserved fabric 83
4.5.1.4 Finely to coarsely crystalline dolomite cement 85
4.5.1.5 Scattered finely to medium crystalline dolomite in limestone 86
4.5.2 Replacive dolomite fabric distribution 86
4.6 Dolomite geochemistry 91
4.6.1 Mole % $CaCO_3$ 91
4.6.2 Strontium and sodium 91
4.6.3 Iron and manganese 94
4.6.4 Oxygen and carbon isotopes 97
4.6.5 Strontium isotopes 106
4.6.6 Fluid inclusions 106
4.7 Interpretation 109
4.7.1 Dolomite distribution constraints for paleoflow direction 109
4.7.2 Petrographic constraints 112
4.7.3 Geochemical constraints 116
4.7.3.1 Stoichiometry 116
4.7.3.2 Strontium and sodium 117
4.7.3.3 Iron and manganese 119
4.7.3.4 Oxygen and carbon isotopes 120
4.7.3.5 Strontium isotopes 123
4.7.3.6 Fluid inclusions 124
4.8 Discussion 126
4.8.1 Dolomite models 126
4.8.1.1 Hypersaline reflux models 126
4.8.1.2 Mixing-zone models 128

4.8.1.3 Burial compaction models 128
4.8.1.4 Seawater and modified seawater models 129
4.8.1.5 Thermal convection models 130
4.8.1.6 Hydrologic system for Guelph dolomitization 132
4.8.2 Dolomite origin 136
4.8.2.1 Diagenetic fluids 136
4.8.2.2 Early stage dolomite (Type 1 dolomite) 137
4.8.2.3 Middle stage dolomite (Type 2 dolomite) 140
4.8.2.4 Late stage dolomite (Type 3 dolomite) 142
4.8.2.5 Saddle dolomite 144
4.8.2.6 Scattered dolomite 144
4.8.2.7 Thermal convection for dolomite alteration 145
4.9 Dolomite formation model 147
4.10 Conclusions 150

**Chapter 5 Dedolomite and dedolomitization** 153
5.1 Abstract 153
5.2 Introduction 154
5.3 Dedolomite distribution 156
5.4 Dedolomite petrography 159
5.5 Dedolomite geochemistry 163
5.6 Interpretation and discussion 168
5.6.1 Dedolomitizing fluid 168
5.6.2 Source of $Ca^{2+}$ for dedolomitization 170
5.6.3 Environment and timing of dedolomitization 172
5.6.4 Replacement mode 173
5.6.5 Dedolomitization model 174
5.7 Conclusions 178

**Chapter 6 Post-dolomitization diagenesis and porosity** 180
6.1 Abstract 180
6.2 Introduction 181
6.3 Porosity types 184
6.3.1 Interparticle porosity 184
6.3.2 Fenestral porosity 184
6.3.3 Intraskeletal porosity 186
6.3.4 Shelter porosity 186
6.3.5 Intercrystalline porosity 186
6.3.6 Moldic and intracrystalline porosity 186
6.3.7 Vuggy porosity 188

6.3.8 Fracture porosity 188
6.4 Porosity and permeability distribution 188
6.5 Post-dolomitization diagenesis 194
6.5.1 Mechanical and chemical compaction 194
6.5.2 Fracturing 196
6.5.3 Carbonate dissolution 196
6.5.4 Anhydrite and halite cementation 197
6.5.5 Evaporite dissolution 198
6.5.6 Hydrocarbon emplacement 198
6.6 Interpretation and discussion 199
6.6.1 Porosity-creating processes 200
6.6.1.1 Stylolitization 200
6.6.1.2 Fracturing and carbonate dissolution 202
6.6.1.3 Dolomite coarsening 204
6.6.1.4 Evaporite dissolution 204
6.6.2 Porosity-destroying processes 204
6.6.2.1 Mechanical compaction 205
6.6.2.2 Dedolomitization 205
6.6.2.3 Anhydrite cementation 205
6.6.2.4 Halite cementation 207
6.7 Conclusions 207

**Chapter 7 Summary** 209
7.1 Reef facies and diagenesis 209
7.2 Dolomite type and origin 210
7.3 Dedolomitization 212
7.4 Porosity type and evolution 214
7.5 Implication and further Studies 216

**References** 217

**Appendices** 251
Appendix I 251
Appendix II 255
Appendix III 259
Appendix IV 262
Appendix V 263
Appendix VI 264
Appendix VII 265

# LIST OF FIGURES

## Chapter 1


| | | |
|---|---|---|
| Fig. 1.1 | Location map for the Michigan Basin and the Study area | 2 |
| Fig. 1.2 | Location map for reefal carbonate distribution in the study area | 3 |
| Fig. 1.3 | Previously proposed dolomitization models for the Michigan Basin | 7 |


## Chapter 2


| | | |
|---|---|---|
| Fig. 2.1 | Structural cross section across the Michigan Basin | 22 |
| Fig. 2.2 | Middle Silurian facies distribution in the Michigan Basin | 24 |
| Fig. 2.3 | Lithostratigraphic profile of Paleozoic strata in the study area | 28 |
| Fig. 2.4 | Middle and Upper Silurian strata in southwestern Ontario | 31 |
| Fig. 2.5 | Regional cross-section for Guelph reefal facies distribution | 33 |
| Fig. 2.6 | Guelph reefal facies distribution in the study area | 39 |
| Fig. 2.7 | Generalized burial history curve of Silurian strata in the study area | 44 |


## Chapter 3


| | | |
|---|---|---|
| Fig. 3.1 | Representative lithology log for pinnacle reefal facies | 52 |
| Fig. 3.2 | Summerized reefal facies in Guelph reefs | 53 |
| Fig. 3.3 | Reef growth model for Guelph reefs in southwestern Ontario | 56 |
| Fig. 3.5 | Previously suggested reef models for the Niagaran reefs | 58 |
| Fig. 3.6 | Summarized paragenetic sequence for Guelph carbonate | 61 |
| Fig. 3.7 | Microphotographs of pre-dolomitization diagenesis | 64 |


## Chapter 4


| | | |
|---|---|---|
| Fig. 4.1 | A-1 and A-2 dolomite distribution around Guelph pinnacle reef | 78 |
| Fig. 4.2 | Dolomite fabric types in the Guelph Formation | 81 |
| Fig. 4.3 | Microphotographs of Type 1 replacive dolomite | 82 |
| Fig. 4.4 | Microphotographs of Type 2 replacive dolomite | 84 |
| Fig. 4.5 | Microphotographs of Type 3 replacive dolomite | 87 |
| Fig. 4.6 | Microphotographs of dolomite cements and scattered dolomite | 88 |
| Fig. 4.7 | Microphotographs of replacive dolomite fabric distribution | 90 |
| Fig. 4.9 | Mole % $CaCO_3$ histogram for three replacive dolomites | 92 |
| Fig. 4.10A | Na vs. Sr for major carbonate fabrics | 93 |
| Fig. 4.10B | Na vs. Sr for three replacive dolomites | 93 |
| Fig. 4.11A | Mole%$MgCO_3$ vs. Sr for three replacive dolomites | 95 |
| Fig. 4.11B | $\delta^{18}O$ vs. Sr for three replacive dolomites | 95 |
| Fig. 4.12A | Fe vs. Mn for major carbonate fabrics | 96 |
| Fig. 4.12B | Fe vs. Mn for three replacive dolomites | 96 |

| | | |
|---|---|---|
| Fig. 4.13 | $\delta^{18}O$ vs. $\delta^{13}C$ for major carbonate fabrics | 98 |
| Fig. 4.14A | $\delta^{18}O$ vs. $\delta^{13}C$ for Guelph replacive dolomites | 99 |
| Fig. 4.14B | $\delta^{18}O$ vs. $\delta^{13}C$ for three replacive dolomites | 99 |
| Fig. 4.15 | Location of seven representative reefs along the ramp | 101 |
| Fig. 4.16 | $\delta^{18}O$ and $\delta^{13}C$ trend along the ramp in Fig. 4.15 | 102 |
| Fig. 4.17 | $\delta^{18}O$ vs. $\delta^{13}C$ for three replacive dolomites in seven reefs | 103 |
| Fig. 4.18 | $\delta^{13}C$ vs. Mn for three replacive dolomites | 104 |
| Fig. 4.19 | $\delta^{18}O$ vs. $\delta^{13}C$ for A-1 carbonates | 105 |
| Fig. 4.20 | Sr vs. $^{87}Sr/^{86}Sr$ for major carbonate fabrics | 107 |
| Fig. 4.21A | $^{87}Sr/^{86}Sr$ vs. $\delta^{18}O$ for three replacive dolomites | 108 |
| Fig. 4.21B | $^{87}Sr/^{86}Sr$ vs. Fe for three replacive dolomites | 108 |
| Fig. 4.22 | Estimated precipitation paleotemperatures of replacive dolomites | 110 |
| Fig. 4.23 | General dolomitization models | 127 |
| Fig. 4.24 | Proposed evaporative drawdown related paleohydrologic model | 133 |
| Fig. 4.25 | Temperature vs. $\delta^{18}O_{dolomite}$ (PDB) for three replacive dolomites | 139 |
| Fig. 4.26 | Summarized flowchart for dolomite alteration paths | 141 |
| Fig. 4.27 | Proposed dolomite formation model for three replacive dolomites | 149 |


## Chapter 5


| | | |
|---|---|---|
| Fig. 5.1 | Representative lithology log for dedolomite in pinnacle reefs | 158 |
| Fig. 5.2 | Photomicrographs of replacive fabrics in dedolomite | 161 |
| Fig. 5.3 | Photomicrographs of replacive fabrics in dedolomite | 162 |
| Fig. 5.4 | Na vs. Sr for limestone, dolomite and dedolomite | 164 |
| Fig. 5.5 | Fe vs. Mn for limestone, dolomite and dedolomite | 165 |
| Fig. 5.6 | $\delta^{18}O$ vs. $\delta^{13}C$ for limestone, dolomite and dedolomite | 166 |
| Fig. 5.7 | Sr vs. $^{87}Sr/^{86}Sr$ for major carbonate fabrics including dedolomite | 167 |
| Fig. 5.8 | Proposed model for dedolomite formation | 177 |


## Chapter 6


| | | |
|---|---|---|
| Fig. 6.1 | Major porosity types in Guelph carbonates | 185 |
| Fig. 6.2 | Photomicrographs of porosity types | 187 |
| Fig. 6.3 | Photomicrographs of porosity types and late diagenesis | 189 |
| Fig. 6.4 | Permeability vs. porosity for dolomite and limestone | 190 |
| Fig. 6.5 | Porosity vs. permeability for porous and low-porosity limestones | 192 |
| Fig. 6.6 | Porosity vs. permeability for three replacive dolomites | 193 |
| Fig. 6.7 | Porosity vs. permeability for limestone and dedolomite | 195 |
| Fig. 6.8A | Major porosity-creating processes in Guelph carbonate | 201 |
| Fig. 6.8B | Major porosity-destroying processes in Guelph carbonate | 201 |
| Fig. 6.9 | Porosity vs. permeability for dedolomite and Type 2 dolomite | 206 |

# LIST OF TABLES


| | | |
|---|---|---|
| Table 2.1 | Representative composition of formation waters | 48 |
| Table 4.1 | Dolomite distribution in partially dolomitized reefs | 79 |

# Chapter 1 Introduction

## 1.1 Study area

Southwestern Ontario is located at the southeastern margin of the Michigan Basin, one of the oldest and most important hydrocarbon production regions in North America (Fig. 1.1). The study area includes Huron, Middlesex, Elgin, Lambton, Kent and Essex counties in southwestern Ontario, covering a total area of approximately 7,000 $km^2$ (Fig. 1.2).

Regionally and pervasively dolomitized pinnacle and patch reefs of the Guelph Formation in southwestern Ontario are the most important reservoirs for hydrocarbon production and they have produced prolific amounts of oil and gas for several decades (Sanford 1969; Carter 1992; Carter et al. 1994). In addition to its economic importance, the Guelph Formation is an excellent unit for studying the origin of ancient massive dolomite in a reefal sequence covered and encased by cyclic evaporite-carbonate strata, a common association in the Great Lakes Region and in many other evaporative basins. The Middle Silurian Guelph Formation contains a variety of lithologies and diagenetic phases representing different stages of diagenesis from primary limestones to later altered dolomites. In addition, there is a large data set consisting of more than 1000 borehole records and more than 100 cores of the Guelph Formation in the study area.

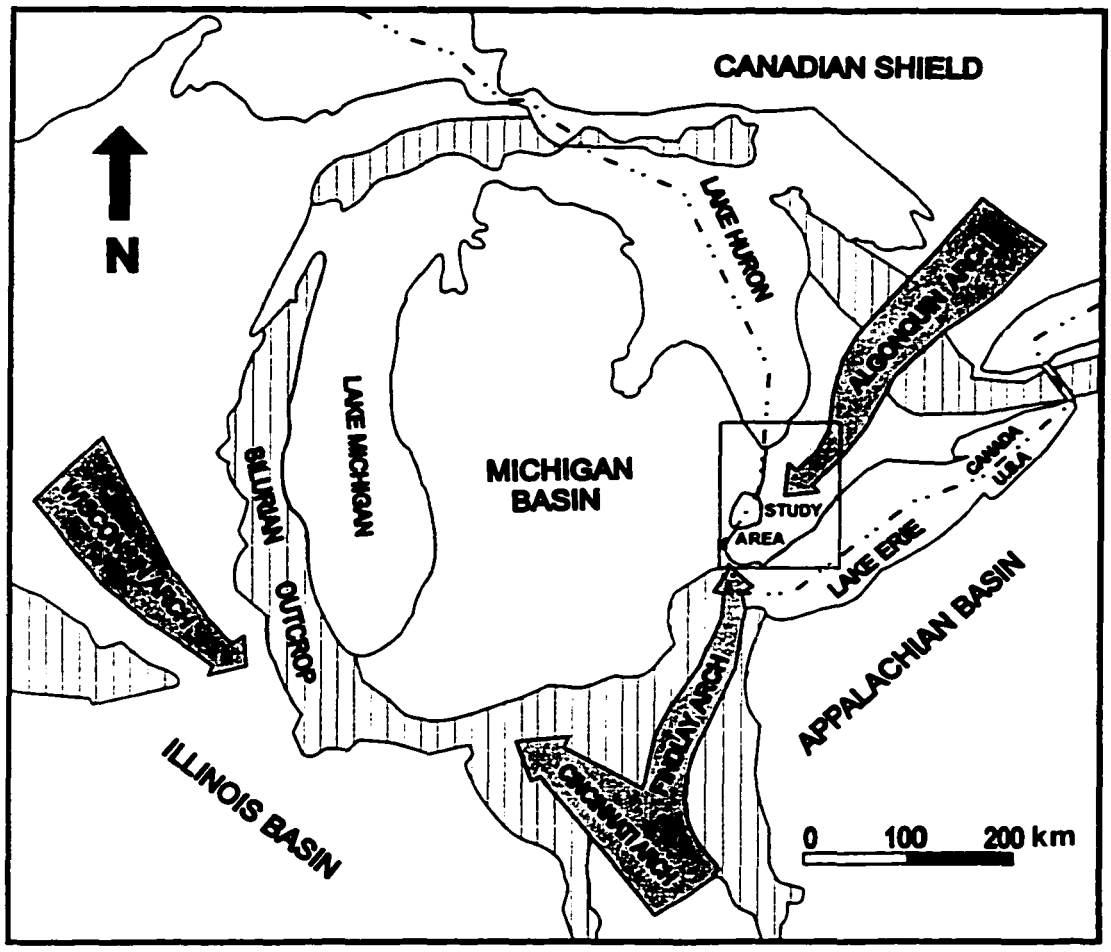



Fig. 1.1 The Michigan Basin is a circular intracratonic basin in the Great Lakes Region (modified after Sanford 1969). The study area is located at southwestern Ontario on the southeastern margin of the Michigan Basin.

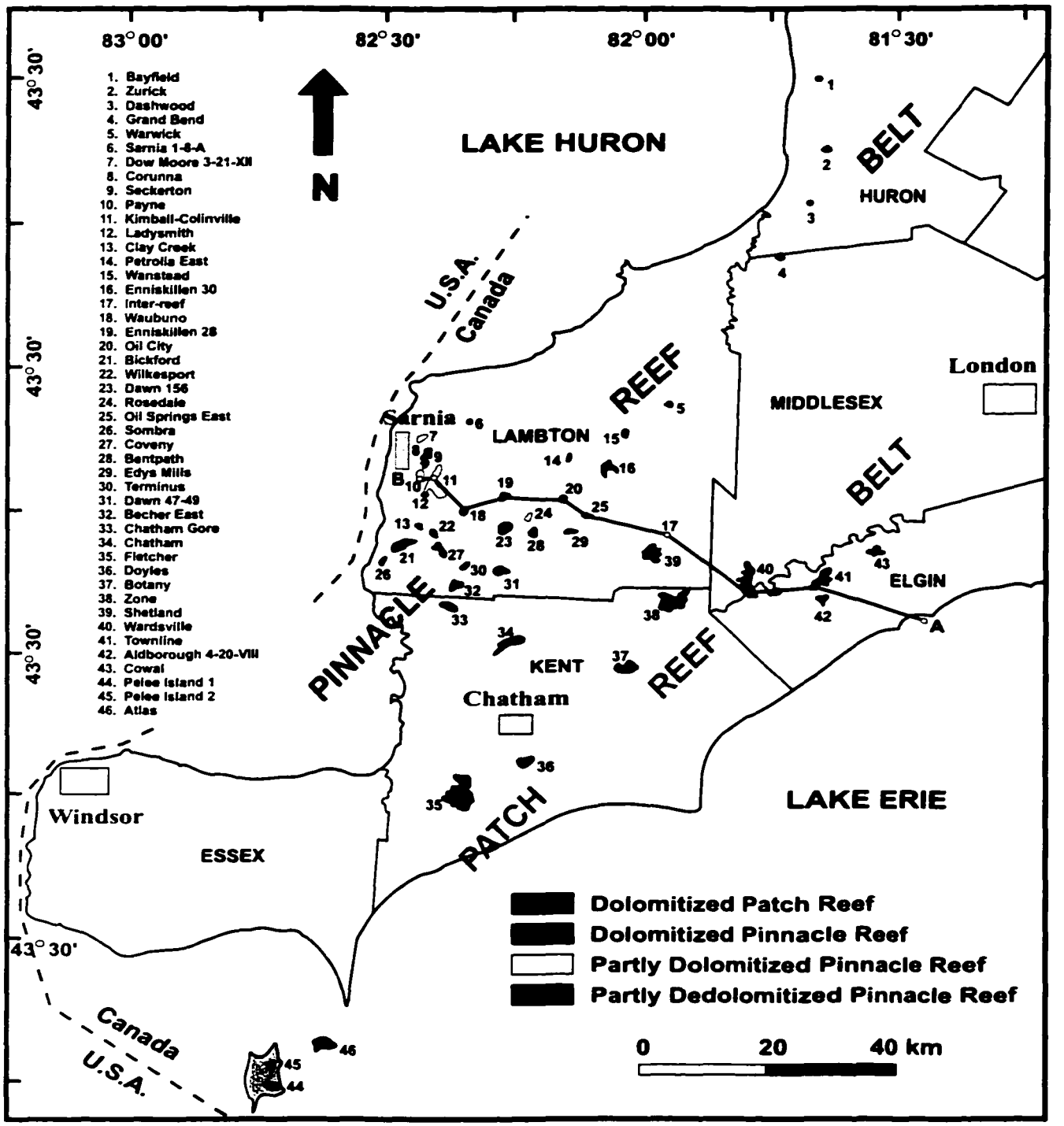



Fig. 1.2 Location map showing the study area including six counties in southwestern Ontario, the distribution of patch reefs and pinnacle reefs, the location of completely dolomitized reefs, partially dolomitized reefs, and dedolomitized reefs. An east-west regional cross-section (A-B) is across the middle of study area and is shown in Fig. 2.5.

## 1.2 Hydrocarbon occurrence

The first oil discovery well in the Michigan Basin was drilled to a depth of approximately 20 m in the Devonian beds at Oil Springs in Lambton County in 1858, making southwestern Ontario the birthplace of the petroleum industry in North America (Gould 1976). The Oil Springs field and the Petrolia field, which was discovered in 1862, produced oil until the 1980s (Rybanksky and Trevail 1983).

The first discovery well in Middle Silurian (Niagaran) reefs was drilled on the Kingsville patch reef in Gosfield South Township of Essex County in 1889. The initial open flow was 10,000 Mcfd of natural gas (Sanford 1969). Following that discovery, especially during the 1930s and 1940s, more and more oil and gas pools were discovered in Niagaran reefs. Exploration activities gradually spread into southeastern Michigan State during the 1950s, followed by numerous discoveries in the 1960s. The application of both 'Niagaran play' concepts developed from extensive exploration in southwestern Ontario and southeastern Michigan, along with new methods in seismic data collection and computerized data processing, created great success in northwestern Michigan during the mid-1960s to 1970s. Drilling in Ontario and Michigan has since extended the known boundaries of the Niagaran reef trend to the shores of Lake Huron and Lake Michigan, indicating the likelihood of its offshore extension and the presence of a complete circular reef belt around the basin. 156 oil and/or gas pools in southwestern Ontario, over 100 pools in southeastern Michigan, and over 700 pools in northern Michigan have been discovered in Niagaran reefs. These pools have produced over 300 million $m^3$ of oil and

40 billion $m^3$ of gas (Armstrong and Goodman 1990).

In southwestern Ontario, the total 156 Niagaran pools include 35 oil pools, 91 gas pools, and 30 oil and gas pools (Koepke and Sanford 1966; Bailey and Cochrane 1990; Carter 1991). Most of the pools were discovered in shelfward patch reefs and basinward pinnacle reefs in the Guelph Formation. Of the total 87 pinnacle reefs that were discovered, 53 reefs contained commercial oil and/or gas, 18 reefs were completely plugged by anhydrite and halite, and 16 reefs were filled with salt or fresh water. Examples of the productive pinnacle reefs include Corunna, Dawn 156, Kimball-Colinville, Payne, Seckerton and Waubuno (Fig. 1.2). The shelfward patch reefs contain some of the most prolific Silurian gas fields in southwestern Ontario, such as the Fletcher and Wardsville reefs (Fig. 1.2). Currently, approximately 70 of the total 156 Silurian pools are either suspended or abandoned. More than 20 drained pinnacle reefs were converted to gas storage facilities by the Ontario Energy Board to serve the pipeline network for storing natural gas from western Canada in the summer and supplying gas for Ontario and Quebec in the winter (Carter et al. 1994). Although the Niagaran play in southwestern Ontario has entered its mature stage, Guelph reefs are still potential targets for further development (Bailey 1986; Bailey and Cochrane 1990). Hydrocarbon exploration for Guelph reefs continues at a moderate pace in the 1990s (Carter et al. 1994).

## 1.3 Previous studies

The diagenetic histories of Middle Silurian pinnacle reefs in the Michigan Basin have been documented in several studies carried out in northern Michigan (Huh 1973; Huh et al. 1977; Sears and Lucia 1980; Cercone and Lohmann 1985, 1987), southeastern Michigan (Gill 1973, 1977a; Kaleem 1994), and southwestern Ontario (Grimes 1987; Charbonneau 1990). Some workers (e.g., Gill 1977a; Grimes 1988; Charbonneau 1990; Smith et al. 1993) attributed much of the reef diagenesis to meteoric water in the phreatic zone, mixing zone, and especially vadose zone. Other studies do not support this conclusion (e.g., Sears and Lucia 1979; Sarg 1982; Cercone 1984b; Cercone and Lohmann 1985). For example, Sears and Lucia (1979) considered the pisoliths and leached crusts at the top of the pinnacles to be related to higher salinity brines. Sarg (1982) proposed a pinnacle growth model without subaerial exposure.

To date, only a couple of studies (e.g., Grimes 1987; Charbonneau 1990; Smith et al. 1993) present petrographic and limited geochemical data from six reefs. Only one study (Carter 1991) shows the dolomite distribution within A-1 and A-2 carbonates based on subsurface mapping of Sombra Township in Lambton County. Most of the knowledge of the Silurian reefs in the Michigan Basin, including dolomitization, has been based on earlier studies conducted in southeastern (Felber 1964; Sharma 1966; Jodry 1969; Gill 1977a) and northwestern Michigan (Huh et al. 1977; Sears and Lucia 1980; Cercone 1984b; Cercone and Lohmann 1985, 1987) on the U. S. side. A variety of dolomitization models have been proposed based on dolomite distribution in different locations in southeastern Michigan (Sharma 1966; Jodry 1969; Gill 1977a) and the only study of

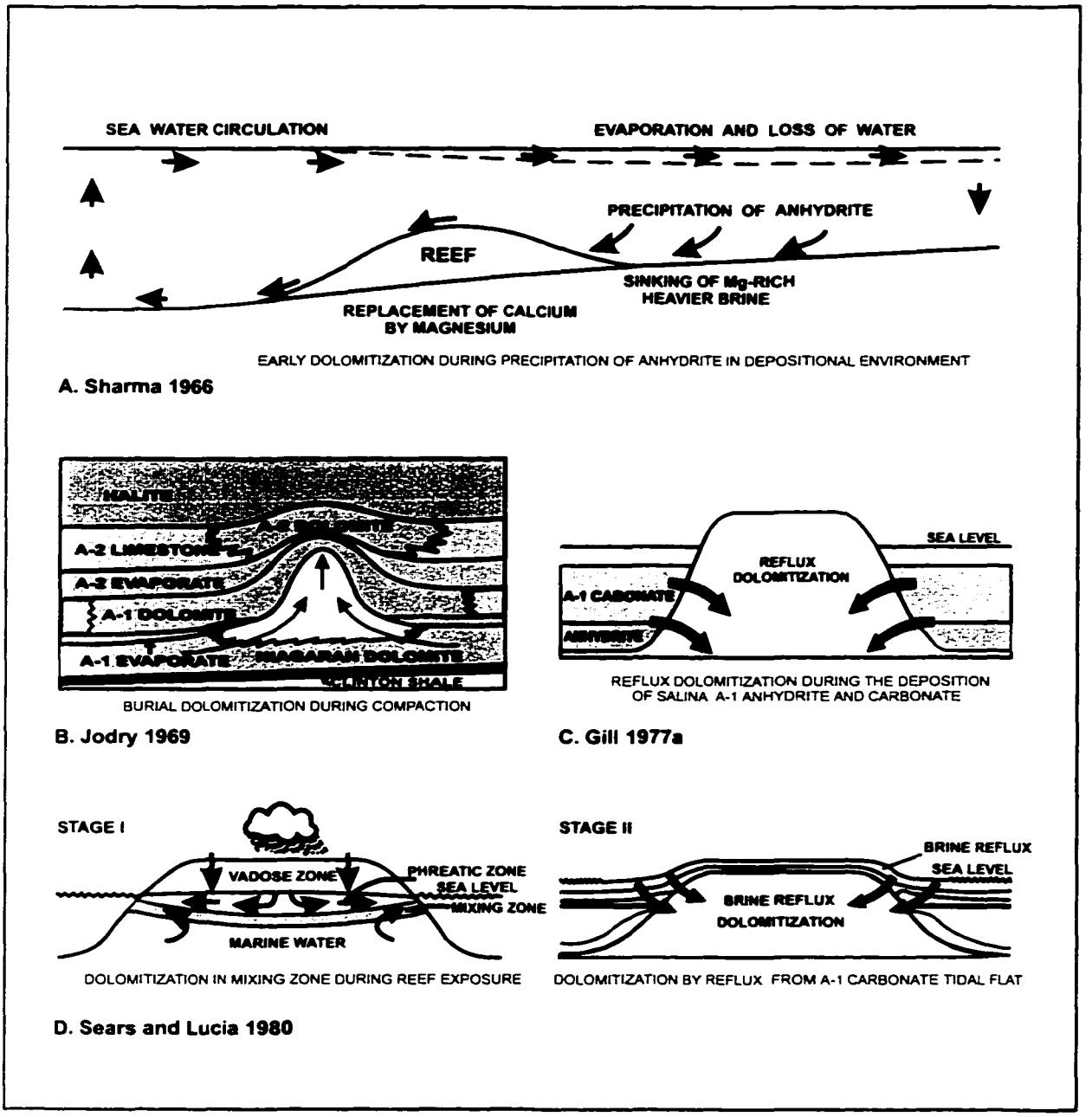



Fig. 1.3 Previouly suggested models for the dolomitization of Guelph pinnacle reefs in the Michigan Basin.

regional dolomitization was carried out by Sears and Lucia (1980) in northwestern Michigan (Fig. 1.3). The origin of the massive dolomite and main controlling factors on reservoir formation in the Guelph Formation of southwestern Ontario remain unclear.

In southeastern Michigan, an early comprehensive study of Silurian reefs by Felber (1964) concluded that the reefs developed in three growth stages in response to increasing salinities with no depositional break separating Salina from Niagara deposition. He suggested that the dolomitization occurred very early, before the deposition of the Salina A-1 Anhydrite. Sharma (1966) attributed dolomitization of the Peters pinnacle reef in St. Clair County to a one-step refluxion of the pinnacle reef by Mg-rich brines produced by extensive surface evaporation during deposition of the overlying A-1 Evaporite unit. The heavier brines sank downward to the seafloor, then moved basinward through the porous reefal sediments. He attributed the shelfward increasing abundance of dolomite to an earlier seal of the basinward seafloor by A-1 anhydrite (Fig. 1.3A). Jodry (1969) observed that the dolomitization of A-1 and A-2 carbonates around completely dolomitized pinnacle reefs extended nearly equally in all directions based on the mapped Mg/Ca ratio distribution in St. Clair and Macomb Counties. He also found that the degree of dolomitization in A-1 and A-2 Carbonates was directly proportional to the distance from the dolomitized reefs, implying a reef-related flow system. Instead of invoking refluxion of evaporative seawaters, Jodry (1969) assumed that the reef growth was contemporaneous with the deposition of lower Salina interreef carbonates and evaporites. He proposed a compaction model, in which reefal limestones and their surrounding A-1 and A-2 limestones were dolomitized by an upward

compaction flow of connate water from the adjacent interreef muddy carbonates during progressive burial (Fig. 1.3B). Gill (1977a) found that the Guelph Formation in the Belle River Mills Gas Field was entirely dolomitized without any limestone remains. He attributed dolomitization of the pinnacle reefs and surrounding A-1 Carbonate to the downward reflux of hypersaline brines in a supratidal sabkha environment during reef exposure and A-1 Evaporite deposition (Fig. 1.3C).

In northern Michigan, Sears and Lucia (1980) observed a general basinward dolomite-decreasing trend, where the shelfward reefs were completely dolomitized and basinward reefs were only partially dolomitized or remained as limestone. They believed that the dolomitization pattern of Niagara reefs followed the dolomitization pattern of A-1 Carbonate and suggested that downward refluxing fluid from the overlying A-1 Carbonate sea was responsible for dolomitization of both A-1 Carbonate and the underlying Niagara reefs. Sears and Lucia (1980) invoked a two-step model, including a first step of mixing-zone dolomitization for the partial dolomitization (10 to 30% dolomite content) of reefs during reef subaerial exposure and a hypersaline seawater reflux dolomitization for the massive dolomitization of shelfward reefs and A-1 Carbonate during deposition of A-1 tidal flat carbonate (Fig. 1.3D). Cercone (1984b) and Cercone and Lohmann (1985) further supported the two-step model of Sears and Lucia (1980), although they believed that the influence of meteoric water on reefs was relatively insignificant.

In southwestern Ontario, Sanford (1969) found that the A-1 Carbonate unit was preferentially dolomitized around completely dolomitized pinnacle reefs and oil and gas accumulations within A-1 Carbonate occurred in porous dolomite near the reefs. Carter (1991) mapped the dolomite distribution pattern in both A-1 and A-2 carbonate units based in Sombra Township of Lambton County. He also recognized that the dolomite in the A-1 carbonate unit is most common in the basal 1 to 3 m portion and is associated with dissolution of overlying halite of the B unit. Carter (1991) further pointed out that the close association of the dolomitization of A-1 and A-2 carbonates around dolomitized pinnacle reefs and overlying halite dissolution suggests that they may have been caused by the same fluid in a subsurface environment, although the source, timing and flow direction were not deduced. Grimes (1987) and Charbonneau (1990) described in detail the depositional facies and common diagenetic phases in cores from six reefs. They suggested several episodes of reef exposure and the importance of karsting to reservoir distribution, as indicated by the observed features such as large V-shaped vertical cavities filled by calcite and anhydrite cements and paleosol horizons. Note, however, that the reported paleosol horizons are more likely dedolomite intervals formed in subsurface conditions (see Chapter 5).

## 1.4 Study objectives

This study is the first attempt to investigate the distribution, origin, and diagenetic evolution of Guelph dolomites on a regional scale in southwestern Ontario. Despite the economic and geological importance and ready accessibility of the Guelph Formation in the study area, comprehensive diagenetic studies of these reefs on a regional scale have

not been carried out. Although some earlier studies have suggested a dominant influence by depositional facies or textures on the porosity and permeability of Niagaran reefs (e.g., Gill 1977a; Sears and Lucia 1980), it is also apparent from the present study that various diagenetic alterations of the reefal carbonates, especially dolomitization and post-dolomitization alteration, have resulted in an array of textural changes that played important roles in the development of carbonate reservoirs in the Guelph Formation. The development of a suitable model for the origin of Guelph dolomite and its diagenetic history depends on recognition of the nature and origin of diagenetic fluids responsible for the alteration and understanding of the relative timing of diagenetic events. In addition, the three-dimensional pattern of dolomite distribution in a sedimentary basin is a direct record of the paleohydrologic flow system for the dolomitization. In this study, a regional examination of the Guelph dolomite and a reappraisal of the previous literature in light of recent concepts in carbonate diagenesis and particularly dolomite diagenesis permits a better understanding of the controls over the distribution of dolomite fabrics and their influence on the quality of dolomite reservoirs in the Guelph Formation.

The prime objectives of this study are: (1) to determine the occurrence and distribution of Guelph dolomite in the study region based on core and well logging data; (2) to document its petrographic characteristics and geochemistry in order to build a regional data base for this study and future studies; (3) to develop a suitable model to explain the origin and diagenetic history of dolomite, on the basis of the dolomite distribution pattern, petrography and geochemistry within a regional stratigraphic framework; and (4) to determine the importance of post-dolomitization diagenetic processes in the Guelph

Formation, such as dolomite-to-dolomite and dolomite-to-calcite alteration, and to assess their influence on both porosity evolution and reservoir formation.

This integrated investigation of data from (1) borehole records, (2) core observations, (3) standard transmitted light and cathodoluminescence petrographic study of thin sections, (4) geochemical analyses for major elements (Ca and Mg), trace elements (Sr, Na, Fe, and Mn), stable isotopes (O and C), and radiogenic isotopes (Sr), and (5) fluid inclusion analysis of Guelph dolomites and associated limestones, provides a better understanding of the origin and distribution of dolomites, especially the source of dolomitizing fluids, the timing of dolomitization, and the pumping mechanism. Geochemical data from different dolomite types are compared to determine whether present-day geochemistry of the dolomites still reflects the original signatures of initial dolomitization, or whether subsequent diagenetic alteration of early-formed dolomites occurred as suggested in some recent studies (e.g., Land 1985; Hardie 1987; Gao and Land 1991; Mazzullo 1992). A hydrologic model is proposed for early dolomitization and later dolomite alteration, including dolomite dissolution, dolomite recrystallization, dolomite overgrowth or cementation, and dedolomitization, as well as other related diagenesis. This model may have important implications for the understanding of dolomite formation and reservoir distribution in Middle Silurian reefs in other areas of the Michigan Basin and for other similar basins.

## 1.5 Methodology

A total of 76 cores from 32 pinnacle and patch reefs and inter-reef areas in the study region (Appendix I), including 15 limestone-bearing cores and 8 dedolomite-bearing cores, were systematically described and logged at the Subsurface Core Laboratory of the Ontario Ministry of Natural Resources, London. Numerous slabbed core samples were polished to study textures in detail. The lithology was described using the classification of Dunham (1962) and its subsequent modification by Embry and Klovan (1971). The porosity was described using the classification of Choquette and Pray (1970). The excellent preservation of depositional and early diagenetic textures in undolomitized pinnacle and patch reefs permitted the reconstruction of original sedimentary facies and pre-dolomitization diagenesis. In addition, good to moderate preservation of limestone fabrics can be found in most dolomites, especially in mimetically replaced microcrystalline dolomites, allowing the extrapolation of information obtained from limestones.

A total of 180 representative samples, including 161 samples from Guelph carbonates and 19 samples from A-1 carbonates (Appendix II), were chosen for detailed petrographic and geochemical analysis. They were selected to provide geographic and stratigraphic coverage of the study area to represent different reefs and lithologies. 157 polished thin sections, including 35 limestone, 106 dolomite and 16 dedolomite, were prepared and half of each thin section was stained with Alizarin Red S and potassium ferricyanide solution (Dickson 1966). Petrographic analysis was based on examination of thin sections under transmitted light on a conventional Nikon microscope and under

cathodoluminescence on a Technosyn 8200 Cold Cathode Luminoscope operating at 15-17 kV beam voltage and 0.7-0.8 mA beam current.

Based on observation of stained thin sections, all limestone samples are nearly pure with less than 8% dolomite; all dolomite samples are pure dolomite; dedolomite samples contain approximately 10-45% of dolomite. 103 representative samples of whole rock and individual diagenetic fabrics such as calcite and dolomite cements from dolomite and associated limestone and dedolomite, including 83 samples from Guelph carbonates and 19 samples from A-1 carbonates, were chosen for geochemical analyses. For comparative purpose, samples of different types of dolomites were also selected for geochemical study. Powdered samples were obtained from thin section cut-offs or hand specimens using a rotary Dremel tool with dental drill bits. All powdered samples were pretreated by roasting at 470°C using a helium flow for 45 minutes to remove the volatile organics (Epstein et al. 1953). Both elemental and stable isotopic analyses were carried out using the same powdered samples. The solutions for elemental analyses were prepared using acid decomposition and following a procedure similar to that developed by Robinson (1980), placing about 0.2 g of powder in 10 mL 1M dilute HCl at room conditions for 30 minutes for calcite (including dedolomite) and 2 hours for dolomite. The solutions were filtered using ashless paper to remove insoluble residue. The insoluble fraction for each sample was weighed and subtracted from the total sample weight during calculation. The non-carbonate residues range from less than 1% by weight in most samples to up to 2% in a few samples.

85 samples were analyzed by Atomic Absorption Spectrometry (AAS) for major elements (Ca, Mg) and trace elements (Na, Sr, Fe and Mn) and an additional 17 samples were analyzed by Inductively Coupled Plasma (ICP) Spectrophotometry for Ca, Mg, Na, Sr, Fe, Mn and Al in the Water Quality Laboratory at the University of Waterloo (Appendix III). Interference due to ionization was avoided by adding KCl to both standards and unknowns. The results from AAS and ICP are comparable. Duplicates and blanks were run for determining the precision and accuracy of the analyticai results. Analytical errors are less than ±5% for Sr and Mn and lower than ±10% for Na and Fe, respectively. Robinson (1980) suggested that the contamination from leaching of the non-carbonate fraction in low non-carbonate content samples (< 5%) would be less than 10% for Sr, Na, and Mn and less than 20% for Fe. Based on ICP analyses, Al concentrations in Guelph carbonates are all below the detection limit (<1 ppm). Some reported carbonates with high Al contents (e.g., Lu and Meyers 1998, 140-2200 ppm) are interpreted to have resulted from leaching of terrigenous impurities. The low contents of Al in Guelph carbonates also indicate an insignificant contribution from possible leaching of non-carbonate residuals to the trace element compositions and the $^{87}Sr/^{86}Sr$ ratios.

94 samples from Guelph and A-1 carbonates, including 64 replacive dolomite or dolomite cement, 22 bulk limestone or calcite cement, and 8 dedolomite, were analyzed for oxygen and carbon stable isotopes in the Environmental Isotope Laboratory at the University of Waterloo (Appendix III). Following the method developed by McCrea (1950), the $CO_2$ was obtained by reacting 10-20 mg roasted powder sample with 100% phosphoric acid at 50°C, 48 hours for dolomite and 30 minutes for calcite and dedolomite

samples and then analyzed on a Prism Series II mass spectrometer. Results are reported in per mil (‰) notation relative to the PDB standard using standard correction procedures. Dolomite $\delta^{18}O$ values are not corrected for dolomite-phosphoric acid fractionation of approximately 0.8‰ enrichment (Sharma and Clayton 1965). Precision of the data was determined using at least one laboratory standard (EIL21 for calcite and EIL22 for dolomite) and one duplicate sample in each group of 6 to 7 samples. Reproducibility on duplicates is better than ± 0.3 ‰ for both $\delta^{18}O$ and $\delta^{13}C$ values. Based on observation of stained thin sections, all the dolomite samples were pure dolomite. In order to remove the $CO_2$ produced by reacting with possible trace amounts of calcite in dolomite samples, the reaction vessels were pumped for 5 minutes after mixing the powdered samples with pure $H_3PO_4$ for 15 minutes. For calcite and dedolomite samples, only the $CO_2$ collected in the first 15 minutes was used for analysis.

Twenty-seven powdered samples, including 3 bulk limestone, 1 calcite cement, 20 bulk dolomite, 1 dolomite cement, and 2 dedolomite, were sent to the Radiogenic Isotope Facility, Department of Earth and Atmospheric Sciences, at the University of Alberta for analysis, for measuring of $^{87}Sr/^{86}Sr$ ratios (Appendix III). Carbonate powders were first dissolved in cold 0.75N HCl solution and Sr was separated by conventional cation exchange chromatography using BioRad AG50-X8, a 200 to 400 mesh resin. The purified Sr was loaded to a single Re filament together with Ta activator then was analyzed for isotopic composition on a VG354 mass spectrometer. All results are reported relative to $^{87}Sr/^{86}Sr = 0.71027$ for the National Institute of Standards and Technology Standard Reference Material SRM987. Precision was better than ±0.00002.

All analyses were corrected for variable mass-discrimination to a value of $^{86}Sr/^{88}Sr$ = 0.1194.

Fifteen doubly polished 100-200 μm-thick sections were prepared for fluid inclusion analysis following the method of Barker and Reynolds (1984). Homogenization and melting temperatures of two-phase inclusions in different diagenetic fabrics, including 1 equant calcite, 3 Type 2 dolomite, 2 dedolomite, 3 Type 3 dolomite, 2 saddle dolomite, 1 megaquartz cement, and 1 halite (Appendix IV), were examined on a Nikon microscope with a USGS-type gas-flow heating and freezing stage. The fluid inclusion temperatures were calibrated using the lab standards. The fluid inclusions in 2 Type 1 dolomite samples were too small (<5 μm) to be measured. The measured inclusions are all isolated primary two-phase fluid inclusions ranging from 5 to 15 μm in size (Roedder 1984; Goldstein and Reynolds 1993). All measurements were duplicated and values were reproducible to ±2°C. Several factors, including pressure, thermal stretching and leaking, contamination by hydrocarbon liquid and gases ($CO_2$, $CH_4$ and $H_2S$, etc.) trapped or altered from trapped organic material in inclusions, may affect the readings of fluid inclusion data (Crawford 1981; Roedder 1984). Homogenization temperatures (Th) listed in Appendix II are not corrected for pressure difference. The initial melting or eutectic temperature (Te) and final melting temperature (Tm) were also measured in most of the studied inclusions whenever possible. Many two-phase inclusions in Type 3 dolomites contain very small (visually <5%) vapor bubbles which have extremely high Th. These small bubbles do not disappear until overheating to approximately 270 to 300°C. These erroneously high measured values of Th are likely caused by $CH_4$–dominated vapor

trapped in two-phase inclusions, as suggested by Jones and Kesler (1992) for the inclusions in dolomites from the eastern Tennessee mining districts.

## 1.6 Organization of the thesis

This thesis is presented in seven chapters. The first chapter mainly introduces the study area and strata, previous related studies, study objectives and methodology. The second chapter reviews the regional geological setting for the Michigan Basin and the study area of southwestern Ontario based on the information from numerous former studies and new data from this study. This chapter includes discussion of paleoclimate, stratigraphy, paleogeography and depositional environments, especially during the Middle to Late Silurian. Burial and geothermal history, and chemical compositions of present-day formation waters in the study area are also reviewed. Chapter 3 describes the major facies in the Guelph Formation using core descriptions obtained in this study. A general paragenetic sequence is constructed based on thin section observation, but only pre-dolomitization diagenesis including early calcite cementation, calcite neomorphism and early limestone dissolution is documented in this chapter. Other diagenetic events are treated in chapters 4, 5 and 6. Chapter 4 is the most comprehensive chapter of this thesis and it focuses on the origin of different dolomite fabrics that occur in the Guelph Formation. Chapter 5 deals with local dedolomite that occurs in five pinnacle reefs on the basinward lower ramp. Dedolomitization is interpreted to have resulted from $Ca^{2+}$-rich fluids generated from the local dissolution of associated limestone. Chapter 6 introduces the major porosity types and their distribution in Guelph carbonates. The post-dolomitization diagenesis, especially dolomite alteration is the main process to control

the porosity evolution and final porosity. The major conclusions from this study and recommendations for further study are summarized and presented together in Chapter 7.

# Chapter 2 Geological Setting

## 2.1 Regional geology

The Michigan Basin is a nearly circular basin with a diameter of approximately 650 km and an area of approximately 300,000 $km^2$ developed on a Precambrian basement. The study area of nearly 7000 $km^2$ in southwestern Ontario is located on the southeastern margin of the Michigan Basin (Fig. 1.1, 1.2). The Michigan Basin is bounded on the west by the Wisconsin Arch in Wisconsin, on the south by the Cincinnati Arch and Findlay Arch in Ohio, on the east by the Algonquin Arch in Ontario, and on the north by the Precambrian Canadian Shield.

The Michigan Basin has traditionally been considered as a classic intracratonic basin within the North American craton. Several mechanisms have been proposed to explain the formation and subsidence of the Michigan Basin. These include crustal rifting or continental extension (Howell and van der Pluijm 1990), thermal subsidence (Sleep and Sloss 1978; Nunn et al. 1984; Nunn 1986), downwarping caused by continental compression triggered by plate motion (Sanford et al. 1985), and increase in crustal density due to eclogite phase transformation or dense material intrusion (Haxby et al. 1976). Recent studies indicate that its formation involved a succession of basin-forming processes, which included rifting, thermal subsidence and later isostatic readjustment (Klein 1995). The Michigan Basin formed following the reactivation of an earlier rift system, the Mid-Continental Rift, caused by partially melted lower crust and intrusion of anorogenic granite during the Late Precambrian breakup of the super-continent Rodinia.

This rift is traceable from Kansas to Lake Superior (Quinlan 1987; Howell and van der Pluijm 1990). Cooling of anorogenic granite and related thermal contraction caused subsequent thermal subsidence (Sleep and Snell 1976; Nunn et al 1984; Nunn 1986).

The Paleozoic strata in the Michigan Basin have been documented in several regional studies (e.g., Burgess and Benson 1969; Sanford 1969; Carter 1987; Johnson et al. 1992). The Michigan Basin contains up to 4.5 km of preserved sedimentary strata, consisting largely of a thick lower Paleozoic succession and a thinner upper Paleozoic sequence, with minor Mesozoic (Jurassic) strata in the basin center (Sleep and Sloss 1978). The general thickness variations of the Paleozoic strata in the Michigan Basin are shown in a north-south profile across the basin (Fig. 2.1) (Gardner and Bray 1985). Cambrian strata are marine sandstones and shales and the Ordovician succession is composed of shallow marine carbonates and siliciclastics. Silurian sequence consists of Lower Silurian shallow-water platform carbonates, which pass upward into Middle Silurian deeper-water basinal carbonates rimmed by pinnacle and patch reefs on the ramp with barrier reefs and back-reef carbonates on the platform shelf, and Late Silurian restricted marine deposits consisting of interbedded evaporites and carbonates. Devonian and Mississippian strata are dominated by shallow marine carbonates that give way to Pennsylvanian non-marine siliciclastics. Jurassic fluvial red beds were deposited only in the basin center. The basin is mostly covered by up to 400 m of the Pleistocene glacial sediments. Subsidence rate of the Michigan Basin varied with time. The average rates in the basin center were 20 to 30 m/Ma from the Middle Ordovician to Early Devonian, whereas the rates were only 5 to 10 m/Ma in southwestern Ontario for the same time period (Sloss 1988).

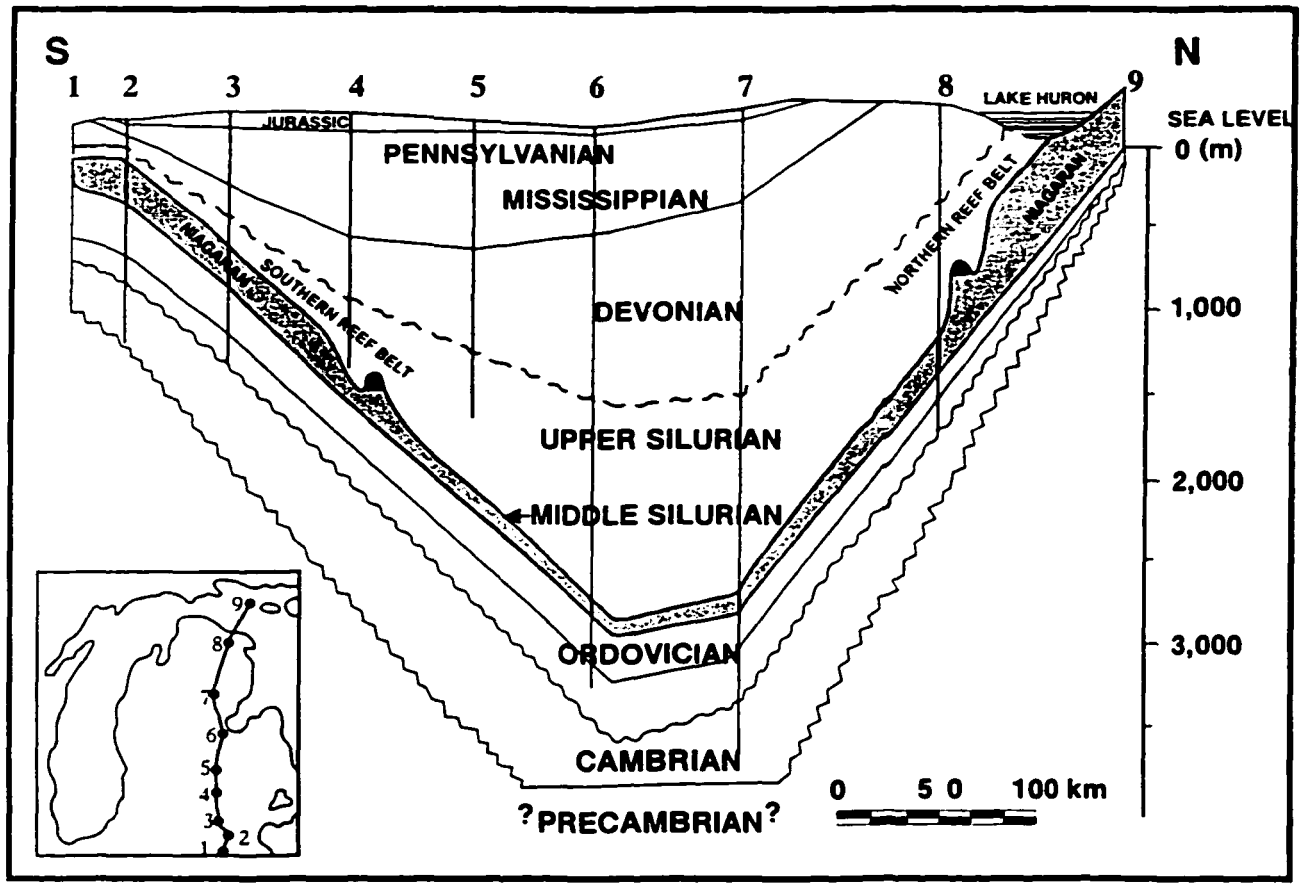



Fig. 2.1 Structural cross section across the Michigan Basin (modified after Gardner and Bray 1985).

During the Middle Silurian, the Michigan Basin retained a climatically and nutritionally favorable environment for reef growth. A nearly concentric reef ring consisting of a southern reef belt and a northern reef belt was developed along the margin of the basin (Sanford 1969; Burgess and Benson 1969; Gill 1977a, 1979, 1985; Sears and Lucia 1979; Bailey 1986) (Fig. 2.2). The southern reef belt extends from southern Michigan to southwestern Ontario with a linear length of at 210 km and maximum width of approximately 60 km. The northern reef belt that is developed in northeastern Michigan stretches for at least 280 km and is 40 km wide. In both reef belts, the reefs increase in height basinward from the shelf, and the morphologies and the internal facies are very similar (Gill 1979; Sears and Lucia 1979). In southwestern Ontario, the pinnacle reefs have maximum heights of 140 m, and are shorter than their counterparts in northern Michigan (Gill 1979).

The growth of Niagaran reefs during the Middle Silurian was mainly controlled by differential subsidence, as indicated by a basinward increase in the height of reefs (Sears and Lucia 1979). The general concordance between deeper water facies and thicker units in the Upper Silurian sequence also suggests that the sedimentation was mainly controlled by basin subsidence rather than eustatic sea-level changes (Fig. 2.1).

The regional depositional setting of southwestern Ontario through the Paleozoic was generally controlled by three major structural elements developed on the Precambrian basement: the northeast-plunging Findlay Arch, the southwest-plunging Algonquin Arch, and the Chatham Sag between the two arches (Fig. 1.1). The Algonquin-Findlay Arch

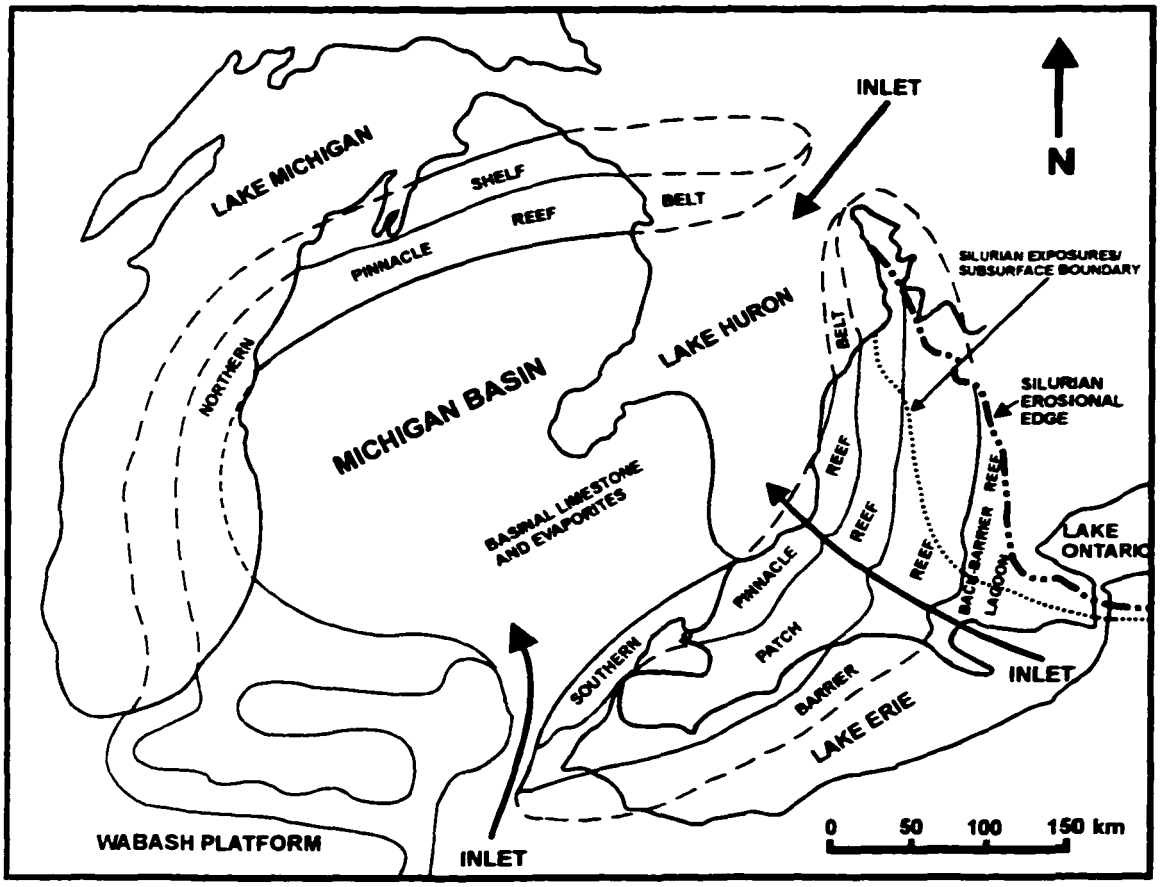



Fig. 2.2 Generalized paleogeographic environments and facies distribution in the Michigan Basin during the Middle to Late Silurian. Four facies zones including pinnacle reef, patch reef, barrier reef, and back-barrier-reef lagoon (Eramosa Member) were developed in the Guelph Formation. Compiled based on the information from Burgess and Benson (1969), Sanford (1969), Winder and Sanford (1972), Briggs and Briggs (1974), Gill (1977a, 1979, 1985), McMurray (1985), Bailey (1986), Cercone (1988), Armstrong and Goodman (1990), Sonnenfeld and Al-Aasm (1991), and this study.

system was reactivated from time to time, and exhibited vertical relief up to 100 to 200 m during the Paleozoic (Sanford 1962; Sanford et al. 1985). The Findlay-Algonquin Arch system separates the Michigan Basin and the Appalachian Basin. The Appalachian Basin was an elongate foreland basin for the most of Paleozoic Era (Quinlan and Beaumont 1984; Noor 1989). The study area is located in the Chatham Sag and on the westward side of the Algonquin Arch in the Michigan Basin.

Brigham (1971) suggested that the Findlay and Algonquin arches were the passive result of differential subsidence in the two basins on the opposite sides of the arches. Quinlan and Beaumont (1984) proposed that the primary controls on the development of the arches were the location and magnitude of Appalachian orogenic events and the rheological (elastic) behavior of lithosphere. Sanford et al. (1985) suggested that the Findlay and Algonquin arches, which parallel the Appalachian orogen, were initiated by the compressive stresses of plate motion in Precambrian time and were reactivated from time to time during the Paleozoic. Large quantities of siliciclastics were deposited in the Appalachian Basin with an estimated maximum thickness of approximately 11,000-12,000 m to the southeast of Lake Erie, but were greatly diminished northwestward over the Algonquin Arch and into the Michigan Basin (Liberty and Bolton 1971; Mesolella 1978; Carter 1987).

Tectonic activity was relatively weak and the structural features are relatively simple in the study region, with small to medium-size normal faults, local folds, and halite-dissolution-related structures (Brigham and Winder 1966; Brigham 1971; Sanford et

al.1985). Sanford et al. (1985) proposed that the relative vertical movements of basement arches probably caused faulting and fracturing of the overlying strata and resulted in the development of a regional fault and fracture framework in southern Ontario. These faults and fractures likely influenced the distribution of reefs, the flow conduits for both water and hydrocarbons, and the traps for hydrocarbon accumulation.

## 2.2 Paleoclimate

Paleomagnetic evidence and reconstructed paleocontinental positions indicate that the North American plate (continent) was located at approximately 30°S during the Ordovician. Later this plate moved northward then rotated in a clockwise direction back to near an equatorial position by the Late Devonian (Ziegler et al. 1977; Irving 1979). Collective palaeomagnetic and palaeobotanic data indicate that the Michigan Basin was positioned in a tropical paleolatitude between 10°S and 15°S during Silurian time (Roy et al. 1967; Van der Voo 1982, 1988; Shannon and Naylor 1989).

Several regional stratigraphic and sedimentary studies (e.g., Briggs and Briggs 1974; Shaver et al. 1978; Droste and Shaver 1983) also support the idea that the Michigan Basin was in a near equatorial paleolatitude and filled by warm shallow seas. Prevailing southeast trade winds during the Middle Silurian would have provided an ideal situation for reef growth. The climate of southwestern Ontario changed from a humid tropical climate in the Middle Silurian (Niagaran) to an arid to semi-arid tropical climate with high evaporation rates in the Late Silurian (Cayugan), as indicated by prolific reef development in the Guelph Formation followed by deposition of a thick sequence of

interbedded evaporites and carbonates in the Salina Formation.

## 2.3 Stratigraphy

The detailed stratigraphy of the sedimentary succession in the subsurface of southwestern Ontario has been described by Pounder (1962), Sanford (1969), Brigham (1971), Winder and Sanford (1972), Bailey (1986), Carter (1987, 1990), Johnson et al. (1992). In southwestern Ontario, the Paleozoic strata consist of a variety of carbonates, siliciclastics, and evaporites ranging in age from Late Cambrian to Late Devonian and locally Mississippian (Sanford 1962, 1969; Sanford et al. 1985) (Fig. 2.3). Upper Cambrian sandstones at the base are disconformably overlain by thick sequence of Middle Ordovician limestones, which are in turn overlain by thick Upper Ordovician shales. Silurian succession consisting of mainly carbonates and evaporites is well developed in the southwestern Ontario subsurface and exposed to the northeast along the Niagara Escarpment from the Bruce Peninsula across the Algonquin Arch to the Niagara Peninsula (Liberty and Bolton 1971; Carter 1987; Armstrong and Goodman 1990). The Devonian succession is mainly composed of carbonate and evaporite rocks with some shale and Mississippian consists of alternating shales and sandstones. These rocks were tilted to form the present-day, southwestward regional dip of approximately 6-9 m/km toward the center of the Michigan Basin, with maximum preserved thicknesses of approximately 1400 m in the Chatham Sag and approximately 500 to 1000 m over the Algonquin Arch (Sanford 1969; Winder and Sanford 1972). These strata unconformably overlie Precambrian basement (1000 Ma) rocks of the Grenville Province at the southern margin of the Canadian Shield. The Precambrian rocks include granite, gneiss and

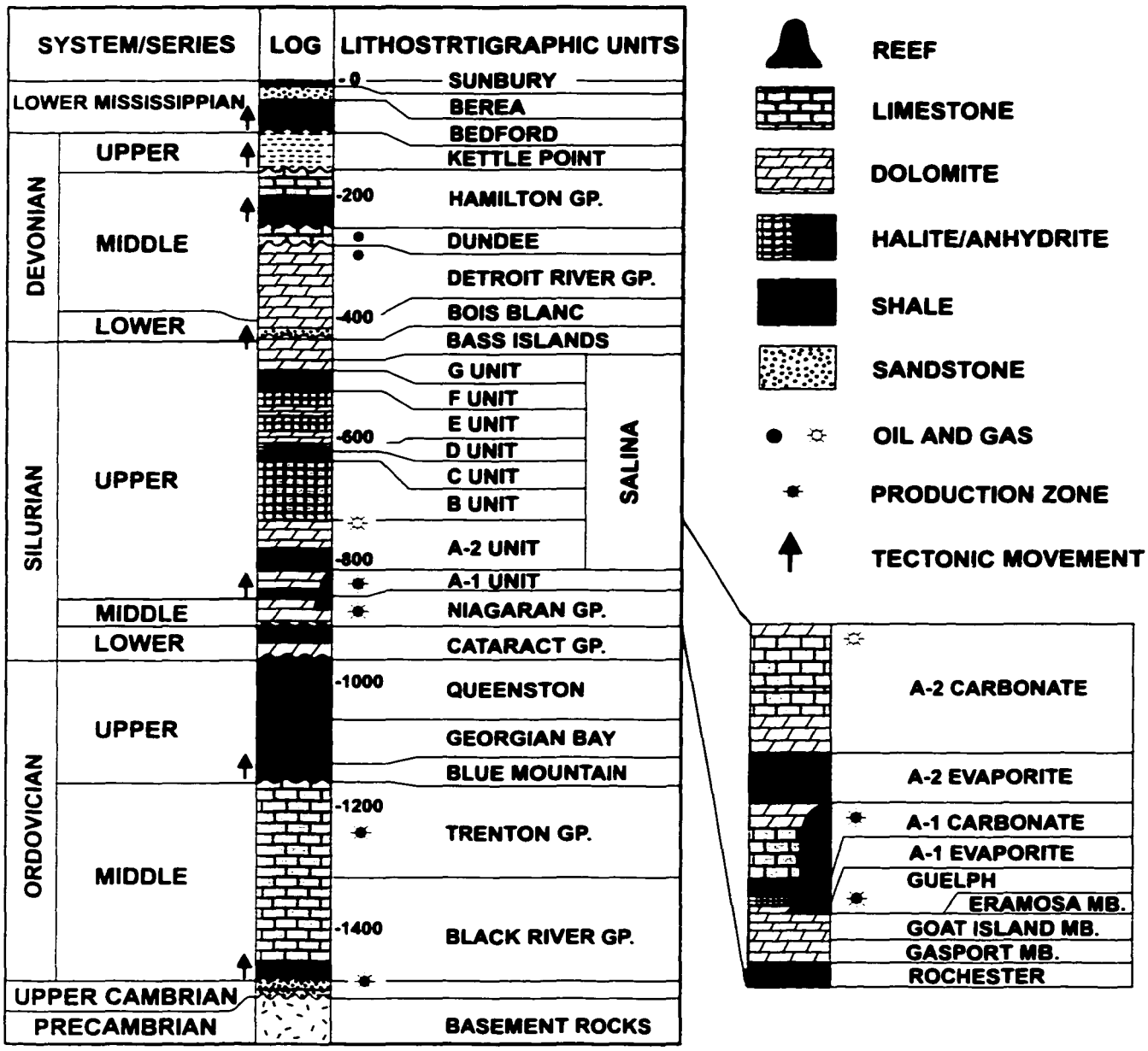



Fig. 2.3 Lithostratigraphic profile of Paleozoic strata in southwestern Ontario (modified from Sanford et al. 1985).

metasedimentary rocks, with minor marble and metaclastics (Carter 1987; Carter and Easton 1990).

The Silurian sequence includes the Lower Silurian Cataract Group and Clinton Group, the Middle Silurian Albemarle (Niagaran) Group, and the Upper Silurian Salina Formation and Bass Islands Formation. The Middle and Upper Silurian successions in the study area are shown in Figure 2.4. The Cataract and Clinton groups are composed of a 20 to 40 m thick sequence of carbonates and shales with minor sandstones, deposited in a broad regional platform along the Algonquin Arch (Sanford 1969). The Albemarle (Niagara) Group is dominated by platformal and reefal carbonates. The Salina Formation consists of interbedded carbonates and evaporites and Bass Islands Formation is composed of dolomites (Fig. 2.4).

Cohee (1948) introduced the term 'Niagara' for the Middle Silurian carbonate sequence in southern Michigan. The terms 'Brown Niagara' and 'Grey Niagara' were often used in oil exploration for an upper portion of buff to brown porous dolomite (Guelph Formation equivalent) and a lower grey dolomite (Lockport Formation equivalent), respectively. The term 'Albemarle' was used in southern Ontario for the correlative sequence. More detailed stratigraphic studies prompted by oil exploration in southwestern Ontario have further divided the Albemarle Group into the Rochester, Lockport, and Guelph formations, which represent a transgressive sequence of carbonate sediments and buildups deposited in shallow open shelf to deeper carbonate ramp environments (Sanford 1969; Smith and Legault 1985) (Fig. 2.4).

The Rochester Formation, the lowermost unit of the Albemarle Group (Fig. 2.4), is a dark grey to black shale and/or calcareous to dolomitic shale unit with numerous crinoid fragments and thin dolomite interbeds. It blankets the study area with a relatively uniform thickness of 10 to 15 m and represents deposition on a storm-influenced, moderately shallow and muddy shelf environment (Brett 1983).

The Lockport Formation was subdivided into a lower Gasport Member and an upper Goat Island Member (Fig. 2.4). The Gasport and Goat Island members have a total thickness of 20 to 60 m in the study area with thinning basinward to a few meters in the basin center and thickening shoreward up to 90 m in the shelf margin, representing an open shallow carbonate shelf (Sanford 1962; Crowley 1973; Brett et al. 1990). The Lockport Formation grades eastward into the equivalent Amabel Formation along a boundary from the Bruce Peninsula to the Niagara Peninsula (Smith and Legault 1985).

The Eramosa Member at the base of the Guelph Formation (Fig. 2.3) is composed of dark grey to brown, laminated to thin-bedded, burrowed, organic-rich and bituminous, dolomitic mudstone and wackestone with petroliferous smell, fragments of brachiopods, trilobites and bryozoans, local chert nodules and preserved gypsum (Bolton 1957; Sanford 1969; Liberty and Bolton 1971). It also contains scattered, small reef knolls in southern Ontario and northwestern New York (Crowley 1973; Smith and Legault 1985). The Eramosa Member was only developed in the eastward part of the study region where it represents a restricted back-barrier-reef lagoon environment (Armstrong and Goodman

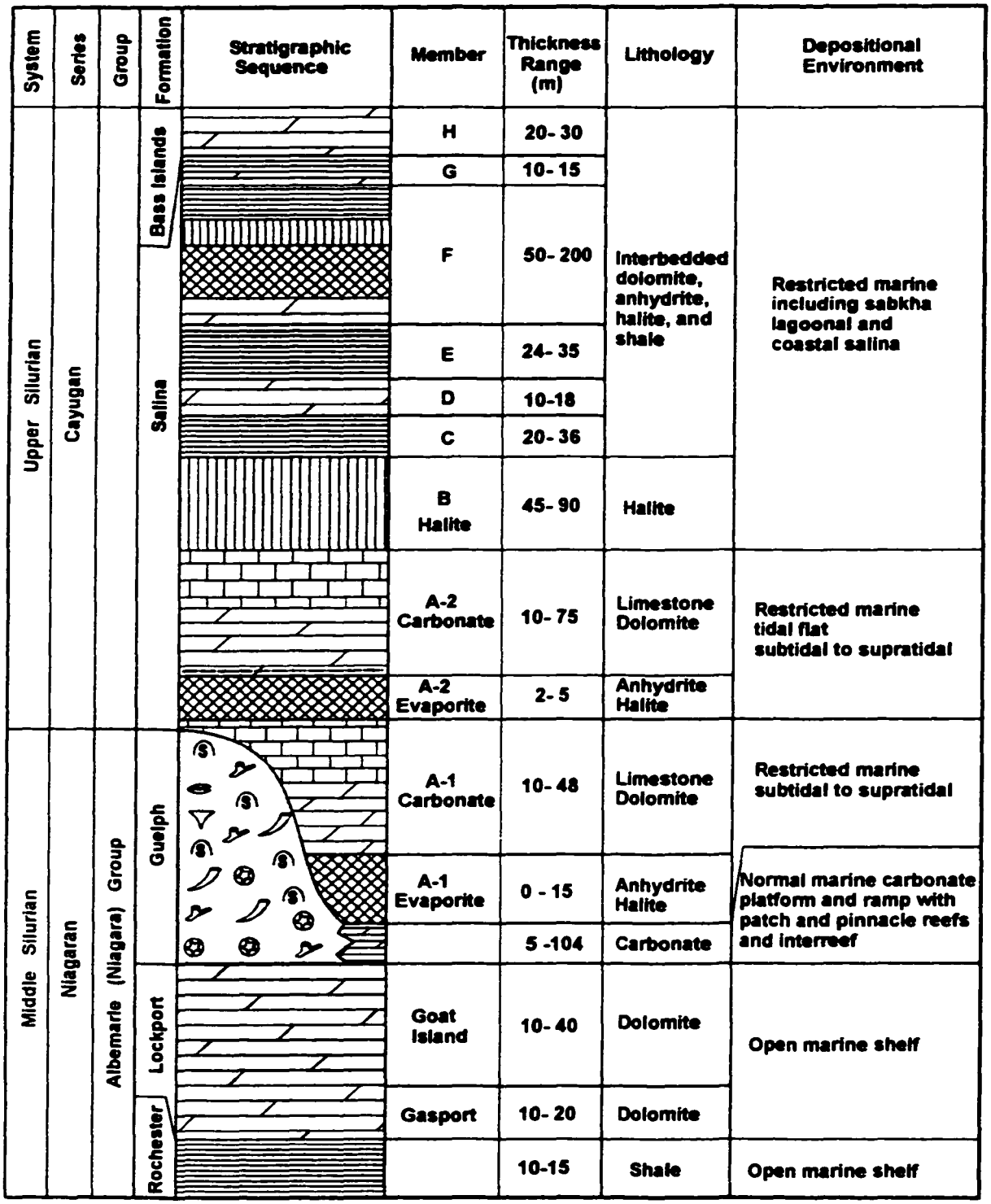
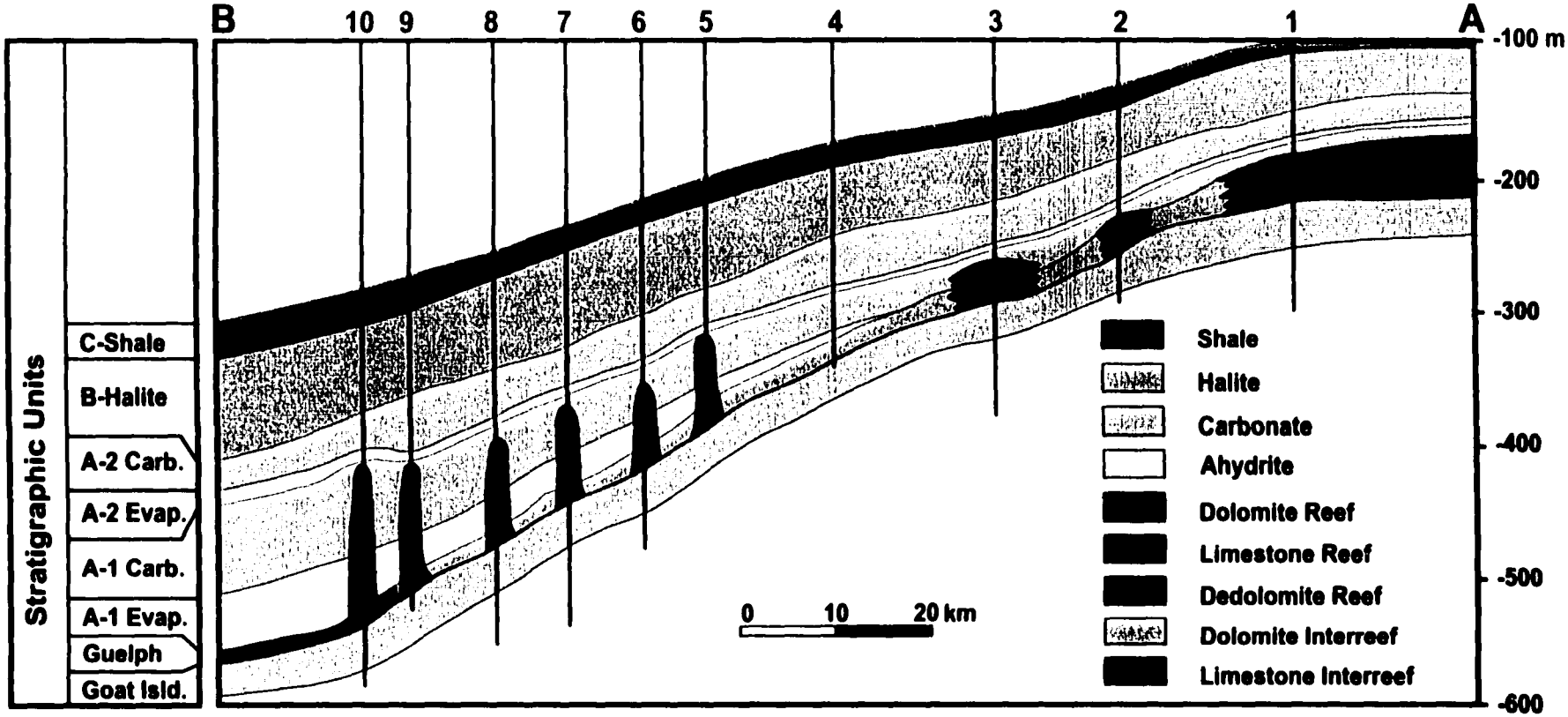



Fig. 2.4 General stratigraphic sequence of the Middle and Upper Silurian for study area in southwestern Ontario. Compiled Based on data from Sanford (1969), Liberty and Bolton (1971), Carter (1987), Haynes and Hughes-Pearl (1990), and Johnson et al. (1992). The Middle Silurian Guelph Formation is dominated by reefal carbonates and is mostly composed of tan to dark brown, microcrystalline to finely crystalline, pervasive dolomite, which is overlain by interbedded carbonates and evaporites of the Upper Silurian Salina Formation.

1990; Brett et al. 1990).

The Guelph Formation, which is the focus of this study, is the uppermost unit of the Albemarle Group (Fig. 2.4). It consists mostly of tan to dark brown, microcrystalline to coarsely crystalline pervasive dolomites with local dedolomite and limestone. The term 'Guelph Formation' was originally named by Logan (1863) in his "Geology of Canada" for the series of rocks typically developed in the vicinities of Galt (now part of Cambridge) and Guelph. The Guelph Formation outcrops along a belt 15 to 30 km wide from the tip of the Bruce Peninsula to the Niagara River and extends southwest to the subsurface of southwestern Ontario (Sanford 1969). An approximately east-west oriented regional cross-section through southwestern Ontario (Fig. 2.5) shows that the Guelph Formation consists of shelfward barrier reefs, basinward patch reefs and pinnacle reefs, and their thin equivalent interreef facies developed over an gently-dipping carbonate ramp of the Goat Island Member of the Lockport Formation. The thickness of the Guelph Formation ranges from 5-10 m in inter-reef areas to up to 140 m in pinnacle reefs (Fig. 2.4). More basinal facies are relatively thin and nonporous micritic limestones (Sanford 1969). The contact between the Lockport Formation and the overlying Guelph Formation is a conformable transition (Gill 1977a; this study), although several previous studies suggested this contact might represent a major erosional or karsting surface or an unconformity (Charbonneau 1990; Smith et al. 1993).

The Upper Silurian succession (Cayugan) was divided into eight units, A to H in ascending order, by Landes (1945) (Fig. 2.4). The uppermost unit H was later renamed




| Depositional Environment | Basin | Lower Ramp | Upper Ramp | Platform Margin |
|---|---|---|---|---|
| Guelph Main Facies | | Pinnacle Reef | Patch Reef | Barrier Reef |
| Guelph Lithology | Limestone | Dolomite, Limestone, and Dedolomite | Dolomite | Dolomite |

Fig. 2.5 Regional cross-section, showing the distribution of main facies and lithologies in the Guelph Formation and the relationship between the Guelph Formation and overlying A, B, and C units of the Salina Formation. Location of cross-section (A-B) is shown in Figure 1.2.

the Bass Islands Formation. The Salina Formation includes seven units from A to G and consists of cyclically interbedded evaporites and carbonates. Evans (1950) further subdivided unit A into, from base to top, A-1 Evaporite, A-1 Carbonate, A-2 Evaporite, and A-2 Carbonate. Droste and Shaver (1977) interpreted the evaporite units to have been deposited from hypersaline seawater, whereas the interbedded carbonate units were deposited under more normal marine conditions.

The A-1 Evaporite (mainly anhydrite) thickens basinward from 0 to 20 m and occurs in the interreef areas against the pinnacle reefs, but it does not cover the reefs and is absent in the shelf area (Fig. 2.4, 2.5). The A-1 Carbonate occurs between the reefs and extends over the reef tops with a thickness from 10 to 50 m, which thins basinward. The A-1 Carbonate unit consists of light brown to tan, fine to medium crystalline, stromatolitic and laminated dolomites on the shelf and around and above patch and pinnacle reefs on the ramp. A-1 carbonate containing few brachiopods and intraclasts was interpreted as have been deposited in a low energy subtidal to supratidal environment (Gill 1977b) or a tidal flat to restricted shallow marine environment (Sears and Lucia 1980).

The relatively thin A-2 Evaporite, ranging from 2 to 15 m in thickness, is an excellent regional cap rock that covers the A-1 Carbonate and Guelph reef rocks (Fig. 2.4, 2.5). It consists of halite in the interreef areas and basin center but changes to anhydrite on the crests of pinnacle reefs. It pinches out shelfward above the barrier reefs (Fig. 2.5). A-2 Carbonate thickens basinward from 10 to 75 m. It is composed of dark grey to brown, laminated to massive, microcrystalline to finely crystalline dolomites and lime

mudstones.

Following the deposition of A-1 and A-2 units, the B Halite occurred as a widespread unit in a much larger area than the A-1 and A-2 evaporites in the Michigan Basin and extended into the adjacent Appalachian Basin (Carter 1987; Haynes and Hughes-Pearl 1990). It is a widespread unit and varies from 45 to 90 m in thickness in the study area (Fig. 2.4, 2.5). The B Halite is absent above several pinnacle reefs due to later dissolution.

The C unit is a uniform grey or green shale with minor anhydrite, 20 to 30 m thick (Fig. 2.4). It is an excellent regional time-stratigraphic marker (Fig. 2.5). The D unit is another halite unit, 10-20 m thick, with millimeter to centimeter thick thin dolomite bands (Fig. 2.4). It is also been removed by dissolution on top of some pinnacle reefs. Unit E consists of grey to brown dolomite and shaly dolomite, grading upward into grey shale with local anhydrite beds. Its thickness ranges from 20 to 35 m (Fig. 2.4). Unit F is composed of dolomite and dolomitic shale unit with anhydrite, halite, and red shale interbeds, ranging from 20 to 200 m in thickness. Unit G varies from 10 to 15 m and consists of tan dolomite and anhydrite overlain by grey dolomitic shale. Bass Islands Formation consists of 20 to 30 m thick dark brown microcrystalline to finely crystalline dolomite with evaporite mineral molds (Fig. 2.4). Sonnenfeld and Al-Aasm (1991) concluded that the evaporites of the Salina Group progressively extended shoreward from the deeper basin area to the shallow shelf. The depositional environments for the Salina Group are interpreted as subtidal through intertidal and supratidal to terrestrial settings, including

lagoon, sabkha and coastal salina (Gill 1977a, 1977b; Nurmi and Friedman 1977; Haynes 1989).

The contact between the Salina Group and the overlying Devonian succession is conformable (Landes 1945). However, as mentioned earlier, the contact between the Guelph Formation and overlying Salina Group has long been a subject of controversy and opinions regarding the existence of an unconformity are still widely divided, although all authors do believe that this contact represents a fundamental change in depositional environment. Some workers (e.g., Evans 1950; Pounder 1962; Gill 1973, 1977a; Bay 1983) believed that the tops of Guelph reefs were subaerially exposed and eroded prior to and during deposition of the A-1 Unit and this contact represents an erosion surface or an unconformity. Other workers (e.g., Charbonneau 1990; Smith 1990; Smith et al. 1993) suggested that this contact is a major karsting surface due to long-term subaerial exposure but there were also multiple periods of karsting occurring between episodes of reef growth. On the other hand, many workers (e.g., Jodry 1969; Liberty and Bolton 1971; Alling and Briggs 1961; Mesolella et al. 1974; Droste and Shaver 1977, 1982, 1985; Shaver et al. 1978; Sarg 1982) suggested that this contact is a conformable one without significant exposure or erosion or that it only represented a possible short exposure and local erosion at the tops of some reefs.

If it can be proven that the Guelph reefs on the slope were indeed widely eroded in pre-Salina time, it would be expected that the same erosion should also have occurred along the more elevated margins of the Michigan Basin, but this is not observed. In the

shelfward regions such as the Niagara Peninsula, Haynes and Hughes-Pearl (1990) observed that the boundary between the Guelph Formation and overlying Salina Group in the Domtar gypsum mine is a thin (approximately 2-5 cm) green shale layer. This green shale was interpreted to represent continued underwater deposition, but also reflecting a short period of increasing clastic supply. This shale layer is similar to the thin green shale layer commonly observed on the tops of patch and pinnacle reefs, implying that this contact is also a conformable one in more basinward areas.

## 2.4 Depositional setting of the Guelph Formation

An epicontinental sea extended throughout most of the central part of the North America during the Silurian, including the Great Lakes region and further north to Hudson Bay on the Canadian Shield (Briggs and Briggs 1974). During the Middle to Late Silurian, the Michigan Basin was a shallow continental sea with a broad marginal carbonate platform rimmed by barrier reefs (Sanford 1969; Gill 1985; Johnson et al. 1992). The depositional environment of the Michigan Basin including southern and southwestern Ontario during the Middle and Late Silurian has been well documented in several previous studies and the relationship between the Middle Silurian Niagara reefs and overlying Upper Silurian Salina evaporites in the Michigan Basin is well known (Sanford 1969; Huh 1973; Briggs and Briggs 1974; Mesolella et al. 1974, Gill 1977a, b; Mesolella 1978; Smith and Legault 1985; Bailey 1986; Anastas and Coniglio 1993; Johnson et al. 1992; Carter et al. 1994).

In southern and southwestern Ontario, the Middle Silurian succession consisting of the Lockport-Amabel Formation and conformable overlying Guelph Formation represents a

continuous transgressive sequence deposited on a 150-200 km wide, gentle-slopping, carbonate ramp (Sanford 1969; Liberty and Bolton 1971; Smith and Legault 1985). The Guelph Formation in southern and southwestern Ontario has been divided into four facies zones (Sanford 1969; Winder and Sanford 1972; Bailey 1986). From east to west, there are a shoreward back-barrier-reef lagoon zone, a shelf-rimmed barrier reef or carbonate bank zone, a basinward patch reef zone on the upper ramp, and a pinnacle reef zone on the lower ramp (Figs. 2.5, 2.6). Further development of the shelf-rimmed barrier reef complexes formed a partially closed, 50-70 km-wide band around the Michigan Basin during the late Silurian (e.g., Mesolella et al. 1974). This band acted as an effective barrier to isolate the Michigan Basin from the surrounding seas. Several authors (e.g., Droste and Shaver 1985; Bailey 1986; Armstrong and Goodman 1990; Sonnenfeld and Al-Aasm 1991) have suggested that there were three inlets, including the Clinton Pass in the south, the Sudbury sag in the north and the Chatham Sag in the east, which breached the barrier reef complex (Fig. 2.2). The main reef builders were corals, stromatoporiods, bryozoans, and blue-green algae. Associated fossils include crinoids, bivalves, gastropods, and cephalopods. The basinal facies are composed of relatively thin and impermeable micritic limestones (Sanford 1969; Mantek 1973; Nurmi and Friedman 1977; Huh et al. 1977; Gill 1979).

The study area is located in the patch and pinnacle reef zones (Fig. 1.2, 2.5). The cross section through the study area shows variations in the thickness of the Guelph Formation and some associated units and the distribution of Guelph reef and interreef facies and their relationship with underlying and overlying rocks. This figure also illustrates the

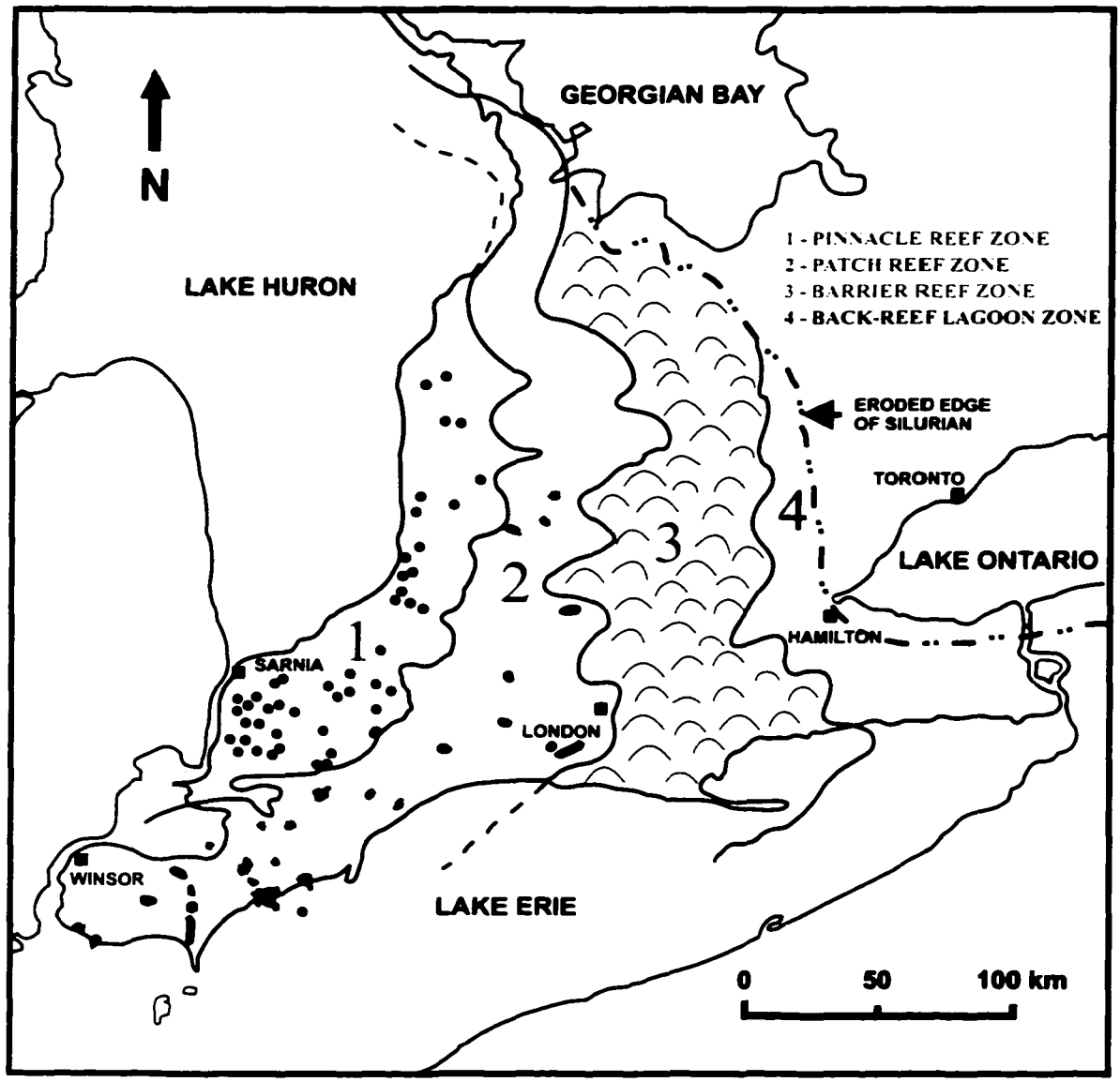



Fig. 2.6 Depositional environment of the Guelph Formation in southwestern Ontario, showing four facies zones including shelfward back-barrier-reef lagoon and barrier reef zones and basinward patch reef and pinnacle reef zones. Compiled based on the data from Sanford (1962, 1969); Winder and Sanford (1972); Bailey (1986); Charbonneau (1990); and this study.

depositional setting for Guelph patch and pinnacle reefs on a typical carbonate ramp with a simple, northwestward-dipping, gently-sloping surface, similar to the setting described by Sears and Lucia (1979) in the northern Michigan and by Read (1985) in other basins.

The pinnacles have different plan-view shapes and were developed on the lower ramp close to basin center. Many pinnacle reefs are elongated parallel to the dip of the carbonate ramp (Fig. 1.2). Their present-day burial depths range from 395 m to 760 m. Their thickness increases basinward systematically from 40 to 140 m and their sizes range from 4 hectares (10 acres) to over 800 hectares (2000 acres). Dip-meter data indicate that the pinnacle reefs have flat tops and steep flanks with slopes of 30° to 40° (Mantek 1973). Several cores from reef flanks show dips of 20° to 45°.

Most pinnacle reefs have been dolomitized and mainly consist of tan to brown, microcrystalline to finely crystalline dolomites (Fig. 1.2). A few basinward pinnacle reefs consist completely or partially of limestones with well preserved depositional and early diagenetic textures or have been partially replaced by dedolomite (Fig. 1.2). The completely dolomitized inter-reef facies are very thin with thickness ranging from 5 to 10 m, and are composed of crinoidal wackestone-packstone and laminated to thin-bedded mudstone.

The patch reefs grew on the upper ramp close to shelf (Fig. 1.2). The patch reefs were dominated by lateral growth and their heights range from 20 to 60 m and sizes range from 1,000 hectares (2500 acres) to up to 16,000 hectares (40,000 acres). The patch reef zone

consists of a number of separated patch reefs such as the Fletcher patch reef, and each individual patch reef commonly consists of several superposed reef knolls. The main reef builders in the patch reef were corals and stromatoporoids. Patch reefs in the study area were completely dolomitized and consist of finely to coarsely crystalline dolomites.

To the northeast of the study region, a barrier reef zone or carbonate bank was developed along the margin of a broad platform over the Algonquin Arch during the Middle to Upper Silurian (Sanford 1969; Gill 1985; Bailey 1986) (Fig. 2.6). The Guelph Formation thickens toward the barrier reef complex zone to the northeast (Fig. 2.5). During late Middle Silurian, the progressive lateral and vertical development of the barrier reef complex formed a nearly continuous barrier that surrounded the sediment-starved basin and the Michigan Basin changed into an isolated evaporative basin during most Late Silurian time (Sanford 1969; Bailey 1986).

The back-barrier-reef lagoon zone, represented by the Eramosa Member of the Guelph Formation, is developed further eastward and outcrops in a 10-30 km wide of zone along the Niagaran Escarpment from the Bruce Peninsula (Liberty and Bolton 1971; Armstrong and Goodman 1990) across the broad Algonquin Arch to the Niagara Peninsula (Sanford 1969) (Fig. 2.6). A similar back-barrier-reef lagoon zone (more than 80 km wide) has been recognized in the northern Michigan, characterized by laminated carbonate mudstones with a few small patch reefs (Burgess and Benson 1969; Briggs and Briggs 1974) (Fig. 2.2). This lagoon facies, which represents an inner shelf environment, probably extended through Early Devonian time but the rock record was eroded (Carter

1987). This broad inner shelf might have been a source or recharge area where supplied diagenetic fluids to more basinward carbonates in the Guelph Formation.

Regional studies (Richard 1969; Carter 1987) have shown that Salina evaporites began to be deposited earlier within the Michigan Basin than in the Appalachian Basin and that the evaporite beds are younger in New York than in Ontario. During the Late Silurian, younger evaporites are successively more widespread and onlap to more shelfward areas (Carter 1987).

## 2.5 Burial and thermal history

The Paleozoic subsidence history of the Michigan Basin records three major unconformities which occurred in: (1) the Late Silurian to Early Devonian, (2) the Late Mississippian, and (3) the end of the Carboniferous to Jurassic (Dorr and Eschman 1971; Gardner and Bray 1985). The unconformity between the Upper Silurian and Lower Devonian succession occurred mainly in the southern portion of the basin, including southwestern Ontario and the Late Mississippian unconformity occurred around the basin margin (Cercone 1984a). These two unconformities lasted for relatively short period of times. The third unconformity played the most important role in controlling the burial history of the Michigan Basin. Several lines of evidence, including a consistent basin subsidence rate during the early Paleozoic; configuration of the erosional surface at the basin's northern margin; comparison with the adjacent Illinois Basin; and elevated organic maturation in pre-Carboniferous source rocks and Pennsylvanian coals, all support that a total of 1700 m rather than the existing 700 m of Carboniferous strata were deposited in the Michigan Basin (Cercone 1984a; Fisher and Barratt 1985). This means

that approximately 1,000 m of Carboniferous strata were removed during a significant erosion event between the Late Carboniferous and the Jurassic (Shannon and Naylor 1989). Vugrinovich's (1988) shale compaction study supports this idea. The basin has remained stable and unaffected by significant erosion since Jurassic time, as indicated by both the poorly consolidated Jurassic sediments (Vugrinovich 1989) and the extremely immature sporopollens in Jurassic sediments (Cercone 1984a).

The burial history of the Michigan Basin is relatively well known compared to its thermal history. Based on well data from OGS 82-1 (core #994) and OGS 82-2 (core #860) in the study area and burial reconstruction of both Coniglio and Williams-Jones (1992) for southwestern Ontario and Manitoulin Island areas and Cercone (1984a) for central and northern Michigan, the inferred burial history curves and maximum burial depths of the Guelph Formation in the study area are summarized in Figure 2.7.

The thermal maturity of organic matter is a direct record of the thermal-burial history of the host rock. Based on conodont and acritarch alteration color data, Legall et al. (1981) concluded that the Devonian, Silurian and Late Ordovician rocks in southwestern Ontario are immature with maximum burial temperatures close to 60°C. However, other studies (Gardner and Bray 1985; Cercone 1984a; Powell et al. 1984) have demonstrated that organic matter in Silurian and Ordovician strata has generally attained moderate to high levels of thermal maturity, ranging from 2.7 to 4.0 on the Thermal Alteration Index (TAI) scale and from 0.7% to 3.5% in vitrinite reflectance values (Ro). These values are within the ranges of TAI ($2.65 < TAI < 3.70$) and Ro ($0.65\% < Ro < 2.0\%$) for the oil window.

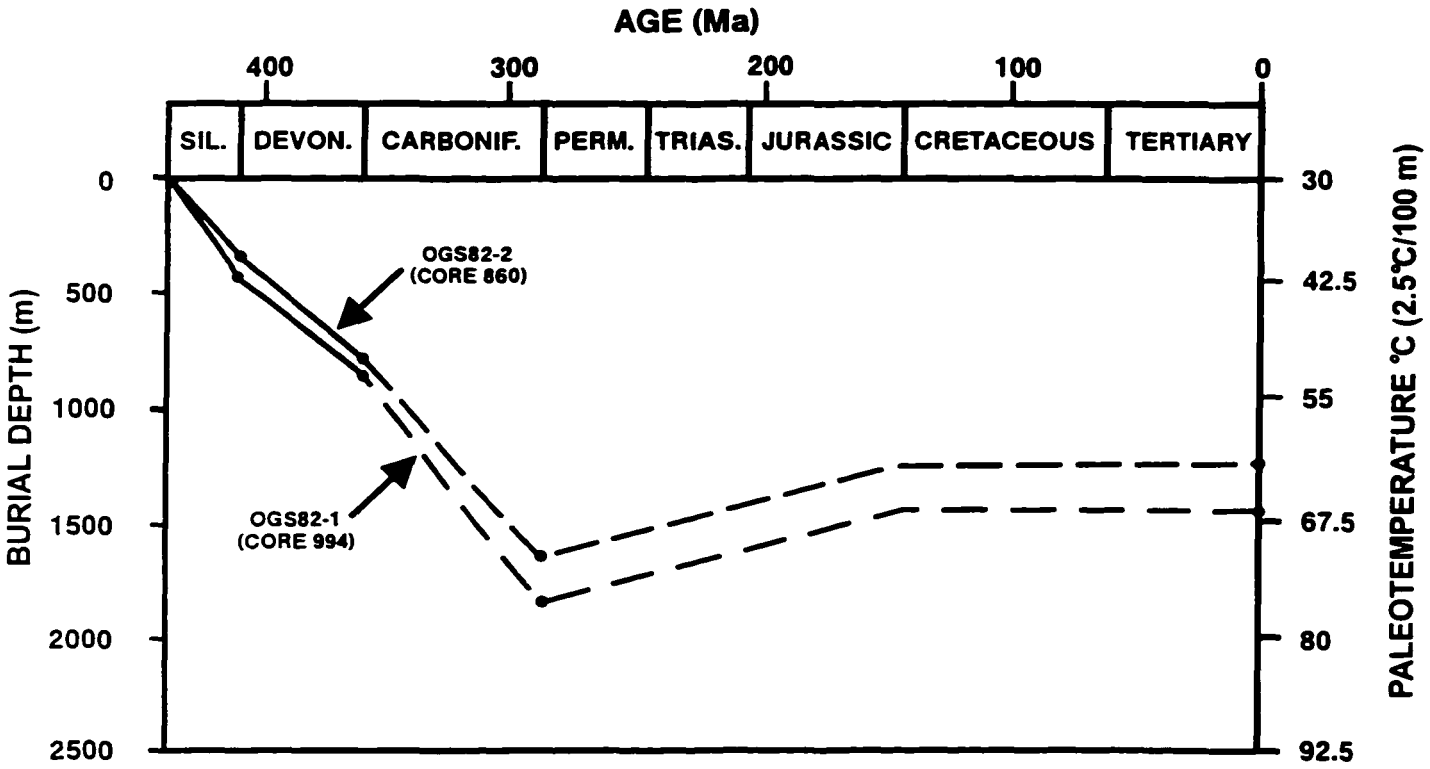



Fig. 2.7 Generalized burial history curve of Silurian strata in the southwestern Ontario, constructed using the core data from Ontario Geological Survey wells OGS82-1 and OGS82-2 and the results from Cercone (1984a), Nunn et al. (1984), Mareschal (1987), Coniglio and Williams-Jones (1992). Dashed lines indicate inferred burial depth and subsequent uplift tracks, assuming that Carboniferous strata were 1000 m thick.

The elevated organic maturity in the Silurian and Ordovician succession cannot be explained by the burial history and present-day geothermal gradient studies. Cercone (1984a) and Coniglio and Williams-Jones (1992) suggested that the Middle Silurian succession was probably never been buried more than 1500 to 2000 m. The reported present-day regional geothermal gradient based on well log temperature data is only approximately 1.9°C /100 m (Gardner and Bray 1985; Vugrinovich 1989). Hogarth and Sibley (1985) suggested a slightly higher paleogeothermal gradient of 2.3°C/100 m for southern Michigan based on their conodont color study. Similarly, the higher thermal maturation of organic matter cannot be explained by existing geophysical models either. Proposed models for the subsidence history of the Michigan Basin attribute the thermal history of the Michigan Basin to a Precambrian thermal high event that was followed by a thermal sag or low geothermal gradient (2.2°C/100 m) period throughout the early Paleozoic (Haxby et al. 1976; Nunn et al. 1984).

Vugrinovich (1989) suggested that the present-day geothermal gradients are only valid for post-Jurassic time and the actual levels during the Cambrian to Carboniferous were probably much higher. By use of the Lopatin (1971) method, Cercone (1984a) proposed higher geothermal gradients between 3.5 and 4.5°C/100 m and approximately 1000 m of missing Carboniferous strata to explain the deficit between observed higher levels of organic maturity and present-day burial depths. Furthermore, burial depth alone may not be the sole major parameter influencing paleotemperatures in the Michigan Basin (Vugrinovich 1989). Paleogeothermal gradient and paleotemperature are also affected by several other factors, including thermal conductivity, groundwater flow and hydraulic

conductivity, basement heat flow and geothermal anomalies, basin geometry, water table configuration, and climate (Garven and Freeze 1984). The upward movement of hydrothermal fluids from the deep basin along faults or fractures as suggested by Coniglio et al. (1994) for the Ordovician carbonates in southwestern Ontario could have also caused temperature and geothermal gradient anomalies in the Silurian sequence.

## 2.6 Formation water composition

In southwestern Ontario, the chemistry and isotopic composition of present-day formation fluids in Precambrian to Devonian rocks have been investigated in several recent studies (McNutt et al. 1987; Dollar et al. 1988; Frape et al. 1989). These studies confirmed that the formation waters in different strata are concentrated brines with highly variable chemical compositions (Table 2.1). The brines in Guelph and Salina A-1 carbonates contain mainly $Ca^{2+}$, $Na^{+}$, and $Cl^{-}$ with Total Dissolved Solids (TDS) ranging from 198,000 to 391,000 mg/L and average values of approximately 300,000 mg/L (McNutt et al. 1987; Frape et al. 1989). Formation waters from Niagaran carbonates along the reef trends in southeastern and northern Michigan are extremely concentrated $CaCl_2$ brines with similar compositions and average TDS value of 353000 mg/L (n=25; Wilson and Long 1992; Table 2.1). The most important cations in the brines are $Ca^{2+}$, $Na^{+}$, and $Mg^{2+}$. $Cl^{-}$ is the dominant anion, followed by $Br^{-}$ and $SO_4^{=}$.

The salinities of present-day formation waters in the Michigan Basin are much higher than those of normal seawater (35,000 mg/L). Elevated salinities of subsurface brines relative to their marine precursors could have resulted from downward flow of surface-evaporated brine or subsurface dissolution of evaporites (Hanor 1994). Present-day

formation brines in southwestern Ontario have been modified by mixing processes and water-rock interaction (McNutt et al. 1987; Frape et al. 1989). In Michigan, Wilson and Long (1992) suggested that the generally good agreement between brines and seawater in $Cl^-$ and $Br^-$ concentrations or Cl/Br ratios in brines from reefal carbonates indicate that they evolved from concentrated seawaters. In southwestern Ontario, Cl/Br and Na/Cl ratios in the Guelph Formation waters are not compatible with the ratios in concentrated seawater (Table 2.1). These ratios can be explained by halite dissolution and mixing between two or more fluids from different strata or sources (Frape et al. 1989). Variations in $Cl^-$ and $Br^-$ concentrations may have been affected by fluid mixing processes and precipitation/dissolution of halite, as recently reported for brines in carbonate aquifers in the Permian Basin (Stueber et al. 1998).

In southwestern Ontario and in Michigan, brines in Niagaran carbonates are all enriched in $Ca^{2+}$, $Na^+$, and $Cl^-$ but depleted in $Mg^{2+}$, $K^+$, and $SO_4^=$ relative to seawater (Table 2.1). The extremely high levels of $Na^+$ (100,000 mg/L) and $Cl^-$ (207,000 mg/L) in Guelph carbonates was most likely acquired through halite dissolution. Both Frape et al. (1989) and Wilson and Long (1992) suggested that brines with enriched $Ca^{2+}$ and depleted $Mg^{2+}$ relative to equally concentrated seawater might have resulted from subsurface dolomitization. Depleted $K^+$ concentrations probably relate to water-rock interaction with aluminosilicate minerals (Wilson and Long 1992). Low $SO_4^=$ concentrations indicate subsurface sulfate reduction and/or $CaSO_4^=$ precipitation. High $Ca^{2+}$ and low $SO_4^=$ concentrations could also imply that anhydrite dissolution was not an important process in the generation of present formation waters.

Table 2.1 Representative compositions of formation waters and brines from Precambrian basement and Paleozoic strata in the Michigan Basin, including southwestern Ontario, southern and northern Michigan (adapted from Frape et al. 1984; McNutt et al. 1987; Dollar et al. 1988; Frape et al. 1989; and Wilson and Long 1992).

| | Precambrian[1] basement | Cambrian[1] | Trenton[1] Group | Guelph[1] Fm. | Salina[1] Fm. | Dundee[1] Fm. | Michigan[2] Basin | Concentrated[3] seawater |
|---|---|---|---|---|---|---|---|---|
| Ca | 65000 | 48000 | 32500 | 31300 | 8200 | 31500 | 76300 | <126 |
| Mg | 10 | 6090 | 4960 | 7770 | 2850 | 5410 | 11800 | 48200 |
| Na | 16900 | 43800 | 49700 | 65500 | 100000 | 70600 | 31300 | 53800 |
| K | 120 | 1390 | 2070 | 1880 | 2600 | 3030 | 9770 | 14500 |
| Sr | 1390 | 1210 | 620 | 435 | 215 | 750 | N/A | N/A |
| Rb | N/A | 1.5 | 2.4 | 1.5 | N/A | 3.0 | N/A | N/A |
| Cl | 156000 | 179800 | 150290 | 189000 | 207000 | 179000 | 215000 | 185000 |
| Br | 1090 | 1530 | 1190 | 1390 | 590 | 1050 | 2590 | 2440 |
| $SO_4$ | 1140 | 260 | 335 | 250 | 750 | 165 | 48 | 644000 |
| ALK | N/A | N/A | N/A | N/A | N/A | N/A | 91 | N/A |
| TDS | 241000 | 282000 | 242700 | 297600 | 322200 | 291600 | 353000 | 368340 |
| $\delta^{18}O$ | −10.8 to -7.8 | -2.5 | -2.2 | -0.72 | N/A | -9.3 | N/A | N/A |
| $\delta^{2}H$ | -22.2 to 5.0 | -24.6 | -29.8 | -44.8 | N/A | -59.7 | N/A | N/A |
| $^{87}Sr/^{86}Sr$ | 0.712-0.725 | 0.70957 -0.71032 (0.70990) | 0.70901 -0.71041 (0.70993) | 0.70908 -0.70946 (0.70911) | N/A | 0.70816 -0.70949 (0.70860) | N/A | N/A |

ALK – alkalinity; TDS – total dissolved solid; N/A - not available: chemical concentrations are reported in mg/L; O and H isotopic values are reported in relative to SMOW standard, $^{87}Sr/^{86}Sr$ ratios are reported relative to NBS standards and the means are given in parentheses. Superscript notes: 1 – elemental and isotopic data reported by Frape et al. (1984) for Precambrian brines in Canadian Shield and by McNutt et al. (1987), Dollar et al. (1988), and Frape et al. (1989) for more than 80 water samples from Paleozoic strata in southwestern Ontario; 2 – elemental data reported by Wilson and Long (1992) for 25 water samples from Middle Silurian reefs in southern and northern Michigan; 3 – composition of concentrated seawater from McCaffery et al. (1987).

$\delta^{2}H$-$\delta^{18}O$ values indicate that formation waters may have experienced variable mixing and that meteoric water was unimportant in the formation of present-day brines hosted in Cambrian to Devonian strata (McNutt et al. 1987). $\delta^{2}H$-$\delta^{18}O$ values in Precambrian basement are greatly different from those in the overlying sedimentary rocks (Table 2.1).

The $^{87}Sr/^{86}Sr$ ratios in formation waters from southwestern Ontario show elevated values (McNutt et al. 1987; Table 2.1) relative to their corresponding coeval seawaters (Burke et al. 1982). Decay of $^{87}Rb$ to $^{87}Sr$ during prolonged water-rock interaction with Rb-bearing minerals elevates the $^{87}Sr/^{86}Sr$ ratios in late diagenetic fluids (Banner 1995). The elevated $^{87}Sr/^{86}Sr$ ratios in formation waters from Guelph carbonates and other strata indicate that these formation waters must have acquired more radiogenic $^{87}Sr$ through either water-rock interactions with Rb-bearing minerals such as clay, mica, and K-feldspar within the carbonate rocks and nearby siliciclastic units or mixing with more radiogenic fluids from deeper formations or Precambrian basement (McNutt et al. 1987; Harper 1993).

In southwestern Ontario, McNutt et al. (1987) concluded that formation waters in sedimentary strata and Precambrian brines may have different origins, as evidenced by their significant differences in elemental and isotopic (O, H, and Sr) compositions, although some mixing between them may have occurred. Vertical inter-formational and cross-formational water mixing along fracture conduits very likely occurred. Based on regional mapping of Ca/Na ratio and TDS, Frape et al. (1989) suggested that large-scale northward flow of dilute Na-Cl brines may have migrated into the southwestern Ontario within porous strata and along fracture networks developed on or in the proximity of the Findlay-Algonquin Arch system. Regional flow may have mixed with or displaced preexisting formation brines.

# Chapter 3 Reefal facies and pre-dolomitization diagenesis

## 3.1 Abstract

In southwestern Ontario, the Middle Silurian Guelph Formation is mainly composed of patch reefs, pinnacle reefs, and interreef facies developed on a gently-sloping carbonate ramp. The main reefal facies in the Guelph Formation include basal crinoidal mud mound facies, coral-stromatoporoid reef core facies, crinoidal-bryozoan inter-reef-core facies, stromatolitic cap facies, and interreef mud facies. The general reef growth history consists of three major stages, including an initial mud mound stage, an organic reef buildup stage, and a final reef cap stage. The patch reefs and pinnacle reefs show similar facies, except patch reefs typically lack the basal crinoidal mud mound facies. The observations in this study support the interpretation that reef growth was followed by evaporite deposition without significant erosion or karsting between.

Petrographic study shows that Guelph carbonates have undergone a complicated diagenetic history. The most important diagenesis is regional pervasive dolomitization, which will be treated in detail in Chapter 4. This chapter focuses on the pre-dolomitization diagenesis, including fibrous and equant calcite cementation, neomorphism, and limestone dissolution that occurred between deposition and shallow burial. Post-dolomitization diagenesis includes dolomite alteration, dedolomitization, hydrothermal dolomite formation, anhydrite cementation, halite plugging, and hydrocarbon emplacement under moderate to deep burial conditions, which will be discussed in Chapter 5 and Chapter 6.

## 3.2 Reefal facies

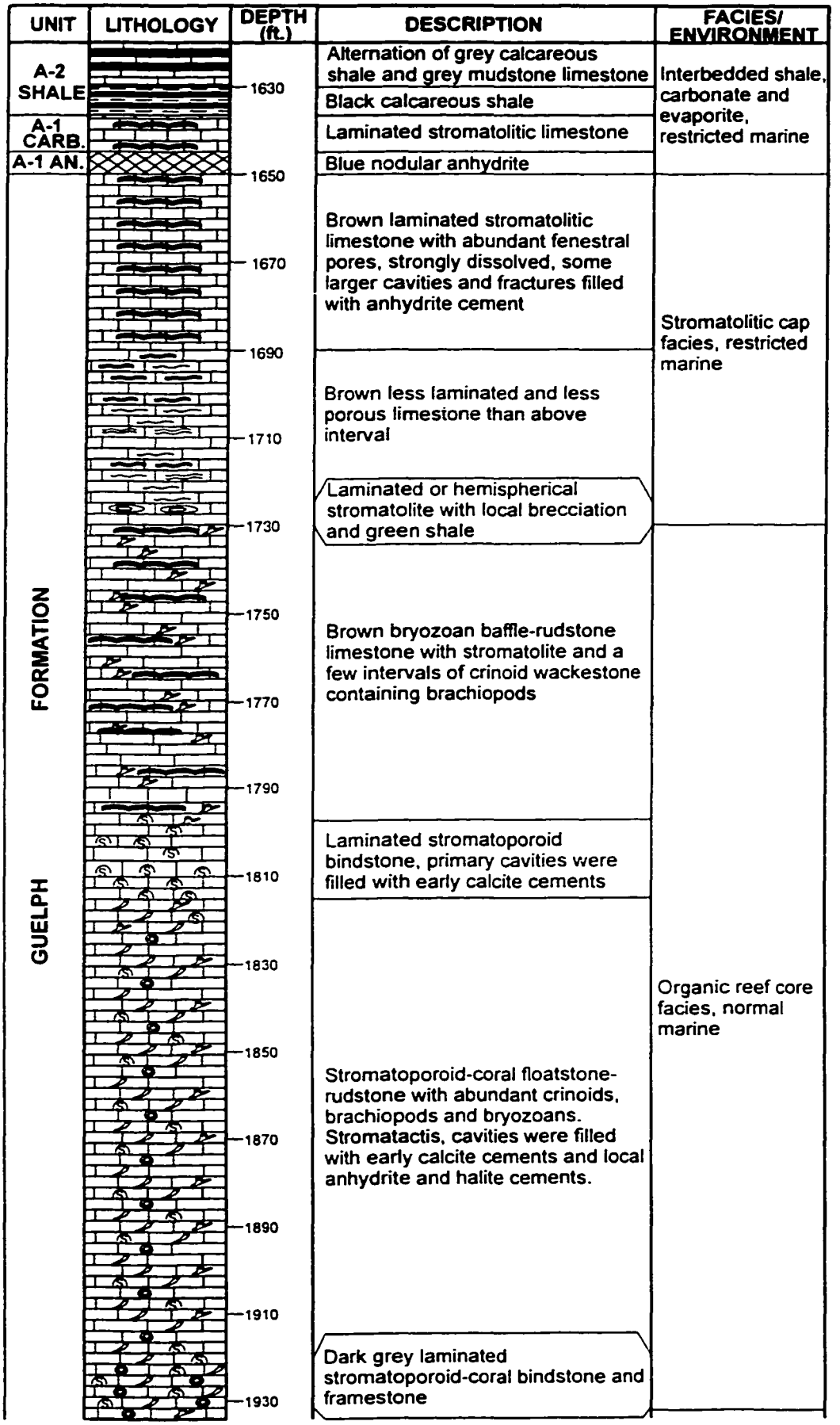
From observation of more than 70 cores from 32 reefs in this study, especially the limestone cores from partially dolomitized pinnacle reefs in southwestern Ontario, the reefal rocks in the Guelph Formation are classified into five main facies. They are: (1) basal crinoidal mud mound facies; (2) coral-stromatoporoid reef core facies; (3) crinoidal-bryozoan inter-reef-core facies; (4) stromatolitic cap facies; and (5) interreef mud facies. The profile of a limestone reef core from Rosedale pinnacle reef and a summarized facies model show the main reefal facies and a general upward-shallowing sequence in typical pinnacle reefs (Figs. 3.1 and 3.2).

### 3.2.1 Basal crinoidal mud mound facies

This facies consists of grey colored and completely dolomitized crinoidal mudstone-packstone with whole fossils and fragments of laminar stromatoporoids, brachiopods, bryozoans, gastropods, and cephalopods. It varies from 15 to 55 m in thickness and constitutes the initial mound-like substrate for further reef growth in the basinward pinnacle reefs, but this facies is absent in shelfward pinnacle reefs and all patch reefs. The contact between this facies and overlying coral-stromatoporoid reef core facies is commonly sharp.

### 3.2.2 Coral-stromatoporoid reef core facies

The dominant rock types in this facies include: (1) branching tabulate coral-laminar stromatoporoid-branching bryozoan bindstone with most of these metazoans in growth


UNIT
LITHOLOGY
DEPTH (ft.)
DESCRIPTION
FACIES/ ENVIRONMENT
A-2 SHALE
A-1 CARB.
A-1 AN.
GUELPH FORMATION
1630
1650
1670
1690
1710
1730
1750
1770
1790
1810
1830
1850
1870
1890
1910
1930
Alternation of grey calcareous shale and grey mudstone limestone
Black calcareous shale
Laminated stromatolitic limestone
Blue nodular anhydrite
Brown laminated stromatolitic limestone with abundant fenestral pores, strongly dissolved, some larger cavities and fractures filled with anhydrite cement
Brown less laminated and less porous limestone than above interval
Laminated or hemispherical stromatolite with local brecciation and green shale
Brown bryozoan baffle-rudstone limestone with stromatolite and a few intervals of crinoid wackestone containing brachiopods
Laminated stromatoporoid bindstone, primary cavities were filled with early calcite cements
Stromatoporoid-coral floatstone-rudstone with abundant crinoids, brachiopods and bryozoans. Stromatactis, cavities were filled with early calcite cements and local anhydrite and halite cements.
Dark grey laminated stromatoporoid-coral bindstone and framestone
Interbedded shale, carbonate and evaporite, restricted marine
Stromatolitic cap facies, restricted marine
Organic reef core facies, normal marine

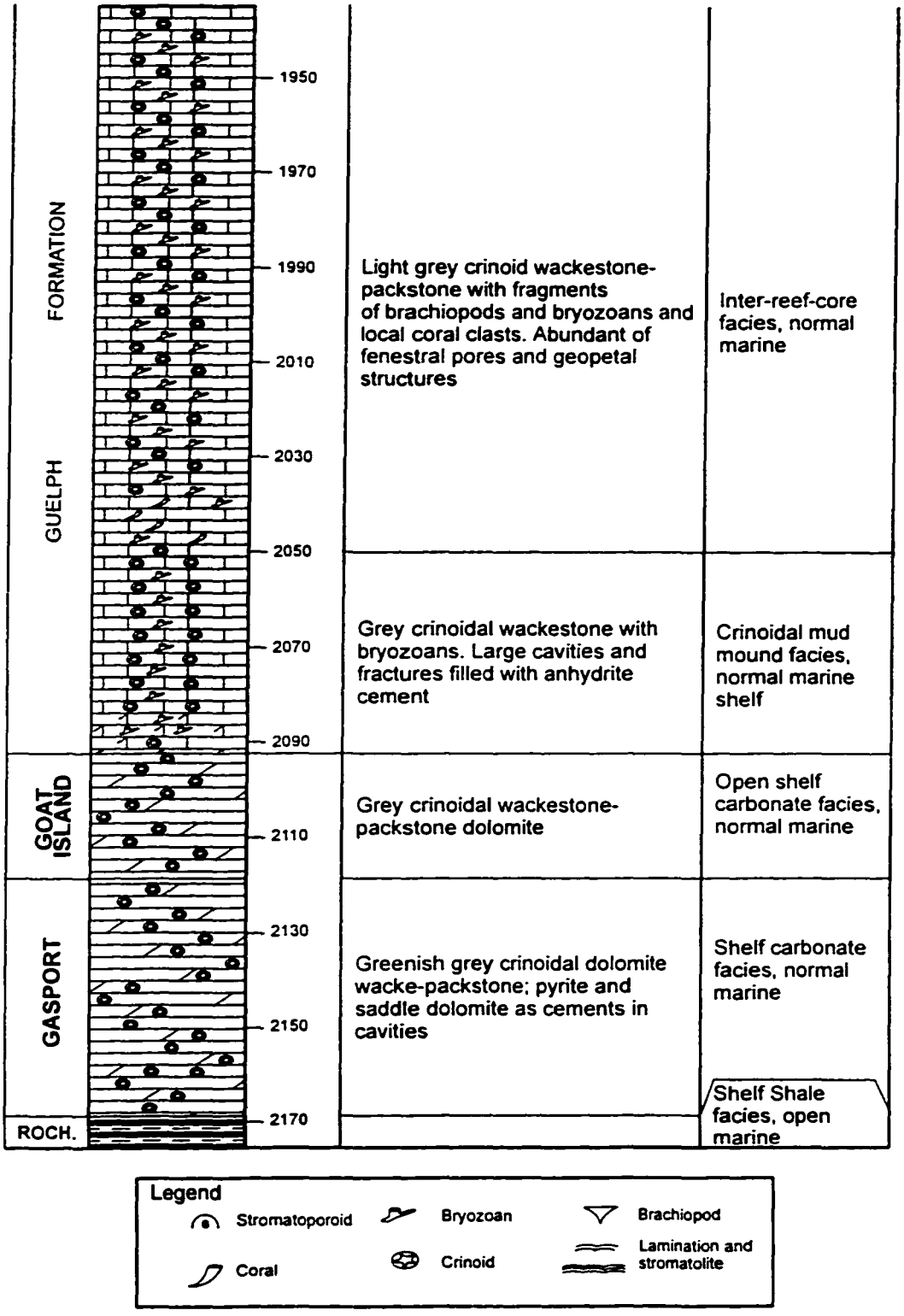



Fig. 3.1 Representative core log of core 578 from Rosedale pinnacle for showing the reefal facies in Guelph reefs

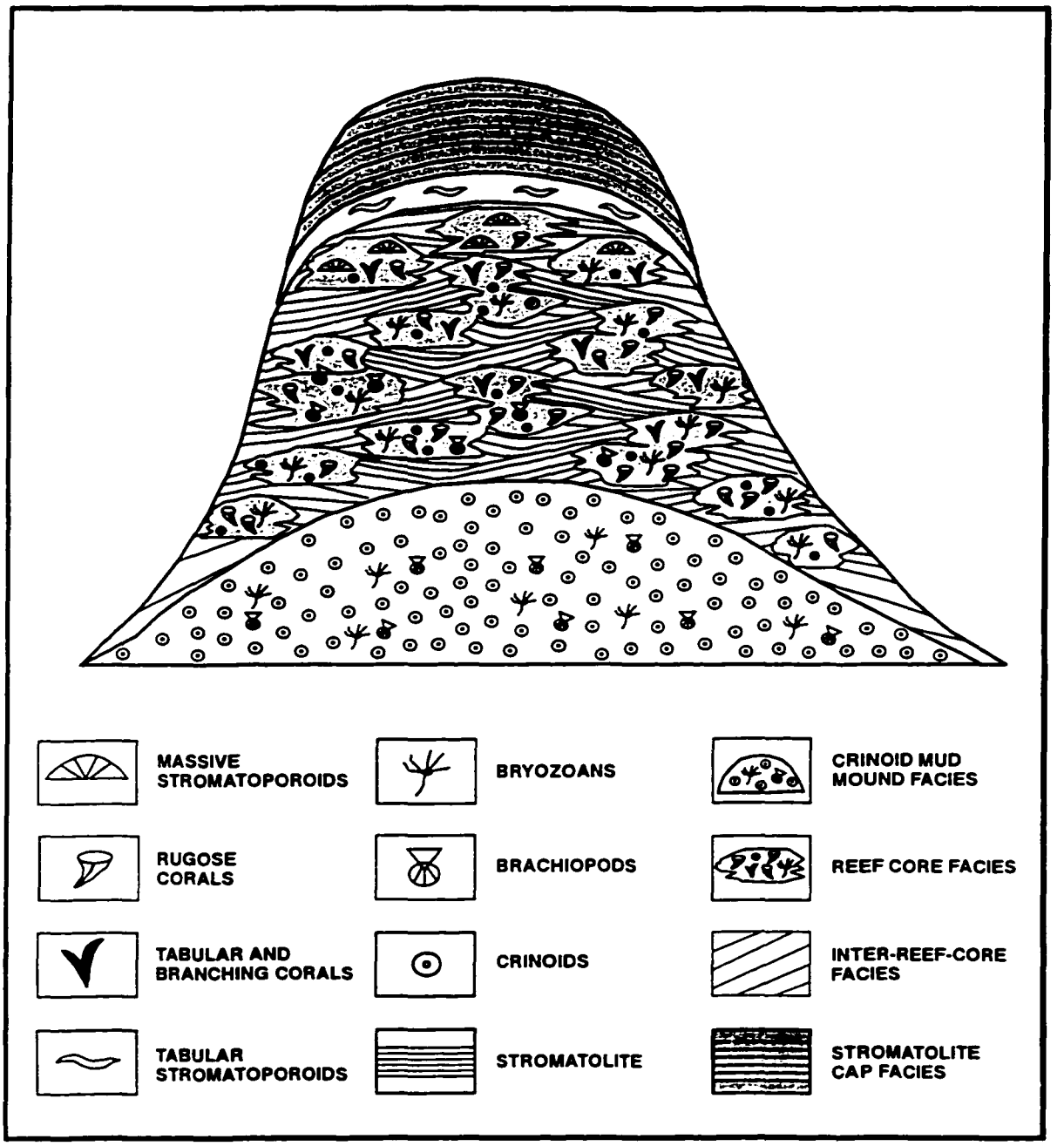



Fig. 3.2 Major reefal facies and fossil zones in Guelph reefs in southwestern Ontario.

position; and (2) coral-stromatoporoid rudstone-floatstone with local corals, stromatoporoids and bryozoans in growth position, large numbers of pebble- to boulder-sized clasts of tabulate corals, rugose corals, laminar and massive stromatoporoids, and abundant whole and fragmented bryozoans, brachiopods, crinoids, gastropods, bivalves, and cephalopods. Encrusting bryozoans and calcareous algae occur locally. This facies occurs as grey to brown colored, massive rocks in all reefs and ranges from 20 to 65 m in thickness. This facies represents the organic reef core (e.g., Sanford 1969; Gill 1977a). A thin laminar stromatoporoid bindstone (0.2-1.5 m) commonly occurs on top of reef core facies as the boundary between this facies and overlying stromatolite cap facies.

### 3.2.3 Crinoidal-bryozoan inter-reef-core facies

This facies consists of bioclastic-intraclastic wackestone-packstone and local bryozoan bafflestone, with detritus of corals and stromatoporoids and variable amounts of crinoids, bryozoans, brachiopods, and ostracods. It represents a contemporaneous facies beside or between the coral-stromatoporoid reef core facies as inter-reef-core sediments (Sears and Lucia 1979). Its thickness ranges from 2 to 15 m.

### 3.2.4 Stromatolitic cap facies

This facies occurs in the uppermost part of all reefs and consists of brown colored, stromatolitic bindstone and laminated to thin-bedded fenestral mudstone-wackestone and peloidal-intraclastic wackestone. Stromatolites include laminated and hemispherical forms. This facies commonly contains only a few brachiopods but abundant fenestral pores. Bioturbated rocks and flat pebble conglomerate consisting of broken and probably

slightly transported stromatolite occur in some intervals. This facies ranges from 10 to 30 m in thickness and it represent the final reef growth stage (e.g., Gill 1977a).

### 3.2.5 Interreef mud facies

Interreef facies occurs between reefs and consists of grey colored, thin-bedded crinoidal mudstone-wackestone with minor amounts of fossil debris from the reefs. The total thickness of this facies varies from 3 to 10 m.

## 3.3 Reef growth history

The vertical facies in Guelph pinnacle reefs indicate three major stages of reef growth in different environments (Figs. 3.2, 3.3). The basal crinoid mud mound facies represents the initial stabilization and carbonate buildup by crinoid community in a relatively deep, below wave base, low energy subtidal environment on an open carbonate ramp. The coral-stromatoporoid reef core facies reflects major colonization and rapid buildup of organic core by framework builders including mainly tabular and rugose corals and stromatoporoids in a shallow, close to or above wave base, agitated subtidal environment. The crinoidal-bryozoan inter-reef-core facies represents the detrital material derived from nearby reef core facies and reworked by high-energy waves and currents. Basinward pinnacle reefs were initialized on crinoidal mud mounds and developed in a deeper water area. The stromatolite cap facies represents the final stage of reef growth in a subtidal to supratidal island environment in a restricted marine setting. More shelfward pinnacle and patch reefs evidently started as coral-stromatoporoid facies without the crinoidal mound substrate. These three reef growth stages observed in this study (Figs. 3.3) are identical to

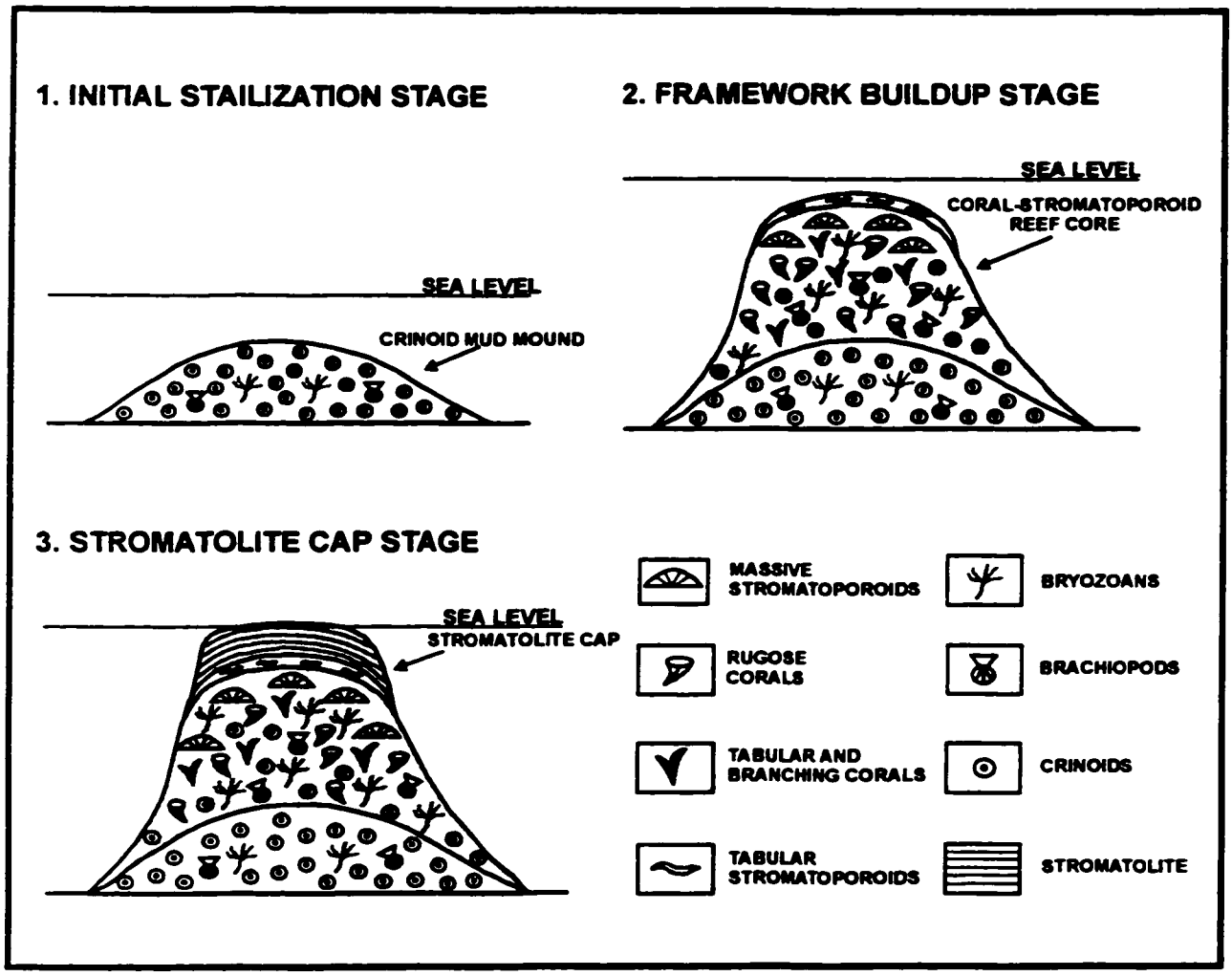



Fig. 3.3 Reef growth model for Middle Silurian Guelph reefs developed in southwestern Ontario.

those described in previous studies in southwestern Ontario (e.g., Grimes 1988; Charbonneau 1990) and Michigan (e.g., Mantek 1973; Mesolella et al. 1974; Gill 1977a; Huh et al.1977; Sears and Lucia 1979) (Fig. 3.4).

The abundance of skeletons of shallow-water organisms in the reefal facies indicates that they were deposited in a relatively shallow marine environment. The stromatolitic cap facies may record the initial transition from a normal marine environment to a hypersaline setting at the end of Guelph reef growth. Following the development of Guelph reefs, the depositional environment changed to restricted marine, and Guelph pinnacle and patch reefs are surrounded by the A-1 Evaporite and A-1 Carbonate and further capped by the A-2 Evaporite and A-2 Carbonate (Figs. 2.4, 2.5).

## 3.4 Reef-evaporite relationship

Based on the interpretations of the temporal relationship between Guelph reefs and the surrounding and overlying Salina evaporites and carbonates, three different reef growth models have been proposed (Mesollela et al. 1974). They are: (1) complete reef growth prior to evaporite formation (Gill 1977a; Huh et al. 1977; Sears and Lucia 1979); (2) reef growth alternating with evaporite deposition (Burgess and Benson 1969; Messolella et al. 1974); and (3) entirely contemporaneous reef growth and evaporite deposition (Alling and Briggs 1961; Jodry 1969; Mantek 1973) (Fig. 3.4). Most authors (Gill 1977a; Huh et al. 1977; Pearson 1980; Petta 1980; Sears and Lucia 1980; Cercone 1984b) believed that the Niagaran reefs had a continuous reef growth history with only one short exposure and possible leaching event at the top of the reefs during sea level lowering. Grimes (1988),

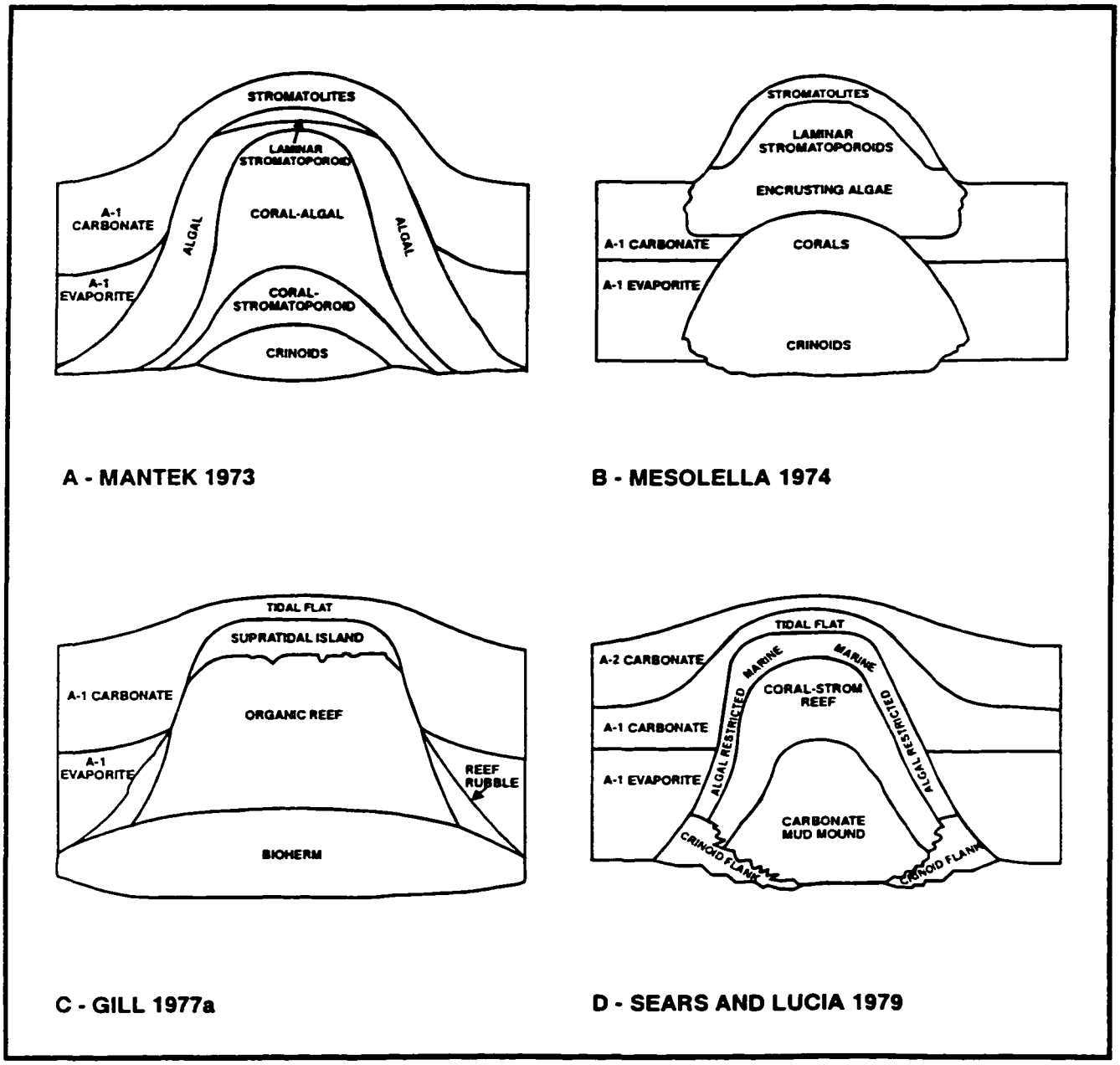



Fig. 3.4 Previously suggested reef models for the Niagaran reefs in both southern and northern reef belts the Michigan Basin. Compiled based on information from Sanford (1969); Mantek (1973); Mesolella et al. (1974); Gill (1977a); Sears and Lucia (1979); and Cercone (1984b).

Charbonneau (1990), and Smith et al. (1993), suggested eight episodes of major subaerial exposure and karsting during Guelph reef growth, based on their studies of one patch reef (Fletcher) and six pinnacle reefs (Payne, Rosedale, Terminus, Warwick, Wilkesport and Bayfield) in southwestern Ontario. They believed that multiple episodes of subaerial karsting occurred due to cyclic sea level lowering during Guelph reef development, although only the karst surfaces on the top and at the base of each pinnacle reefs can be correlated with other reefs. Sarg (1982) believed that the onset of hypersaline water caused the cessation of reef growth. Core examination in this study support the interpretation that reef growth entirely predated the deposition of Salina carbonates and evaporites (e. g., Gill 1977a; Sears and Lucia 1979).

Grimes (1988), Charbonneau (1990), and Smith et al. (1993) listed several features, including severe dissolution, karst breccias, mini-caves, paleosols, karstic crusts, laterally porous zones, and meteoric blocky calcite cementation, to support their fresh water karsting hypothesis. However, these features can be the result of other fluids and processes. For example, the "paleosol" in the Terminus pinnacle reef in their studies is recognized in the current study to be dedolomite. If the suggested major karsting zones existed in reefs on the basinward ramp, these zones should also be developed on the shelfward carbonate platform, a much wider area for gathering fresh water. Many regional investigations (e.g., Cercone and Lohmann 1985), including observations in the current study, do not support the idea of significant fresh water alteration. A greenish shale layer of 5-30 cm thickness was developed on the top of many reefs and rounded clasts of this shale occur within immediately overlying carbonates. However, no obvious

erosional or karst contact between the Guelph Formation and overlying A-1 Carbonate is observed in this study and the view that Niagara reefs grew continuously without significant or long interruption is supported by the observations from this study. Furthermore, if the suggested major karsting zones existed at the top of the pinnacle reefs on the basinward lower ramp, these zones should have extended to the shelfward carbonate platform, an area that was much shallower, much closer to land, and much larger for the gathering of fresh water. Regional studies in the landward areas, such as the Niagara Peninsula (Haynes and Hughes-Pearl 1990), however, have not born this out. Instead, Haynes and Hughes-Pearl (1990) found that the boundary between Guelph Formation and overlying A-1 Carbonate of the Salina Group at the Domtar gypsum mine, represented by a thin green shale layer (approximately 2-5 cm), is a conformable contact. This green shale is similar to but thinner than the green shales (10-50 cm) occurring at the top of the pinnacle reefs.

## 3.5 Paragenetic sequence

The diagenetic histories of Middle Silurian pinnacle reefs in the Michigan Basin have been documented by several earlier studies in northern Michigan (Huh 1973; Huh et al. 1977; Sears and Lucia 1980; Cercone and Lohmann 1985, 1987), southeastern Michigan (Gill 1973,1977a; Kaleem 1994), and southwestern Ontario (Grimes 1987; Charbonneau 1990; Smith et al. 1993). Petrographic examination in this study shows that the Guelph reefal carbonates have undergone a complicated and variable diagenetic history. An ideal paragenetic sequence representing the diagenetic history of the Guelph Formation was

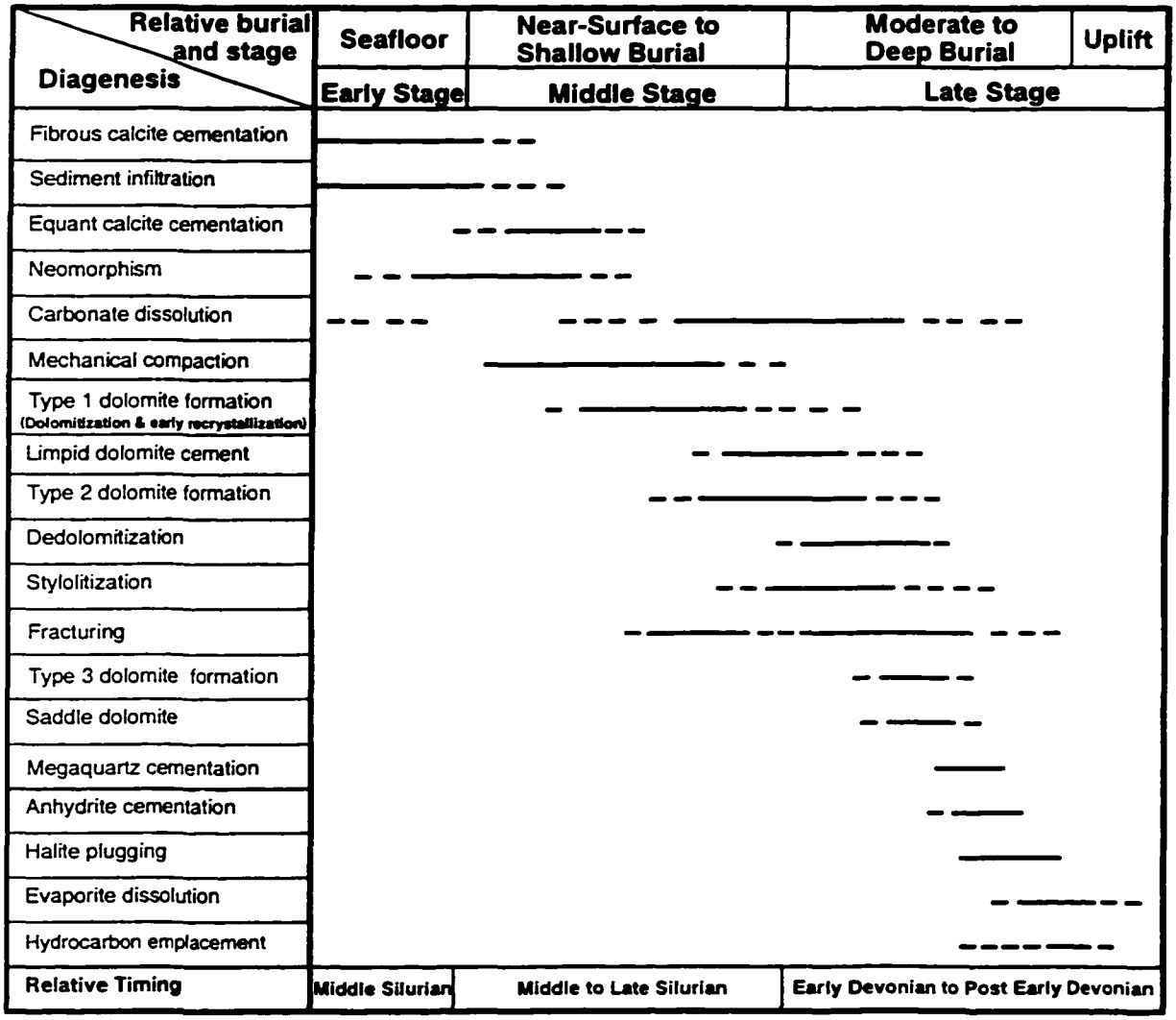



Fig. 3.5 Paragenetic sequence constructed for Guelph carbonates in the study area. Dashed lines are inferred.

constructed based on core and thin section examination of the well-preserved diagenetic phases (Fig. 3.5).

The complete diagenetic history can be divided into pre-dolomitization diagenesis, regional pervasive dolomitization, and post-dolomitization diagenesis. Pre-dolomitization diagenesis occurred between deposition and shallow burial under the influence of seawater, which is characterized by early marine cementation and neomorphism. Internal sedimentation occurred at near surface conditions. Subsequent regional dolomitization occurred under shallow to moderate burial conditions. Post-dolomitization diagenesis includes dolomite dissolution, dolomite alteration, dedolomitization, saddle dolomite formation, megaquartz cementation, anhydrite cementation, halite plugging, and hydrocarbon emplacement that occurred under moderate to deep burial conditions. This chapter will focus on pre-dolomitization diagenesis. Dolomitization, dolomite alteration and hydrothermal dolomite formation will be discussed in detail in Chapter 4, dedolomitization will be treated in detail in Chapter 5, and other major late diagenesis will be documented in Chapter 6.

## 3.6 Pre-dolomitization diagenesis

In reefal limestones, the main pre-dolomitization diagenesis includes fibrous and equant calcite cementation, internal sedimentation, neomorphism, and limestone dissolution (Fig. 3.5).

### 3.6.1 Fibrous calcite cement

In Guelph reefal limestones, an isopachous rim of fibrous calcite cement is typically developed as the first cement in relatively large cavities (>5 mm) within all reefal facies (Fig. 3.6A). Its abundance varies from 2% to 30% of the rock volume. The isopachous rims consist of radiaxial elongate crystals ranging from 10 to 30 μm in width and 100 to 800 μm in length, showing undulose extinction, cloudy appearance (inclusion-rich), and irregular crystal boundaries. Fibrous calcite cement is nonluminescent to very dull orange luminescent with no obvious zones (Fig. 3.6B). In some reefs, such as the Warwick pinnacle reef, it occurs as multiple phases consisting of several isopachous layers. Stromatactis (e.g., Gill 1977a) containing fibrous calcite cement is common in the stromatolitic cap facies. In some dolomite intervals (Type 1 dolomite, see Chapter 4), the morphology of fibrous calcite cement is preserved, but the mineralogy was altered to dolomite.

### 3.6.2 Equant calcite cement

Equant calcite cement commonly occurs in limestones as blocky, euhedral to subhedral calcite spar ranging in size from 50 to 250 μm as a second phase cement overlying fibrous calcite cement (Fig. 3.6A) or as first phase cement in some pores or intervals where fibrous calcite cement is absent. This cement partly to completely fills the remaining pore space. In many cavities equant calcite occurs as first phase pore-lining or pore-filling cement. The equant calcite cement commonly shows zoned orange luminescence, and is more brightly luminescent than the fibrous calcite cement (Fig. 3.6B). It is less common than fibrous calcite cement, and normally occurs in amounts of

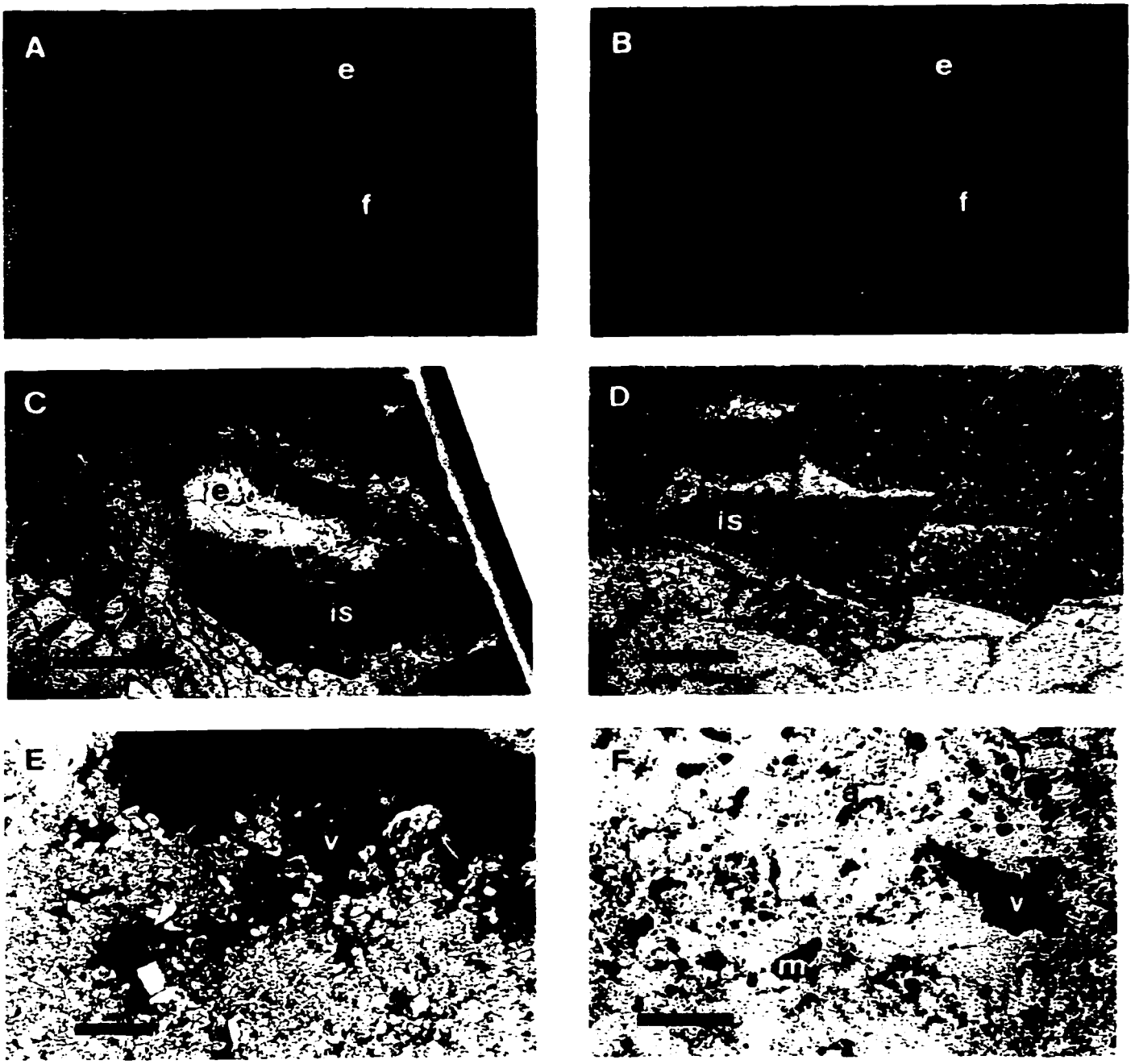



Fig. 3.6 (p.64) Photomicrographs of pre-dolomitization diagenesis in polished limestone thin sections. **A.** Isopachous rim of fibrous calcite cement (f) occurs as the first cement in a filled primary pore. Equant calcite cement (e) occurs as the second cement toward pore center. Sample W34, plane light, scale bar = 0.2 mm. **B.** Same view as in A but under CL view. Fibrous calcite cement (f) exhibits nonluminescence to very dull reddish luminescence and equant calcite cement (e) shows brighter zoned orange luminescence. Scale bar = 0.2 mm. **C.** A shelter pore was floored with darker internal sediments (is) to form a geopetal structure, and later was filled by fibrous (f) and equant (e) calcite cements. Sample W34, plane light, scale bar = 1.0 mm. **D.** Intraskeletal pores in a coral was floored with internal sediments (is) and later filled by equant calcite cement (e). Sample W24, stained, plane light, scale bar = 1.0 mm. **E.** Neomorphosed calcite mosaics around a vug (v). Sample W92, stained, plane light, scale bar = 0.2 mm. **F.** Strongly dissolved stromatolitic limestone with numerous molds (m) and vugs (v). Most pores are cement-free and anhydrite cement (a) occurs in a few pores. Sample W92, plane light, scale bar = 1.0 mm.

less than 3% of the rock volume. No pendant or meniscus cements were observed in the Guelph limestones. In Type 1 dolomite intervals (see Chapter 4), equant cement is commonly mimetically replaced by dolomite.

### 3.6.3. Internal sediments

In reefal limestones, internal sediment consists of calcite micrite, variable amounts of fossil fragments, and minor siliciclastics and organic matter. It partly fills the lower part of primary pores, such as shelter and intraskeletal pores, to form geopetal structures (Fig. 3.6 C,D). Internal sediment is commonly overlain by fibrous calcite cement, although the reverse relationship is also observed in a few cavities.

### 3.6.4 Neomorphosed calcite

In some porous limestones, coarser crystalline (20-50 μm) calcite mosaics within a finer lime matrix consisting of 5-15 μm crystals were observed (Fig. 3.6E).

### 3.6.5 Limestone dissolution

Porous reefal limestones are widely present at different levels within the partially dolomitized pinnacle reefs on the lower ramp. The intensity of dissolution in these limestones is highly variable and commonly the most extensive leaching is present in the stromatolitic facies in the upper parts of reefs. Thin section study indicates that the earliest limestone dissolution postdates fibrous calcite cement but predates equant calcite cement. Some fossils such as brachiopods, gastropods and corals were selectively dissolved to form partial to complete molds and porous intervals (Fig. 3.6F). In limestones, irregular vugs occur more commonly than molds, but many vugs are likely

enlarged or modified molds. In some limestone intervals, these secondary pores contain variable amounts of equant calcite cement, anhydrite cement, halite cement, sometimes bitumen, and occasionally limpid dolomite and saddle dolomite cements, but many moldic and vuggy pores are cement-free (Fig. 3.6F).

## 3.7 Interpretation of pre-dolomitization diagenesis

Fibrous calcite cement in the Guelph Formation is similar to ancient fibrous cements in the pinnacle reefs in northern Michigan and elsewhere. These cements were interpreted to be the product of early submarine cementation of primary porosity by numerous authors (e.g., Sears and Lucia 1980; Davies 1977). Its morphology is also similar to the submarine fibrous Mg-calcite calcite cements observed in modern reefs (e.g., James et al. 1976; Grammer et al. 1995) and its original mineralogy was probably Mg-calcite (Cercone and Lohmann 1985).

Equant cement commonly occurs in meteoric phreatic settings (Folk 1974; Longman 1980), but this cement can also be formed in non-freshwater environments (Given and Wilkinson 1987). Identical equant calcite cements from pinnacle reefs in southwestern Ontario and elsewhere in the Michigan Basin have been interpreted as having been precipitated in the shallow subsurface phreatic zone from either meteoric fluids (Gill 1977a; Sears and Lucia 1980; Charbonneau 1990) or seawater-derived evaporitic fluids (Cercone and Lohmann 1985). Based on its relative timing in the paragenetic sequence and geochemistry (see Chapter 4), equant calcite cement in Guelph limestones is considered to be a shallow burial cement formed in seawater-derived pore fluids.

The relatively early timing of internal sediment and its content of fossil fragments and clastics indicate that it formed in the depositional environment. Charbonneau (1990) interpreted similar internal sediment as the product of vadose processes during reef exposure, based on its coexistence with equant cement in solution-enhanced pores.

Coarser crystalline calcite mosaics within finer lime matrix may reflect aggrading neomorphism (e.g., Folk 1965; Sears and Lucia 1980; Cercone and Lohmann 1985). The most likely fluids for calcite neomorphism are seawater-derived fluids, as suggested by the geochemistry of calcitic components in the Guelph Formation (see Chapter 4).

In northern Michigan, Sears and Lucia (1980) attributed limestone dissolution, equant calcite cementation, and aggrading neomorphism in limestone to early freshwater diagenesis during reef exposure. Similar features such as severe dissolution, "paleosol", and "karstic crusts" described by Smith et al. (1993) (discussed earlier) in southwestern Ontario could have resulted from other diagenetic fluids such as modified marine waters (e.g., Sun 1992). Carbonate dissolution could also extend to late burial stage (e.g., Mazzullo and Harris 1992). Many of the molds and vugs in Guelph limestone and dolomite likely formed after regional dolomitization during burial, as suggested by their lining or filling by late stage anhydrite and/or halite cements, which will be discussed in Chapter 6. The "paleosol" in the Terminus pinnacle reef, which was interpreted to have resulted from long exposure (Smith et al. 1993), is reinterpreted in the present study to be dedolomite that formed in the subsurface (see Chapter 5).

Seawater and hypersaline seawater can be effective agents for limestone dissolution (e.g., Sun 1992). Geochemical data obtained from samples of bulk limestone and major diagenetic fabrics in Guelph limestone do not support any significant involvement of fresh water (see Chapter 4). In addition, Cercone and Lohmann (1985) provided several lines of evidence to argue strongly against the presence of a long-lived influence by meteoric water or a major influence of meteoric water in the pinnacle reefs in northern Michigan. Their main arguments include: (1) absence of a major unconformity between the Niagaran and Cayugan rocks; (2) presence of a semi-arid to arid climate with high evaporation and low precipitation during Salina A-1 Evaporite and A-1 Carbonate time; and (3) absence of extensive meteoric lenses in modern islands similar in size to Guelph pinnacle reefs, even in a humid climate. Their arguments can also be applied to southwestern Ontario. Post-dolomitization dissolution of limestones may have also acted as a Ca source for local dedolomitization in partially dolomitized pinnacle reefs (see Chapter 5).

## 3.8 Conclusions

1. The Guelph Formation consists of five major facies. They are: (1) basal crinoidal mud mound facies; (2) coral-stromatoporoid reef core facies; (3) crinoidal-bryozoan flank facies; (4) stromatolitic cap facies; and (5) interreef mud facies.

2. The vertical facies and fossil zonation in Guelph reefs indicate three major stages of reef growth, including: (1) initial crinoidal mud mound buildup in a relatively low energy

subtidal environment; (2) rapid growth of a coral-stromatoporoid organic reef core and accumulation of detrital flank deposits in an agitated normal marine environment; and (3) growth of a stromatolite cap in a restricted environment. Basinward pinnacle reefs were initialized on crinoidal mounds whereas more shelfward pinnacle and patch reefs were started as coral-stromatoporoid facies without the crinoidal mound substrate.

3. Guelph reefal carbonates exhibit a complicated diagenetic history. An ideal paragenetic sequence representing the complete diagenetic history of the Guelph Formation can be divided into three main stages: (1) pre-dolomitization diagenesis; (2) regional pervasive dolomitization; and (3) post-dolomitization diagenesis. Pre-dolomitization diagenesis is characterized by early marine cementation and neomorphism under the influence of seawater during deposition and shallow burial. Subsequent regional dolomitization and post-dolomitization diagenesis includes dolomite dissolution, dolomite alteration, dedolomitization, saddle dolomite formation, anhydrite cementation, halite plugging, and hydrocarbon emplacement that occurred under shallow to deep burial conditions. These topics will be discussed in the following chapters.

# Chapter 4 Dolomite and dolomite origin

## 4.1 Abstract

The Guelph Formation is a regionally dolomitized reefal carbonate unit developed on a Middle Silurian ramp (150-200 km wide) in the southeastern part of the Michigan Basin. A general basinward dolomite-decreasing trend, consisting of completely dolomitized patch reefs on the upper ramp, completely and partially dolomitized pinnacle reefs on the lower ramp, and undolomitized basinal lime mudstone in the basin center, indicates that dolomitizing fluids were derived from shelfward sources. The selectively dolomitized A-1 and A-2 carbonates in the overlying Salina Group, which completely surround dolomitized pinnacle reefs, suggests that their dolomitization relates to the dolomitization of reefs.

Guelph dolomites mainly consist of three replacive dolomite fabrics: (1) microcrystalline (20-50 μm, Type 1) anhedral mosaics, characterized by well preserved and mimetically replaced bioclastic-intraclastic grains and earlier calcite cement textures; (2) finely crystalline (50-150 μm, Type 2) euhedral to subhedral dolomite with partially preserved grains and precursor textures; and (3) medium to coarsely crystalline (150-400 μm, Type 3) euhedral to anhedral dolomite without preserved grains or precursor textures. Type 1 dolomite is only developed in nonporous intervals. Type 2 dolomite is the most common type and occurs in porous intervals containing moldic and vuggy pores. Type 3 dolomite is dominated by intercrystalline pores and commonly occurs as porous patches or thin layers within Type 2 or Type 1 dolomites.

Type 1 dolomite is interpreted to represent the 'least-altered' dolomite phase produced by early seawater dolomitization, which is supported by its well preserved limestone textures, identical $^{87}Sr/^{86}Sr$ ratios (0.70853-0.70864) to both Middle Silurian limestone and coeval seawater. However, the coarser crystal size and greatly depleted $\delta^{18}O$ values (-4.5‰ to –8.5‰ PDB) of Type 1 dolomites relative to modern dolomite values (1‰ to 3‰ PDB, e.g., McKenzie et al. 1980; Gregg et al. 1992) suggest early recrystallization of a metastable precursor phase.

A hydrologic model related to evaporation and sea-level fall is proposed for early dolomitization. In this model, the regional subsurface reflux of seawater through porous Guelph carbonates was induced by evaporative drawdown and the driving force for basinward flow was the hydraulic head difference between the open sea level and drawdowned sea level in the isolated Michigan Basin. Early dolomitization of Guelph carbonates occurred in this reflux system during the first few hundred meters of burial, probably during the Late Silurian.

The coexistence of three dolomite fabrics with relict textures, and their crosscutting relationships, in conjunction with progressively elevated $^{87}Sr/^{86}Sr$ ratios (0.70860-0.70910) and enriched Fe concentrations (700-3500 ppm) and Mn contents (100-300 ppm) in Type 2 and Type 3 dolomites, indicate that Type 1 dolomite was altered to Type 2 and Type 3 dolomite. $\delta^{18}O$ values (-5‰ to -10‰ PDB) and fluid inclusion data (Th: +64.5 to +74.7°C; Tm: -9.9 to -13.5°C) from Type 2 dolomite indicate that Type 1 dolomite was further altered by saline water during shallow to moderate burial. Localized Type 3 dolomite and saddle dolomite cement were probably related to hydrothermal brines during later burial, as evidenced by their

fracture-related occurrence and high Th values (+95.8 to +128.2°C).

## 4.2 Introduction

The basic requirements for regional dolomitization are (1) a dolomitizing fluid source with sufficient Mg; (2) a geochemical environment with the required thermodynamic and kinetic conditions for dolomite formation; (3) an adequate regional hydrologic flow system to deliver Mg to and remove Ca from the reaction sites; and (4) a sufficient period of time for complete replacement (e.g., Machel and Mountjoy 1986; Morrow 1990). Several dolomitization models have been proposed mainly over the last four decades, including: (1) hypersaline models related to seepage reflux of a denser/heavier hypersaline brine (Adams and Rhodes 1960; Deffeyes et al. 1965; Murray 1969) or evaporative pumping in a sabkha or supratidal zone (Shinn et al. 1965; Hsü and Siegenthaler 1969); (2) mixing-zone models for islands and platforms (Hanshaw et al. 1971; Badiozamani 1973; Land 1973); (3) burial compaction models related to deep connate seawaters expelled from adjacent shales by burial compaction, basinal brines driven by sedimentary loading and/or tectonic compression (Mattes and Mountjoy 1980; Gawthorpe 1987; Mountjoy et al. 1994), and pressure solution of underlying older dolomites (Barnaby and Read 1992); and (4) seawater or modified seawater models for subtidal to subsurface environments (Sass and Katz 1982; Bein and Land 1983; Carballo et al. 1987; Land 1991). Thermal convection of seawater was proposed to explain the dolomitization in several atolls or isolated platforms developed on volcanic basement or associated with volcanic activity (e.g., Simms 1984; Saller 1984; Aharon et al. 1987; Hein et al. 1992). Recently, a combined "thermoflux" dolomitization model was also proposed by Wendt et al. (1998) and hydrothermal dolomite models were reviewed by Morrow (1998).

Significant temporal and spatial variations in both dolomite texture and chemistry have been recognized and reviewed in several recent studies of dolomite (e.g., Land 1985; Banner et al 1988; Mazzullo 1992), although the interpretations of these changes are still controversial. Many previous studies of ancient dolomites have interpreted original textures and geochemical signatures to have been modified or reset by later dolomite diagenesis in fluids with different chemistry and/or under different diagenetic conditions, for example, elevated temperatures (Zenger 1983; Sperber et al. 1984; Gregg and Sibley 1984; Sibley and Gregg 1987; Land 1980, 1985; Hardie 1987; Coniglio et al. 1988; Banner et al 1988; Cander et al. 1988; Sass and Bein 1988; Zenger and Dunham 1988). Numerous more recent studies have further confirmed that the petrographic textures and chemical compositions mainly represent the products of later diagenetic events or multiple stages of dolomite modification rather than original dolomitization (Gao 1990; Gao and Land 1991; Land 1991; Gregg and Shelton 1990; Gregg et al. 1992; Smith and Dorobek 1989; Mazzullo 1992; Kupecz and Land 1991, 1994; Montañez and Read 1992; Ye and Mazzullo 1993).

Extensively dolomitized pinnacle and patch reefs in the Guelph Formation of southwestern Ontario, which is located at the eastern part of the southern reef trend, have produced prolific amounts of oil and gas for more than four decades (Sanford 1969; Carter 1992). Earlier studies of Guelph carbonates in the southern reef trend have focused primarily on the controls of their porosity and permeability by depositional environments and early diagenesis including possible karsting (e.g., Sanford 1969; Gill 1977a; Smith et al. 1993). The Guelph Formation in southwestern Ontario provides an excellent opportunity to examine the origin of economically important, massive reefal dolomites encased by cyclic evaporite-carbonate strata, as it contains

different dolomite fabrics and minor preserved limestone precursors.

The main objectives of this chapter are: (1) to describe the distribution of Guelph dolomites on a regional scale; (2) to document the petrography and geochemistry of different dolomite fabrics; and (3) to evaluate the importance of post-dolomitization alteration of early-formed dolomite. The pattern of dolomite distribution provides a direct record of the paleohydrologic flow system for the dolomitization in a sedimentary basin. Combined petrographic and geochemical evidence can constrain the source of diagenetic fluids and the timing of diagenetic events. A conceptual model for Guelph dolomite formation is proposed based on the dolomite fabric distribution and geochemistry in the context of the regional stratigraphic and hydrological framework.

## 4.3 Terminology

Several different but commonly used terms for "dolomite formation" including "dolomitization", "dolomite diagenesis", "dolomite modification", "dolomite stabilization", "dolomite recrystallization", and "dolomite neomorphism" have been used in the literature to describe the initial formation of dolomite by replacing a limestone precursor and the further alteration of the early-formed dolomite. "Dolomitization" is commonly used for the replacement of limestone by dolomite. "Dolomite diagenesis" includes all alteration that occurred subsequently to the initial dolomite. Dolomite "modification" (textural and/or chemical change) is also a very broad term for many processes occurring after initial dolomite formation, including dolomite dissolution or corrosion, overgrowth of later dolomite on earlier dolomite, dolomite cementation, or dolomite replacement by later dolomite (Banner et al.

1988; Gao and Land 1991; Barnaby and Read 1992; Montañez and Read 1992; Kupecz and Land 1994). "Stabilization" is another general term for the transformation of a thermodynamically unstable or metastable dolomite phase to a more ordered, more stoichiometric, and more stable dolomite phase (Land 1985, 1991). "Recrystallization" is the most common used term in recent dolomite studies. It refers to the replacement of an early-formed dolomite by a later dolomite with significant changes in texture and chemical composition through a dissolution-reprecipitation process on the thin fluid film scale (Land 1985). "Neomorphism" was introduced by Folk (1965) to emphasize changes in both texture and chemical composition of limestone, but this term is often used synonymously with "recrystallization" in many recent dolomite studies (Sibley and Gregg 1987; Gregg and Shelton 1990; Durocher and Al-Aasm 1998). Machel (1998) suggested redefining the meaning of recrystallization and abandoning the usage of neomorphism in dolomite study. The above mentioned terms for the diagenesis of an earlier dolomite are often used as substitutes for one another in the literature without clear definition (e.g., Gao 1990; Montañez and Read 1992; Kupecz et al. 1993). A general term 'dolomite recrystallization' as defined by Machel (1998) will be used in this study to include all the processes involved in dolomite-to-dolomite transformation and the corresponding textural changes (in crystal size, crystal shape, and zonation), structural changes (in ordering and strain), and compositional changes (in stoichiometry, trace elements, isotopes, and fluid inclusion properties). The common processes involved in dolomite-to-dolomite transformation in Guelph dolomites include: (1) earlier, finer dolomite replaced by later coarser dolomite through a thin-film dissolution-reprecipitation process; and more importantly (2) combined old dolomite dissolution and new dolomite

formation through both precipitation on old dolomite cores as overgrowths and precipitation as new crystals.

## 4.4 Dolomite distribution

In southwestern Ontario, the Guelph Formation is underlain by completely dolomitized platform carbonates of the Lockport Formation and overlain by the partially dolomitized Salina A-1 Carbonate unit (Fig. 2.4). In the Guelph Formation, the barrier reef complex on the platform margin, all patch reefs on the upper ramp and most pinnacle reefs on lower ramp are entirely dolomitized (Fig. 2.5). However, a few pinnacle reefs on the basinward side of the lower ramp are only partially dolomitized or remain undolomitized and further basinward facies consist of thin and nonporous lime mudstones (Figs. 1.2, 2.5). This general basinward dolomite-decreasing trend is similar to the dolomite distribution trend found in northern Michigan (Gill 1979; Sears and Lucia 1980; Cercone 1984b). Partially dolomitized pinnacle reefs consist of interbedded dolomite and limestone layers in sharp contacts. Dolomite beds are always completely dolomitized without limestone relicts. Within all observed partially dolomitized pinnacle reefs on the lower ramp, the lower portions of the reefs were always preferably dolomitized (Table 4.1). Some partly to completely dolomitized pinnacle reefs on the lower ramp were also partially dedolomitized (Figs. 1.2 and 2.5, see Chapter 5 for details). Inter-reefal carbonates in the study region consist entirely of dolomite. Facies-related dolomitization such as preferentially dolomitized burrows and mudstones (Saller and Yaremko 1994) are absent in the Guelph Formation.

A-1 and A-2 carbonate units in the study area are generally composed of thin-bedded to

stromatolitic lime mudstone-wackestone and less laminated to stromatolitic, finely to medium crystalline dolomite. In the platform margin and on the upper ramp, A-1 and A-2 units consist of only dolomite, but they change to mainly limestone in the pinnacle reef zone on the lower ramp (Fig. 2.5). Similar dolomite distribution trend was observed in northern Michigan (Sears and Lucia 1980). On the lower ramp, A-1 and A-2 carbonates occur as limestone in the interreef areas and around or above the undolomitized limestone reefs (e.g., Rosedale pinnacle reef) and partially dolomitized reefs (e.g., Wilkesport, Payne, and Sarnia 1-8-A pinnacle reefs), but dolomitized A-1 and A-2 carbonates always occur around or above (in close proximity to) the dolomitized pinnacle reefs (e.g., Sombra, Bickford, Duthill, Enniskillen 28, Seckerton, and Dawn 156 pinnacle reefs) (Figs. 1.2 and 4.1; Table 4.1). However, not all A-1 and A-2 carbonates in the vicinity of dolomitized pinnacle reefs are dolomite.

Table 4.1 Dolomite distribution in partially dolomitized pinnacle reefs

| Reef name | Thickness of cored Guelph (m) | Dolomite distribution |
|---|---|---|
| Dow Moore 28* | 100 m | Bottom 40 m |
| Payne | 115 m | Bottom 33 m |
| Sarnia 1-8-A* | 50 m | Bottom 5 m |
| Warwick | 140 m | Bottom 78 m |
| Wilkesport | 75 m | Bottom 32 m |

* Incomplete Guelph Cores

In southeastern Michigan, Jodry (1969) noted that A-1 carbonate consists of limestone in the interreef area or further away from the pinnacle reefs and the A-1 carbonate was preferentially

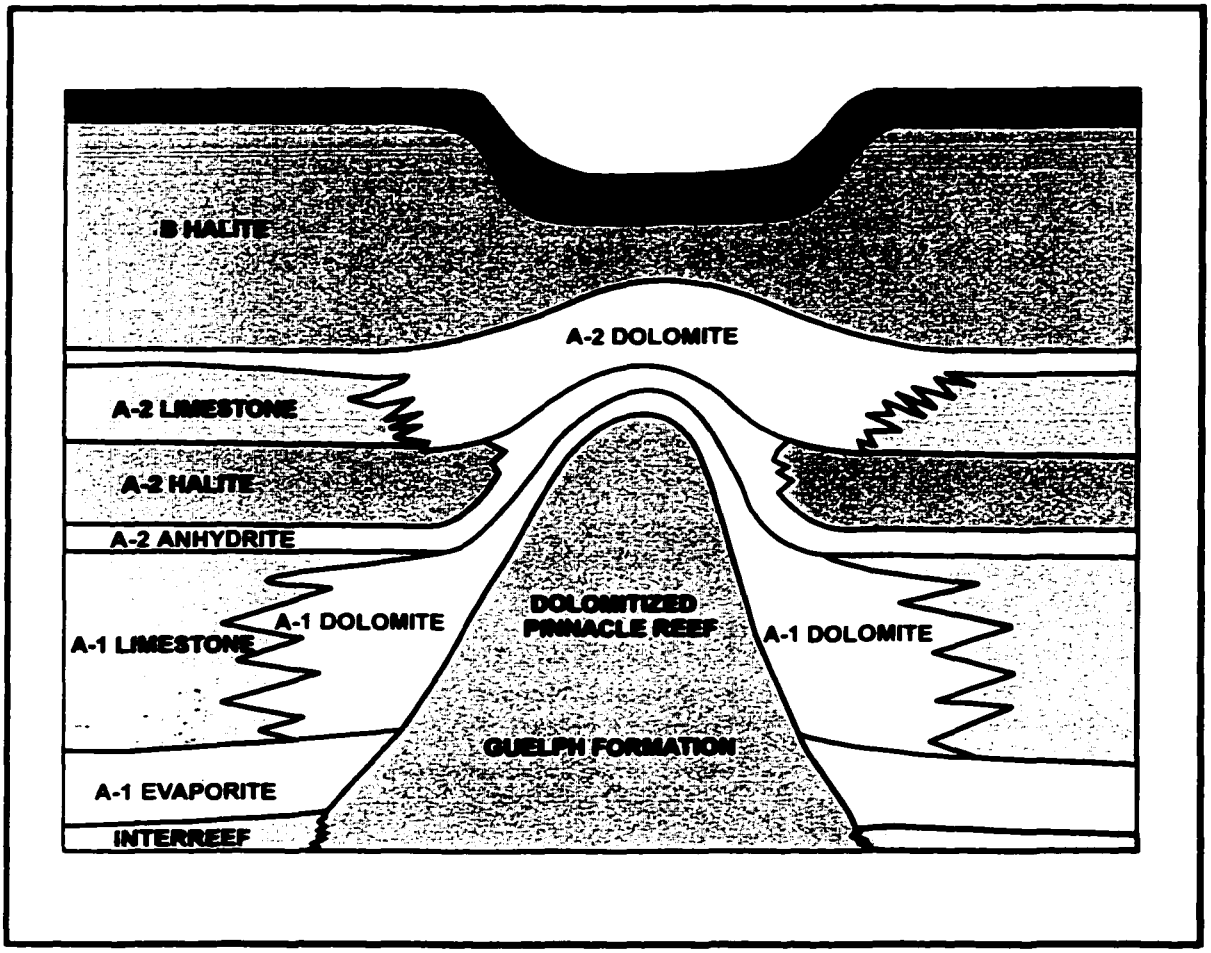



Fig. 4.1 Salina A-1 and A-2 dolomite distribution around dolomitized Guelph pinnacle reefs.

dolomitized around the dolomitized pinnacle reefs to form dolomite halos. In southwestern Ontario, Sanford (1969) found that the A-1 Carbonate unit is preferentially dolomitized around completely dolomitized pinnacle reefs. Oil and gas accumulations within A-1 Carbonate occur where porous dolomite is developed near reefs. Hill (1973) suggested that "A-1 sucrosic dolomite" halo is a useful indicator of underlying reef proximity. Based on regional subsurface mapping in Sombra Township of Lambton County, Carter (1991) reported similar findings in that the A-1 Carbonate unit is composed predominantly of limestone with less than 10% dolomite in interreef areas and dolomite occurs proximal to pinnacle reefs or to the shelfward platform margin. He also observed that dolomitization of the A-2 Carbonate unit followed a similar pattern as in the A-1 Carbonate unit and A-2 halite and B-halite were partly to completely dissolved away above the pinnacle reefs surrounded by A-1 and A-2 dolomites (e.g., Sombra and Duthill pinnacle reefs) (Fig. 1.2).

## 4.5 Dolomite petrography

### 4.5.1 Dolomite fabrics

Guelph dolomite has a tan to dark brown color and mainly consists of dolomite replacing pre-existing reefal limestone with only minor dolomite cement (<3%). Sedimentary textures such as bedding and stromatolites, fossils such as corals, stromotoporoids, crinoids, and brachiopods, and early fibrous and equant calcite cements, which commonly occur in primary reefal limestones, were poorly to well preserved. The replacive dolomitization is typically complete, similar to the pervasive dolomites reported from the pinnacle reefs in northern Michigan (Sears and Lucia 1980; Cercone 1984b). A transition in relative abundance of dolomite in rocks ranging from 0% to 100%, which has been observed in many other ancient

carbonate units (e.g., Qing and Mountjoy 1989), is not observed in the Guelph Formation.

Guelph replacive dolomite consists of microcrystalline to coarsely crystalline crystals ranging from 20 to 400 μm and can be classified into three main fabric types according to their average crystal size, i.e. microcrystalline (Type 1) dolomite, finely crystalline (Type 2) dolomite, and medium-coarsely crystalline (Type 3) dolomite (Fig. 4.2). Minor amounts of finely to coarsely crystalline, limpid and saddle dolomite cements also occur in replacive dolomites.

The relative abundance of three dolomite fabrics in the Guelph Formation has been estimated based on core and thin section observations in this study. Type 2 dolomite is the most common fabric, accounting for more than 80% of replacive dolomites. Type 1 dolomite comprises approximately 15%. Type 3 dolomite is volumetrically minor, accounting for less than 5%.

#### 4.5.1.1 Type 1. Microcrystalline dolomite with preserved fabric

Type 1 dolomite generally consists of tightly packed, microcrystalline (20-50 μm), anhedral and equigranular crystals with non-planar boundaries (Figs. 4.2, 4.3A). It occurs in all depositional facies and contains well-preserved precursor fabrics such as pseudomorphic dolomitized crinoid fragments (Fig. 4.3B) and mimetically replaced early fibrous and equant calcite cements (Fig. 4.3A, C). Type 1 dolomite postdates fibrous and equant calcite cements but predates stylolitization and fracturing. Type 1 dolomite shows a relatively uniform, very dull orange luminescence without obvious CL zones (Fig. 4.3D).

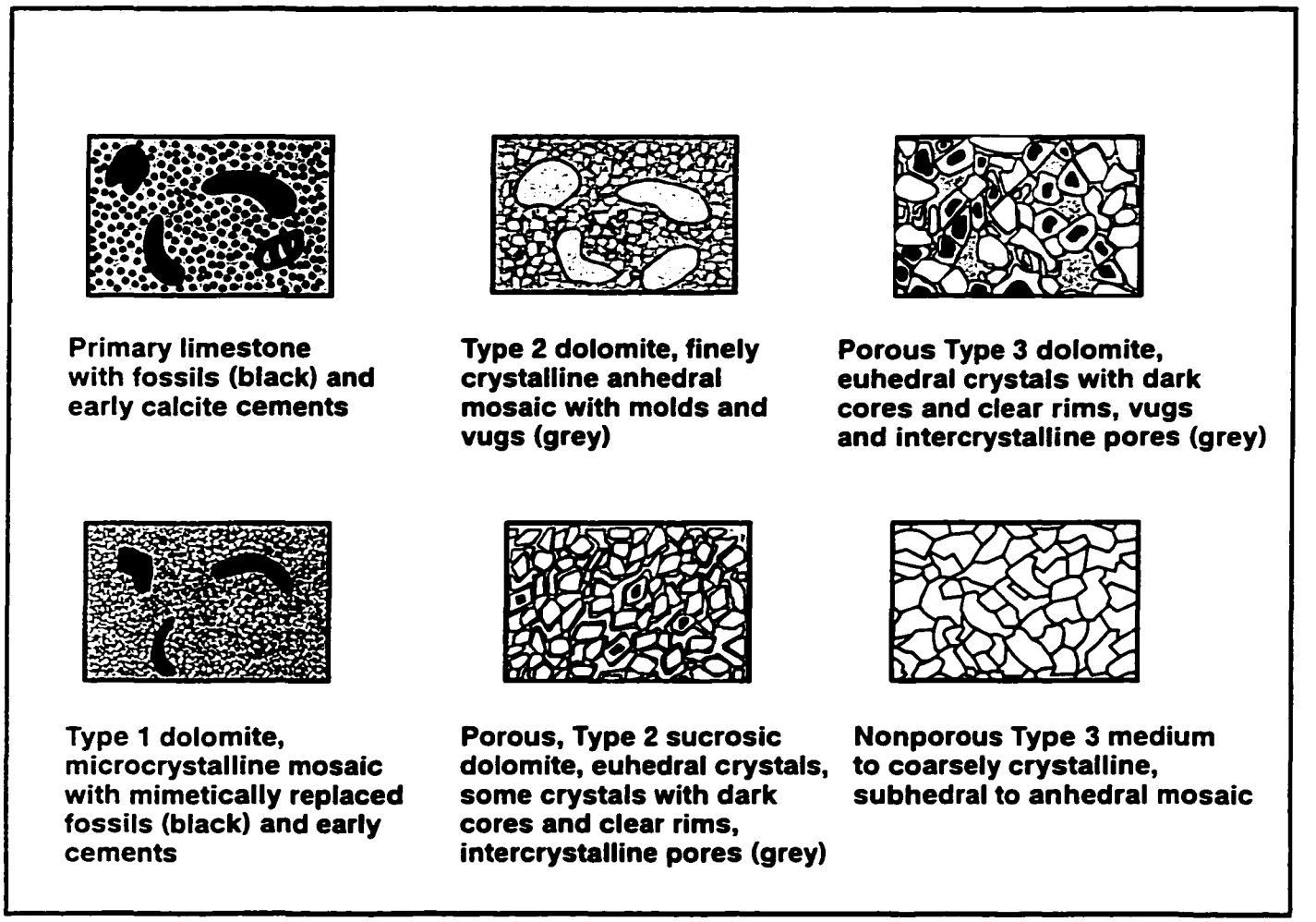



Fig. 4.2 Replacive dolomite fabrics in the Guelph Formation in southwestern Ontario.

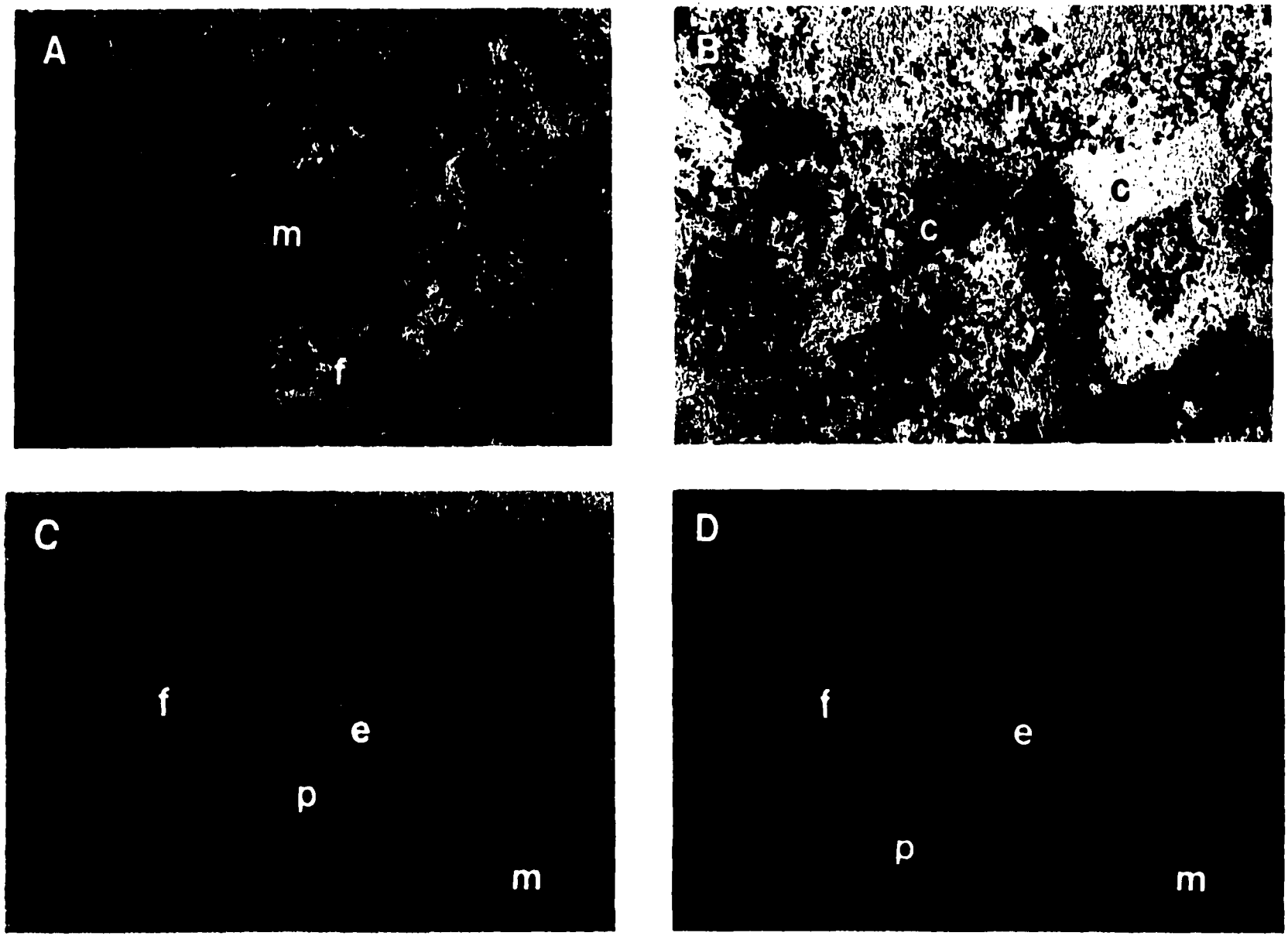



**Fig. 4.3** (p.82) Photomicrographs of Type 1 dolomite in polished thin sections. **A.** Nonporous Type 1 dolomite consists of tightly packed, microcrystalline, anhedral crystals (m). Previous fibrous calcite cement (f) was mimetically replaced by dolomite. Sample W154, crossed-polarized light, scale bar = 1.0 mm. **B.** Mimetically dolomitized crinoid fragments (c) in a Type 1 dolomite. Sample W150, crossed-polarized light, scale bar = 0.2 mm. **C** and **D.** Microcrystalline Type 1 dolomite (m) and mimetically dolomitized fibrous (f) and equant (e) cements around a pore (p) under plane light and CL view. Type 1 dolomite showing dull orange to reddish luminescence without obvious CL zones. Sample W135, scale bar =1.0 mm.

#### 4.5.1.2 Type 2. Finely crystalline dolomite with partially preserved fabric

Type 2 dolomite is typically composed of finely crystalline (50-150 μm), euhedral to anhedral, intergrown rhombic crystals (Figs. 4.2, 4.4A), with uniform extinction. It commonly occurs as a porous sucrosic mosaic with planar crystal boundaries, but sometimes as nonporous mosaic with irregular, non-planar crystal boundaries (Fig. 4.4B). Precursor fabrics of allochems and early fibrous and equant cements are poorly to fairly preserved. Most Type 2 dolomite crystals exhibit inclusion-rich cloudy cores and relatively inclusion-free clear rims (Fig. 4.4A), but some crystals are completely inclusion-rich or inclusion-poor (Fig. 4.4B). The clear rims commonly comprise 10-40% of the crystals with cloudy cores. The cloudy cores and inclusion-rich crystals display dull orange luminescence, which is slightly brighter than the dull orange luminescence of Type 1 dolomite. Clear, relatively inclusion-poor rims show dull reddish luminescent zones (Fig. 4.4C). Some cloudy cores and inclusion-rich crystals of Type 2 dolomite exhibit mottled or irregular patchy luminescence (Fig 4.4C). Many Type 2 dolomite mosaics contain minor amounts of Type 1 dolomite and coexistence of Type 2 and finer Type 1 mosaic on a hand specimen or thin section scale is very common (Fig. 4.4D). In Type 2 dolomite, some fossils including brachiopods, corals, gastropods, cephalopods, and crinoids, were selectively dissolved, partially to completely, to form variable amounts of moldic and vuggy porosity (see Chapter 6).

#### 4.5.1.3 Type 3. Medium to coarsely crystalline dolomite without preserved fabric

Type 3 dolomite mosaics commonly occur as loosely packed, sucrosic aggregates consist of medium to coarsely crystalline (150-400 μm), euhedral to anhedral, intergrown rhombs, usually with cloudy cores and clear rims (Figs. 4.2, 4.5A), sometimes as tightly interlocking

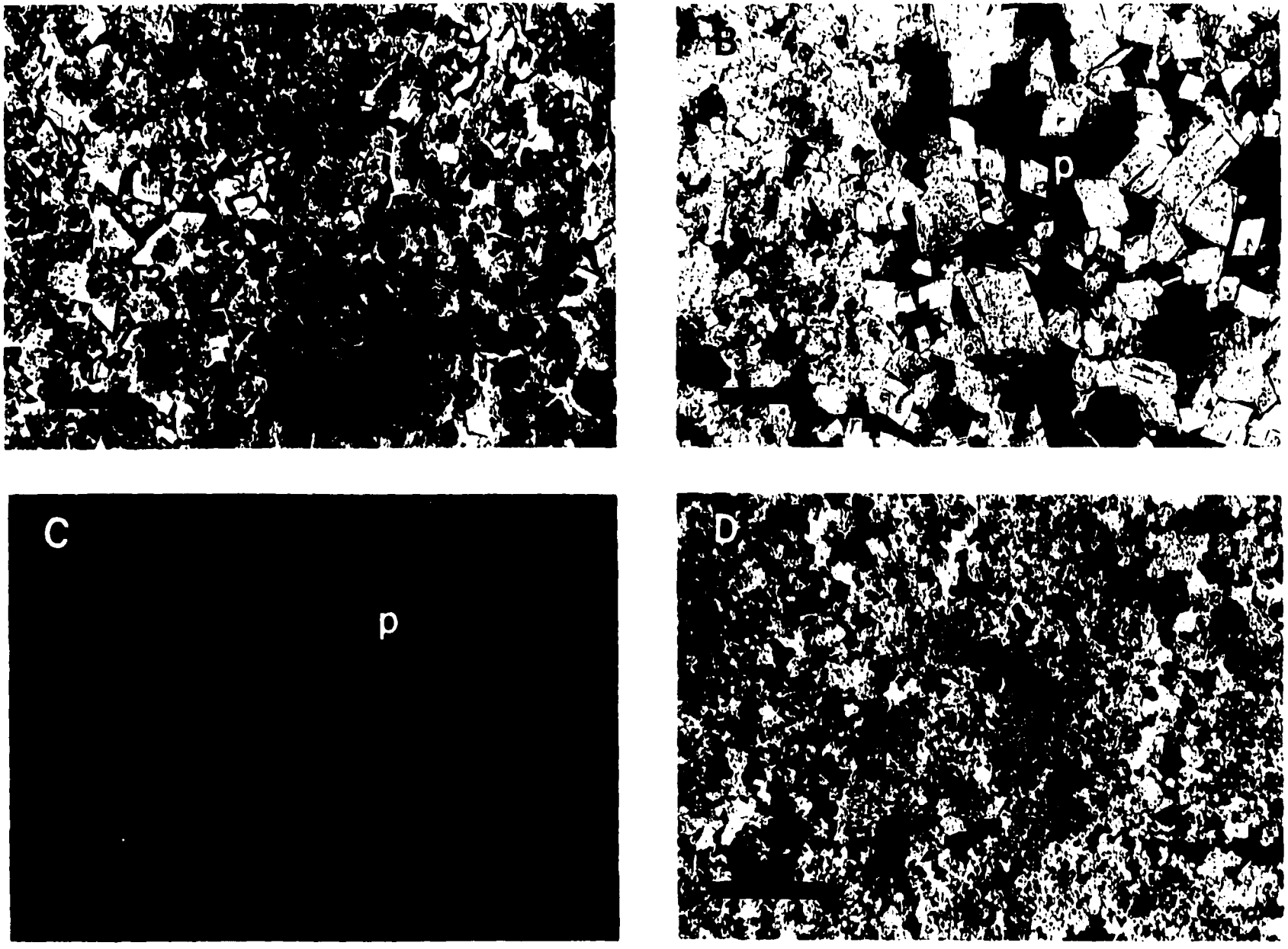



**Fig. 4.4** (p.84) Photomicrographs of Type 2 dolomite in polished thin sections. **A.** Finely crystalline Type 2 dolomite (T2) consisting of anhedral to euhedral crystals. Most crystals have cloudy cores and clear rims. Sample W120, plane light, scale bar =0.2mm. **B.** Type 2 dolomite. The left portion shows a nonporous mosaic consisting of anhedral crystal and the right portion occurs as a porous sucrosic mosaic consisting of euhedral crystals and intercrystalline pores (p). Sample W144, crossed-polarized light, scale bar = 0.2mm. **C.** Type 2 dolomite (T2) shows dull and patchy orange luminescent cores with reddish luminescent rims. Sample W106, CL view, scale bar = 0.2mm. **D.** Type 2 dolomite contains irregular patches of microcrystallice (mp) Type 1 mosaic. Sample W26, plane light, scale bar = 1.0 mm.

mosaics of anhedral non-planar crystals without obvious overgrowth rims (Fig. 4.5B). This dolomite is characterized by a typical non-mimetic, fabric-destructive dolomite where depositional and earlier diagenetic textures are completely obliterated. The overgrowth rims commonly comprise 10-30% of the whole crystals with cloudy cores. Some crystals in Type 3 mosaics exhibit curved crystal faces and sweeping extinction that are similar to saddle dolomite. Type 3 dolomite exhibits uniform to mottled dull orange to reddish luminescence (Fig. 4.5C, D) that is brighter than the dull orange luminescence of cloudy cores and inclusion-rich crystals in Type 2 dolomite mosaics. Clear rims of Type 3 crystals commonly display alternating CL zones of orange and reddish luminescence and non-luminescence (Fig.4.5C).

#### 4.5.1.4 Finely to coarsely crystalline dolomite cement

Dolomite fabrics formed by replacing pre-existing fibrous and equant calcite cements are considered as replacive dolomite. They commonly occur in fabric-preserving Type 1 dolomite and are partially preserved in some Type 2 dolomite intervals. True dolomite cement occurs as limpid dolomite and saddle dolomite cements. Limpid dolomite cement consists of white colored, euhedral to subhedral, finely to coarsely crystalline (100–300 μm) crystals with rhombic terminations and uniform extinction. Limpid dolomite cement commonly occurs in minor amounts (<2%) lining molds, vugs, and fractures in Type 2 and Type 3 dolomites (Fig. 4.6A). It is also present in the vugs and fractures in the rock dominated by Type 1 dolomite fabric. This cement generally shows dull reddish luminescence with thin non-luminescent bands (Fig. 4.6B), similar to the dull reddish luminescent zones occurring in clear rims in Type 2 dolomite mosaics. Limpid dolomite cement in Guelph dolomite is similar to the euhedral "limpid' dolomite occurring as pore-filling cement in many other ancient dolomites (Folk and

Land 1975; Braithwaite 1991) and in Recent carbonate sediments (Sibley 1980; McKenzie et al. 1980; Mitchel et al. 1987).

Saddle dolomite occurs as a cement lining or filling vugs and fractures in porous limestone and Type 2 and Type 3 dolomites in minor amounts (< 1%), characterized by milky white, coarsely crystalline (200-1000 μm), euhedral crystals with curved crystal faces and sweeping extinction (Figs. 4.6C). It is mostly non-luminescent, but may show subtle bands of dull reddish luminescence and non-luminescence. Some crystals show inclusion-rich, cloudy cores and inclusion-free, clear rims.

#### 4.5.1.5 Scattered finely to medium crystalline dolomite in limestone

Scattered, finely to medium crystalline (100-250 μm), subhedral to euhedral rhombs occur in amounts of 1% to 8% by volume in almost all limestone samples (Fig. 4.6D). The dolomite rhombs show dull reddish luminescence with non-luminescent bands, similar to the dull reddish luminescence of limpid dolomite cement. They mostly occur as replacive phase but sometimes as cement in vugs and fractures in more porous limestones.

### 4.5.2 Replacive dolomite fabric distribution

The three different dolomite fabrics occur irregularly throughout the Guelph Formation. Coexistence of two fabrics is common and coexistence of three fabrics is also observed. There is no evidence to suggest that the distribution of different dolomite fabrics or their relative abundance is facies-controlled or related to texture. Type 1 dolomites are more commonly present in basinward pinnacle reefs, whereas Type 2 and Type 3 dolomites are more abundant

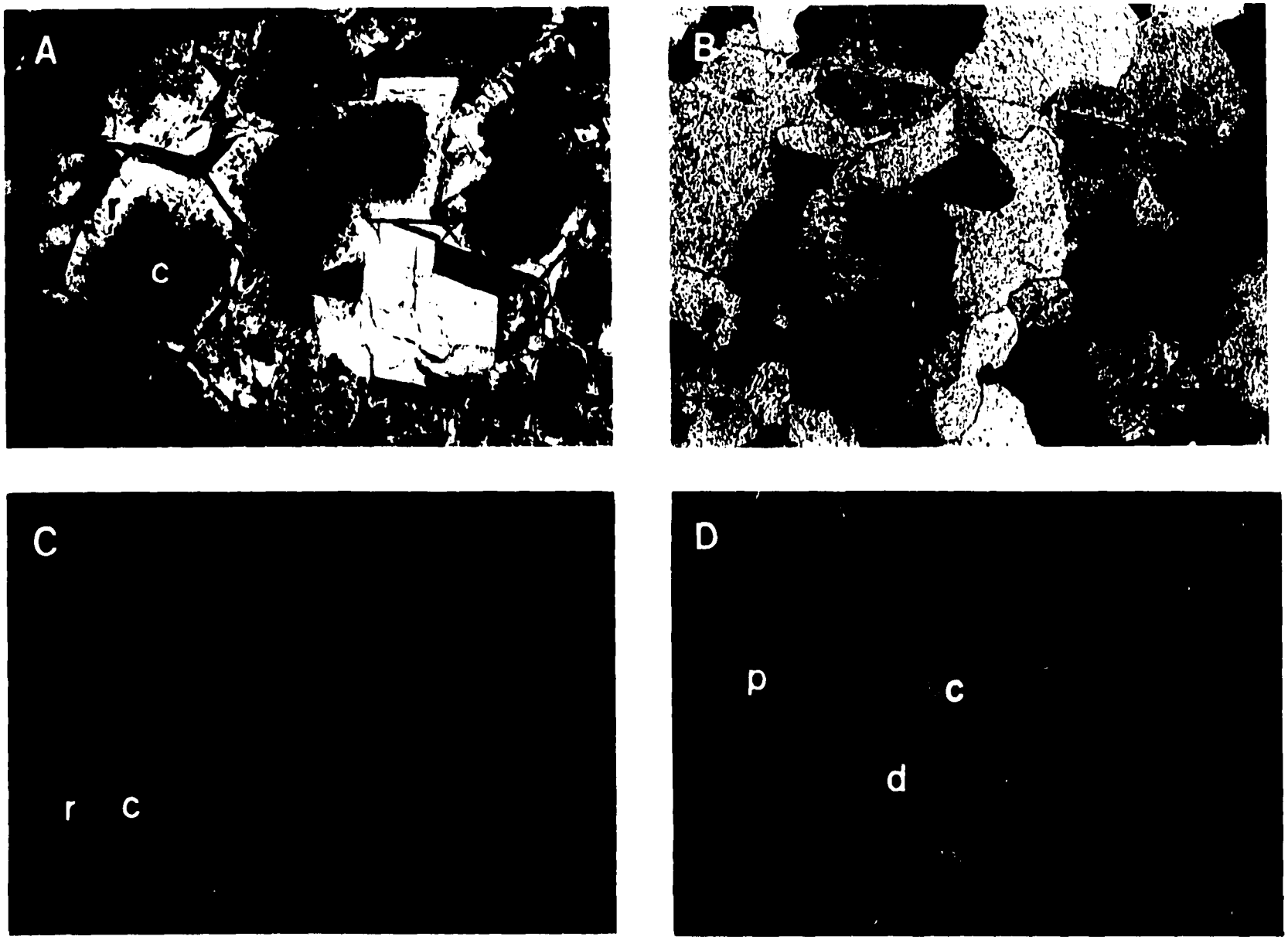



**Fig. 4.5** (P.87) Photomicrographs of type 3 dolomite in polished thin sections. **A.** Type 3 dolomite mosaic consisting of euhedral rhombic crystals with cloudy cores ( c ) and clear rims ( r ). Sample S10, plane light, scale bar = 0.2 mm. **B.** Type 3 dolomite mosaics consisting of euhedral non-planar crystals without obvious overgrowth rims. Sample W51, crossed-polarized light, scale bar = 0.2mm. **C.** Type 3 dolomite exhibits mottled orange luminescent cores ( c ) and reddish luminescent zoned rims ( r ). Sample S10, CL view, scale bar = 0.2mm. **D.** Type 3 dolomite shows relatively uniform dull orange CL without obvious zones. Minor late calcite cement ( c ) around pores (p) showing orange CL. Sample W121, CL view, scale bar = 0.2 mm. W121

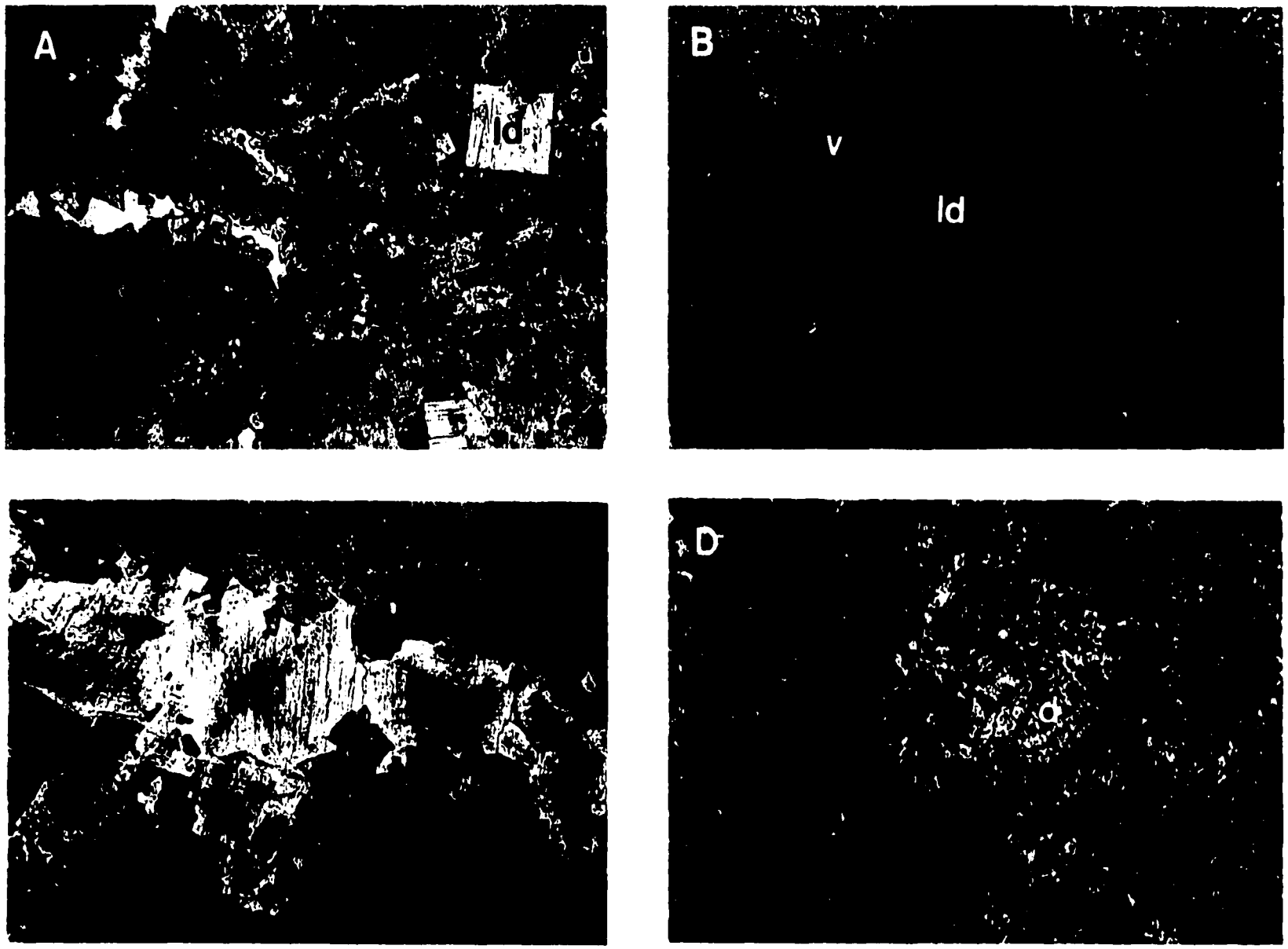



**Fig. 4.6** (p.88) Photomicrographs of dolomite cements and scattered dolomite in polished thin sections. **A.** Limpid dolomite cement (ld) lines vugs (v) in a Type 2 dolomite. Sample W137, plane light, scale bar = 1.0 mm. **B.** Limpid dolomite cement (id) exhibits reddish luminescence with zones. Sample W137, CL view, scale bar = 0.2mm. **C.** Saddle dolomite cement (sd, white) filling a fracture in limestone and postdating the equant calcite cement (c, purple) that lines the fracture. Sample W24, stained, plane light, scale bar = 0.2 mm. **D.** Scattered dolomite (d) around fibrous calcite cement (f) in limestone. Sample W34B, plane light, scale bar = 1.0 mm.

in the shelfward pinnacle and patch reefs.

In some Type 1 dolomite samples, minor Type 2 fabric occurs as millimeter- to centimeter-sized patches around voids and along fractures (Fig. 4.7A). Type 2 dolomite also occurs as alternating intervals with Type 1 dolomite. In places, stylolites separate Type 1 and Type 2 fabrics (Fig. 4.7B). Some Type 2 dolomites contain minor amounts of Type 1 fabric as patches or thin layers (Figs. 4.4D, 4.7C). Sharp boundaries between Type 2 and Type 3 fabrics are observed (Fig. 4.7D). Type 3 dolomite mosaics occur along fractures and stylolites within Type 2 fabric dominated dolomites in places. Type 3 fabric commonly occurs as millimeter to decimeter-sized local patches or lenses, and as thin layers (1-30 cm) within Type 1 and Type 2 dolomites, although it also makes up massive intervals up to 2-10 m thick. Type 2 fabric patches within Type 1 dolomite and Type 3 fabric patches within Type 1 and Type 2 dolomites are always related to local vugs and fractures.

Mottled fabrics in core are commonly observed in partly or selectively dolomitized rocks (e.g., Qing and Mountjoy 1986). Some Type 2 dolomite also occurs with mottled appearance in core. Mottled Type 2 dolomite is caused by differences in crystal size and porosity. Dark brown patches consist of more coarsely crystalline and more porous dolomite mosaics, with more bitumen or residual oil stain. Lighter brown or grey background dolomites are composed of more finely crystalline and relatively less porous Type 2 dolomite mosaics, with less or no bitumen or residual oil stain.

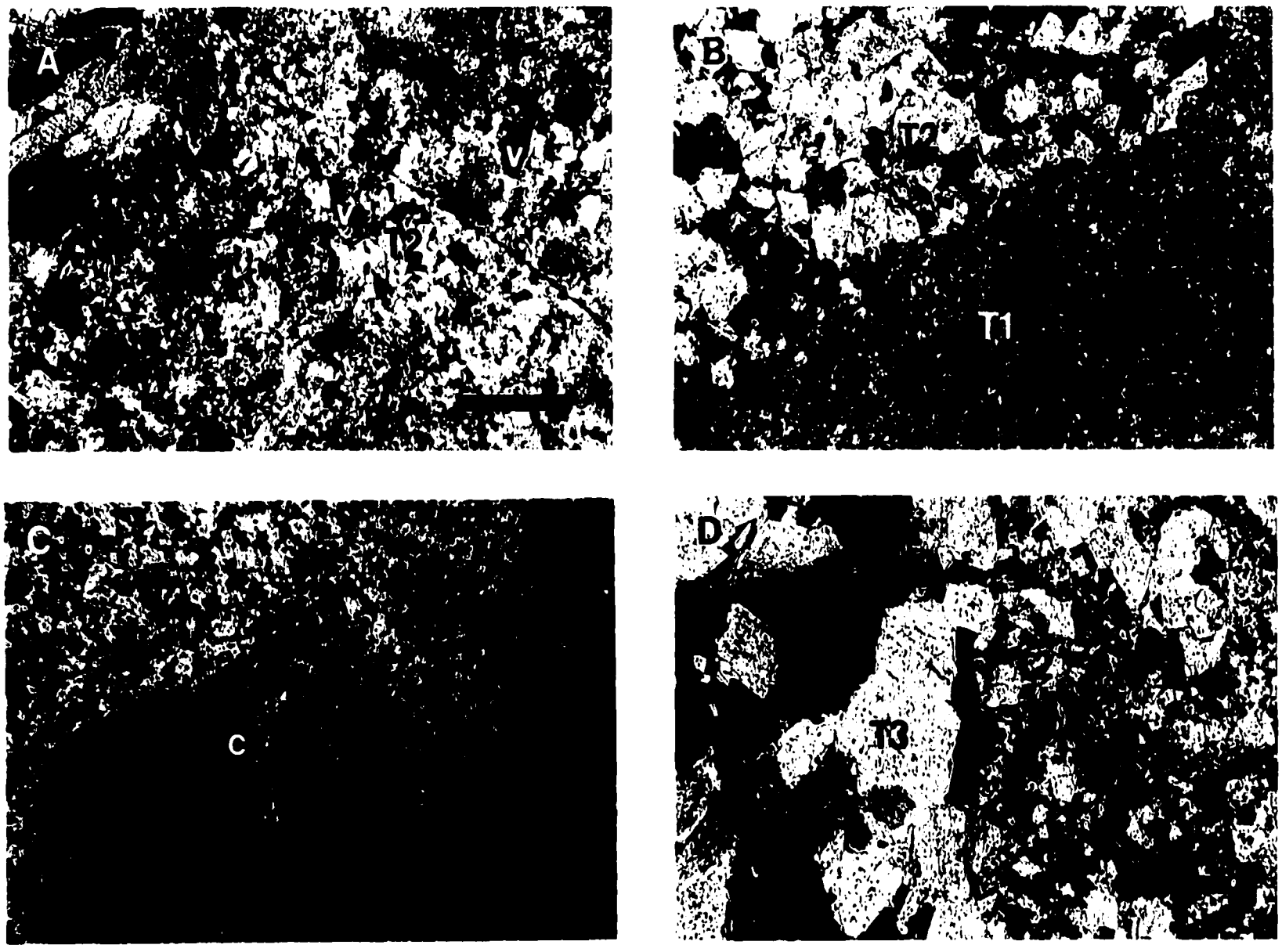



**Fig. 4.7** (p.90) Photomicrographs of replacive dolomite fabric distribution in polished thin sections. **A.** Type 2 dolomite fabric (T2) occurs as patches around vugs (v) in a Type 1 dolomite. Sample W108, crossed-polarized light, scale bar = 1.0 mm. **B.** Sharp stylolitic boundary (st) between Type 1 (T1) and Type 2 (T2) dolomites. Sample W108, crossed-polarized light, scale bar = 0.2 mm. **C.** A Type 1 dolomite patch with a mimetically replaced crinoid fragment (c) is surrounded by Type 2 dolomite mosaics (T2). Sample W86, crossed-polarized light, scale bar = 1.0 mm. **D.** Boundary between Type 2 dolomite (right side) and Type 3 dolomite (left side). Sample W147, crossed-polarized light, scale bar = 0.2 mm.

## 4.6 Dolomite geochemistry

### 4.6.1 Mole % $CaCO_3$

Dolomite mole % $CaCO_3$ histogram shows that most dolomite samples in three types of dolomite are nearly stoichiometric to stoichiometric and there is no obvious relationship between dolomite stoichiometry and crystal size (Fig. 4.9). Type 1 dolomite has 48 to 55 mole % $CaCO_3$ with an average of 51.7 mole % $CaCO_3$ (n=10). Type 2 dolomite varies from 48 to 55 mole % $CaCO_3$ with a slightly lower average of 51.6 mole % $CaCO_3$ (n=22). Type 3 dolomite ranges from 49 to 55 mole % $CaCO_3$ with an average of 52.3 mole % $CaCO_3$ (n=14).

### 4.6.2 Strontium and sodium

Na concentrations in limestones (porous and nonporous; n=12), calcitic skeletal fragments (brachiopod, coral, and stromatoporoid; n=7), calcite cement (fibrous and equant; n=2), replacive dolomite (Type 1, Type 2 and Type 3; n=46), and dolomite cement (replacive and non-replacive; n=8) range from approximately 140 ppm to 55,400 ppm. Samples containing greater than 1600 ppm of Na are excluded since they contain variable amounts of halite cement. Halite-free carbonate samples having approximately 140 to 1600 ppm Na are considered to be valid (Fig. 4.10A). The average Na contents in calcitic and dolomitic samples are approximately 390 and 595 ppm, respectively. Na contents of replacive dolomites and dolomite cements largely overlap Na concentrations in limestone and calcite cement but show a larger range. Na contents of replacive dolomites exhibit no obvious correlation with dolomite type (Fig. 4.10B).

The Sr concentrations of limestones, calcitic skeletal fragments, and calcite cements, vary

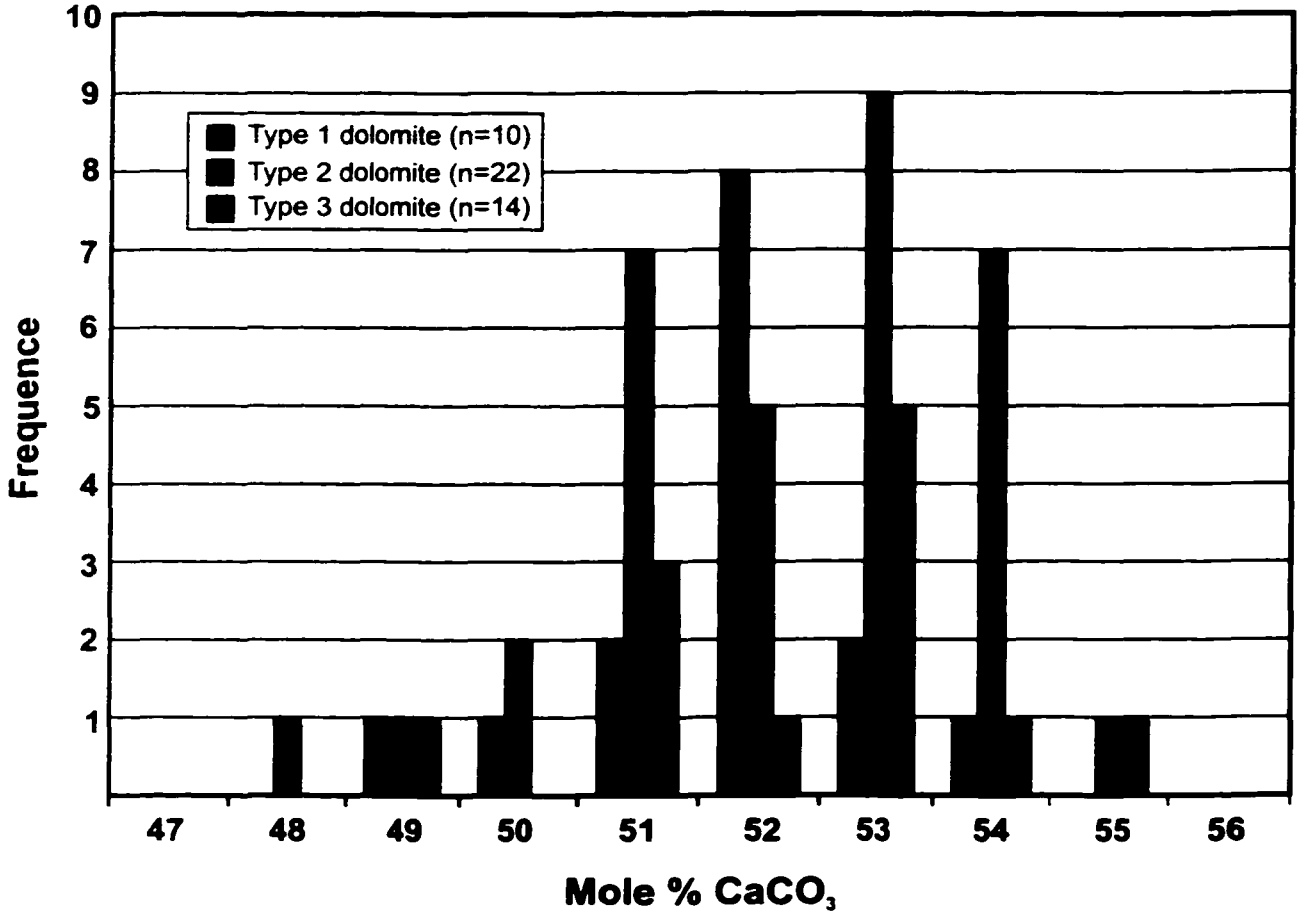



Fig. 4.9 Mole % $CaCO_3$ histogram for Type 1, Type 2 and Type 3 dolomites in the Guelph Formation.

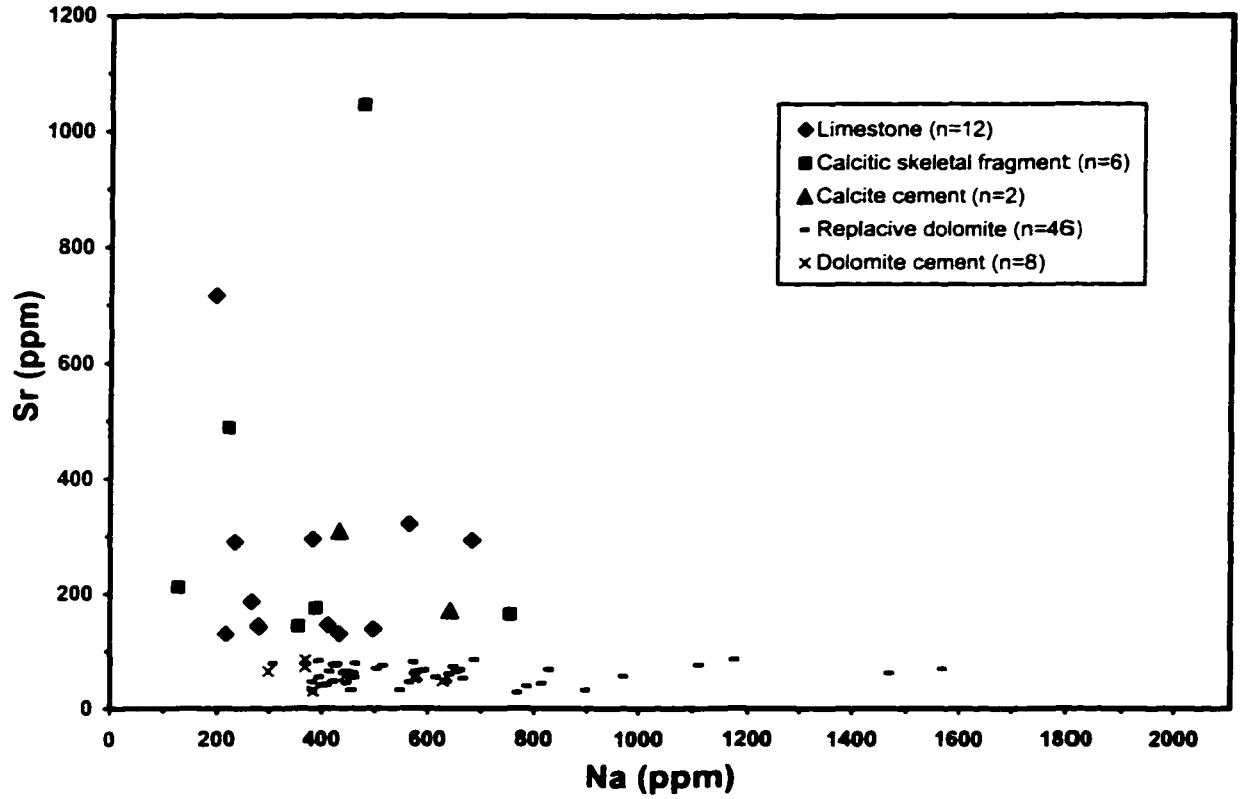



Fig. 4.10A Na vs. Sr for major carbonate fabrics in the Guelph Formation.

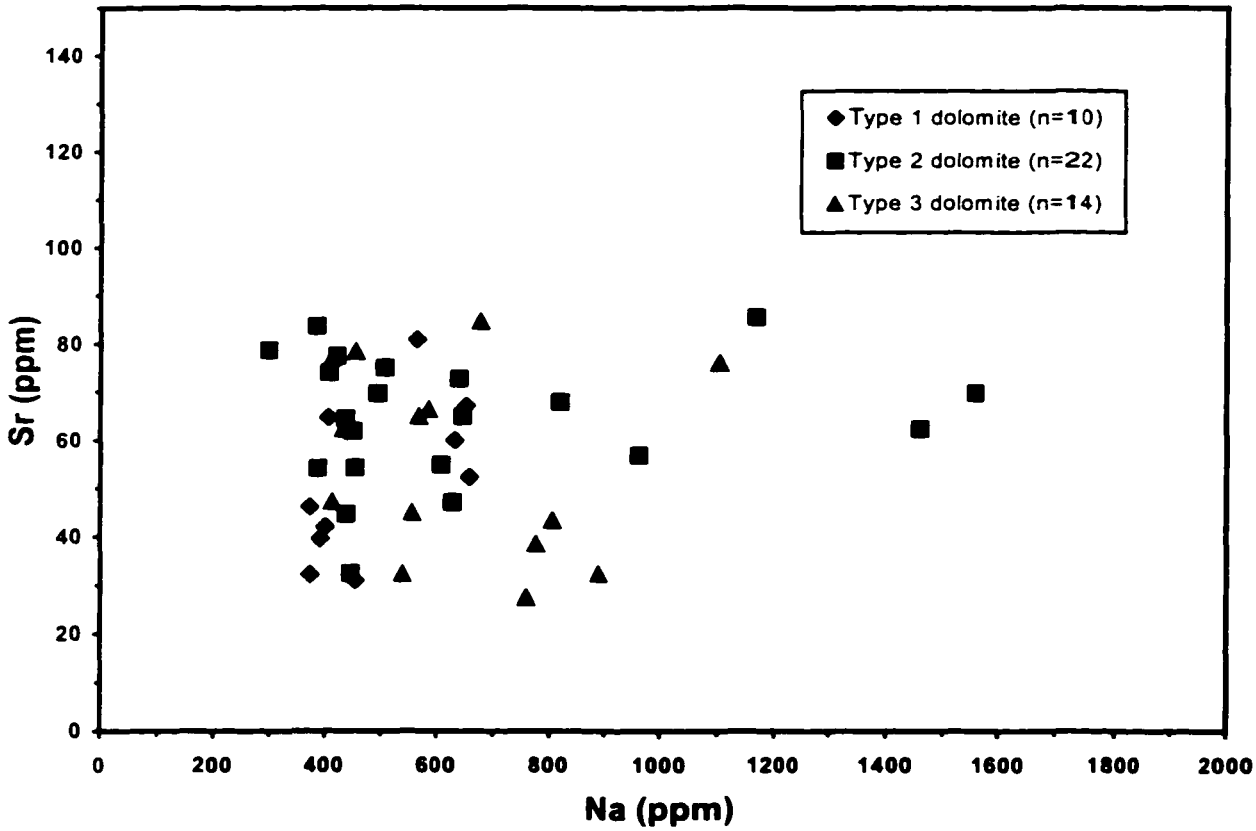



Fig. 4.10A Na vs. Sr for Type 1, Type 2 and Type 3 dolomites in the Guelph Formation.

from approximately 140 to 2050 ppm, with an average of 412 ppm. In contrast, replacive dolomites and dolomite cements show low Sr contents varying in a narrow range from approximately 30 to 85 ppm, with an average of 58 ppm (Fig. 4.10A). This average dolomite Sr content is close to the average value of dolomite (74 ppm) in the Niagara pinnacle reefs of northern Michigan (Sears and Lucia 1980). Guelph replacive dolomites do not show obvious relationship between Sr content and dolomite type (Fig. 4.10B). The correlation between Sr and mole % $MgCO_3$ and between Sr and $\delta^{18}O$ for three replacive dolomites are generally poor (Fig. 4.11A,B).

### 4.6.3 Iron and manganese

Fe contents in limestone, calcitic skeletal fragments, and calcite cement samples range from approximately 105 to 710 ppm with an average of 300 ppm. Mn concentrations vary from approximately 20 to 95 ppm with an average of 50 ppm (Fig. 4.12A). Fe and Mn contents in replacive dolomite and dolomite cement are enriched relative to almost all calcitic samples, ranging from 240 to 3600 ppm and from 50 to 360 ppm, respectively. Type 1 dolomite has relatively low Fe and Mn concentrations of approximately 240 to 1360 ppm (average 781 ppm) and 50 to 200 ppm (average 93 ppm), respectively, whereas Type 2 and Type 3 dolomites show much higher Fe and Mn contents of approximately 500 to 3600 ppm (average 1476 ppm) and 60 to 360 ppm (average 140 ppm), respectively (Fig. 4.12B). Fe and Mn contents of Type 2 dolomite largely overlap with the Fe and Mn concentrations of Type 3 dolomite (Fig. 4.12B). Dolomite cements (replacive and non-replacive) have high contents of Fe and Mn ranging from approximately 1030 to 3120 ppm (average 1839 ppm) and from 90 to 310 ppm (average 193 ppm), respectively.

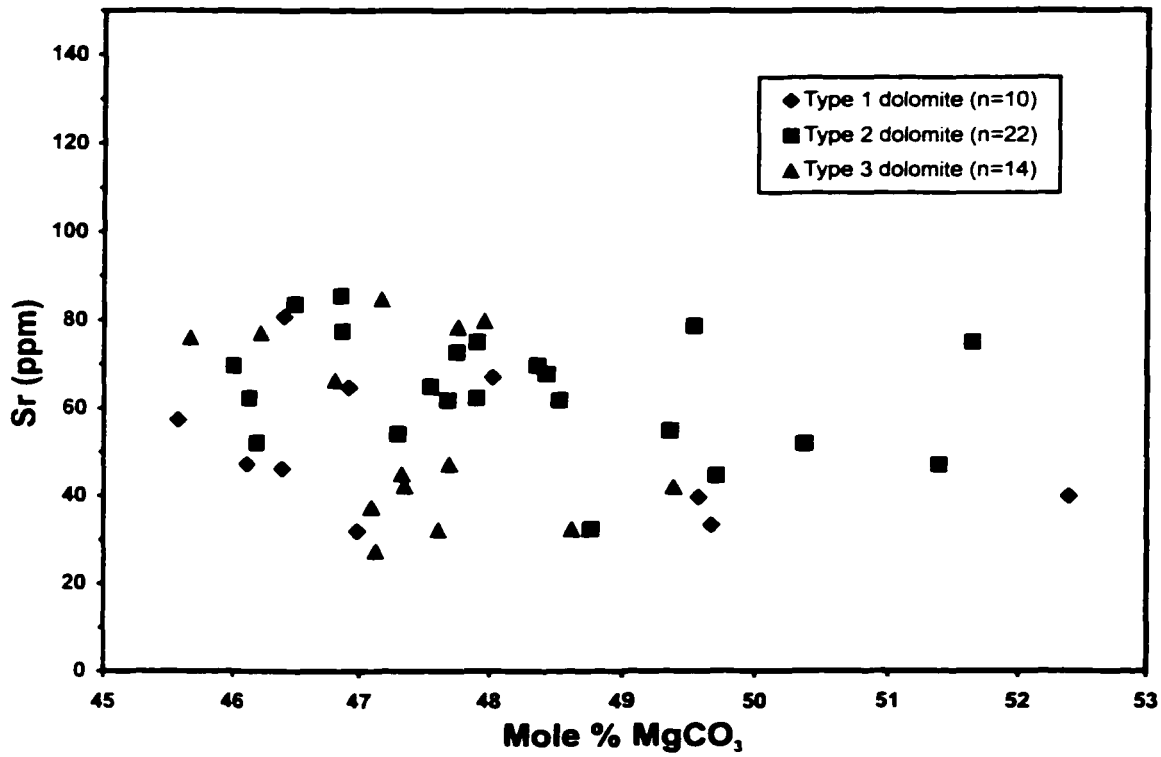



Fig. 4.11B Mole % $MgCO_3$ vs. Sr for Type 1, Type 2 and Type 3 dolomites in the Guelph Formation.

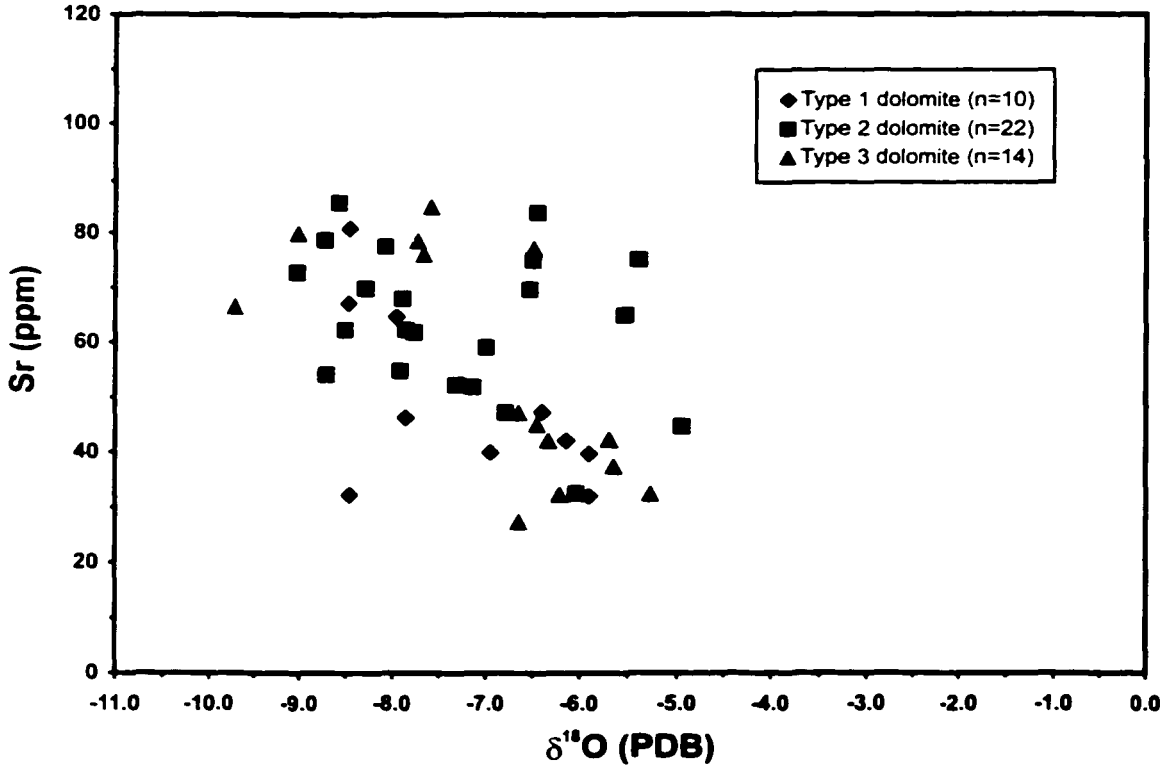



Fig. 4.11B $\delta^{18}O$ vs. Sr for Type 1, Type 2 and Type 3 dolomites in the Guelph Formation.

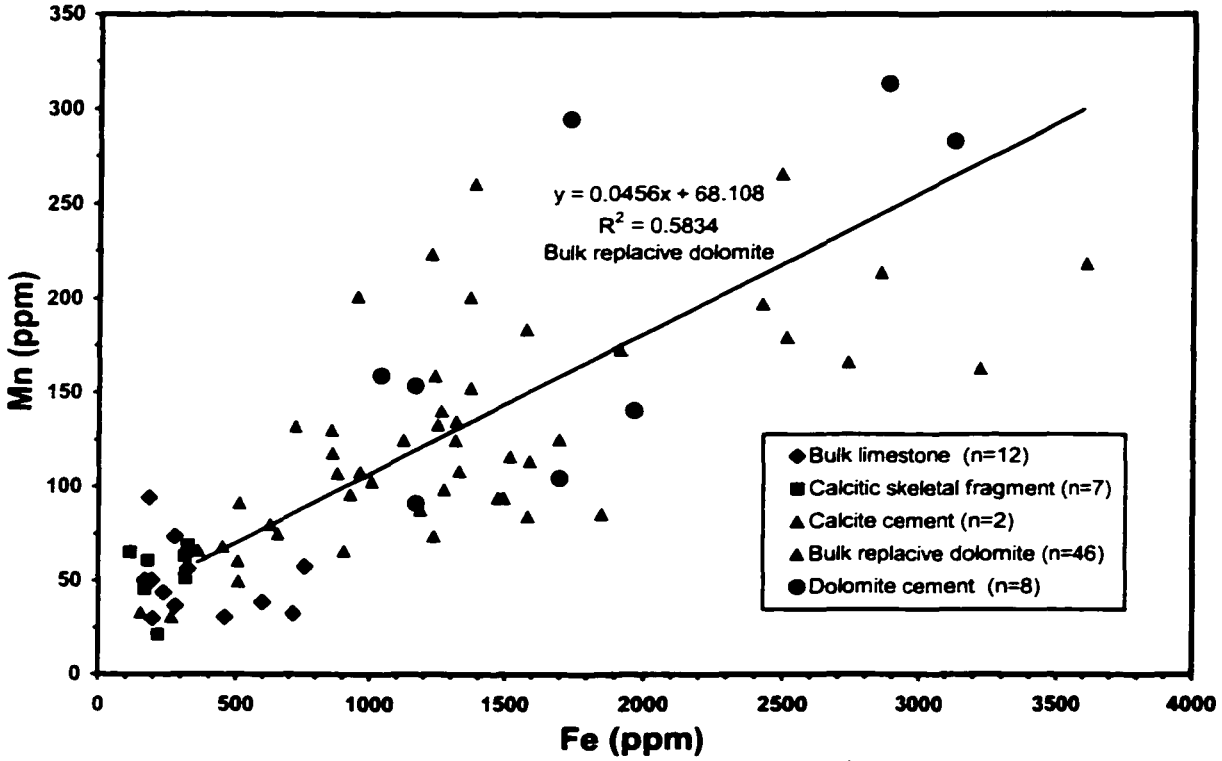



Fig. 4.12A Fe vs. Mn for major carbonate fabrics in the Guelph Formation.

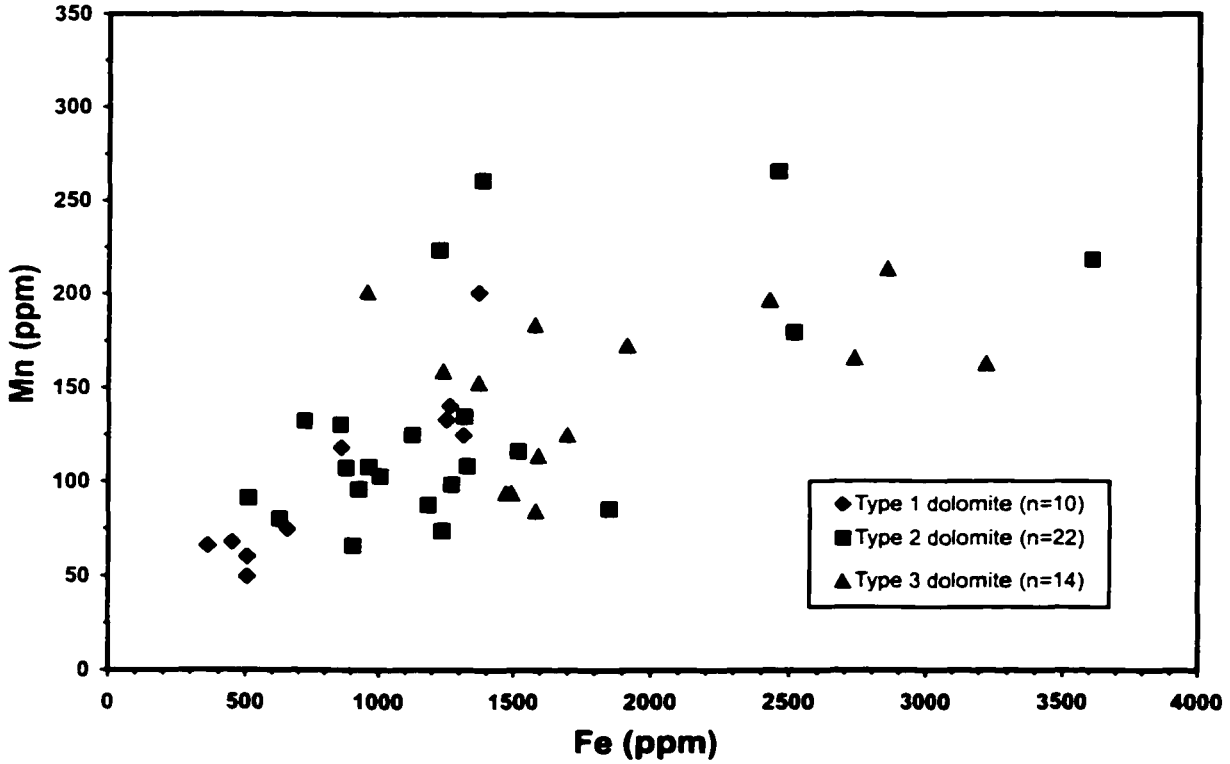



Fig. 4.12B Fe vs. Mn for Type 1, Type 2 and Type 3 dolomites in the Guelph Formation.

### 4.6.4 Oxygen and carbon isotopes

The $\delta^{18}O$ and $\delta^{13}C$ values of samples from limestones (porous and nonporous; n=12), calcitic skeletal fragments (brachiopod, coral, crinoid, and stromatoporoid; n=7), calcite cements (fibrous and equant; n=2), replacive dolomites (Type 1, Type 2, and Type 3; n=46), replacive dolomite cements (n=3), limpid dolomite cements (n=3), and saddle dolomites (n=2) in the Guelph Formation distribute over a relatively narrow range (Fig. 4.13). In the Guelph Formation, the highest $\delta^{18}O$ value of approximately -5‰ (PDB) was encountered in one nonporous limestone and one fossil fragment sample, which is within the estimated $\delta^{18}O$ value range (-3.2‰ to -5.4‰ PDB) for Silurian marine invertebrates and calcite cements (Allan and Wiggins 1993). This most-enriched value (-5‰ PDB) is considered to represent the best preserved and the closest value to the original signature of Middle Silurian marine limestone and used as a base line for interpreting $\delta^{18}O$ values of Guelph carbonates. Three different types of replacive dolomite fabrics exhibit narrow $\delta^{18}O$ and $\delta^{13}C$ value ranges varying approximately from -5‰ to –10‰ (PDB) and from +1‰ to +5‰ (PDB) (Fig. 4.14A). Type 1 dolomite $\delta^{18}O$ and $\delta^{13}C$ values vary from –5.9‰ to –8.5‰ (PDB) (average –7.3‰) and from +1.2‰ to + 4.4‰ (PDB) (average +2.3‰) (Fig. 4.14B); Type 2 dolomite $\delta^{18}O$ values range from –5.4‰ to –9.0‰ (PDB) (average -7.3‰) and $\delta^{13}C$ values from +1.1‰ to +5.0‰ (PDB) (average +3.0‰); and Type 3 dolomite $\delta^{18}O$ values vary from –5.3‰ to –9.7‰ (PDB) (average -7.0‰) and $\delta^{13}C$ values from +1.4‰ to +4.6‰ (PDB) (average +2.5‰). The $\delta^{18}O$ and $\delta^{13}C$ values of both dolomitized preexisting calcite cement and limpid dolomite cement, ranging from –6.5‰ to –9.3‰ (PDB) and from +2.5‰ to +4.1‰ (PDB) are similar to the values of replacive dolomites, but saddle dolomite cements show slightly lower $\delta^{18}O$ and

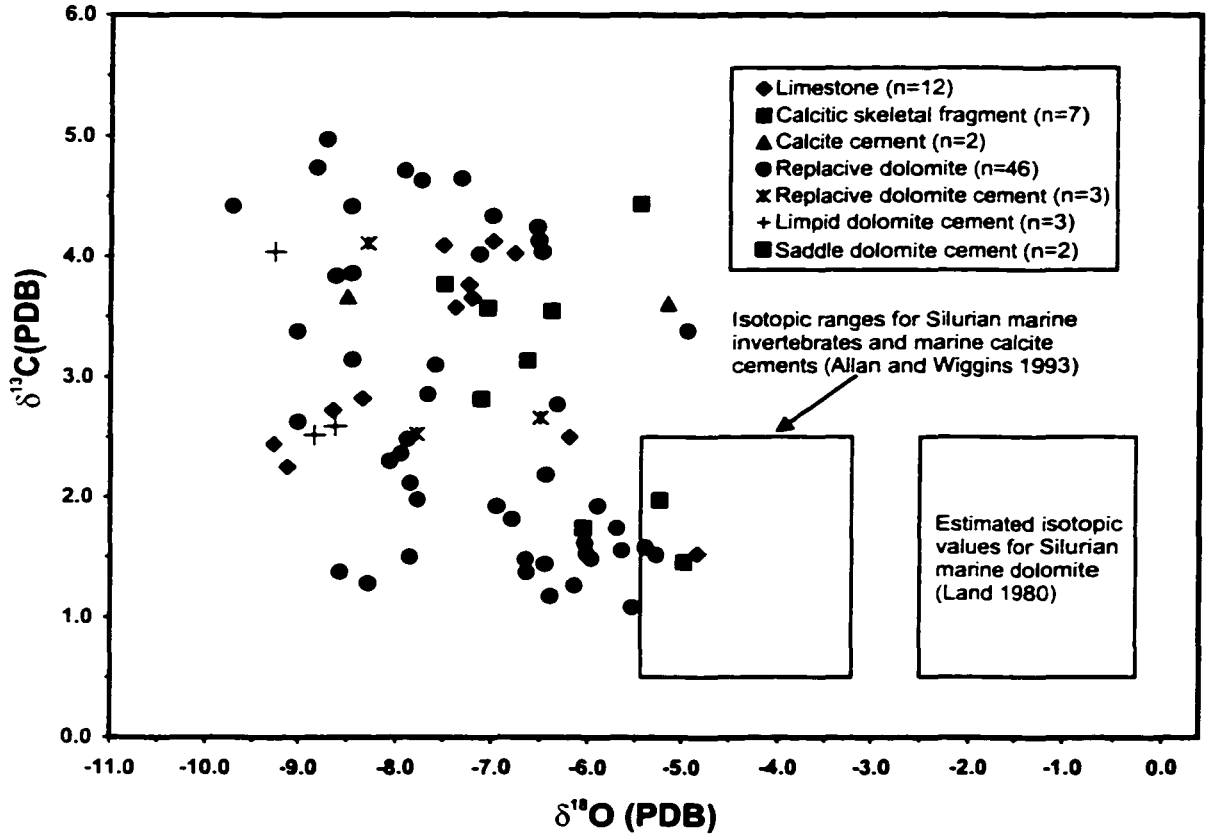



Fig. 4.13 Oxygen and carbon isotopic compositions of major carbonate fabrics in southwestern Ontario.

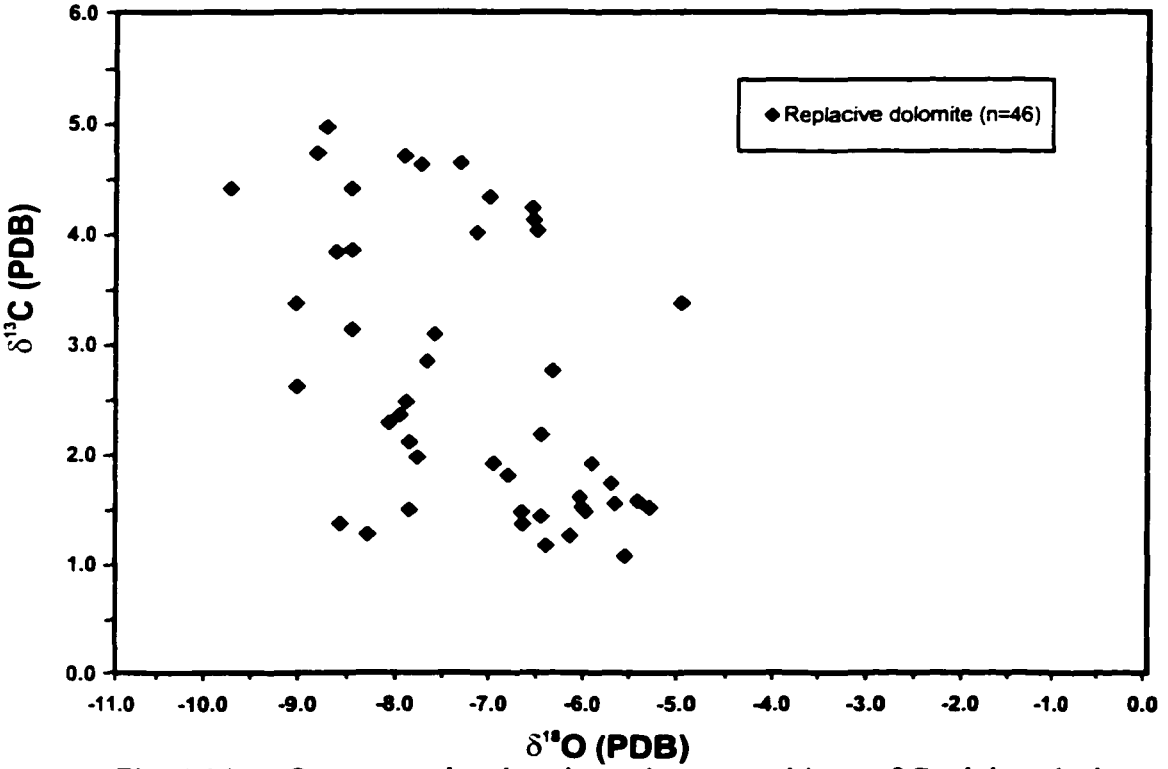



Fig. 4.14A. Oxygen and carbon isotopic compositions of Guelph replacive dolomites in southwestern Ontario.

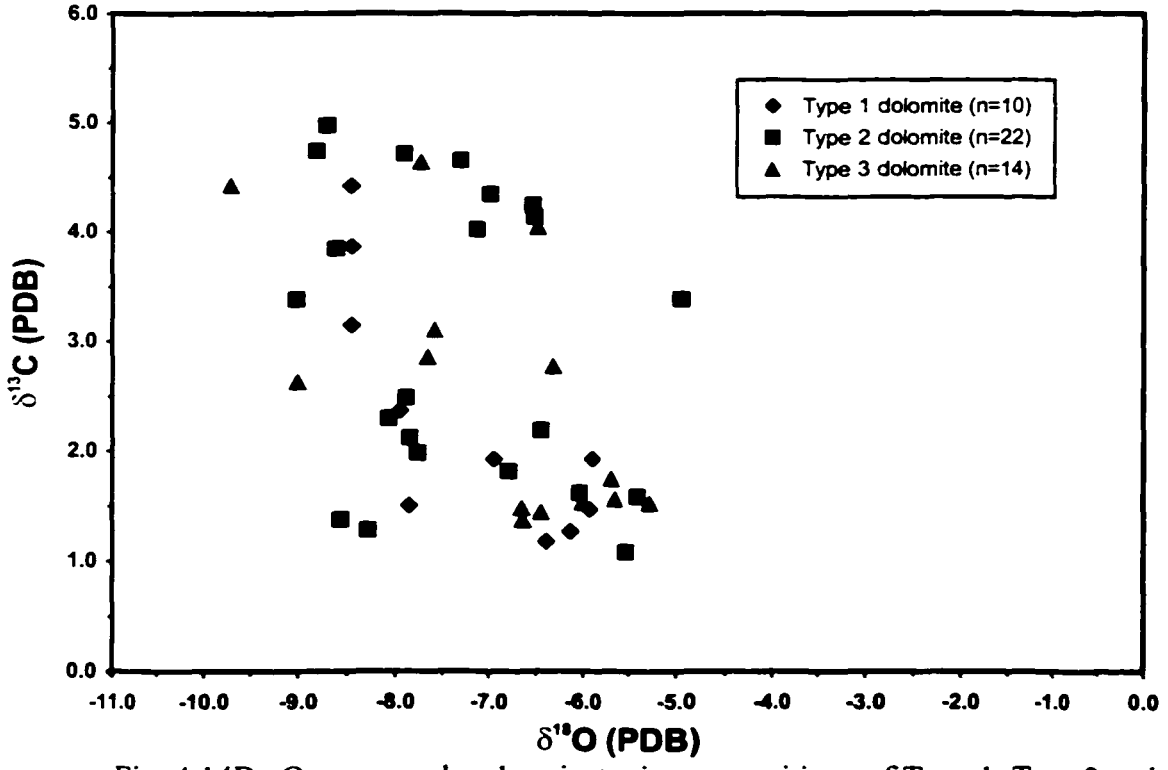



Fig. 4.14B. Oxygen and carbon isotopic compositions of Type 1, Type 2 and Type 3 dolomites in southwestern Ontario.

$\delta^{13}C$ values than these dolomite cements (Fig. 4.13). $\delta^{18}O$ values of replacive dolomites and dolomite cements ranging from approximately -5‰ to –10‰ (PDB) are greatly depleted relative to the estimated values of -3.2‰ to -5.4‰ (PDB) for Silurian marine calcite (Allan and Wiggins 1993) and marine dolomite (Land 1980). Dolomite $\delta^{13}C$ values from approximately +1‰ to +5‰ (PDB) are similar or slightly enriched compared to the estimated marine calcite values of +0.5‰ to +2.5‰ (PDB) (Allan and Wiggins 1993) (Fig. 4.13).

In the study region, $\delta^{18}O$ and $\delta^{13}C$ values of three different replacive dolomites (n=32) from one patch reef and six pinnacle reefs along the dip of the ramp define a general basinward $\delta^{18}O$-decreasing and $\delta^{13}C$-increasing trend (Figs. 4.15 and 4.16). This $\delta^{18}O$ trend does not exhibit obvious correlation with dolomite fabric type and different dolomite fabrics from same reef show similar $\delta^{18}O$ values (Fig. 4.17). Three types of replacive dolomites display weak to strong positive correlation between $\delta^{13}C$ and Mn (Fig. 4.18).

Isotopic compositions of 1 limestone and 10 dolomite samples from the Salina A-1 Carbonate were also analyzed in this study (Appendix II). Their $\delta^{18}O$ and $\delta^{13}C$ values range from –4.7 to –7.9‰ and from +1.5 to +3.7‰ (PDB), respectively (Fig. 4.19), similar to the values in Guelph carbonates determined in this study ($\delta^{18}O$: -5‰ to -10‰; $\delta^{13}C$: +1.5‰ to +4.5‰, PDB) (Fig. 4.14) and close to the values ($\delta^{18}O$: –5.4‰ to –8.3‰; $\delta^{13}C$: +0.1‰ to +3.3‰, PDB; n=53) obtained by O'Shea (1988) from A-1 dolomites in southwestern Ontario (Fig. 4.19).

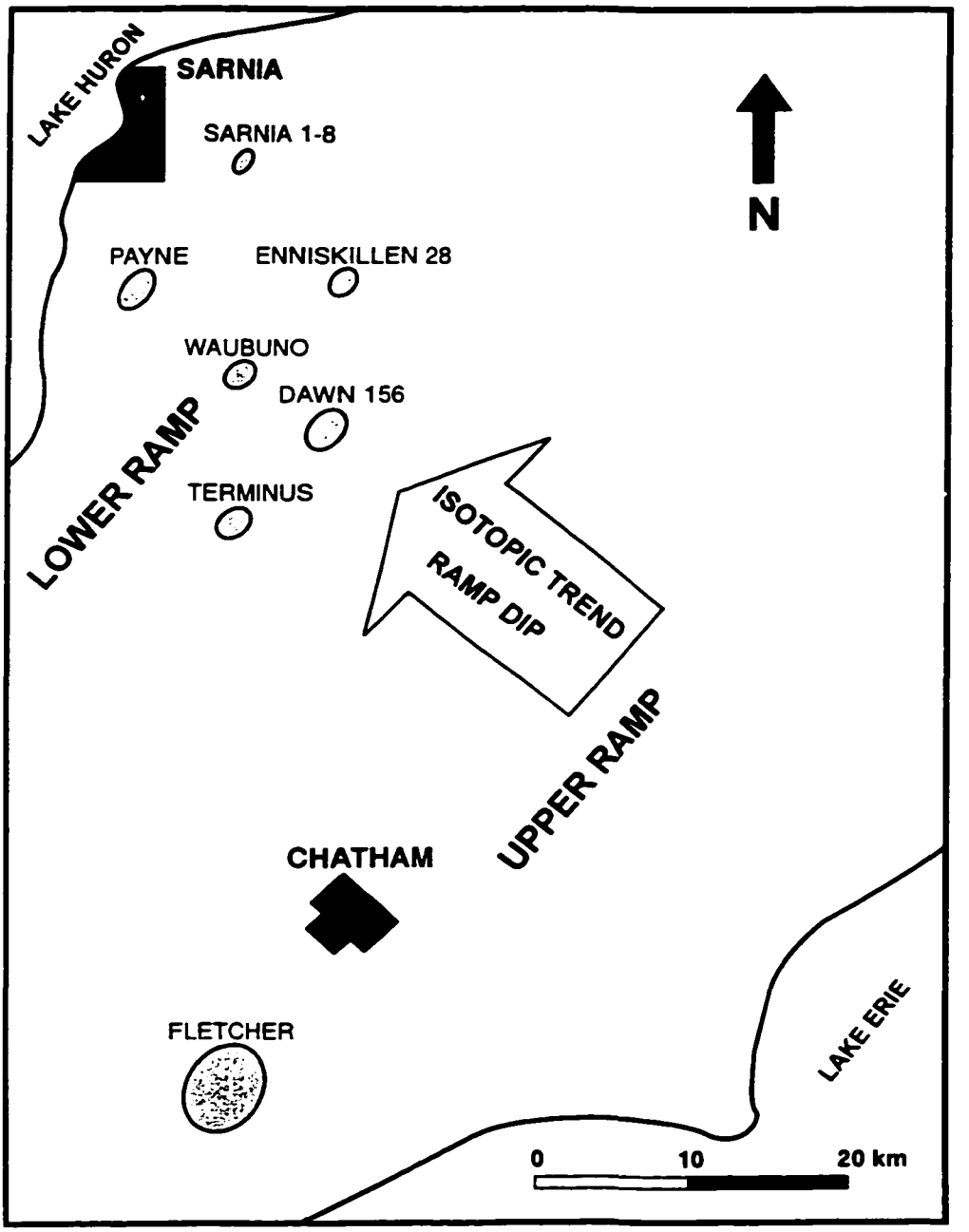



Fig. 4.15 Location map showing the relative location of seven representative reefs on the Middle Silurian ramp in the study area. The oxygen and carbon isotopic values of dolomite from these reefs define a general $^{18}O$-decreasing and $^{13}C$-increasing trend toward northwest or along the ramp dip. The isotopic trend is shown in Fig. 4.16.

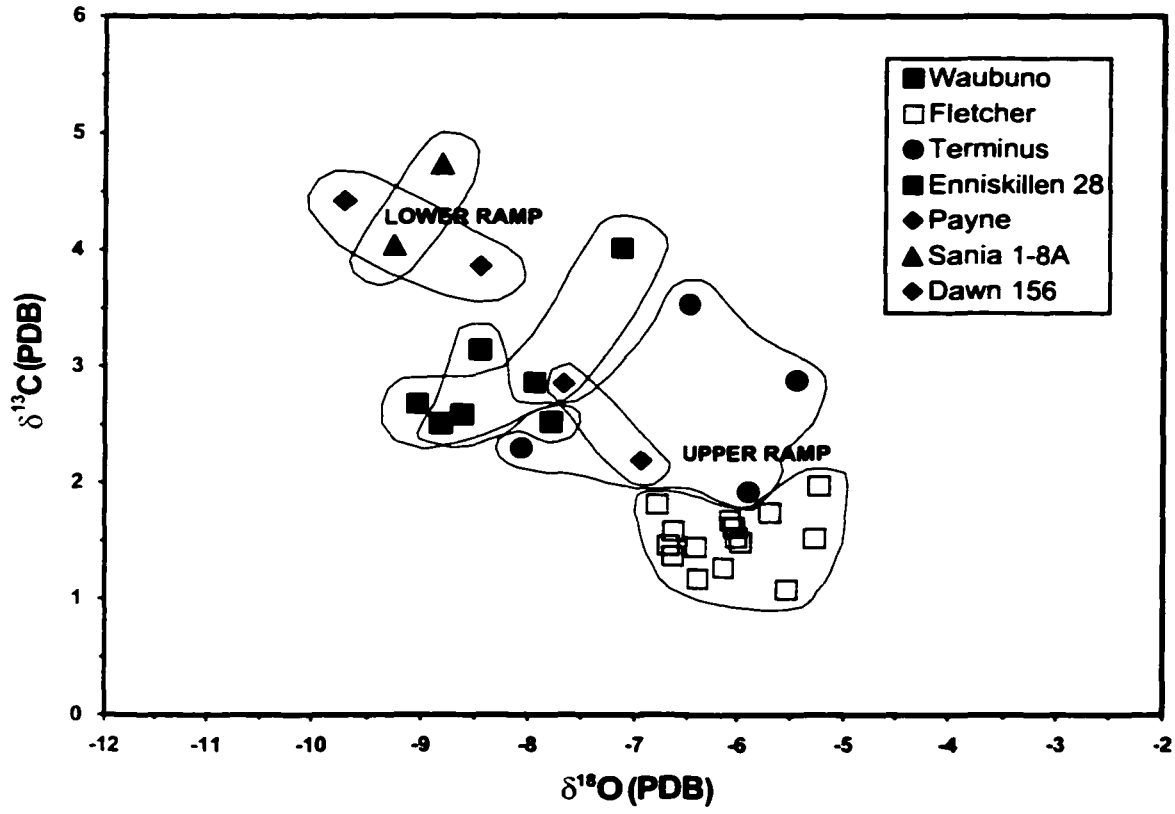



Fig. 4.16 Stable isotopic compositions of Guelph replacive dolomites from seven reefs along the Middle Silurian ramp indicated in Fig. 4.14.

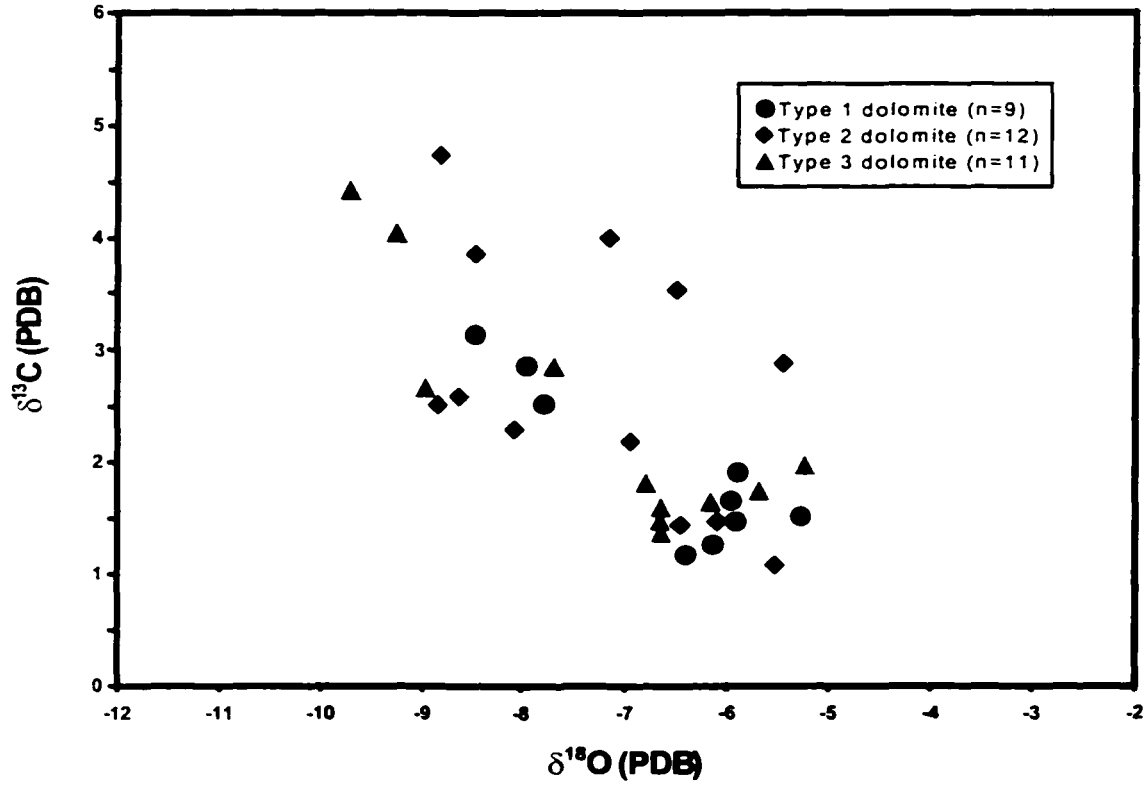



Fig. 4.17 Stable isotopic compositions for Type 1, Type 2 and Type 3 dolomites in seven selected Guelph reefs along the Middle Silurian ramp indicated in Fig. 4.15.

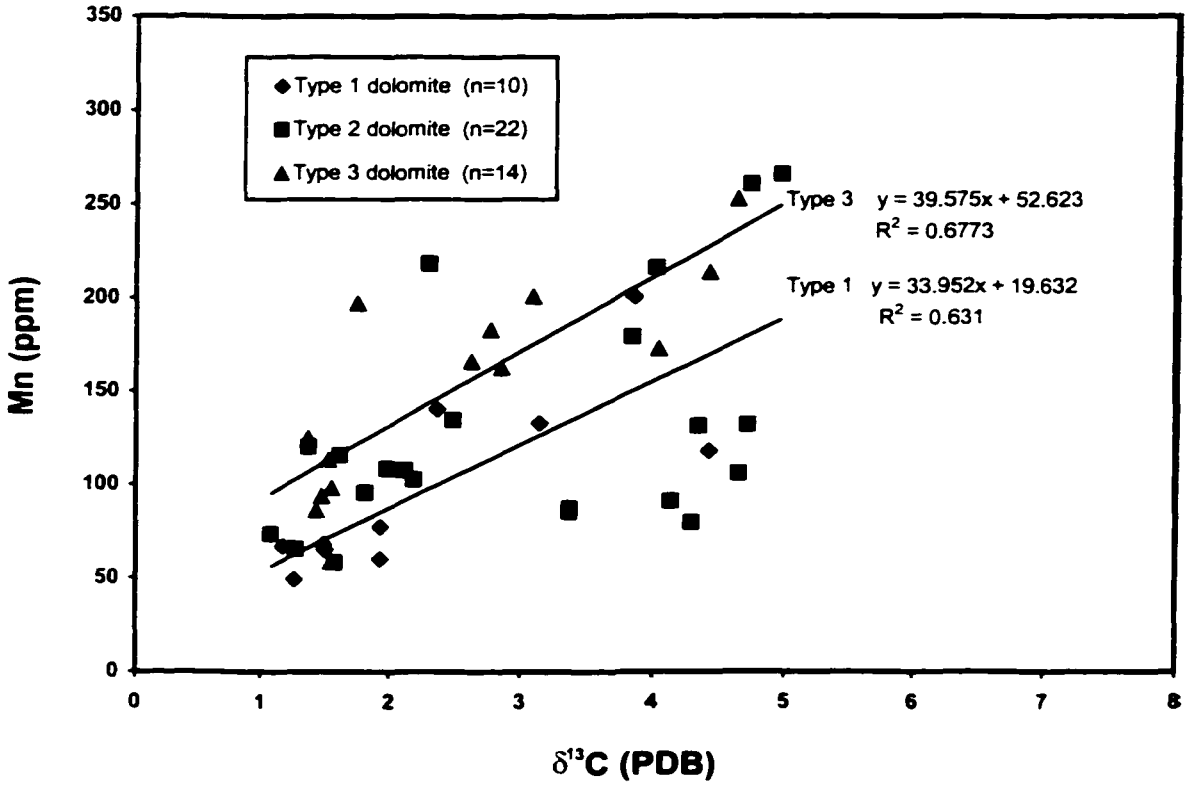



Fig. 4.18 $\delta^{13}C$ vs. Mn for Type 1, Type 2 and Type 3 dolomites in the Guelph Formation.

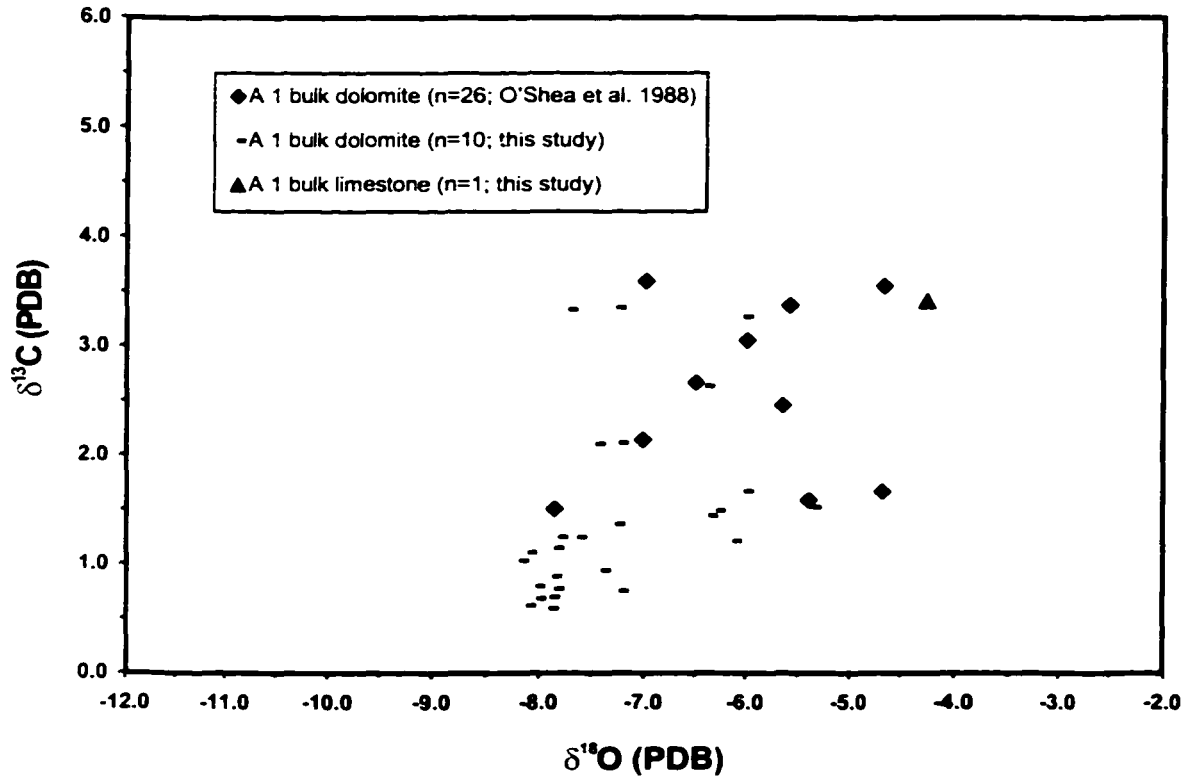



Fig. 4.19 Oxygen and carbon isotopic compositions of A-1 carbonates in southwestern Ontario.

### 4.6.5 Strontium isotopes

The $^{87}Sr/^{86}Sr$ ratios of 3 of 4 calcitic samples, including three limestone and one calcite cement samples, fall within the range of ratios for Middle Silurian seawater (0.70845 to 0.70865; Burke et al. 1982), with one coral skeletal sample in a strongly dissolved limestone having a higher $^{87}Sr/^{86}Sr$ ratio of 0.70870 (Fig. 4.20). The $^{87}Sr/^{86}Sr$ ratios of Type 1 dolomite samples (n=4) vary from 0.70845 to 0.70861 and all fall in the $^{87}Sr/^{86}Sr$ range of Middle Silurian seawater (0.70845 to 0.70865; Burke et al. 1982) (Fig. 4.20). $^{87}Sr/^{86}Sr$ ratios of Type 2 dolomite samples (n=10) vary from 0.70865 to 0.70877 and Type 3 dolomites (n=6) have the highest $^{87}Sr/^{86}Sr$ ratios ranging from 0.70879 to 0.70910. $^{87}Sr/^{86}Sr$ ratios of Type 2 and Type 3 dolomite rocks (0.70865-0.70910) are significantly higher than the coeval seawater, but lower than the ratios of present-day formation waters (0.70908 to 0.70946, average 0.70916, n=10) for Guelph formation brines (McNutt et al. 1987). A plot of replacive dolomite $^{87}Sr/^{86}Sr$ ratio versus Sr content show a generally increase of $^{87}Sr/^{86}Sr$ ratio with increasing dolomite crystal size, although there is no obvious correlation between $^{87}Sr/^{86}Sr$ and Sr (Fig. 4.20). $^{87}Sr/^{86}Sr$ versus $\delta^{18}O$ for three replacive dolomites displays no obvious covariance (Fig. 4.21A), but $^{87}Sr/^{86}Sr$ versus Fe exhibits good correlation for Type 1 and Type 3 dolomites (Fig. 4.21B).

### 4.6.6 Fluid inclusions

15 doubly polished thin sections were used to study fluid inclusions. Measurable two-phase primary inclusions (5-15 μm) in 13 samples including 1 equant calcite, 3 Type 2 dolomite, 2 dedolomite, 3 Type 3 dolomite, 2 saddle dolomite, 1 megaquartz cement, and 1 halite cement, were analyzed for both homogenization and melting temperatures. The homogenization temperatures are not corrected for pressure differences. Fluid inclusions in 2 Type 1 dolomite

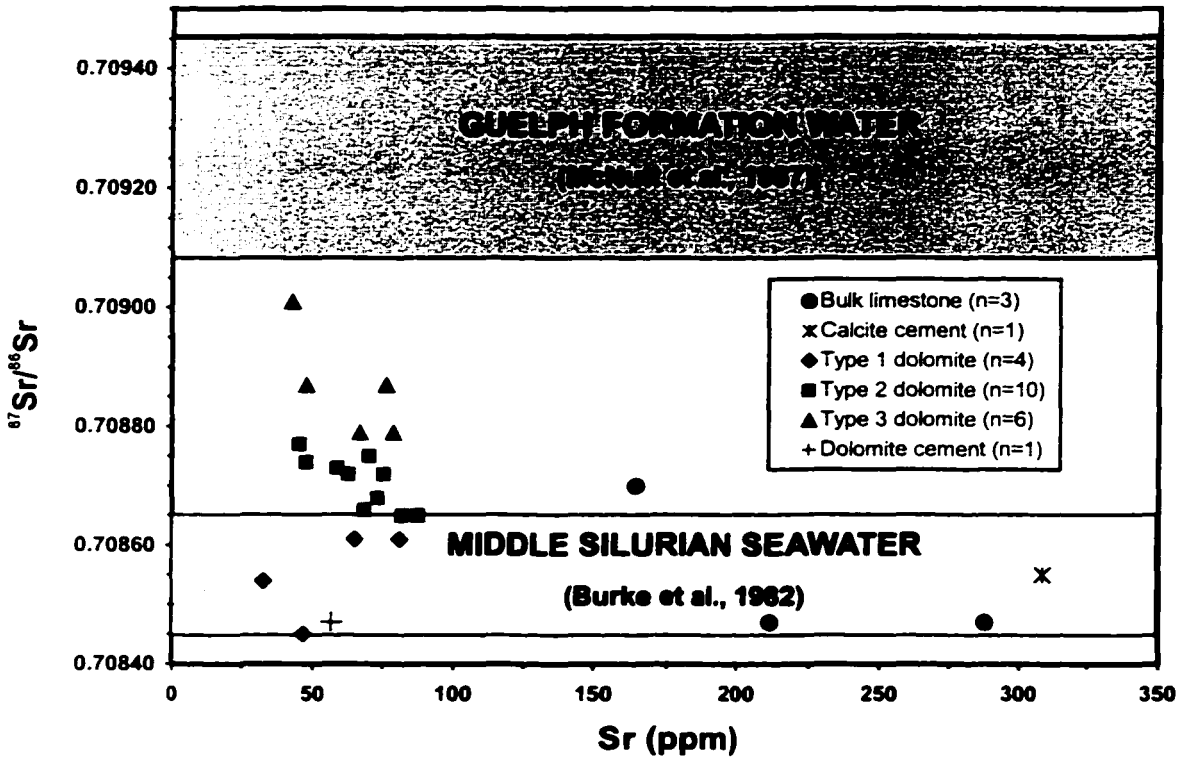



Fig. 4.20 Sr vs. $^{87}Sr/^{86}Sr$ for major calcitic and dolomitic fabrics in the Guelph Formation.

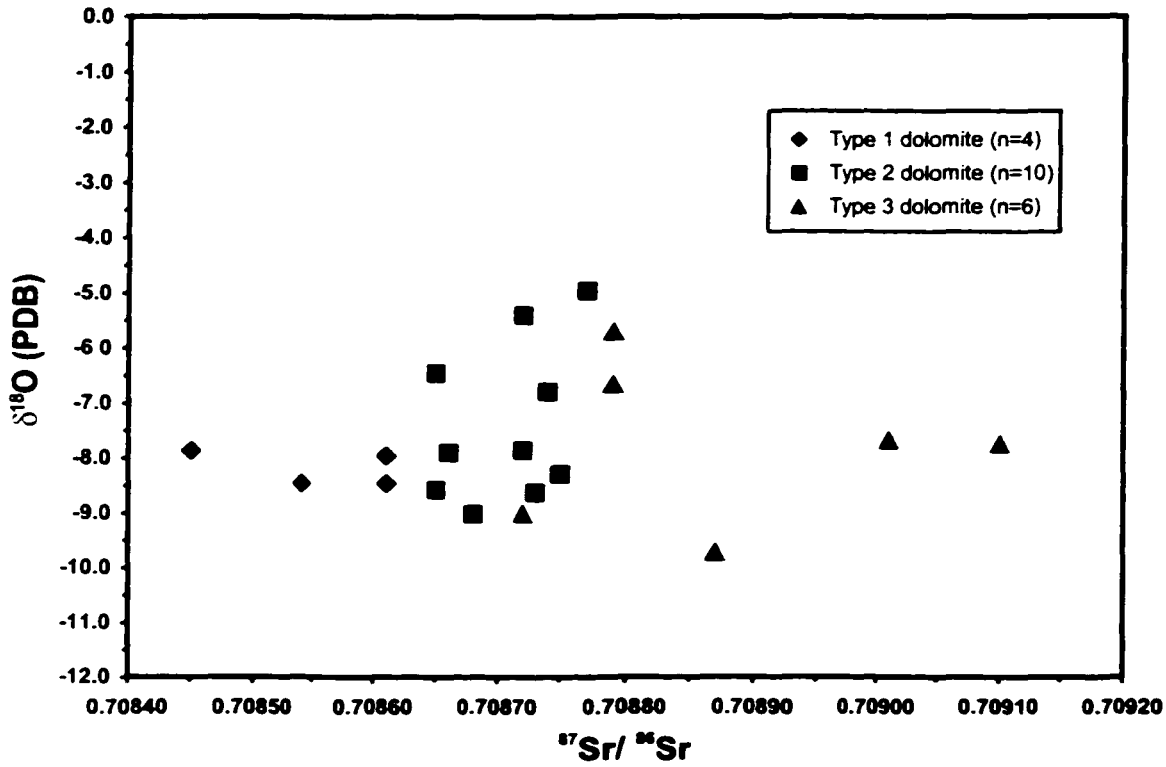



Fig. 4.21A $^{87}Sr/^{86}Sr$ vs. $\delta^{18}O$ for Type 1, Type 2 and Type 3 dolomites in the Guelph Formation.

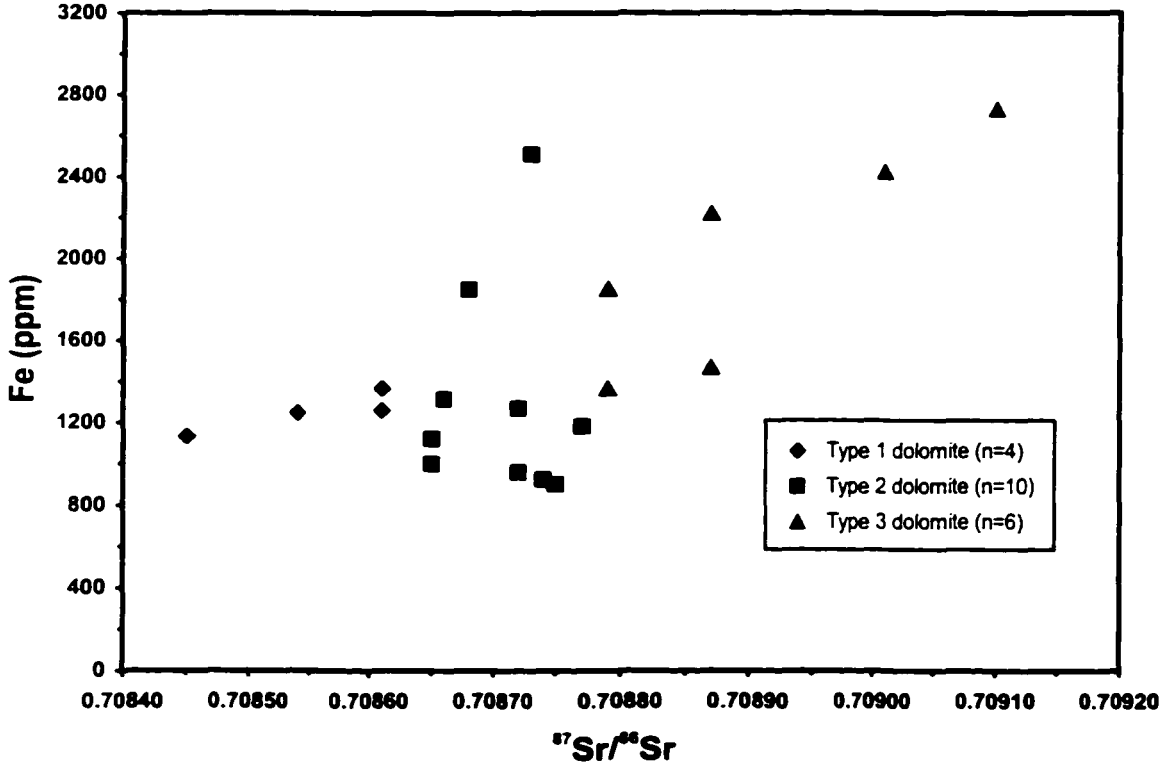



Fig. 4.21B $^{87}Sr/^{86}Sr$ vs. Fe for Type 1, Type 2 and Type 3 dolomites in the Guelph Formation.

samples are too small (< 5 μm) to be measured. The measured homogenization temperatures and melting temperatures are listed in Appendix IV.

Homogenization temperature (Th) values from Type 2 and Type 3 dolomites are in the range of +64.5 to +74.7°C and +95.8 to +116.7°C, respectively (Fig. 4.22). Th readings from saddle dolomite range from +98.7 to +128.2°C. Th values in megaquartz cement vary from +97.2 to +102.3°C.

Initial melting temperature (Te) values of fluid inclusions in Type 2, Type 3, and saddle dolomites range from –28.0 to –47.6°C. Te values in the megaquartz cement vary from –48.2 to –52.3°C. Final melting temperature (Tm) values of Type 2, Type 3, and saddle dolomites range from –9.9 to –32.4°C. Tm values in megaquartz vary from –27.9 to –28.6°C.

## 4.7 Interpretation

### 4.7.1 Dolomite distribution constraints for paleoflow direction

Dolomite distribution patterns and trends in the Guelph Formation and associated A-1 and A-2 Carbonate units provide useful evidence for deducing the paleoflow directions of dolomitizing fluids. The general basinward dolomite-decreasing trend in the Guelph Formation suggests a basinward flow along the Guelph carbonate aquifer on the ramp (Fig. 2.6). The dolomitizing fluids were probably generated in the shelfward back-barrier-reef lagoon environment now represented by the Eramosa Member, the uppermost member of the Lockport Formation. This unit is only present in the shelfward back-barrier-reef and is absent in the study area. Completely dolomitized interreef facies at bottom of the Guelph Formation and preferentially

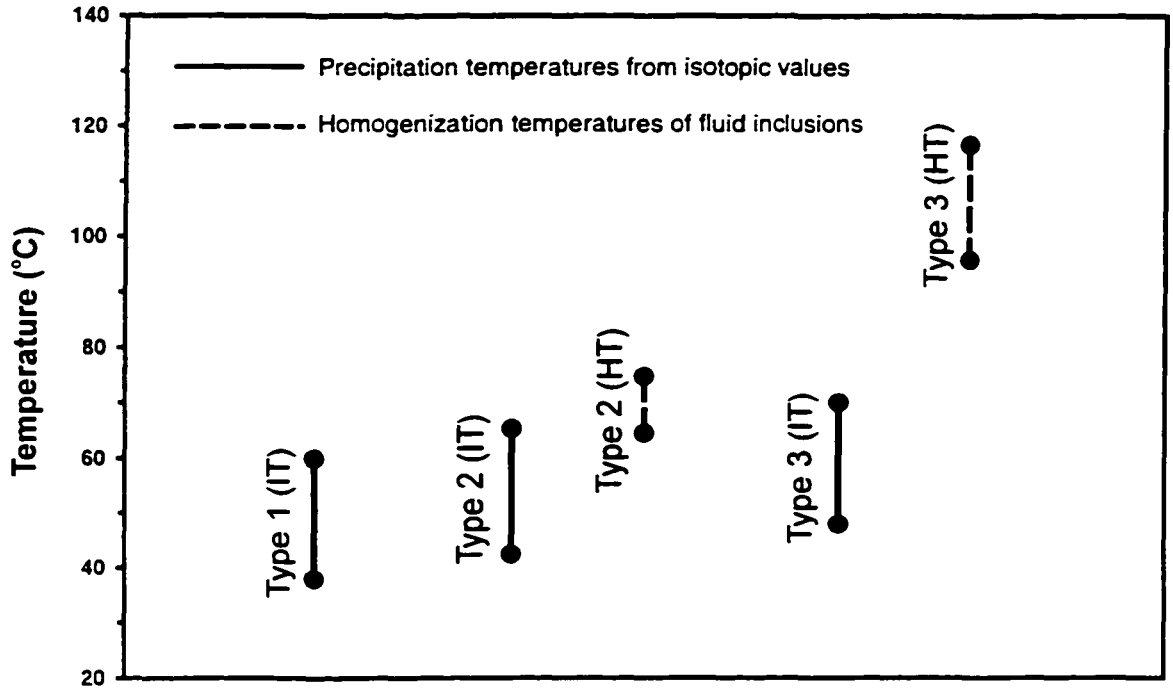



Fig. 4.22 Summary diagram for estimated paleotemperatures for precipitation of three types of replacive dolomites in the Guelph Formation. Solid lines represent temperature ranges calculated from oxygen isotopic values (IT) using Land's (1985) equation and assuming a 30°C surface temperature and a -4‰ (SMOW) of $\delta^{18}O_{water}$ value (see Fig. 4.25). Dashed lines represent temperature ranges estimated from fluid inclusion homogenization temperatures (HT).

dolomitized lower portions in partially dolomitized pinnacle reefs on the lower ramp are inconsistent with a downward reflux of hypersaline waters from the overlying A-1 Carbonate sea as suggested in previous studies (Gill 1977; Sears and Lucia 1980) (Fig. 1.3). Rather, a basinward reflux of dolomitizing fluids through an aquifer developed in bottom interreef facies and the lower portion of reefs can readily explain the dolomite distribution observed in the Guelph Formation (Fig. 2.5, see later discussion for detailed explanation). Local upward flow within individual reefs must have occurred in order to dolomitize the upper portions of the completely dolomitized reefs. The selective dissolution of A-2 and B halite layers above some pinnacle reefs and preferential dolomitization of A-1 and A-2 carbonates immediately surrounding and above the dolomitized pinnacle reefs (Fig. 4.1) also supports upward escape flow through the reefs. Dolomite in A-1 and A-2 carbonate units on the limestone-dominated lower ramp selectively occurs around dolomitized pinnacle reefs. This suggests that the dolomitization of A-1 and A-2 limestones resulted from the same fluids as those for dolomitization of Guelph limestone and the reflux system persisted until after deposition of A-1 and A-2 carbonates.

Why were some basinward pinnacle reefs on the lower ramp left undolomitized or only partially dolomitized? Lack of effective contact with dolomitizing fluids or poor connection with the regional flow system is probably the main reason for the completely undolomitized Rosedale limestone pinnacle reef (Fig. 1.2). Preferably dolomitized lower portions of partially dolomitized reefs likely resulted from insufficient hydraulic head to drive upward flow to the upper portions of the reefs. Alternatively, there may have been poor connection due to the absence of permeable conduits caused by strong calcite cementation. A similar situation occurs

in the Rimbey-Meadowbrook reef trend in the Alberta Basin. Lack of dolomitization in Redwater and Golden Spike reefs within the almost entirely dolomitized reef trend is believed to relate to their poor connection to the reef trend and the flow system (Machel and Mountjoy 1987; Amthor et al. 1993).

### 4.7.2 Petrographic constraints

A paucity of transitions between limestone and pure dolomite and lack of dolomitic limestones in the Guelph Formation in the study area may indicate that dolomitization was a relatively rapid process in an open system, as suggested by Sperber et al. (1984) for other dolomites.

Many microcrystalline dolomite mosaics with mimetic precursor textures, similar to the Type 1 dolomite in the Guelph Formation, have been interpreted by others to indicate high nucleation rates or density of nucleation sites and normally a high degree of dolomite saturation (e.g., Sibley 1982; Purser et al. 1994). Fabric-preserving replacement which characterizes Type 1 dolomite likely resulted from balanced limestone dissolution and contemporaneous dolomite nucleation and growth in a dolomite saturated fluid (Sun 1995). Sibley and Gregg (1987) suggested that microcrystalline mimetic dolomite consisting of tightly packed mosaics of anhedral crystals (<50 μm) was typically formed in near surface to shallow burial, low-temperature (<50°C) diagenetic environments, whereas coarsely crystalline dolomite is commonly formed during deeper burial and at elevated temperatures. The pervasive but fabric-preserving nature of Type 1 dolomite argues that dolomitization likely occurred relatively early when the limestone precursor was still fairly porous and permeable, because extensive replacement needs large amounts of dolomitizing fluid moving through the host rock. In

contrast, late deep burial dolomites are commonly coarsely crystalline, fabric-destructive, crosscut the bedding and commonly contain limestone relicts (Zenger and Dunham 1988; Mountjoy and Amthor 1994).

Type 1 dolomite is similar to the microcrystalline dolomites in several recent studies of ancient platform dolomites (e.g., McManus and Wallace 1991; Mutti and Simo 1994). These dolomites consist of anhedral mosaics with mimetic fabrics and they have been interpreted to represent early replacive dolomites. However, Type 1 dolomites show coarser crystal sizes (20-50 μm) than these dolomites and many reported recent dolomites (commonly < 4 μm) (e.g., Milliman 1974), suggesting that early recrystallization led to an increase in crystal size in Type 1 dolomite. This interpretation of early recrystallization is further supported by the oxygen isotopic data (discussed below). The initial dolomitization may have led pervasive replacement of the Guelph reefal limestones and produced massive mimetic dolomite that was subsequently modified into Type 1 dolomite.

Pseudomorphic and partially dolomitized allochems are considered as diagnostic criteria for replacement of calcite by dolomite. But similar petrographic evidence for dolomite-to-dolomite replacement is not readily observed using conventional transmitted microscopy in the Guelph Formation. Cathodoluminescence petrography, however, is a powerful tool for studying dolomite alteration (e.g., Cander et al. 1988; Dorobek and Filby 1988; Smith and Dorobek 1989; Montañez and Read 1992; Kupecz and Land 1994). The overall CL characteristics of the three Guelph dolomite fabrics vary in a relatively narrow range from very dull orange luminescence in Type 1 dolomite to slightly brighter orange luminescence in Type 2 dolomite

then to brighter orange to reddish luminescence in Type 3 dolomite. But Type 1 crystals have no obvious CL zones that commonly occur in Type 2 and Type 3 dolomites. Some Type 2 and Type 3 crystals show mottled or irregular patchy CL, similar to some other ancient dolomites (e.g., Dorobek and Filby 1988; Smith and Dorobek 1989), and imply partial dolomite-to-dolomite replacement within these crystals. Well-preserved CL zones indicate that dolomite overgrowth played an important role in forming more coarsely crystalline crystals in Type 2 and Type 3 dolomite.

Dolomite crystal size is considered to be primarily controlled by the balance between nucleation rate and growth rate (two kinetic processes) that relate to differences in precursor fabric and mineralogy (aragonite, high-Mg-calcite, or low-Mg-calcite) (Sibley 1981, 1982), micrite content (Vahrenkamp and Swart 1994), bulk chemistry of the dolomitizing fluid and physical conditions, such as temperature (Gregg and Sibley 1984; Sibley and Gregg 1987; Hardie 1987). Generally, high-Mg-calcite and aragonite precursors, fine precursor crystals with high surface area to volume ratio, and highly supersaturated fluids with respect to dolomite, favor high nucleation rate and the formation of microcrystalline and mimetic texture. Dawans and Swart (1988) suggested that finely crystalline mimetic dolomite formed from fast precipitation and coarser crystalline sucrosic dolomite formed from slow precipitation. Under higher than near-surface temperatures, crystal size tends to coarsen with temperature increase (Sibley and Gregg 1987). Dolomite crystal size may provide useful information to interpret dolomite alteration (e.g., Mazzullo 1992; Kupecz et al. 1993). Dolomite crystal coarsening can occur through recrystallization of finer precursors and/or dolomite overgrowth of younger dolomite on earlier cores (e.g., Land 1986, 1991; Sibley and Gregg 1987; Sibley et al. 1993).

Sibley and Gregg (1987) suggested that polymodal (inequigranular) distribution of dolomite crystal size could result from nucleation in an inhomogeneous substrate or multiple nucleation events. In the Guelph Formation, the coexistence of three dolomite fabrics with different crystal sizes, patchy and relict textures, and their crosscutting relationships, support an early dolomite formation followed by later dolomite alteration. The general increase of both dolomite overgrowth and moldic and vuggy porosity with increase in crystal size in Type 2 and Type 3 dolomites suggests that dolomite crystal coarsening in these dolomites is largely related to partial dissolution of earlier dolomite and precipitation of newer dolomite as overgrowth.

The degree of preservation of limestone precursor fabrics in dolomite can indicate the degree of dolomite alteration (e.g., Kupecz et al. 1993). Mimetically replaced allochems are common in modern dolomites but relatively rare in Paleozoic dolomites (Sibley 1982). Pervasively dolomitized Guelph rocks show a full range of textures from well-preserved or mimetic precursor fabric in microcrystalline Type 1 dolomite to complete destruction of fabric in medium-coarsely crystalline Type 3 dolomite. Sedimentary and pre-dolomitization textures were mostly well preserved during initial dolomitization and early recrystallization to form Type 1 dolomite, but further alteration to Type 2 and Type 3 dolomites partially to completely destroyed earlier fabrics.

Most Type 2 and Type 3 dolomites consisting of crystals with cloudy cores and clear rims were probably formed from alteration of Type 1 dolomite and subsequent overgrowth, as a result of changes in pore fluid chemistry (Sibley 1980). Cloudy cores in Type 2 and Type 3 fabrics

show similar dull orange luminescence as Type 1 crystals, suggesting that these cloudy cores probably formed from earlier Type 1 dolomite. Finely to coarsely crystalline cloudy cores showing brighter and patchy CL imply that core dolomites were formed from recrystallization of earlier Type 1 dolomite. Clear rims exhibiting luminescent zones represent later dolomite direct precipitation as overgrowth. Selective partial dissolution of Type 1 dolomite may have provided pore space and material for later dolomite overgrowth.

The occurrence of Type 2 fabric as patches around voids and along fractures in pervasively replaced Type 1 dolomite rocks further supports the interpretation that these Type 2 patches were most likely produced from the alteration of surrounding Type 1 dolomite rather than from directly replacement of limestone. Type 3 dolomites could have formed either directly by non-mimetic replacement of limestone precursor by dolomite or alteration of Type 1 and Type 2 dolomites under higher temperatures, as suggested in recent dolomite studies (Sibley and Gregg 1987; Soussi and M'rabet 1994). Direct replacement of limestone by medium to coarsely crystalline dolomite during deep burial commonly produces limestone relicts (e.g, Mountjoy et al. 1994), but no limestone remains are encountered in Type 3 dolomite in the Guelph Formation. Coexistence of Type 2 and Type 3 dolomite mosaics in the same fossil or clast strongly suggests that Type 3 dolomite resulted from alteration of Type 2 dolomites.

### 4.7.3 Geochemical constraints

#### 4.7.3.1 Stoichiometry

Ca-rich nonstoichiometric compositions in dolomites have been linked to several factors such as bulk chemistry (salinity and Mg/Ca ratio), rapid crystal growth rate, low nucleation rate, and

low temperatures (e.g., Folk and Land 1975; Sass and Katz 1982; Machel and Mountjoy 1986; Hardie 1987; Frisia 1994). Numerous dolomite studies (e.g., Carpenter 1980; Lumsden and Chimahusky 1980; Land 1980, 1985; Sperber et al. 1984; Sibley 1990; Mazullo 1992; Gregg et al. 1992; Vahrenkamp and Swart 1994) have suggested that many originally finely crystalline, calcian metastable dolomites were subsequently altered to more coarsely crystalline, more stoichiometric, thermodynamically stable and less-soluble phases during early to late burial. Alterations of Type 1 dolomite to Type 2 and Type 3 dolomites evidently did not cause significant changes in stoichiometry perhaps due to alteration occurring in a relatively closed or low water-rock ratio system, in which very limited excess Ca was eliminated (Searl 1994). The stabilization from initial calcian dolomite to stoichiometric dolomite in Guelph dolomite likely have taken place through a single early recrystallization (discussed below) as suggested by Sperber et al. (1984) for other dolomites, but not through multiple steps of recrystallization as suggested by Land (1980), since three different dolomite fabrics in the Guelph Formation show a similar range of stoichiometries.

#### 4.7.3.2 Strontium and sodium

The low Sr concentrations in all Guelph dolomites (50 to 100 ppm) are similar to the reported concentrations of generally less than 100 to 300 ppm for many ancient dolomites interpreted to have been precipitated from marine waters (e.g., 40-150 ppm, Machel and Anderson 1989). But these concentrations are much lower than the values of many modern protodolomites (approximately 500 to 700 ppm) precipitated from evaporitic and marine environments (Behrens and Land 1972; Land 1980; Banner 1995). A decrease in Sr content with increasing crystal size is not observed in Guelph dolomites. Such a trend in other studies has been

interpreted to have resulted from dolomite recrystallization in Sr-depleted meteoric waters (e.g., Dunham and Olson 1980; M'Rabet and Soussi 1994).

Sr depletion in replacive dolomites could be related to diagenetic alteration of early-formed dolomite by Sr-depleted meteoric waters or in a lower Sr/Ca ratio fluid (Land 1980, 1985; Gao 1990), low precipitation rates (Katz and Matthews 1977), or precipitation under lower effective distribution coefficients ($D_{sr}$ ranging from less than 0.0165 to 0.060, Jacobson and Usdowski 1976; Katz and Matthews 1977; Land 1980; Baker and Burns 1985; Vahrenkamp and Swart 1990; Banner 1995). The low Sr concentrations in all Guelph dolomites relative to limestones, calcitic skeletal fragments, and calcite cements (Fig. 4.10A), indicate that a large amount of Sr has been removed from the calcitic precursors during earlier dolomitization. Low and similar Sr concentrations in all three types of dolomites (Fig. 4.10B), also suggest that Sr depletion mainly occurred before or during Type 1 dolomite formation.

The Na concentration of dolomite has been suggested to be a useful tool in estimating paleosalinity of diagenetic fluids (e.g., Fritz and Katz 1972; Land and Hoops 1973; Veizer et al. 1978). However, a great amount of Na in dolomite can be derived from brine inclusions and halite solid inclusions (Land 1980), or contamination of bulk samples by halite cement. Based on core and thin section examinations, Na concentrations above 1600 ppm are caused by halite contamination; halite-free dolomite samples have Na contents ranging from approximately 200 to 1600 ppm. These values fall in the reported Na values (approximately 190 to 2750 ppm) for evaporative and marine origin dolomites (Land and Hoops 1973; Sibley 1980; Humphrey 1988). Na contents do not show any obvious correlation with dolomite crystal size. A positive

covariation trend between Na and Ca, which in recent studies (Malone et al. 1996; Lu and Meyers 1998) is interpreted to have resulted from dolomite alteration, is not found in Guelph dolomites.

#### 4.7.3.3 Iron and manganese

Fe and Mn contents in carbonates are mainly controlled by redox conditions (Eh), ion concentrations in precursor rock and pore fluid, precipitation rate, and associated detrital and diagenetic minerals including Fe-Mn oxides and hydroxides, pyrite, and clay minerals (Allen 1980; Bein and Land 1983; Veizer 1983). Incorporation of Fe and Mn into calcite and dolomite require low Eh or reducing conditions to reduce their trivalent or tetravalent states to the divalent states. Fe concentrations (150-1300 ppm) and Mn contents (50-150 ppm) in Type 1 dolomites are largely overlapped by values of Fe (100-700 ppm) and Mn (20-100 ppm) in limestones, calcitic skeletal fragments, and calcite cements (Fig. 4.11A, B). This suggests that pore fluid composition and redox conditions were similar for both limestone lithification and Type 1 dolomite formation and the Fe and Mn in Type 1 dolomites were mainly derived from their limestone precursors.

Recent dolomite studies (Gao 1990; Barnaby and Read 1992; Montañez and Read 1992) have attributed the relative enrichments of Fe and Mn in later dolomites to dolomite recrystallization. Higher content of Fe and Mn in later, coarser dolomites could be related to either enhanced leaching from Fe- and Mn-bearing minerals under relatively reduced conditions (Frank 1982) or higher Fe and Mn distribution coefficients resulting from higher temperatures or slower precipitation rates (Lorens 1981). The distribution coefficient of Sr also

commonly changes with temperature and precipitation rate (e.g., Lorens 1981; Barnaby and Read 1992), but the Sr concentrations in Guelph dolomites do not co-vary with either Fe or Mn contents. Furthermore, the limited variation in dolomite $\delta^{18}O$ values does not indicate a great temperature change. Therefore, higher contents of Fe and Mn in Type 2 and Type 3 dolomites relative to the values of Type 1 dolomites are interpreted to have formed from Fe and Mn-enriched fluids under more reduced conditions. The identical ranges of Fe and Mn contents in both Type 2 and Type 3 dolomites can be attributed to their formation in a similar redox environment or a rock-buffered system.

#### 4.7.3.4 Oxygen and carbon isotopes

The $\delta^{18}O$ values of carbonates are primarily controlled by temperature and oxygen isotopic composition of precipitating fluid (Dickson and Coleman 1980; Veizer 1983; Land 1986). Numerous studies have demonstrated that there have been secular changes in the initial isotopic composition of marine carbonates due to changes in ocean isotopic composition through time (Popp et al. 1986 a, b; Veizer et al. 1986; Walker and Lohmann 1989; Lohmann and Walker 1989; Lavoie 1993). Theoretically, dolomite should show 2-4‰ enrichment relative to the coexisting calcite for isotopic equilibrium exchange in the same fluid (Land 1980). However, the average $\delta^{18}O$ value of Type 1 dolomites (approximately -8.0‰ PDB) is slightly more depleted than the average $\delta^{18}O$ value of calcitic components (bulk limestones, calcitic skeletal fragments, and calcite cements) (approximately -7.0‰ PDB), which is incompatible with isotopic cogenesis or equilibrium. This is consistent with the petrographic observation that dolomitization postdates calcite cementation and limestone lithification.

The depleted $\delta^{18}O$ values of Type 1 dolomites (-5‰ to –8.5‰ PDB) relative to Silurian marine calcite values (-3.2‰ to -5.4‰ PDB) (Allan and Wiggins 1993) is not consistent with a hypersaline seawater origin which commonly produces relatively enriched isotopic compositions in ancient dolomites (e.g., Budai et al. 1987).

The major causes for negative $\delta^{18}O$ values in ancient carbonates have been outlined in several studies (e.g., Hudson 1977; Land 1980, 1983, 1992; Veizer 1983; Lohmann 1988). The dolomite $\delta^{18}O$ depletion in Guelph dolomites is most likely related to later oxygen isotopic exchange with earlier dolomite either at higher temperatures or in lighter $\delta^{18}O$ fluids. The much lighter $\delta^{18}O$ values of calcitic components in the Guelph Formation relative to estimated Middle Silurian marine calcite values (Allan and Wiggins 1993) suggest that Guelph limestones were also modified either at elevated temperatures or by $^{18}O$-depleted fluids.

The involvement of meteoric water is commonly invoked to explain negative $\delta^{18}O$ values in carbonates (e.g., Land 1986), but dolomite precipitation at higher temperatures remains as a most likely explanation for depleted $\delta^{18}O$ values in Guelph dolomites. The mixed water line or coupled depletion of $\delta^{18}O$ and $\delta^{13}C$ suggested for mixing-zone and vadose zone origin carbonates (e.g., Lohmann 1988; Lu and Meyers 1998) is not observed in Guelph dolomite. Furthermore, as mentioned in Chapter 2, the regional paleoclimate and paleogeography of the Middle Silurian in Ontario argue against a large fresh water supply. In addition, the small size of individual pinnacle reefs on the lower ramp were unlikely to experience suitable conditions for receiving substantial amounts of fresh water. Finally, core and petrographic studies and positive $\delta^{13}C$ values (+1.5‰ to +5.0‰ PDB) do not provide evidence to support meteoric

diagenesis in Guelph carbonates.

Sulfate reduction is another possible cause of depletion of $\delta^{18}O$ values in carbonate minerals. Sass et al. (1991) concluded that the depleted $\delta^{18}O$ values in organic-rich (average 10% TOC) carbonates of the Upper Cretaceous in Israel were directly caused by the degradation of organic matter in the sulfate reduction zone during early diagenesis. The potential of $^{18}O$ depletion caused by sulfate reduction would likely have been negligible due to low organic carbon content in the Guelph Formation, although this effect cannot be ruled out. Furthermore, this mechanism can not explain the basinward $\delta^{18}O$-depletion trend.

Oxygen isotopic depletion or enrichment trends associated with crystal size changes (e.g., Gao 1990; Gao and Land 1991; Kupecz and Land 1994) are not observed in Guelph dolomites (Fig. 4.17). The oxygen isotopic values of Type 1 dolomites are interpreted to have been largely retained in later Type 2 and Type 3 dolomites. The alteration of finer Type 1 dolomites to Type 2 dolomite likely occurred in fluids with similar oxygen isotopic composition and temperature. Type 3 dolomite may have formed under higher temperature but in a relatively closed or rock-buffered system.

In the Guelph Formation, the $\delta^{13}C$ values of calcitic components range from +1.5‰ to +3.5‰ (PDB) and the lowest $\delta^{13}C$ values of approximately +1.5‰ (PDB) occur in nonporous limestones. The narrow range of $\delta^{13}C$ values (+2.0‰ to +5.0‰ PDB) in all dolomite fabrics and their identical values to those of calcitic samples suggest that the carbon in the dolomites was mainly derived from seawater. Positive $\delta^{13}C$ values throughout Guelph dolomites also

support a deeper subsurface dolomitization by seawater-dominated fluids, because fresh water involvement and organic-matter oxidation in near-surface vadose and phreatic zones in an arid climate should at least cause depletion of $\delta^{13}C$ values (e.g., Allan and Matthews 1982; Lohmann 1988), although whether this is applicable to Silurian time is uncertain. Slightly enriched $\delta^{13}C$ values in Guelph dolomites may have resulted from the increased input of organically-derived heavier $CO_2$ due to bacterial fermentation of organic matter ($2CH_2O = CO_2 + CH_4$) or methanogenesis (e.g., Irwin 1977; Kelts and McKenzie 1984; Burns et al. 1988; Lohmann 1988). Sears and Lucia (1980) and Cercone and Lohmann (1985) reported similar $\delta^{13}C$ values for Niagaran dolomites in pinnacle reefs of northern Michigan. They interpreted positive $\delta^{13}C$ values to have been caused by a flux of fluids with $^{13}C$-enriched bicarbonate produced by anaerobic methanogenesis in reducing tidal flats during A-1 deposition.

Guelph dolomites and A-1 dolomites show similar oxygen and carbon isotopic compositions (Fig. 4.19), suggesting that both Guelph and A-1 carbonates were likely dolomitized by a common dolomitizing fluid. This is consistent with occurrence of A-1 and A-2 dolomites around dolomitized pinnacle reefs.

#### 4.7.3.5 Strontium isotopes

$^{87}Sr/^{86}Sr$ ratios in carbonate minerals are the direct record of the $^{87}Sr/^{86}Sr$ ratios of precipitating fluids without fractionations caused by temperature or biological influence (Banner 1995). The strontium isotopic composition of seawater has varied with time as result of change in relative influxes of continental and mantle strontium (e.g., Burke et al. 1982). Type 1 dolomites show slightly higher $^{87}Sr/^{86}Sr$ ratios than the ratios of associated limestones

but similar $^{87}Sr/^{86}Sr$ ratios to the Middle Silurian seawater (0.7045-0.7065; Burke et al. 1982) (Fig. 4.20), suggesting that the fluids for Type 1 dolomite formation were derived from seawater.

The $^{87}Sr/^{86}Sr$ ratios of present-day Guelph Formation waters are much higher than the Middle Silurian seawater values, ranging from 0.70908 to 0.70946 with an average value of 0.70916 (n=10) (McNutt et al. 1987) (Fig. 4.20). The elevated $^{87}Sr/^{86}Sr$ ratios in present formation waters were probably caused by diagenetic interaction with siliciclastics and clay minerals within the Guelph Formation (McNutt et al. 1987); by mixing with $^{87}Sr$-rich cross-formation fluids migrated from nearby siliciclastics-rich beds; or intrusion of deep basinal $^{87}Sr$-rich brines which reacted with K-feldspar in Precambrian basement rocks (Harper 1993).

The $^{87}Sr/^{86}Sr$ ratios of Guelph dolomites fall between the lowest values of coeval seawater and the highest ratios of present-day formation water and exhibit a systematic increase with increasing crystal size (Fig. 4.20). This trend is consistent with Type 1 dolomites being modified by more radiogenic, younger formation waters during the formation of Type 2 and Type 3 dolomites. Fe ions were probably also leached from associated detrital minerals at the same time, as suggested by the general covariation trend between $^{87}Sr/^{86}Sr$ ratios and Fe contents in replacive dolomites (Fig. 4.21B).

#### 4.7.3.6 Fluid inclusions

By assuming a commonly accepted geothermal gradient of 2.5°C/100 m (e.g., Hogarth and Sibley 1985; Coniglio and William-Jones 1992; Middleton et al. 1993) and a surface

temperature of 30°C for study area, Th values of +64.5 to +74.7°C in Type 2 dolomite are interpreted to have formed at moderate burial depths of approximately 1400-1800 m. Th values of +95.8 to +116.7°C in Type 3 dolomites are close to the Th values of +98.7 to +128.2°C in saddle dolomite and similar to the Th values of +83°C to +122°C (without pressure correction) reported for late fracture-filling calcite and saddle dolomite from Niagaran pinnacle reefs in northwestern Michigan (Cercone and Lohmann 1987). These high Th values from Type 3 dolomites are compatible with the calculated entrapment temperatures if assuming both extremely high geothermal gradients of 3.5-4.5°C/100 m (a possible hydrothermal event) and a maximum burial depth of 1000 m deeper than present-day depths (Cercone 1984a) occurred in southwestern Ontario during Type 3 dolomite formation. For example, by assuming a geothermal gradient of 3.5°C/100 m and a surface temperature of 30°C, the entrapment temperatures for the maximum burial depths of 1500 to 2000 m (1000 m more than present-day maximum burial) in the study area range from 82.5 to 100°C.

Fluid inclusion data from megaquartz are commonly considered to be more reliable than data from carbonates due to the high potential of stretching and leaking of inclusions in carbonate minerals (Prezbindowski and Larese 1987). Th values in two-phase inclusions in megaquartz cement in the Guelph Formation vary from +97.2 to +102.3°C and are identical to Th values obtained from Type 3 dolomites and saddle dolomite cements.

Te gives an indication of type of salt system in the fluid and Tm can be used to determine the total salinity and ionic strength of the fluid within the inclusion (Crawford 1981). Te values ranging from –27.6 to –52.3°C in all samples are much lower than the eutectic temperature of

-20.8°C in the NaCl-$H_2O$ system, suggesting the existence of Ca and/or Mg ions in the fluid (Crawford 1981). Tm values ranging from -6.2 to –32.4°C indicate that the diagenetic fluids have high salinities varying from 9.5 to 30.7 wt.% NaCl equivalent (Potter et al. 1978) (Appendix IV) and high ionic strengths of ranged from 2.5 to 5, which are several times higher than normal seawater (0.8) (Crawford 1981).

## 4.8 Discussion

### 4.8.1 Dolomitization models

#### 4.8.1.1 Hypersaline reflux models

Hypersaline dolomitization models call upon seepage reflux of denser/heavier hypersaline brines (Adams and Rhodes 1960; Shields and Brady 1995) or evaporative pumping in a sabkha or supratidal zone (Shinn et al. 1965) (Fig. 4.23A). Previous studies (Gill 1977a,b; Sears and Lucia 1980) suggested that dolomitization of Guelph pinnacle reefs resulted from reflux of overlying hypersaline brines in a sabkha or tidal flat during A-1 deposition. However, preferentially dolomitized lower portions of partially dolomitized pinnacle reefs and selectively dolomitized A-1 carbonate around the dolomitized pinnacle reefs in study area do not support an downward reflux. Machel et al. (1996) recently suggested that reflux of hypersaline brines from an overlying evaporating sea is inadequate to explain regional-scale (more than 100 km wide) pervasive dolomitization. Based on mathematical modeling, Kaufman (1994) also concluded that large scale brine reflux on a wide platform (one to a few hundred kilometers wide) requires unrealistically high densities of brines or a basinward progradation of the reflux system. Hypersaline reflux is unlikely to explain the Guelph dolomitization on such a wide ramp, although supratidal dolomitization can not be ruled in the back -barrier-reef lagoon.

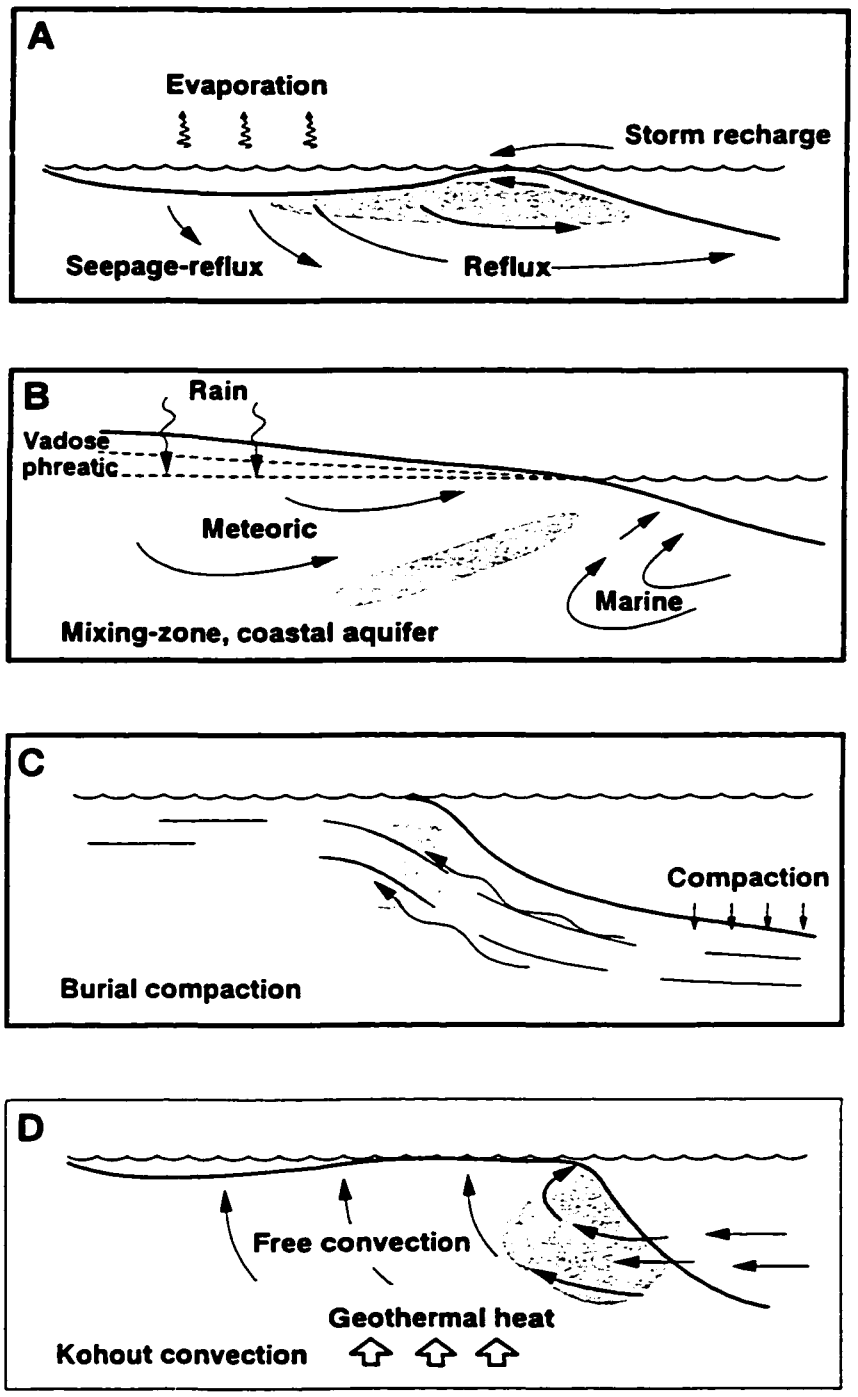



Fig. 4.23 Dolomitization models (after Land 1985, Tucker and Wright 1990).

#### 4.8.1.2 Mixing-zone models

Mixing-zone models are based on the hydrodynamic flow in the transition zone between freshwater and seawater in island and coastal platform settings (Hanshaw et al. 1971; Ward and Halley 1985; Fig. 4.23B). For Guelph dolomites, the main problem in invoking a mixing-zone origin is the source of fresh water in a semi-arid to arid climate during the late Silurian, although some previous studies (Gill 1977a,b; Sears and Lucia 1980; Bay 1983; Smith et al. 1993) suggested that a significant fresh water influence was established during exposure of reefs that were far away from land. In addition, strontium isotope and fluid inclusion data do not support any significant influence of fresh or mixing water. Several recent reviews (Machel and Mountjoy 1986; Hardie 1987; Sun 1994) have suggested that extensive pervasive dolomitization of platform carbonates, like those that comprise most of the Guelph Formation, generally is unlikely to take place in coastal meteoric-marine mixing zones.

#### 4.8.1.3 Burial compaction models

Burial compaction models can involve connate seawater expelled from adjacent sediments by burial compaction or basinal brines driven by sedimentary loading and/or tectonic compression (Mattes and Mountjoy 1980; Gawthorpe 1987; Mountjoy et al. 1994; Fig. 4.23C). For Guelph dolomites, the main problem in Jodry's (1969) compaction model for dolomitization of pinnacle reefs is the amount of connate water in the surrounding sediments. A shelfward compaction flow model might be suitable for other ancient dolomites (Schofield and Adams 1986; Gawthorpe 1987), but it can not explain the basinward dolomite-decreasing trend in the Guelph Formation and the lack of dolomite in the centre of the Michigan Basin. Another problem is that limestone relicts are commonly found in burial dolomites due to low

permeability at deeper burial conditions (e.g., Zenger and Dunham 1988; Mountjoy et al. 1994). Theoretically, a compaction-driven water supply from surrounding sediments is very limited in magnitude and duration relative to the fluid volume and time needed for regional pervasive dolomitization (Shi and Wang 1986; Bjørlykke 1993). Recently, the compaction model based on burial compaction of sediments has been broadened to include tectonic compression (Qing and Mountjoy 1994; Mountjoy et al. 1994; Machel et al. 1996), pressure solution (Barnaby and Read 1992), and topographically-driven flow (Amthor et al. 1993) for regional-scale dolomitization. These broadened models could also likely be applied to Guelph dolomites in southwestern Ontario (discussed below).

#### 4.8.1.4 Seawater and modified seawater models

Land (1985, 1991) suggested that dolomitization by seawater may be more common than is currently recognized and that modified seawater could be a more effective dolomitizing agent than surface seawater. Some recent studies of massive dolomitization (e.g., Land 1985; Given and Wilkinson 1987) favor early dolomitization by seawater or modified seawater due to the availability of Mg, an effective delivery mechanism, relatively permeable limestone host rock, and the distribution patterns of dolomite in carbonate platforms. Seawater and modified seawater models were invoked to explain pervasive dolomitization in many subtidal to subsurface environments (e.g., Sass and Katz 1982; Land 1985, 1991). Although seawater is supersaturated with respect to dolomite and thermodynamically dolomite should precipitate from seawater, seawater has to become modified in order to overcome the kinetic barriers such as magnesium hydration for acting as a dolomitizing agent for extensive dolomitization (Lippman 1973; Machel and Mountjoy 1986). The kinetic barriers could be overcome under

higher temperatures and perhaps over prolonged time periods (Hardie 1987).

Seawater is considered to be the only suitable and widely available dolomitizing fluid to supply the magnesium for the massive dolomitization that occurred in the Guelph Formation. Strontium isotope data from Type 1 dolomite support the interpretation that the Guelph Formation was dolomitized by normal or nearly normal Silurian seawater. Depleted oxygen isotopic values in Type 1 dolomite indicate that the Guelph Formation was dolomitized at elevated temperatures or under shallow to moderate burial conditions. Another important factor for subsurface seawater dolomitization is the existence of an active groundwater flow system during burial. Continuous flow through relatively permeable limestone could carry the required amount of Mg into and bring extra Ca out the reaction sites and allow dolomite nucleation and complete replacement.

#### 4.8.1.5 Thermal convection models

Large-scale circulation of seawater into platform margins under a geothermal convection system was proposed by Kohout (1967) (Fig. 4.23D). Kohout convection is induced by the horizontal density gradients between cold ocean water and geothermally heated groundwater within the platform. Seawater is drawn into the platform margin where it replaces warmer and lighter groundwater, which moves upward as springs on the platform or along its margin (Kohout 1967). Simms (1984) expanded this model to include isolated platforms and atoll reefs that are not in hydrologic communication with a groundwater flow system and applied this transportation mechanism to dolomitization. Mathematical modeling suggested that such open thermal convection, if operating for long periods of time, could pump large amounts of

seawater through the platform and supply sufficient Mg for massive dolomitization (Simms 1984). Thermal convection of seawater was invoked as the main pumping mechanism for dolomitization in several atolls or isolated platforms developed on volcanic basements or associated with volcanic rocks (e.g. Saller 1984; Aharon et al. 1987; Hein et al. 1992). In Enewetak Atoll in the Pacific, Saller (1984) suggested that subsurface seawater convection driven by higher heat flow related to volcanic basement of the atoll, caused dolomitization of Eocene carbonate strata at burial depths rang from 1200 to 1400 m since the early Miocene. In the seawater thermal convection model, basinward platform-margin facies should be preferentially dolomitized but shelfward platform-interior facies would only be partially dolomitized or remain undolomitized (Tucker and Wright 1990). This prediction clearly does not agree with the observed dolomite distribution in the Guelph Formation.

Recently, Wendt et al. (1998) proposed a 'thermoflux' model to explain subsurface (a few hundred meters to 1700 m) dolomitization in the Devonian Swan Hills platform in Wild River area of west-central Alberta. This model combined seawater seepage-reflux and subsurface thermal convection of hypersaline brines to explain the origin of saddle-like replacive dolomites and saddle dolomite cements with high homogenization temperatures of 84.5 to 179.7°C and low final melting temperatures of -17.2 to –22.4°C. They argued that the seepage-reflux system supplied Mg through both porous strata and fault conduits and the thermal convection system was driven by a hydrothermal event during Cretaceous time, providing a long-lasting circulation system for complete replacement. However, it is also possible that Wendt et al.'s (1998) saddle-like dolomites may have resulted from subsequent alteration of earlier formed dolomite in geothermal fluids during later burial. Under deeper

burial conditions, thermal convection could cause extensive dolomite-to-dolomite alteration in a relatively closed system without significant Mg input, since the direct source for newer dolomite is pre-existing dolomite.

#### 4.8.1.6 Hydrologic system for Guelph dolomitization

Interpretation of regional replacive dolomitization is not only a chemical problem, but also a hydrologic problem (Machel and Mountjoy 1986). Recent dolomite studies (e.g., Land 1991; Amthor et al. 1993) suggest that the most important condition for regional replacive dolomitization is a regional-scale flow system.

A regional topography-controlled, gravity-driven flow system (Fig. 4.24), similar to the model described by Garven (1985) and Kendall (1989) readily accounts for many of the features observed in the Guelph Formation. In addition, massive dolomitization of a carbonate platform in an arid climate may have been encouraged by a progressive lowering of sea level (e.g., Coniglio et al. 1988; Tucker 1993). Maiklem (1971) presented a hydrological and diagenetic model based on the evaporative drawdown within the evaporative Elk Point Basin. He concluded that sea level dropped at least 30 m (100 ft) soon after termination of reef development as a result of the development of an almost closed reef barrier around the basin and strong evaporation. In northern Michigan, Cercone (1988) suggested the possibility of regional dolomitization of Niagaran reefs caused by a flow system related to evaporative drawdown. She listed several lines of evidence to support her interpretation that subsurface dolomitization occurred in response to a groundwater flow induced by evaporation drawdown, including the absence of the commonly occurring Mg-rich mineral carnallite in A-1 Evaporite

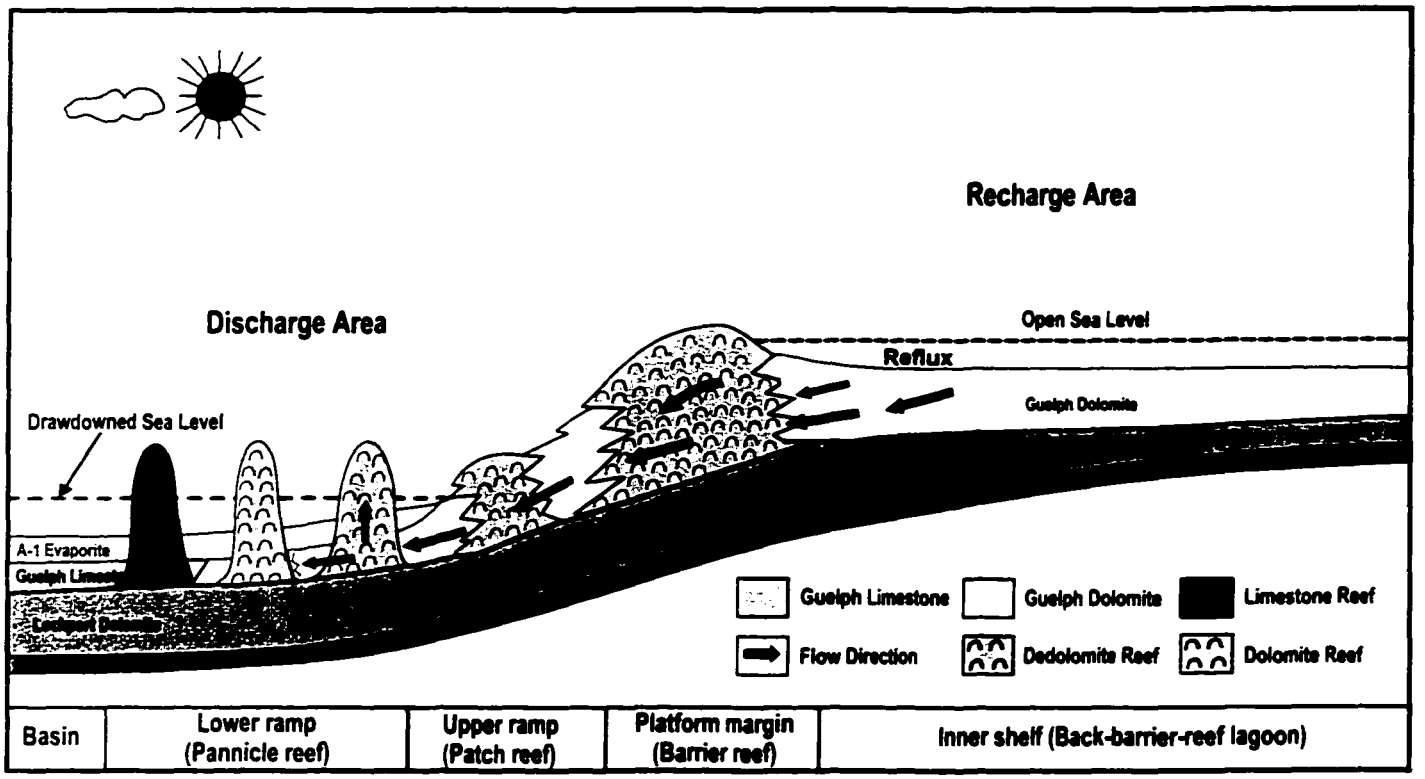



Fig. 4.24 Proposed paleohydrological model for regional topography-controlled, gravity-driven flow system during the Late Silurian. This flow system is interpreted to have been responsible for the regional dolomitization in the Guelph Formation.

which consists of only sylvite (KCl) in northern Michigan. This implies that the hypersaline brine in the basin center was depleted in Mg due to dolomitization along the carbonate flow path. Kendall (1989) suggested that the anhydrite envelopes around the pinnacle reefs in the Elk Point Basin probably represent the precipitates from the escaped Ca-rich springs produced by dolomitization occurring in the reefs. In the study area, nodular anhydrite around and on top of pinnacle reefs within the A-2 Evaporite are common, and the nodular anhydrite on top of pinnacle reefs changes to halite away from reefs (Fig. 4.1). Nodular anhydrite called 'Rabbit Ear" (Gill 1977a) has been found around some pinnacle reefs within A-1 Carbonate in the study area. The similar close association of Guelph dolomite with overlying and surrounding Salina evaporites in southwestern Ontario supports Cercone's (1988) interpretation that evaporative drawdown in the isolated Michigan Basin relative to the surrounding open sea may have driven the flow of dolomitizing fluids.

During the end of the Middle Silurian to Late Silurian, the total evaporation loss in the Michigan Basin exceeded the total inflow from rainfall and the surrounding sea through surface inlets and groundwater seepage (Sonnenfeld 1985). Evaporative drawdown between 100 m and 180 m is thought to have occurred during Salina A-1 Evaporite time (Gill 1977a; Huh et al. 1977; Nurmi and Friedman 1977; Budros and Briggs 1977; Cercone 1988). When the Michigan Basin and the Appalachian Basin were hypersaline environments with carbonates and evaporites during Salina Group time, the southward Wabash Platform of northern Indiana and northeastern Illinois and the Illinois Basin was a normal marine environment (Briggs and Briggs 1974; Droste and Shaver 1985; Cercone 1988), supporting the idea of coexisting low sea level in the isolated Michigan Basin and a high sea level in the adjacent open sea or

platform.

After the initial deposition of A-1 evaporites and some drawdown of sea level, a sea level difference or hydraulic head between the adjacent open sea and the isolated Michigan Basin was established. Reefs were very likely exposed due to evaporative drawdown during Salina A-1 time. The permeable Guelph and underlying Lockport carbonates on the gentle-slopping ramp (Fig. 2.5) likely acted as regional aquifers for this topography-controlled, gravity-driven flow system. This hydraulic head would have forced normal to slightly evaporated seawaters from the back-barrier-reef lagoon connected to the adjacent open sea downward and basinward through permeable reefal and interreef facies (Fig. 4.24). These permeable aquifers were confined by an underlying aquitard consisting of widespread shale of the Rochester Formation and overlying aquitards including relatively thin (3-10 m) but impermeable Salina A-2 anhydrite and halite and the thick B Evaporite unit (up to 90 m).

The timing of this hydrologic flow system probably extended from the time of evaporative drawdown after the onset of deposition of the A-1 Evaporite to the time of the formation of impermeable evaporite seals of B Evaporite or younger Salina evaporites on the floor of the recharge area in the back-barrier-reef lagoon (Fig. 4.24). A progressive overstepping distribution pattern of the Salina evaporites indicates that the evaporites in the Michigan Basin expanded shelfward from the basin to a larger area on the shelf in later time (Sonnenfeld and Al-Aasm 1991).

A modern example of seawater reflux system induced by evaporative drawdown is the East

Salina, a pond of about 30 km long and 20 km wide on West Caicos Island of British West Indies, an isolated carbonate platform near the southeastern end of the Great Bahama Bank (Perkins et al. 1994). Flooded seawater was modified into a dolomitizing agent by heating, evaporation and sulfate reduction under shallow burial conditions. Another example is the MacLeod Basin, a nearshore lagoon 60 km long and 30 km wide, separated from the Indian Ocean on the west by a Pleistocene carbonate ridge up to 60 m in height. The free reflux of seawater occurs as a result of both isolation from the open sea and evaporative sea level drawdown in the lagoon (Logan 1987).

## 4.8.2 Dolomite origin

### 4.8.2.1 Diagenetic fluids

The pore fluid for Type 1 dolomite formation is Middle Silurian seawater, as indicated by its marine $^{87}Sr/^{86}Sr$ signature. Type 1 dolomites have similar Sr contents and $\delta^{18}O$ and $\delta^{13}C$ values as Type 2 and Type 3 dolomites, suggesting that the three different dolomite fabrics precipitated from fluids having similar Sr, $\delta^{18}O$ and $\delta^{13}C$ values or the alteration of the Type 1 dolomites occurred in a relatively closed system. $^{87}Sr/^{86}Sr$ ratios of Type 1 dolomite are in the range of Middle Silurian sweater values and $^{87}Sr/^{86}Sr$ ratios of Type 3 dolomite are closest to the ratios of current formation waters, suggesting that the $^{87}Sr/^{86}Sr$ ratios of pore fluids in the Guelph Formation evolved from seawater ratios to more radiogenic values. The $^{87}Sr$-enriched formation waters in the Guelph Formation and other Paleozoic strata have been attributed to the influence of hydrothermal brines that became more radiogenic by interaction with siliciclastic rocks and clay minerals along the flow path (Dollar et al. 1988; McNutt et al. 1987). During late burial diagenesis, basin-derived hot fluids from deeper strata or basement

may have been locally added to or mixed with the pre-existing diagenetic fluids in the Guelph Formation, as indicated by the elevated Th values in localized Type 3 and saddle dolomites.

#### 4.8.2.2 Early stage dolomite (Type 1 dolomite)

The downdip $\delta^{18}O$ trend in Guelph dolomite is not related to dolomite type (Fig. 4.17). The basinward $\delta^{18}O$-decreasing trend in Guelph dolomite along the ramp most likely resulted from a basinward paleotemperature-increasing trend during burial of the Guelph Formation. A similar basinward $\delta^{18}O$-decreasing trend was observed in the Lower Ordovician Ellenburger Group dolomite in west Texas, but it was interpreted to have been caused by shelfward hydrothermal flow from a basinal source (Kupecz and Land 1991). The temperature difference for Type 1 dolomites in the study area along the downdip trend can be estimated from the oxygen isotopic values. Assuming that the $\delta^{18}O$ value of Silurian seawater was –4‰ (SMOW) (Popp et al. 1986a) and using the paleotemperature equation of Land (1985) for dolomite, a 3.5‰ (PDB) difference in $\delta^{18}O$ value (-5‰ to –8.5‰ PDB) in Type 1 dolomites indicates a temperature range from 38 to 62°C (Fig. 4.25). This temperature difference of approximately 24°C for Type 1 dolomite cannot be explained by burial differences alone, because the maximum downdip burial difference in study area is well below 400 m (Fig. 2.5) and this burial difference represents at most a 10°C temperature difference. A combination of a basinward increase in burial depth and a basinward increase in heat-flow explains this downdip paleotemperature-increasing trend in the Guelph Formation. Laterally convective heat-flow and temperature increase in the basinward discharge area and decrease of geothermal gradient and temperature in the shelfward recharge area are observed in the present-day Michigan Basin (Vugrinovich 1988, 1989) and other basins such as Anadarko Basin of Oklahoma (Carter et al.

1998). This type of lateral thermal gradient increase likely also existed in the Guelph Formation during dolomite formation.

The general basinward $\delta^{13}C$-increasing trend in Guelph dolomite can also be readily explained. The comparable $\delta^{13}C$ values between dolomite (+2.0‰ to +5.0‰ PDB) and their precursor limestone (+1.5‰ to +3.5‰ PDB) indicate that the $^{13}C$ in primary limestone was mostly retained in later dolomite. The more enriched $\delta^{13}C$ values in basinward dolomite likely resulted from an increased flux of $^{13}C$ to the diagenetic fluids during dolomite formation, although the exact source is unclear. A possible reason for the basinward increase of $^{13}C$ input is that more organic material was preserved in the basinward Guelph and overlying A-1 and A-2 carbonates. This organic matter released extra $^{13}C$ to the diagenetic fluids during burial, perhaps due to fermentation or methanogenesis.

Assuming that early dolomitization in the Guelph Formation and the A-1 and A-2 carbonates occurred after the B halite was deposited, the amount of compaction for the carbonates and evaporites in the A and B units can be estimated using Ricken's (1987) compaction equation for a closed system:

$$n^* \text{ (vol\%)} = (1-0.01K)\, n + K$$

where $n^*$ is decompaction porosity, K is the amount of compaction, and n is the current porosity. Assuming a moderate decompaction porosity of 45% (Ricken 1987) and using an average current porosity of 5% for the carbonates and evaporites in the A and B units, the

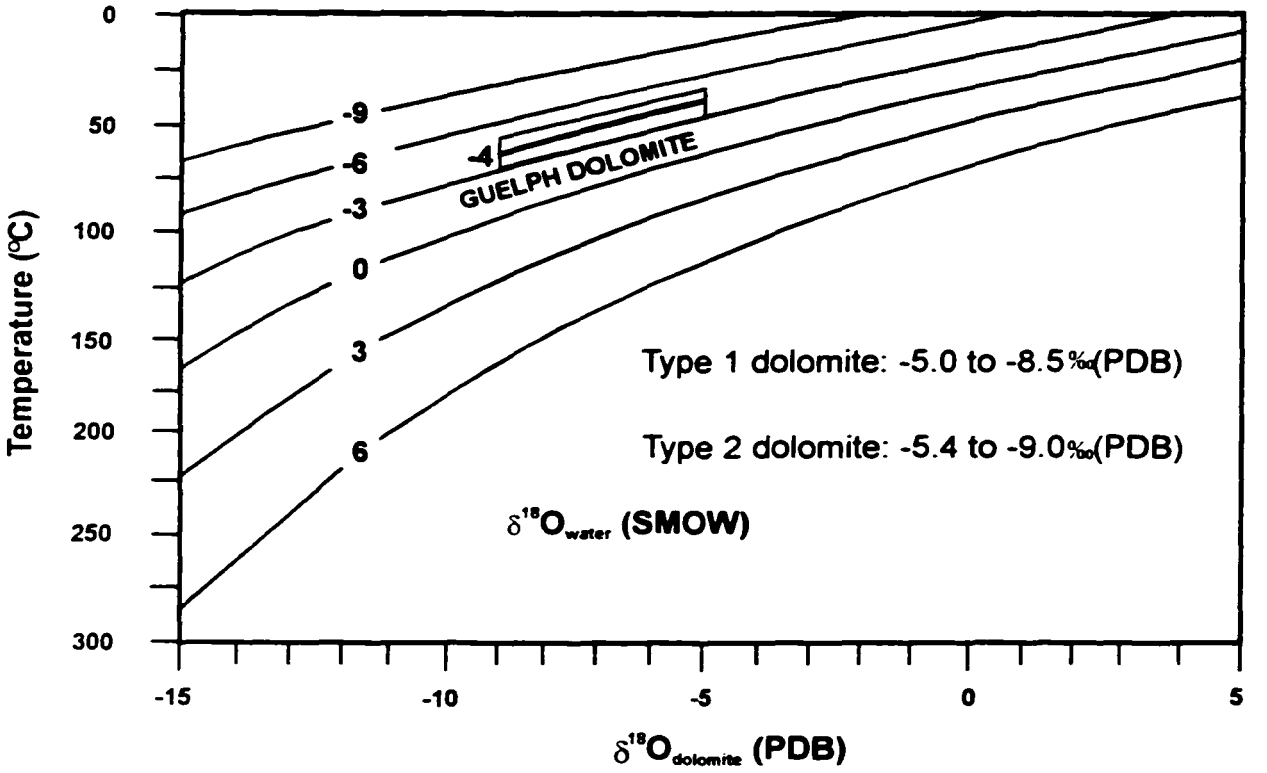



Fig. 4.25 Temperature vs. $\delta^{18}O_{dolomite}$ (PDB) for various $\delta^{18}O_{water}$ values (SMOW), using the equation of Land (1985): $10^3 \ln\alpha_{(dolomite - water)} = 2.78 \times 10^6 T^{-2}(°K) + 0.91$. Shaded area shows the observed $\delta^{18}O$ ranges of Type 1 and Type 2 dolomites. Assuming that $\delta^{18}O$ value of dolomitizing fluids was –4‰ (SMOW), a range of –5.0 to –8.5‰ (PDB) and –5.4 to 9.0‰ (PDB) for Type 1 and Type 2 dolomites Corresponds to temperature ranges of 38 to 62 °C and 42 to 65°C, respectively.

compaction amount is approximately 42%. The actual burial depths of the Guelph Formation when early dolomitization occurred were approximately 170-350 m, which are estimated from the calculated compaction amount (42%) and the present-day thicknesses of the A and B units of approximately 100-200 m (Figs. 2.4 and 2.5). However, the isotopic temperatures estimated using $\delta^{18}O$ values of Type 1 dolomites are 38-62°C which correspond to burial depths of 320-1250 m, by assuming an average surface temperature of 30°C and a commonly accepted geothermal gradient of 2.5°C/100 m. The burial depths of 320-1250 m are much greater than above mentioned burial depths estimated from stratigraphic data. This is consistent with the interpretation that an early recrystallization of initial dolomite occurred at greater burial depths and higher temperatures.

#### 4.8.2.3 Middle stage dolomite (Type 2 dolomite)

Type 2 dolomite is the most common fabric in the Guelph Formation. The mode for dolomite crystal enlargement from early-formed, finer Type 1 dolomite to coarser Type 2 dolomite could have been through either simultaneous dissolution and precipitation on a thin-film scale (Pingitore 1976; Brand and Veizer 1980) or partial dissolution followed by precipitation as overgrowths on earlier dolomite cores and direct precipitation as coarser new crystals in vugs, depending on the relative rates of dissolution (D) and precipitation (P) (Fig. 4.26). In the second mode, the earlier dolomite phases were dissolved in one place and precipitated as overgrowths or new crystals in a nearby place but much larger than thin-film scale.

Porous sucrosic Type 2 dolomite most likely formed by partial dissolution of Type 1 dolomite and subsequent precipitation as overgrowth rims and new crystals, as indicated by its close

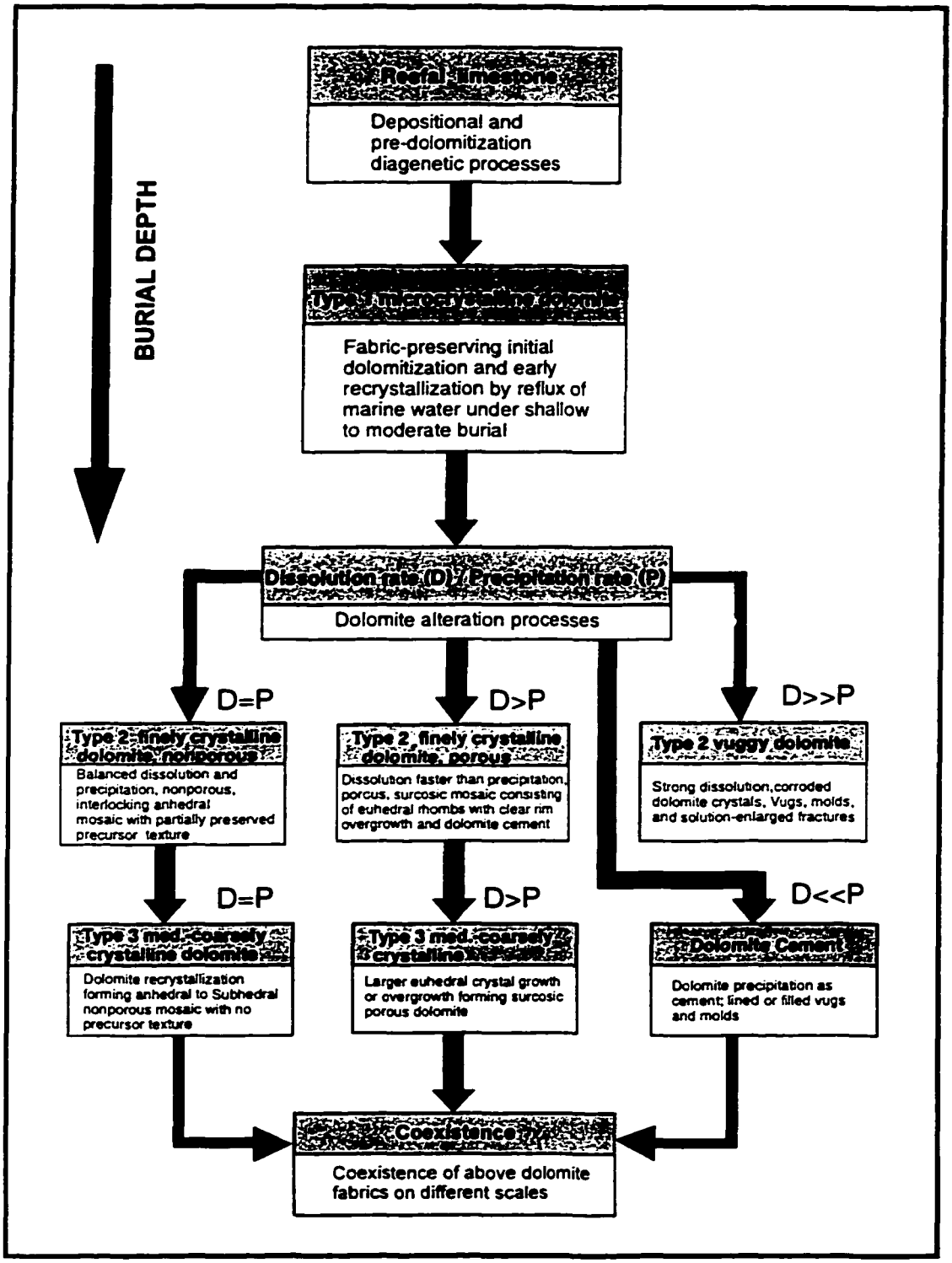



Fig. 4.26 Conceptional flowchart for indicating dolomite formation and further alteration paths in the Guelph Formation in southwestern Ontario.

association with vugs and leached intervals, its coarser crystals consisting of cloudy cores and overgrowth rims or clear euhedral crystals, and its common coexistence with Type 1 fabric with relict textures. Only small portions of Type 2 dolomite occurred as nonporous dolomite consisting of tightly interlocking packed anhedral mosaics, which are interpreted to represent the products of recrystallization. Later dolomite recrystallization may need more strict conditions such as low porosity and permeability for forming and maintaining intercrystal sheet pores and active solution films (Fischer 1988).

Type 2 dolomite Th values range from +64.5 to +74.7°C, which are close to the isotopic temperatures of 42 to 65°C calculated using Land's (1985) equation for dolomite, by assuming an $\delta^{18}O$ value of –4 ‰ (SMOW) for diagenetic fluid and a surface temperature of 30°C (Fig. 4.22). This suggests that Type 2 dolomite formed at moderate burial depths of approximately 480-1400 m.

#### 4.8.2.4 Late stage dolomite (Type 3 dolomite)

There are two popular hypotheses concerning the origin of medium-coarsely crystalline dolomites similar to the Type 3 dolomite in the Guelph Formation. The first hypothesis argues that deep burial dolomitization by warm compactional or basinal fluids could produce medium-coarsely crystalline dolomites with low $\delta^{18}O$ values, high $^{87}Sr/^{86}Sr$ ratios, and high temperature fluid inclusions (e.g., Machel and Anderson 1989; Lee and Freedman 1988; Mountjoy and Amthor 1994). The second hypothesis suggests that later alteration of early-formed finer crystalline dolomite could form similar dolomites (Land 1985, 1991; Banner et al. 1988; Gao and Land 1991; Montañez and Read 1992; Kupecz and Land 1994). Several medium to

coarsely crystalline dolomites were interpreted as being deep burial or hydrothermal in origin (e.g., Lee and Friedman 1988; Qing and Mountjoy 1994), but they could also represent the products of later alteration of earlier, more finely crystalline dolomite in deeper burial or hotter fluids (e.g., Kupecz et al. 1993).

Medium-coarsely crystalline Type 3 dolomites which contain Type 1 and Type 2 dolomite mosaics but no limestone relicts are interpreted to have resulted from the alteration of Type 1 and/or Type 2 dolomites. Elevated temperatures and perhaps pressures (strains) during late burial could be the main driving forces for later alteration of microcrystalline Type 1 and finely crystalline Type 2 dolomites to medium to coarsely crystalline Type 3 dolomites (Land 1985; Hardie 1987; Sibley and Gregg 1987). Several lines of evidence support that the origin of localized Type 3 dolomite being related to late hydrothermal fluids, although the sources for hydrothermal fluids in the study region are uncertain (Coniglio et al. 1994). First, Th values in Type 3 dolomites vary from +95.8 to +116.7°C, which are much higher than the temperatures of 48-70°C calculated from oxygen isotopic compositions (Fig. 4.22) and temperatures of less than 73°C calculated from burial history reconstruction with a maximum burial depth of 1800 m, using an estimated geothermal gradient of 2.5°C/100 m. Second, Type 3 dolomites commonly crosscut Type 2 and Type 1 dolomites along fractures or occur in porous intervals or areas. Third, Type 3 dolomites have similar Th values to those of saddle dolomites and some Type 3 crystals show curved faces and sweeping extinction, which are typical features of saddle dolomite. This suggests that both Type 3 dolomite and saddle dolomite may have been related to the same hydrothermal fluid. The late hydrothermal fluids for localized Type 3 dolomite likely were transported along fractures and permeable intervals or channels and

driven by thermal convection during a hydrothermal episode (e.g., Coniglio et al. 1994; Morrow 1998), or by tectonic forces during orogeny (e.g., Qing and Mountjoy 1994).

#### 4.8.2.5 Saddle dolomite

The origin of saddle dolomite has been suggested to relate to (1) elevated temperatures (60-250 °C) caused by deep burial or hydrothermal fluids (Radke and Mathis 1980; Gregg 1983); (2) 'boiling' of hydrocarbon-related $CO_2$-saturated brines having high carbonate alkalinity (Leach et al. 1991); and (3) thermochemical reduction of sulfate (TSR) by hydrocarbons (Machel 1987; Krouse et al. 1988). More recent studies (e.g., Davies 1996) found that fluid inclusions in many saddle dolomites contain only trace amounts of $H_2S$ that are too low to support a TSR origin. The origin of saddle dolomite in Guelph carbonates likely relates to local fault and fracture-controlled intrusion of hot and saline brines, as indicated by its fracture-related occurrence, high homogenization temperatures ranging from +98.7 to +128.2°C, and low initial melting temperatures ranging from –28.0 to –47.6°C.

#### 4.8.2.6 Scattered dolomite

Minor scattered dolomite in the preserved reefal limestones is interpreted to be late burial in origin, as suggested by their occurrence along fractures and stylolites in limestones. They probably precipitated from the Mg-rich fluids transported along fractures and stylolites. Sears and Lucia (1980) reported similar scattered rhombic crystals, selectively replacing matrix and grains in amounts of 10% to 30% in the pinnacle reefal limestones in northern Michigan and attributed them to an early mixing-zone origin.

#### 4.8.2.7 Thermal convection for dolomite alteration

Morrow (1998) invoked subsurface thermal convection of connate seawaters during a crustal thermal event to explain the origin of fault-fracture controlled hydrothermal dolomite in the Middle Devonian Manetoe and Presqui'ile carbonates in the West Canada Sedimentary Basin. Under burial conditions, thermal convection is driven by an inverse density gradient resulting from thermal expansion of water. In addition, a deep heat source is required (Bjørlykke 1993). Under normal geothermal gradients, there are too many aquitards in most sedimentary sequences for convection to occur (Bjørlykke et al. 1988), but suitable conduits such as networks of faults and fractures could induce large-scale thermal convection and dolomitization (Searl 1991).

Several studies (Sleep and Snell 1976; Nunn et al. 1984; Mareschal 1987) have concluded that there were two or three thermal events during rifting and thermal subsidence of the Michigan Basin. Based on tectonic subsidence data and the assumption that the basin subsidence was primarily controlled by thermal contraction, Mareschal (1987) computed the heat flow history and predicted at least two major thermal anomalies or events at approximately 390 and 330 Ma. These two high heat flow periods correlate to two Appalachian Orogenies and two major unconformities (Sanford et al. 1985). The thermal event of 390 Ma correlates to the Caledonian Orogeny and the unconformity between the Upper Silurian and the Lower Devonian successions. The thermal anomaly at 330 Ma corresponds to the Acadian Orogeny and the Carboniferous unconformity with as much as approximately 1000 m erosion (Cercone 1984a; Fisher et al. 1988).

In Trenton carbonates of the Albion-Scipio and Stoney Point fields in southern Michigan, Hurley and Budros (1990) suggested that the dolomitizing fluids for the fracture-controlled dolomitization ascended along fractures from deeper sources. In southwestern Ontario, Coniglio et al. (1994) invoked a thermal convection model to explain the origin of dolomite in Trenton and Black River strata, where the occurrence of dolomites is closely associated with regional faulting and fracturing. In the study area, Sanford et al. (1985) suggested that a fracture framework consisting of numerous basement-controlled faults and associated fractures in three directions was developed in southwestern Ontario and remained active during basin development and burial history. They also suggested that fault and fracture systems in southwestern Ontario might have acted as conduit systems for late diagenetic fluids and hydrocarbon migration. A fault and fracture network that developed in the Middle Ordovician carbonates (Coniglio et al. 1994) may have continued through the Middle Silurian Guelph carbonates. Long-lived growth faults which directly controlled carbonate deposition and reef growth during sedimentation (Gill 1979; Sanford et al. 1985), could have also provided effective conduits for diagenetic (including hydrothermal) fluids during the burial history.

Subsurface (a few hundred to a few thousand meters) thermal convection is more important as a transport mechanism in circulating fluid and transferring heat than as a mass (such as Mg) supplier, since a large amount of flux through the sediments can be achieved by circulating the same water over and over again (Davis et al. 1985; Shi and Wang 1986; Corbet and Bethke 1992). Dynamic advection flow from outside sources is essential in order to supply Mg and remove Ca for replacement of limestone by dolomite. However, for replacement of pre-existing dolomite by later dolomite, the Mg needed for later dolomite comes from earlier

dolomite. An external Mg source is no longer necessary, even in a relatively closed system during relatively deep burial, as long as sufficient amounts of fluids flowed through the altered rocks. In this regard, thermal convection is the most attractive mechanism to maintain large amounts of flux under deep burial conditions. The occurrence of Type 3 dolomite in the Guelph Formation can be readily explained by Coniglio et al.'s model (1994) for fracture-controlled dolomite in the Middle Ordovician carbonate succession in southwestern Ontario. Coniglio et al.'s model (1994) and the concept of burial dolomite alteration caused by thermal convection may also assist to explain other coarsely crystalline dolomites elsewhere (e.g., Amthor et al. 1993; Qing and Mountjoy 1994), which were interpreted as late burial origin but there was problem of insufficient Mg.

Other late diagenetic processes including dedolomitization, anhydrite and halite cementation, and hydrocarbon migration in Guelph dolomites may have shared some of the conduits formed during Type 2 and Type 3 dolomite formation (see Chapter 5 and Chapter 6).

## 4.9 Dolomite formation model

Numerous authors (e.g., Shukla and Friedman 1983; Qing and Mountjoy 1994; Saller and Yaremko 1994) have attributed the origin of massive ancient dolomite rocks characterized by different dolomite fabrics like those in the Guelph Formation to multistage dolomitization. They argued that different fabrics with variable elemental and isotopic compositions represent the products of different dolomitization stages ranging from early, surface and near-surface dolomitization to late, deep burial replacement of limestone by dolomite in a variety of dolomitizing fluids. However, in the Guelph Formation, the coexistence of three dolomite

fabrics with different elemental and isotopic compositions and the lack of limestone relicts in dolomite rocks can not be readily explained by multistage dolomitization. As an alternative, it is proposed that three different dolomite fabrics in the Guelph Formation represent the products of pervasive early dolomitization and subsequent alteration of early-formed dolomite during burial (Fig. 4.27).

A topography-controlled, gravity-driven seawater reflux system is interpreted to have been responsible for the regional early dolomitization in the Guelph Formation (Fig. 4.24). In this hydrologic model, the main driving force is hydraulic head caused by evaporative drawdown. The recharge area was the inner shelf with normal or nearly normal seawaters without significant evaporite formation. The discharge areas were the ramp and basin center. The sea floor area in the basin was probably rapidly sealed by the deposition of A-1 Evaporite. However, the upper portions or crests of porous patch and pinnacle reefs on the ramp could have acted as effective conduits for upward discharge of topographically driven fluids into the overlying isolated Michigan sea as seepages or springs. Preferentially dolomitized A-1 and A-2 carbonates around and above pinnacle reefs and selectively dissolved A-2 and B halite above the pinnacle reefs also occurred as result of this flow. Flow rates and volumes of seawater seepage may have varied with time depending on the magnitude of evaporative drawdown. The duration of this hydrologic flow system probably extended from initial drawdown during deposition of the A-1 Evaporite to complete seal of the recharge area.

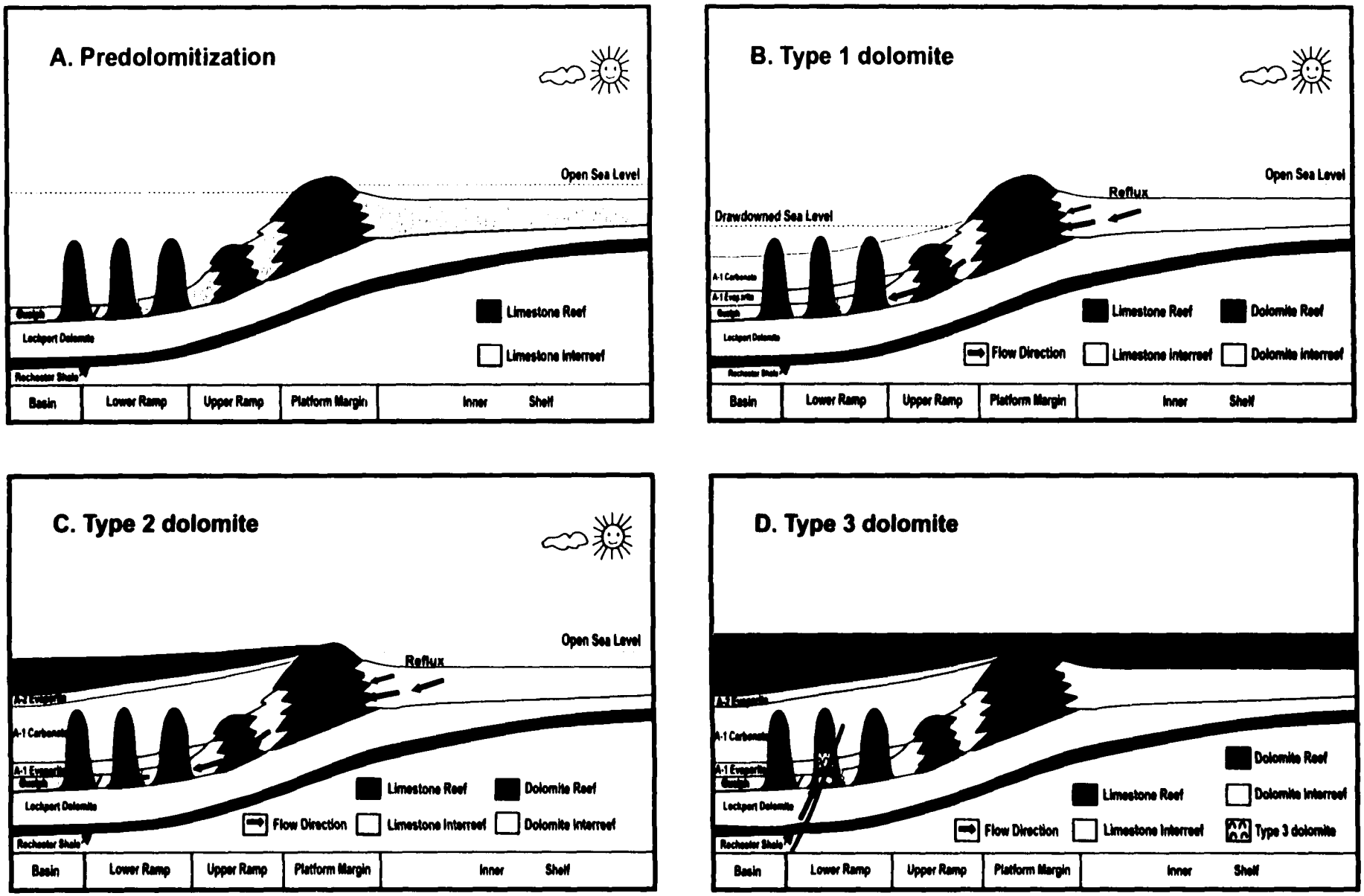



Fig. 4.27 Conceptional model for the origin of three replacive dolomites in the Guelph Formation. Early Type 1 dolomite formation is interpreted to have resulted from seawater reflux driven by a hydraulic head that was induced by evaporative drawdown during the Late Silurian. Later Type 2 and Type 3 dolomites or recrystallization of earlier Type 1 dolomite occurred during deeper burial conditions. .

Guelph reefal limestones were initially extensively dolomitized by active seawater circulation induced by evaporative drawdown during the Late Silurian. Fabric selective and non-selective dissolution in Type 1 dolomites formed variable amounts of biomoldic and vuggy pores opening conduits for further alteration of Type 1 dolomites. Some early dolomites without or with only minor dissolution were preserved as Type 1 dolomites.

Guelph dolomites having different strontium isotopic signatures can be explained by the subsequent alteration of early-formed Type 1 dolomite precursor in the same regional, gravity-driven flow system. Type 1 dolomite represents the 'least altered' dolomite phase that is geochemically closest to the initial replacive dolomite. Type 2 and then Type 3 dolomites represent products of subsequent alteration of early-formed Type 1 dolomite precursors (Figs. 4.26, 4.27).

## 4.10 Conclusions

1. Nonporous, microcrystalline Type 1 dolomite is interpreted to represent the 'least-altered' dolomite phase that is geochemically the closest to the initial replacive dolomite. This is indicated by its best preserved limestone textures, identical $^{87}Sr/^{86}Sr$ ratios to both limestone ratios and coeval seawater values, and low Fe and Mn concentrations similar to those in limestones.

2. Early recrystallization likely occurred in Type 1 dolomite, as suggested by its coarser crystal size (20-50 μm) relative to recent dolomite (commonly less than 4 μm) and depleted $\delta^{18}O$ values. Depleted $\delta^{18}O$ values resulted from early recrystallization in a fluid similar to that

which characterized initial dolomitization but at deeper (shallow to moderate) burial conditions (320-1250 m). The relative timing of Type 1 dolomite formation predates stylolitization but postdates the equant calcite cementation.

3. Petrographic and geochemical constraints and regional paleoclimate and paleogeography argue against any significant influence of meteoric waters in the Guelph Formation. The similarity of strontium isotopic compositions among limestones, Type 1 dolomites, and coeval Silurian seawater, in conjunction with elemental and carbon isotopic compositions in Type 1 dolomites, suggest normal to near-normal marine waters as fluids for initial dolomitization and early recrystallization.

4. Dolomite distribution trends and paleogeography define a topography-controlled seawater reflux flow system. The driving force for this flow system was the hydraulic head between the open sea level and the evaporative drawdowned water level in the isolated Michigan Basin. Regional dolomitization was accomplished by basinward reflux of large volumes of seawater recharged from the back-barrier-reef area connected with the open sea. These waters flowed downward through the porous barrier reefs and inter-reef facies to the individual patch and pinnacle reefs on the ramp. The duration of this flow system extended from the initial drawdown during late Silurian Salina A-1 Evaporite deposition to until the seawater recharge area was completely sealed by evaporites of Salina B and later units. Stratigraphic data suggest that the initial dolomitization probably occurred at shallow burial of less than 350 m.

5. Downdip dolomite $\delta^{18}O$-decreasing trend along the ramp, which is not controlled by

dolomite type, is interpreted to have formed during Type 1 dolomite formation. This trend was mainly caused by downdip increasing burial depths of the Guelph Formation and a basinward geothermal gradient increase along the ramp.

6. Finely crystalline Type 2 dolomite and medium to coarsely crystalline Type 3 dolomite are interpreted to have formed by further alteration of a microcrystalline Type 1 dolomite precursor at deeper burial and/or by warmer fluids, as suggested by their stratigraphic occurrence on a regional scale, petrographic coexistence with Type 1 dolomite in core and thin section scales, later timing relative to Type 1 dolomite, higher $^{87}Sr/^{86}Sr$ ratios and Fe and Mn concentrations, and elevated Th values. Type 2 dolomite formed at moderate to deep burial of approximately 480-1400 m. Type 3 dolomites show the highest Th values and fracture-related occurrences and some Type 3 dolomites exhibit saddle dolomite-like features. They are interpreted to have resulted from fracture-conducted hydrothermal fluids during deeper burial.

7. The systematic covariance between increasing crystal size with increasing $^{87}Sr/^{86}Sr$ ratios and increasing Fe and Mn concentrations indicates a general trend of increasing crystal size with increasing alteration during burial. This trend reflects a continuous alteration of early-formed dolomite in pore fluids with increasing $^{87}Sr$ input from associated siliciclastics or cross formation waters under burial conditions.

# Chapter 5 Dedolomite and dedolomitization

## 5.1 Abstract

Several intervals of partially to nearly completely altered rocks in eight cores from five pinnacle reefs, ranging from 0.2 to 60 m in thickness, previously reported as "paleosols" or marine limestones, are here recognized as dedolomitized rocks. These altered rocks contains variable amount of dedolomite ranging from 5% to 95% and the dedolomitized reefs occur in a narrow zone (10-20 km) on the lower ramp which is between platform dolomites and basinal limestones.

Guelph dedolomites contrast with their dolomite precursors and associated original limestones by their light color, poor lithification, numerous relict dolomite patches, and poorly preserved precursor textures. Dedolomites commonly consist of finely crystalline calcite crystals (20-50 μm), with numerous corroded dolomite relicts and inclusions. Crystal sizes are generally coarser than associated limestones but finer than their dolomite precursors. Replacement fabrics include dolomite rhombs with corroded edges, poikilotopic fabrics with floating dolomite relicts, rhombic calcite pseudomorphs, and micrometer-sized dolomite inclusions. These replacive textures, in conjunction with the common optical continuity and identical dull orange luminescence to nonluminescence of dedolomites and coexisting dolomites, indicate that Guelph dedolomites formed from replacement of preexisting dolomites.

Guelph dedolomites show depleted Sr contents (40-60 ppm), enriched Fe contents (600-1700 ppm) and Mn concentrations (60-200 ppm), and higher $^{87}Sr/^{86}Sr$ ratios (0.70875 and 0.70885), relative to associated original limestones, but similar values to their precursor dolomites. The $\delta^{18}O$ and $\delta^{13}C$ values of Guelph dedolomites range from -6 to -9 ‰ and from +2.5 to +4 ‰ (PDB). Moderate homogenization temperatures (Th: 53.4 to 72.4°C) and low melting temperatures (Te: -28.0 to -31.4°C, Tm: -16.8 to –18.4°C) of primary fluid inclusions within dedolomites suggest a shallow to moderate burial and a saline water origin. Stratigraphic, petrographic, geochemical, and fluid inclusion data support a subsurface dedolomitization by saline brines with higher Ca/Mg ratio but identical trace elemental and isotopic compositions and under identical burial conditions (depth and temperature) to those that led to earlier dolomite formation. The Guelph dedolomitization was neither controlled by fractures or unconformities nor related to fresh waters. The most likely mechanism for localized dedolomitization in the Guelph Formation is related to the circulation of modified seawaters in the same gravity-driven reflux system that led to the formation of earlier Type 1 and Type 2 dolomites. Dedolomitizing fluids acquired extra Ca from the dissolution of local reefal limestones within a narrow limestone-bearing zone on the lower ramp.

## 5.2 Introduction

Several partly to almost completely dedolomitized intervals occur at different stratigraphic levels in eight cores from five pinnacle reefs distributed in a narrow transitional zone on the lower Guelph ramp (Figs.1.2 and 2.5). These altered rocks,

reported as paleosols in previous studies (e.g., Charbonneau 1990), similar to the surface-altered rocks described as "pulverulite" by Chafetz and Butler (1980) and Type II poikilotopic calcite-dolomite by Jones et al. (1989) in their chalky appearance and friable nature, are herein interpreted as dedolomites.

Dedolomitization is a replacement process characterized by dolomite dissolution followed by calcite precipitation. Smith and Swett (1968) and Fairbridge (1979) suggested abandonment of the word 'dedolomitization' and use of the more meaningful term 'calcitization' instead. In this study, the terms 'dedolomitization' for the process of replacing dolomite by calcite and 'dedolomite' for the product of dedolomitization are used due to their prevalence in the literature.

Numerous earlier studies have interpreted dedolomitization to be a surface or near-surface diagenetic phenomenon related to surficial weathering zones, unconformities, or karst (Schmidt 1965; Evamy 1967; Goldberg 1967; Friedman and Sanders 1967; Folkman 1969; Braun and Friedman 1970; Al-Hashimi and Hemingway 1973). Many other studies, however, have suggested that dedolomitization also occurs under shallow burial (e.g. Fritz 1967; Mattavelli et al. 1969; Longman and Mench 1978; Back et al. 1983; Theriault and Hutcheon 1987; Jones et al. 1989; Deike 1990; James et al. 1993) to deep burial conditions (e.g. Land and Prezbindowski 1981; Budai et al. 1984; Sellwood et al. 1989).

Some of the dedolomitized intervals in the Guelph Formation constitute important hydrocarbon reservoirs. Dedolomites as oil and gas reservoir rocks are also reported in the Middle-Late Triassic Taormina Formation of the Gela oil field in Sicily (Mattavelli et al. 1969), Middle Jurassic reservoirs of the Coulommes oil field in the Paris Basin (Purser 1985), and the Upper Devonian Grosmont Formation in northern Alberta (Theriault and Hutcheon 1987).

The main objectives of this chapter are to: (1) report the occurrence and distribution of dedolomites in the Guelph Formation based on core observations; (2) document their petrographic and geochemical characteristics; and (3) discuss the diagenetic processes and conditions, type of fluids, sources of Ca, relative timing, and paleohydrologic system.

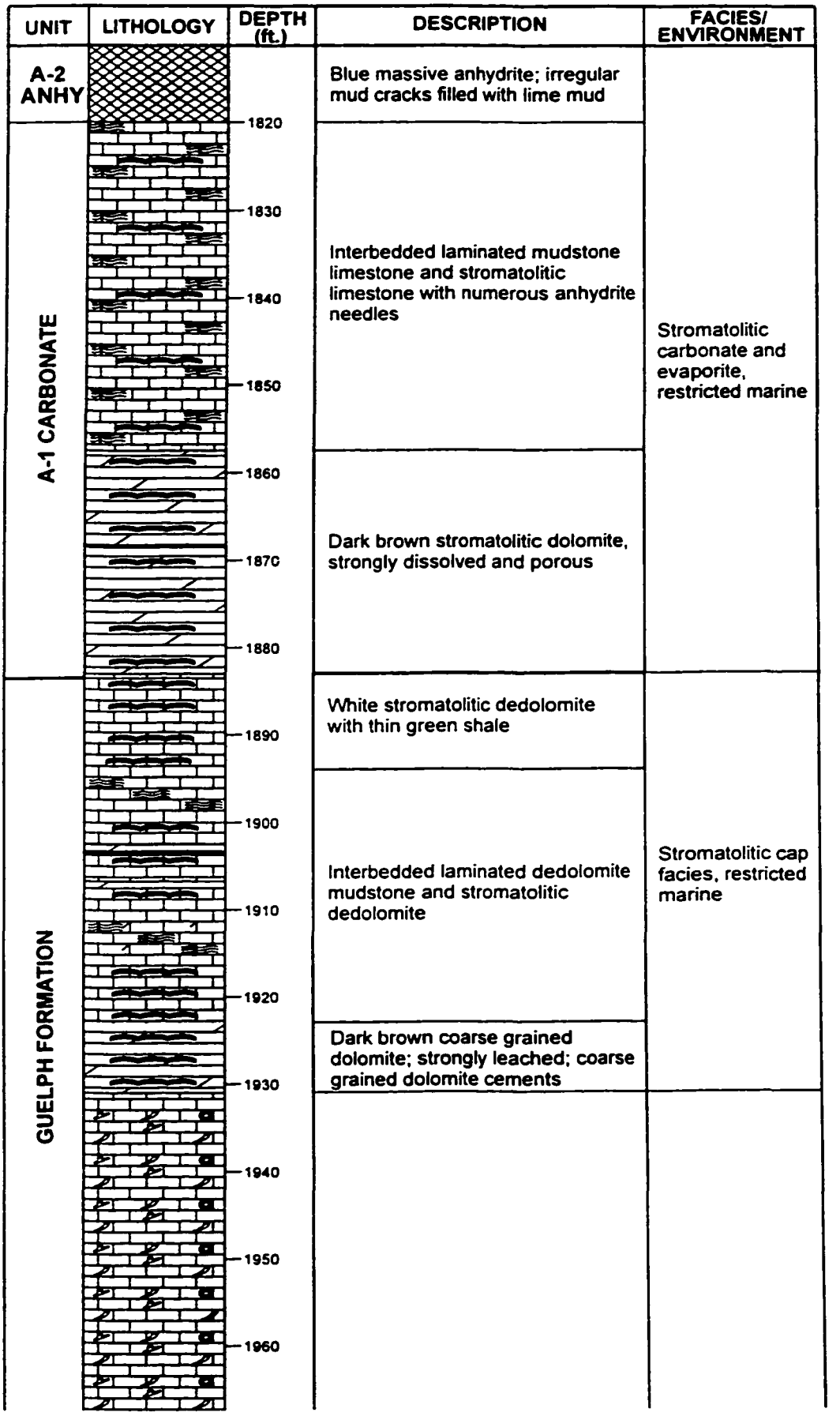
## 5.3 Dedolomite distribution

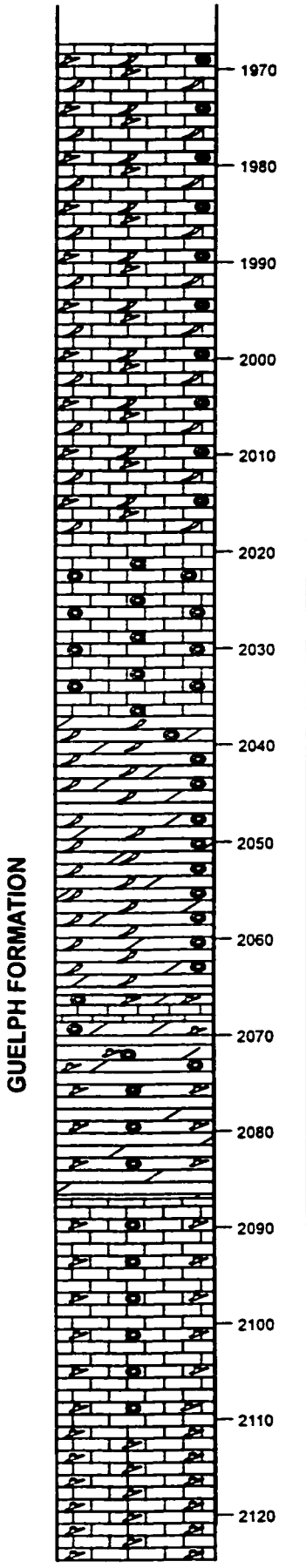
Partially to nearly completely dedolomitized rocks have been observed in 8 cores from five pinnacle reefs, including Sarnia 1-8-A, Waubuno, Wilkesport, Bickford, and Terminus (Appendix I). These reefs distribute within a northeast-southwest oriented, narrow zone (10-20 km) on the lower ramp (Figs. 1.2, 2.5). Four out of the five dedolomite-bearing pinnacle reefs also contain the original limestones as interbeds, whose microscope fabrics show clearly that they had not ever been dolomitized (Fig. 1.2; Appendix I).

The thickness of dedolomitized intervals range from 0.2 to 60 m, interbedded with dark brownish finely crystalline sucrosic (Type 2) dolomite and sometimes with preserved primary limestone. They occur at different stratigraphic levels within the pinnacle reefs without any obvious relation to the Guelph-Salina boundary, which has been interpreted by others as an exposure surface or unconformity (see Chapter 2; Gill 1977a; Charbonneau 1990). Fracture and stylolite-related dedolomites, such as those described by Budai et al. (1984) in Mississippian Madison Limestone in western Wyoming and northeastern Utah, have not been found in the Guelph Formation.

In core, vertical and lateral transitional zones between dolomites and dedolomitized rocks are readily observed due to the lighter color of the dedolomitized rocks. In the dedolomitized intervals, the occurrence of dedolomite varies from scattered patches to nearly complete replacement. Dedolomite content ranges from 5% to 95%. Associated dolomites are commonly tightly packed mosaics, but the dedolomitized rock is considerably more friable and can be easily broken by fingers into powder.

A representative lithological log of core #424 from Waubuno pinnacle reef shows the general lithology and dedolomite distribution (Fig. 5.1). The Terminus reef was almost completely dedolomitized with only a few thin zones of preserved dolomite. Dedolomites in Terminus, Bickford, and Waubuno pinnacle reefs were reported as reefal limestones or paleosols in previous studies (Grimes 1987; Charbonneau 1990). No obvious features related to karsting and subaerial exposure were recognized in dedolomite intervals in this study.


UNIT
LITHOLOGY
DEPTH (ft.)
DESCRIPTION
FACIES/ ENVIRONMENT
A-2 ANHY
Blue massive anhydrite; irregular mud cracks filled with lime mud
A-1 CARBONATE
1820
1830
1840
1850
1860
1870
1880
Interbedded laminated mudstone limestone and stromatolitic limestone with numerous anhydrite needles
Dark brown stromatolitic dolomite, strongly dissolved and porous
Stromatolitic carbonate and evaporite, restricted marine
GUELPH FORMATION
1890
1900
1910
1920
1930
1940
1950
1960
White stromatolitic dedolomite with thin green shale
Interbedded laminated dedolomite mudstone and stromatolitic dedolomite
Dark brown coarse grained dolomite; strongly leached; coarse grained dolomite cements
Stromatolitic cap facies, restricted marine




| | |
|---|---|
| White-grey coral-bryozoan-crinoid bindstone-rudstone-floatstone dedolomite with few thin intervals of bryozoan bafflestone limestone and unaltered brown dolomite. | Organic reef core facies, normal marine |
| Crinoidal wackestone dedolomite | Inter-reef-core facies, normal marine |
| Grey dark grey branching coral bafflestone dolomite and crinoidal wackestone dolomite with dedolomitized patches along fractures | Organic reef core facies, normal marine |
| Grey bryozoan-crinoid wackestone or floatstone dolomite with chalky dedolomitized intervals | Inter-reef-core facies, normal marine |
| Dark grey bryozoan bafflestone and crinoidal wackestone dolomite alternating with dedolomitized intervals.Large cavities lined with saddle dolomite cement | |

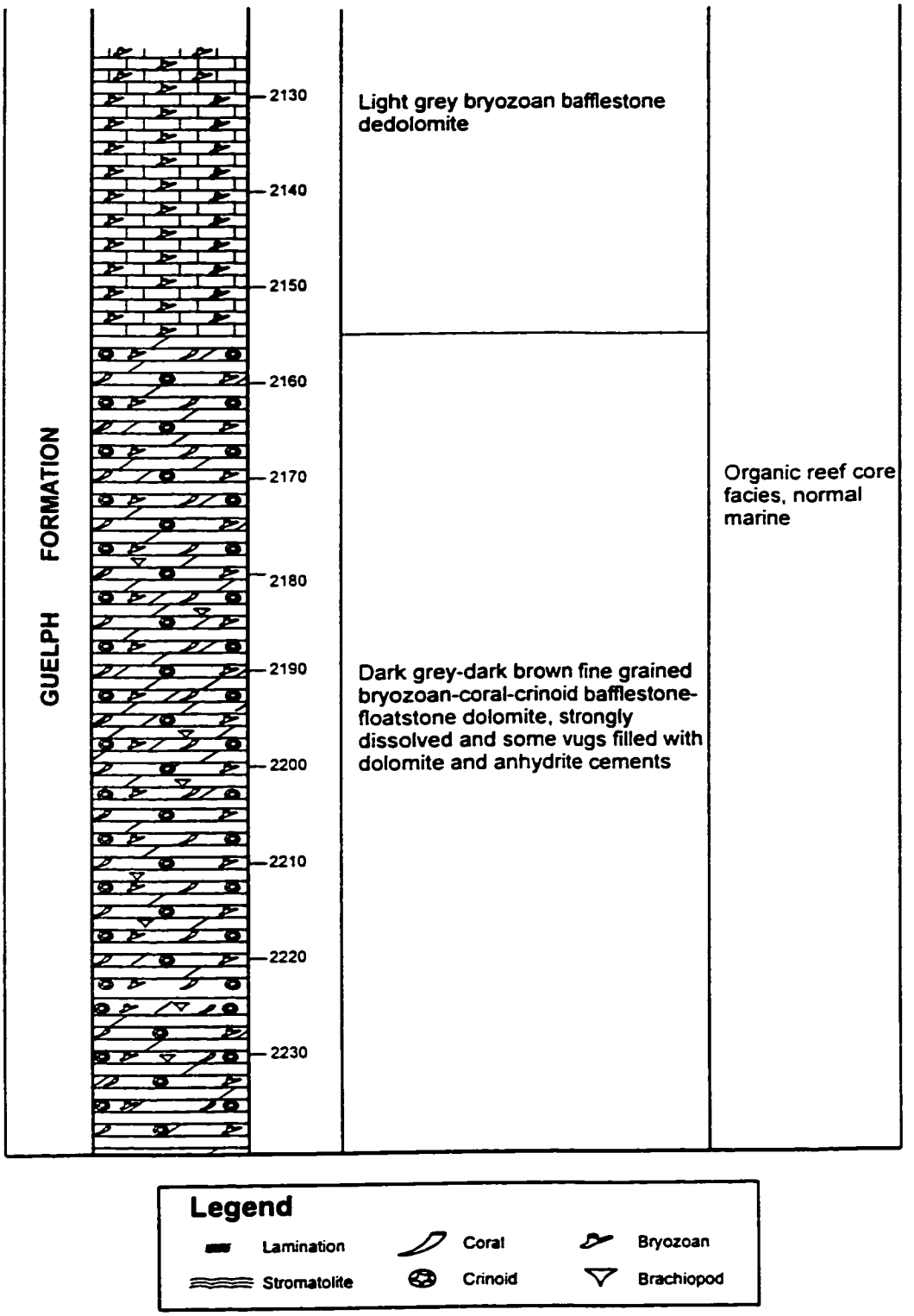



Fig. 5.1 Representative lithology log of Core 424 from Terminus pinnacle reef for dedolomite distribution in the Guelph Formation.

## 5.4 Dedolomite petrography

Guelph dedolomite occurs within finely crystalline (Type 2) dolomite intervals and typically has a chalky white to yellowish color. In Type 2 dolomites, Guelph dedolomite always postdates Type 2 dolomite but predates anhydrite and halite cements (Fig. 3.6). Less commonly, dedolomite occurs around voids or occasionally along fractures in microcystalline (Type 1) dolomites. Guelph dedolomites mostly consist of microcrystalline (20-50 μm), and less commonly finely crystalline (50-150 μm) and medium to coarsely crystalline (150–500 μm) calcite mosaics. Average crystal sizes of dedolomites are finer than their dolomite precursor but much coarser than the associated primary limestones. Dedolomite also has poorer crystal size sorting than its dolomite precursor.

In core and under transmitted light microscopy, partially dedolomitized rocks commonly contain numerous dark brown dolomite relicts as lenses and patches. In places, bryozoans were selectively preserved as relicts of brown dolomite within mostly dedolomitized, lighter color rock. Under CL, dedolomites show a same dull orange to reddish luminescence to nonluminescence as their associated dolomite precursors.

The petrographic criteria for recognition of dedolomites have been discussed in numerous earlier studies (e.g., Lucia 1961; Shearman et al. 1961; Evamy 1967; Goldberg 1967; Folkman 1969; Al-Hashimi and Hemingway 1973; Longman and Mench 1978; Budai et al. 1984; Purser 1985; Theriault and Hutcheon 1987; Jones et al. 1989; Kenny 1992). The

most reliable petrographic evidence for the recognition of dedolomite in the Guelph Formation is a spectrum of replacement textures ranging from minor corrosion on the edges or in the centers of dolomite rhombs to micrometer-sized inclusions of dolomite within calcite crystals. Most Guelph dedolomites exhibit well preserved precursor textures, although they generally more poorly preserve fossils and early diagenetic textures relative to their dolomite precursors and especially primary limestones.

The most commonly occurring replacement fabrics in Guelph dedolomites include: (1) finely crystalline (50-150 μm), euhedral to subhedral dolomite rhombs with corroded and embayed edges in close contact with surrounding finer crystals (20-60 μm) of anhedral calcite (Fig. 5.2A); (2) large dolomite rhombs with or without corroded edges floating in a finer crystalline calcite mosaic (Fig. 5.2A,B); (3) irregular meshwork, consisting of interconnected dolomite relicts (Fig. 5.2C); (4) poikilotopic fabrics, showing coarsely crystalline calcite that poikilotopically encloses rhombic dolomite crystals and corroded dolomite remains (Fig. 5.2D); (5) finely to coarsely crystalline calcite crystals containing numerous micrometer-sized dolomite inclusions (<10 μm) and these dolomite inclusions show the same optical orientation as the calcite host (Fig. 5.3A); (6) dolomitized early fibrous and equant calcite crystals with partially preserved precursor textures (Fig.5.3B); (7) partially to completely dedolomitized rhombic dolomite crystals (Fig. 5.3C); and (8) most replacement extends from the crystal edges or outer rims to cores ("centripetal replacement" of Shearman et al. 1961). Dolomite rhombs replaced by calcite within cores ("centrifugal replacement" of Shearman et al. 1961), as observed in other studies (e.g.

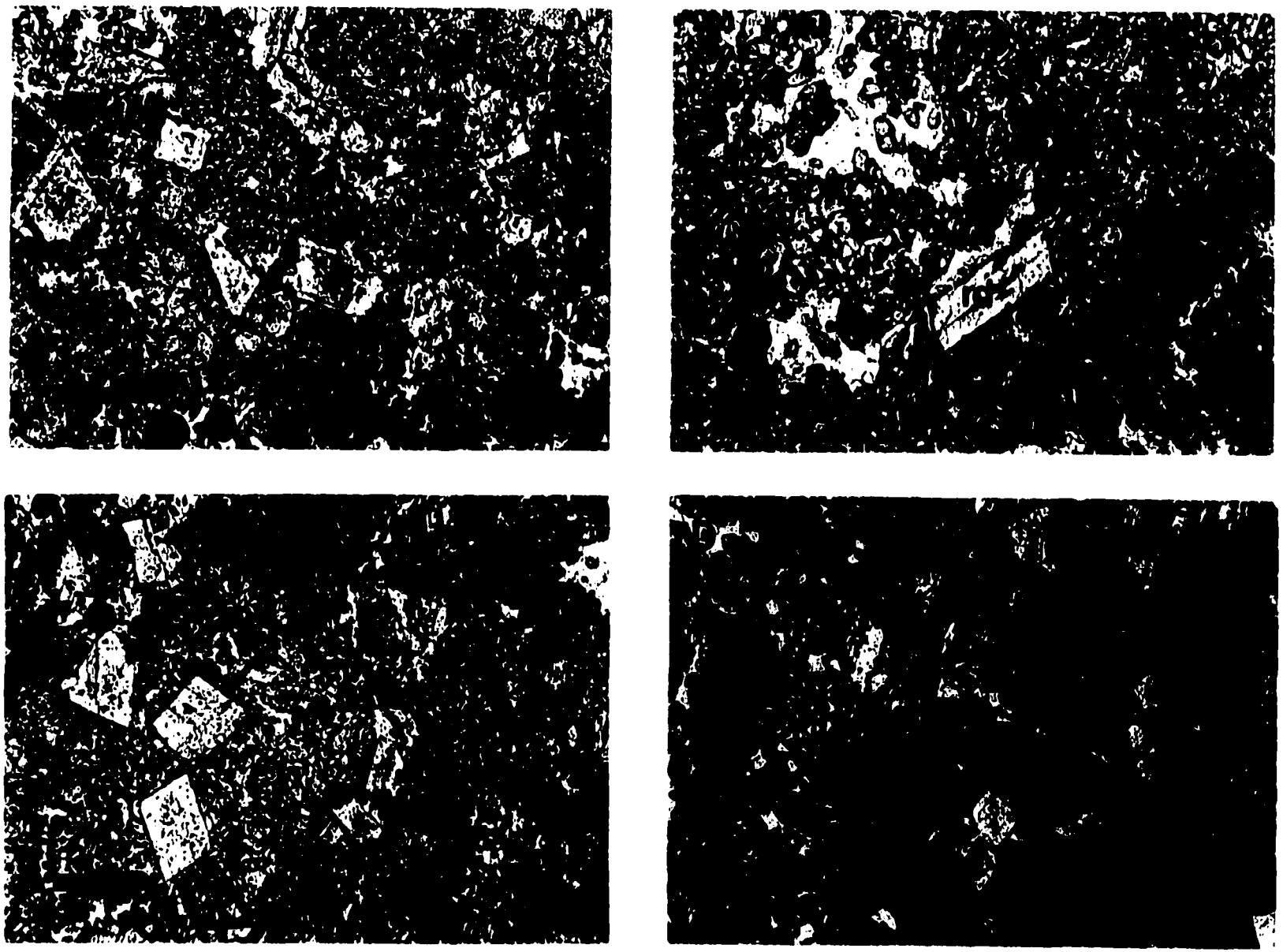


**Fig. 5.2** (p.161) Plane light photomicrographs of dedolomite fabrics in stained and polished thin sections. **A.** Finely crystalline Type 2 dolomite rhombs with corroded edges are closely surrounded by finer crystalline dedolomite crystals (red). Sample W17, scale bar = 0.2 mm. **B.** Corroded Type 2 dolomite rhombs (rd) floating in a finer crystalline mosaic consisting of anhedral dedolomite crystals (red) and irregular dolomite relicts (white). Sample W17, scale bar = 0.1 mm. **C.** A meshwork or net (n) consisting of connected dolomite relicts (unstained), resulted from partial replacement of Type 2 dolomite rhombs by finer crystalline anhedral dedolomite (red). Sample 17, scale bar = 0.2 mm. **D.** A large dedolomite crystal (red) encloses rhombic dolomite crystals and corroded dolomite relicts (white) to form a poikilotopic fabric. Sample W15, scale bar = 0.1 mm.

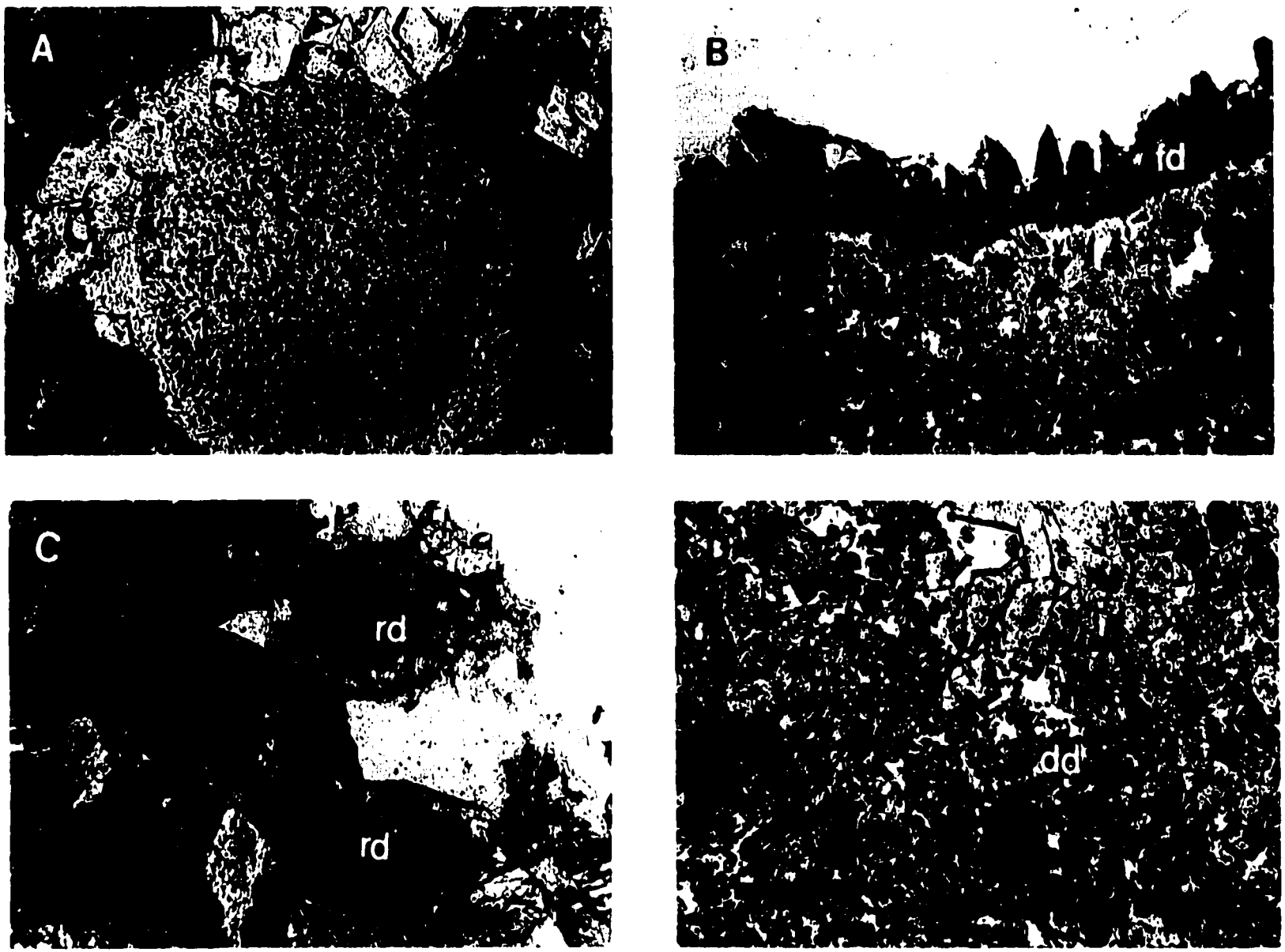



**Fig. 5.3** (p.162) Plane light photomicrographs of dedolomite fabrics in stained and polished thin sections. **A.** A coarsely crystalline dedolomite crystal (red) in the center contains numerous micrometer-sized dolomite inclusions. Sample W95, scale bar = 0.1 mm. **B.** Selectively dedolomitized fibrous cement rim (fd, red) with partially preserved precursor crystal shapes. Sample W16, scale bar = 1.0 mm. **C.** Rhombic dedolomite pseudomorphs. Type 2 dolomite rhombs were partially to nearly completely replaced by dedolomite (red) but with preserved rhombic shapes. Sample W95, scale bar = 0.1 mm. **D.** Replacement boundary between Type 2 dolomite (d, white) and finer crystalline dedolomite (dd, red). Sample W17, scale bar = 0.2 mm.

Budai and Lohmann 1984; Holail et al. 1988; Kenny 1992), are also present but rare. In either case the newly formed dedolomite crystals in the Guelph Formation are optically continuous with the dolomite precursor. Replacement boundaries between Type 2 dolomite and dedolomite are commonly observed in cores and thin sections (Fig. 5.3D). Dolomite rhombs with calcite zones as reported in other studies (e.g. Zenger 1973) were not observed in this study.

## 5.5 Dedolomite geochemistry

Guelph dedolomites are composed of Mg-rich calcites (4-9 wt % $MgCO_3$, Appendix III). Sr and Na contents of Guelph dedolomites vary from approximately 40-60 ppm and 200-2000 ppm, similar to the ranges of Sr (40-100 ppm) and Na (200-1600 ppm) in their dolomite precursors (Fig. 5.4). The concentrations of Fe (600- 1700 ppm) and Mn (60-200 ppm) in Guelph dedolomite are greatly enriched relative to the values of Fe (100-700 ppm) and Mn (20-100 ppm) in associated limestones, but within the ranges of Fe (200-3000 ppm) and Mn (50-350 ppm) for dolomites (Fig. 5.5).

Guelph dedolomites have $\delta^{18}O$ values in the range of -6 to -9 ‰ (PDB) and $\delta^{13}C$ values from +2.5 to +4 ‰ (PDB), values that are similar to those of associated dolomites and most limestone samples (Fig. 5.6). The strontium isotopic ratios ($^{87}Sr/^{86}Sr$) of two dedolomite samples are 0.70876 and 0.70885 (Fig. 5.7), which are similar to the values of Type 2 dolomites.

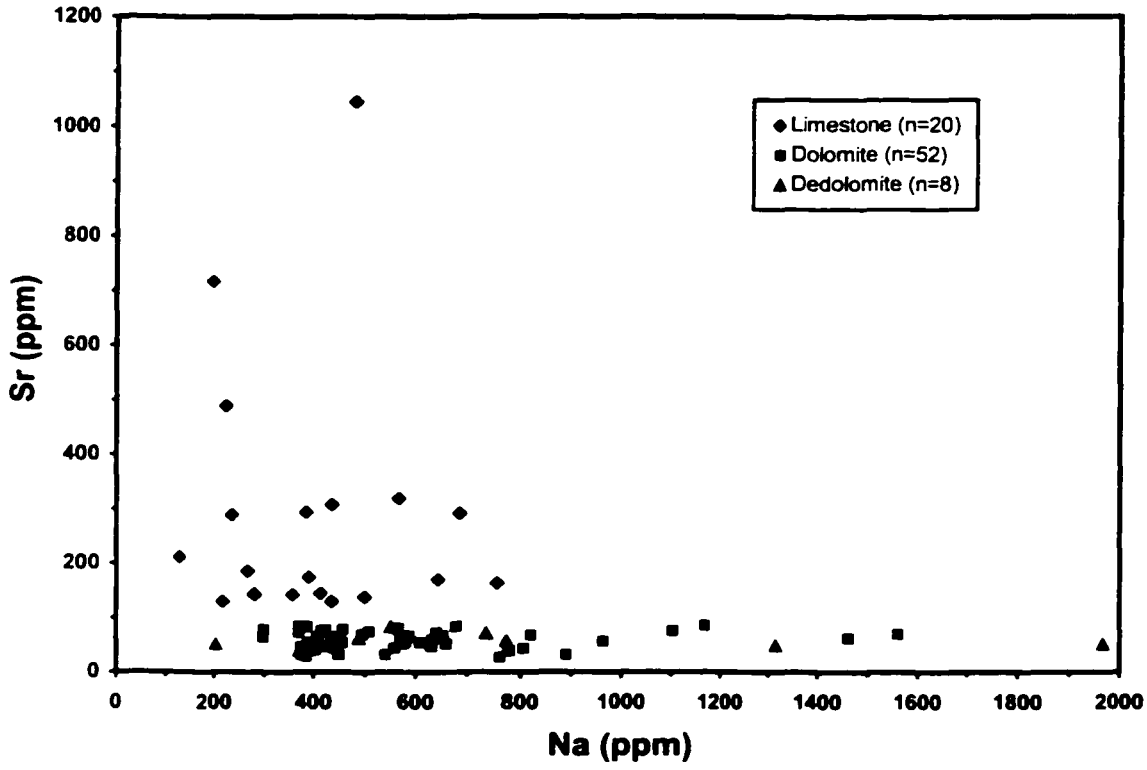



Fig. 5.4 Na vs. Sr for Guelph limestone, dolomite and dedolomite. Dedolomite samples have lower Sr and higher Na concentrations than limestone samples but show similar Sr and Na contents to dolomite samples.

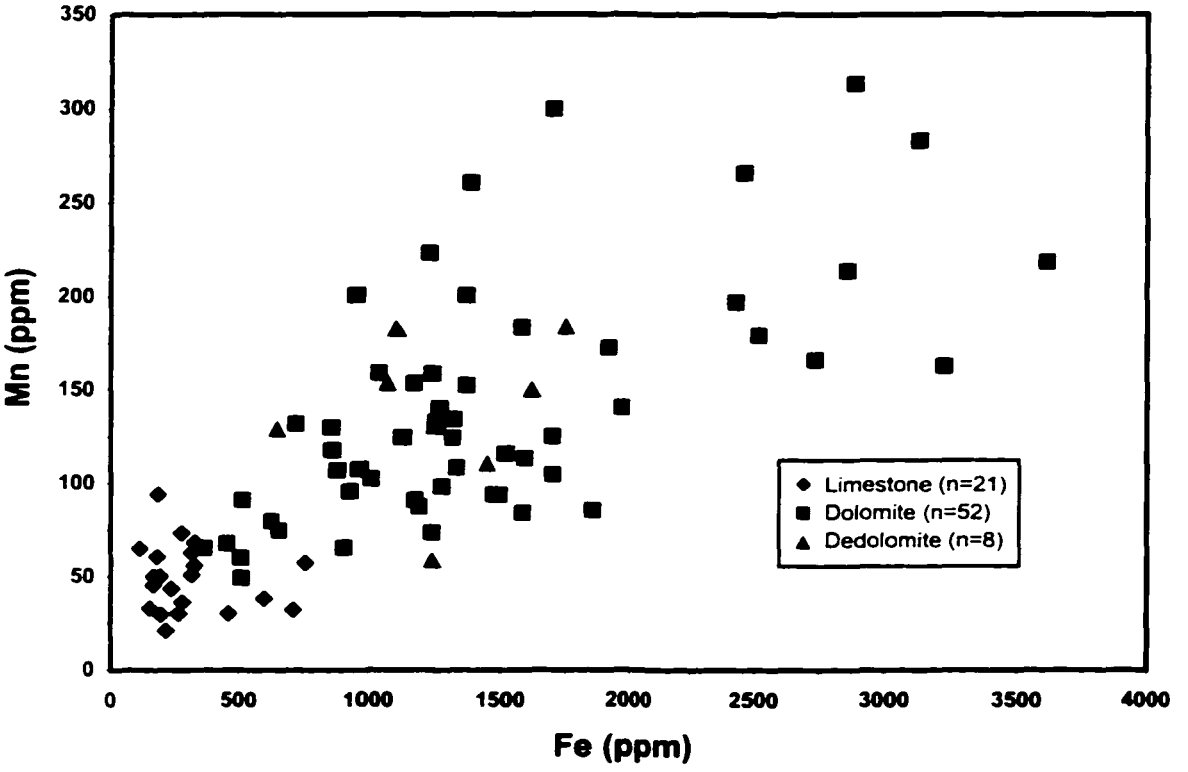



Fig. 5.5 Fe vs. Mn for Guelph limestone, dolomite and dedolomite. Dedolomite samples have higher Fe and Mn concentrations than limestone samples but display similar Fe and Mn contents to dolomite samples.

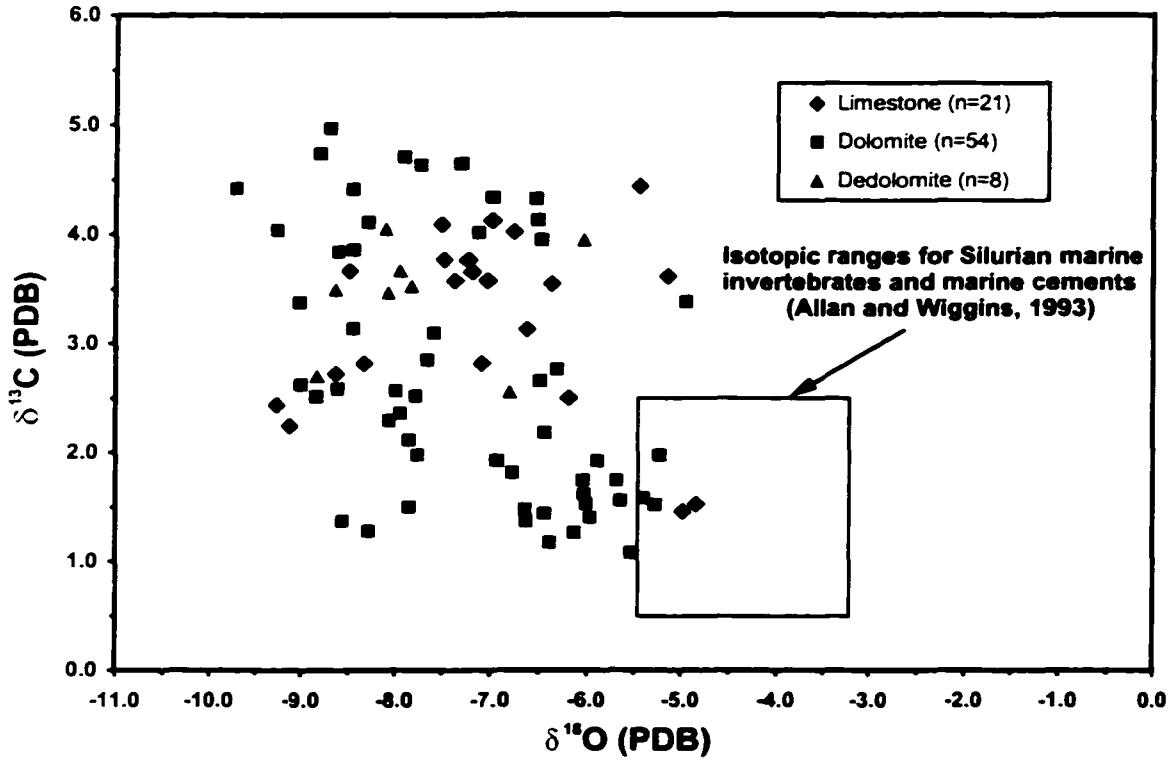



Fig. 5.6 $\delta^{13}C$ (PDB) vs. $\delta^{18}O$ (PDB) for limestone, dolomite, and dedolomite. Dedolomite $\delta^{13}C$ and $\delta^{18}O$ values range from -6 to -9‰ and from +2.5 to +4‰, similar to those of associated dolomite and most limestone samples.

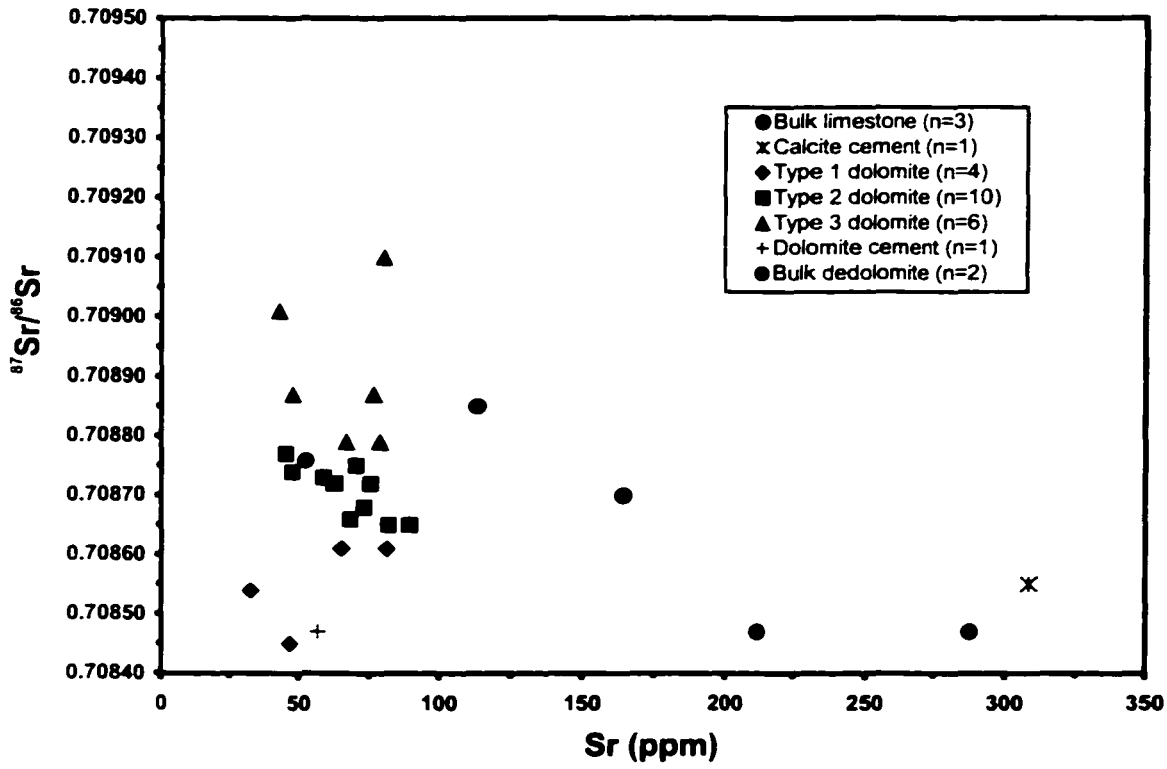



Fig. 5.7 Sr Vs. $^{87}Sr/^{86}Sr$ for major carbonate fabrics including dedolomite. Dedolomite 87Sr/86Sr ratios are higher than ratios of bulk limestone and calcite cement but similar to the ratios of Type 2 dolomite.

Homogenization temperatures (Th) of primary two-phase fluid inclusions within 2 Guelph dedolomite samples range from 53.4 to 72.4°C (Appendix IV). Initial melting temperatures (Te) vary from –28.0 to –31.4°C and final melting temperatures (Tm) range from –16.8 to –18.4°C.

## 5.6 Interpretation and discussion

The general conditions required for extensive dedolomitization in the Guelph Formation include a source of $Ca^{2+}$ ions, a favorable chemical condition maintained for an adequate period of time, and an efficient pump or paleohydrologic system for bringing $Ca^{2+}$ in and flushing $Mg^{2+}$ away.

### 5.6.1 Dedolomitizing fluid

Previous studies have invoked a variety of fluids to explain dedolomitization: (1) fresh meteoric or mixed seawater-meteoric fluids moving downward in a groundwater system, with or without sulfate mineral dissolution (Fritz 1967; Longman and Mench 1978; Magaritz and Kafri 1981; Holail et al. 1988; Kenny 1992); (2) hot, deep, Ca-rich brines moving upward along major faults fault (Land and Prezbindowski 1981); and (3) fluids evolved from seawater (Theriault and Hutcheon 1987), chemically altered by dissolution of carbonate or reacting with non-sulfate minerals in the subsurface (Katz 1971; Land and Prezbindowski 1981; Holail et al. 1988; Jones et al. 1989; James et al. 1993).

Dedolomites formed in fresh water and mixing-zones are characterized by (1) significantly depleted $\delta^{18}O$ values (up to –12‰ PDB) (Kenny 1992) and/or $\delta^{13}C$ values (up to -11‰ PDB) (Fritz 1967; Magaritz and Kafri 1981; Kenny 1992) relative to associated dolomites and limestones; and/or (2) lowed Sr concentrations (<5 to <16 ppm) compared to dolomites (Shearman and Shirmohammadi 1969; Magaritz and Kafri 1981). As discussed above, Guelph dedolomites do not exhibit significant depletions in oxygen and/or carbon isotopic values or Sr concentrations relative to their dolomite precursors or primary limestone. This indicates that the fluids responsible for dedolomitization are isotopically similar to the fluids involved in early Type 1 and subsequent Type 2 dolomite formation, implying seawater or modified seawater as the dedolomitizing fluids.

The seawater origin of dedolomitizing fluids is further supported by strontium isotope and fluid inclusion observations. The $^{87}Sr/^{86}Sr$ ratios of two dedolomite samples (0.70875 and 0.70885) are identical to the ratios of Type 2 dolomite samples and close to the ratios of the Middle Silurian seawater (Fig. 5.7). The low final melting temperatures (Tm) of -16.8 to -18.4°C in dedolomite fluid inclusions indicate that the dedolomitizing fluids were saline waters with higher salinities than normal seawater. These dedolomite Tm values are lower than the final melting temperatures of -10.8 to -13.5°C in Type 2 dolomites (Appendix IV), suggesting a slight increase in salinity in dedolomitizing fluids.

Numerous previous studies have related dedolomitization to fault or fracture systems which served as fluid pathways for vertical upward movement of deep basinal Ca-rich

brines into the site for dedolomitization (Budai et al. 1984; Land and Prezbindowski 1981) or for the downward circulation of fresh surface water (Fritz 1967; Longman and Mench 1978; Deike 1990). However, Guelph dolomites occur as thin layers to massive beds interbedded with dolomite and limestone beds. There is no evidence to support fault or fracture control.

### 5.6.2 Source of $Ca^{2+}$ for dedolomitization

Von Morlot (1847) proposed that dedolomitization was caused by the reaction of dolomite with solutions containing $Ca^{2+}$ from the dissolution of gypsum or anhydrite to form calcite and highly soluble magnesium sulfate, expressed by the following reaction equation:

$$CaMg(CO_3)_2(solid) + Ca^{2+} + SO_4^{=} \rightarrow 2CaCO_3(solid) + Mg^{2+} + SO_4^{=}$$

This hypothesis has been widely applied to many earlier studies of dedolomites (Lucia 1961; Goldberg 1967; Folkman 1969; Longman and Mench 1978; Frank 1981; Back et al. 1983). However, this hypothesis is not well supported in other cases, especially for dedolomites not associated with anhydrite or gypsum beds. Other studies have noted that dedolomites preferably occur within dolomites interbedded with or adjacent to limestones, or within partly dolomitized limestones (Fritz 1967; Magaritz and Kafri 1981; Theriault and Hutcheon 1987), implying that dissolution of associated limestones could be a local source of $Ca^{2+}$ for dedolomitization. Longman and Mench (1978) reported an example of dedolomitization related to limestone dissolution in the Edwards Aquifer of

south and central Texas. Ca-rich groundwater produced by limestone dissolution in the updip recharge area flowed downdip and caused dedolomitization in the Edwards dolomite.

Yanat'eva (1955) found $SO_4^=$ becomes an activator for dedolomitization at low $Pco_2$. More recently, Kastner (1982) conducted a series of experiments at temperatures up to 200°C and concluded that it is the $Ca^{2+}$ content rather than the presence of $SO_4^=$ controlling the replacement of dolomite by calcite. Similarly, Stoessell et al. (1987) concluded that the key requirement for dedolomitization in Na-Ca-Cl brines at up to 200°C is $Ca^{2+}$ concentration but not $SO_4^=$ concentration.

As mentioned in Chapter 3, anhydrite cement occurs throughout the Guelph succession. The brines for precipitating anhydrite cement could have been a $Ca^{2+}$ source for causing dedolomitization. However, anhydrite cement only occurred in larger cavities and fractures in minor amounts (<2%) and anhydrite cementation seems to always postdate dedolomitization. The fluid responsible for anhydrite cementation cannot readily explain the observed massive dedolomitization in both amount and timing.

The brine responsible for deposition of Salina anhydrite beds is another possible $Ca^{2+}$ source. But the late timing of the dedolomitization event and the occurrence of Guelph dedolomites only within a narrow zone do not support the idea that this localized dedolomitization was caused by brines related to deposition of associated anhydrite beds.

The selective dedolomitization within the pinnacle reefs containing interbedded dolomite and limestone suggests that this dedolomitization was most likely resulted from Ca-rich fluids generated from dissolution of remained limestone, which was probably caused by the fluids charged with organic acids and hydrogen sulfide released from organic matter maturation and thermochemical sulfate reduction during burial (e.g., Moore 1989; Mazzullo and Harris 1992). Common occurrence of vuggy and moldic limestones in the eight cores from five dedolomite-bearing reefs further supports this idea.

In light of the above observation and inferences, a more suitable equation to describe dedolomitization in the Guelph Formation is as follows:

$$CaMg(CO_3)_2\ (solid) + Ca^{2+} \rightarrow 2CaCO_3(solid) + Mg^{2+} \quad (K \approx 1 \text{ at } 25°C)$$

For this equation, the equilibrium constant (K) is approximately 1 and the replacement of dolomite by calcite or dedolomite is dominated by the $Ca^{2+}$ concentration in the pore fluids. The most logical explanation for both the restricted occurrence of Guelph dedolomites in a narrow limestone-bearing zone and incomplete dedolomitization in most of the dedolomitized intervals in the pinnacle reefs is that the process was controlled by the limited supply of $Ca^{2+}$ from the local dissolution of limestone beds.

### 5.6.3 Environment and timing of dedolomitization

Dedolomitization can occur under surficial weathering (e.g., Al-Hashimi and Hemingway 1973) or epigenetic diagenesis influenced by oxidized Ca-rich meteoric waters (Shearman

et al. 1961; Evamy 1967; Folkman 1969; Braun and Friedman 1970; Chafetz 1972; Longman and Mench 1978; Frank 1981), early or penecontemporaneous diagenesis (Katz 1968, 1971; Margaritz and Kafri 1981; Purser 1985), and medium to late burial diagenesis (Budai et al. 1984; Theriault and Hutcheon 1987).

Significant depletions in oxygen and/or carbon isotopes of dedolomites relative to associated dolomites have been interpreted to represent alteration from near-surface meteoric or mixed waters (e.g., Magaritz and Kafri 1981; Holail et al. 1988; Wallace et al. 1991; Kenny 1992) and deep burial fluids (Budai et al. 1984). However, oxygen and carbon isotopic compositions of Guelph dedolomites are similar to the values of associated dolomites, suggesting that the isotopic compositions of dedolomitizing fluids and burial conditions (depth and temperature) were similar to those for earlier dolomite formation.

Homogenization temperatures of primary two-phase fluid inclusions within Guelph dedolomites ranging from +53.4 to +72.4°C are similar to or slightly higher than the Th readings of +64.5 to +74.7°C obtained from the fluid inclusions within associated Type 2 dolomites (Appendix IV), indicating a shallow to moderate burial environment.

### 5.6.4 Replacement mode

Dedolomitization is thought to occur by either a one-step thin-film replacement of dolomite by concomitant dolomite dissolution and calcite reprecipitation, or a two-step

time-separated process including dissolution of dolomite to form a void and subsequent precipitation of calcite as cement (e.g., Jones et al. 1989; James et al. 1993). The relative rates of dolomite dissolution and calcite precipitation control the mode of dedolomitization. One-step replacement is more likely to preserve the precursor textures.

Rhombic calcite pseudomorphs indicate one-step replacement (Jones et al. 1989). Partially dedolomitized and preserved precursor fabrics such as fibrous and equant cements were also most likely the products of one-step replacement. In Guelph dedolomites, the common occurrence of several replacement textures including rhombic calcite pseudomorphs, partially dedolomitized fibrous and equant cements, and optical continuity between dedolomite and dolomite suggest that Guelph dedolomites were mainly formed by a one-step replacement. Identical dull orange luminescence to nonluminescence of dedolomites and their dolomite precursors also supports this interpretation.

### 5.6.5 Dedolomitization model

Dedolomitization can result from a chemically evolved pore fluid that was generated by adding fresh water and/or water-rock interaction in a flow system (e.g., Katz, 1971; Theriault and Hutcheon, 1987; Holail et al., 1988; Jones et al., 1989; James et al., 1993). In the Cenomanian-Turonian Upper Judea Group of northern Israel, Magaritz and Kafri (1981) found that dedolomites occurred in a very narrow lateral zone (20-300 m) between shallow-marine hypersaline dolomites and basinal limestones, a situation somewhat

similar to the setting of Guelph dedolomites. They interpreted this dedolomitization to have occurred as a result of exposure to fresh water, as indicated by light carbon isotopes and low Sr concentrations in dedolomite. Theriault and Hutcheon (1987) observed that the dedolomites in the Devonian Grosmont Formation of northern Alberta occurred within partly dolomitized limestones or near undolomitized limestones. They proposed that dedolomitization occurred at the front of a reflux flow of hypersaline brine in the waning stage of dolomitization. $Ca^{2+}$ in the pore fluid at this front was greatly enriched due to the dolomitization reaction along the flow path. Based on the study of an Upper Cretaceous shallow marine carbonate sequence at Baiharija Oasis, northern Egypt, Holail et al. (1988) proposed a similar model in which the dolomitization, dolomite alteration, and selective dedolomitization were caused by an evolving fluid in a similar shallow burial hydrologic system. However, they considered that pore fluid evolved from mixing with fresh water rather than from the dolomitization reaction. Similarly, Jones et al. (1989) suggested that the replacement of dolomite by calcite in the Oligocene-Miocene Bluff Formation of Grand Cayman occurred as groundwater evolved toward less saline with time due to mixing with meteoric waters.

In the study area, Guelph dedolomites occur in pinnacle reefs within a narrow zone on the lower ramp, and their petrographic and geochemical data do not support any significant influence of fresh water. The most likely mechanism for the localized dedolomitization in the basinward pinnacle reefs may involve modified seawater supplied by the same diagenetic flow system which earlier led to regional dolomitization and subsequent Type 2 dolomite formation. The conduits responsible for the formation of earlier Type 2

dolomite likely acted as conduits for their subsequent dedolomitization. The aquifer in this hydrologic system is interpreted to have been a shallow to moderately buried, porous carbonate consisting of Guelph reefal and interreef carbonates developed on the gently-sloping carbonate ramp (Fig. 4.24). The recharge area is presumed to have been on eastward side of the sheif and the discharge area was in the basin center. The driving force for subsurface flow was hydraulic head created by a gravity gradient between the open sea level and the water surface level in the isolated Michigan Basin. Fluids supplied by the recharge sources were similar to the fluids involved in earlier Type 1 and Type 2 dolomite formation, but dedolomitizing fluids acquired extra $Ca^{2+}$ from limestone dissolution during their flow through the partially dolomitized pinnacle reefs on the lower ramp. This subsurface reflux system continued until the water supply was significantly reduced or removed as a result of either that the recharge area in back-barrier-reef lagoon was sealed by thick evaporites, or that the hydraulic head difference between open sea level and drawdown sea level became too low to drive basinward flow (Fig. 4.24).

A general diagenetic model including four major stages is summarized in Figure 5.8 to describe the Guelph dedolomitization during shallow to moderate burial conditions. The first stage was limestone lithification, involving marine and shallow burial calcite cementation and neomorphism (see Chapter 3). The second and third stages involved Type 1 and Type 2 dolomite formation (see Chapter 4). The fourth stage records a shift of the bulk chemical composition of the pore fluid from dolomite stability field to the calcite stability field (e.g., Land 1985). This shift occurred in a narrow transitional zone and is interpreted to represent an increase of Ca/Mg ratio in the pore fluids within dedolomitized

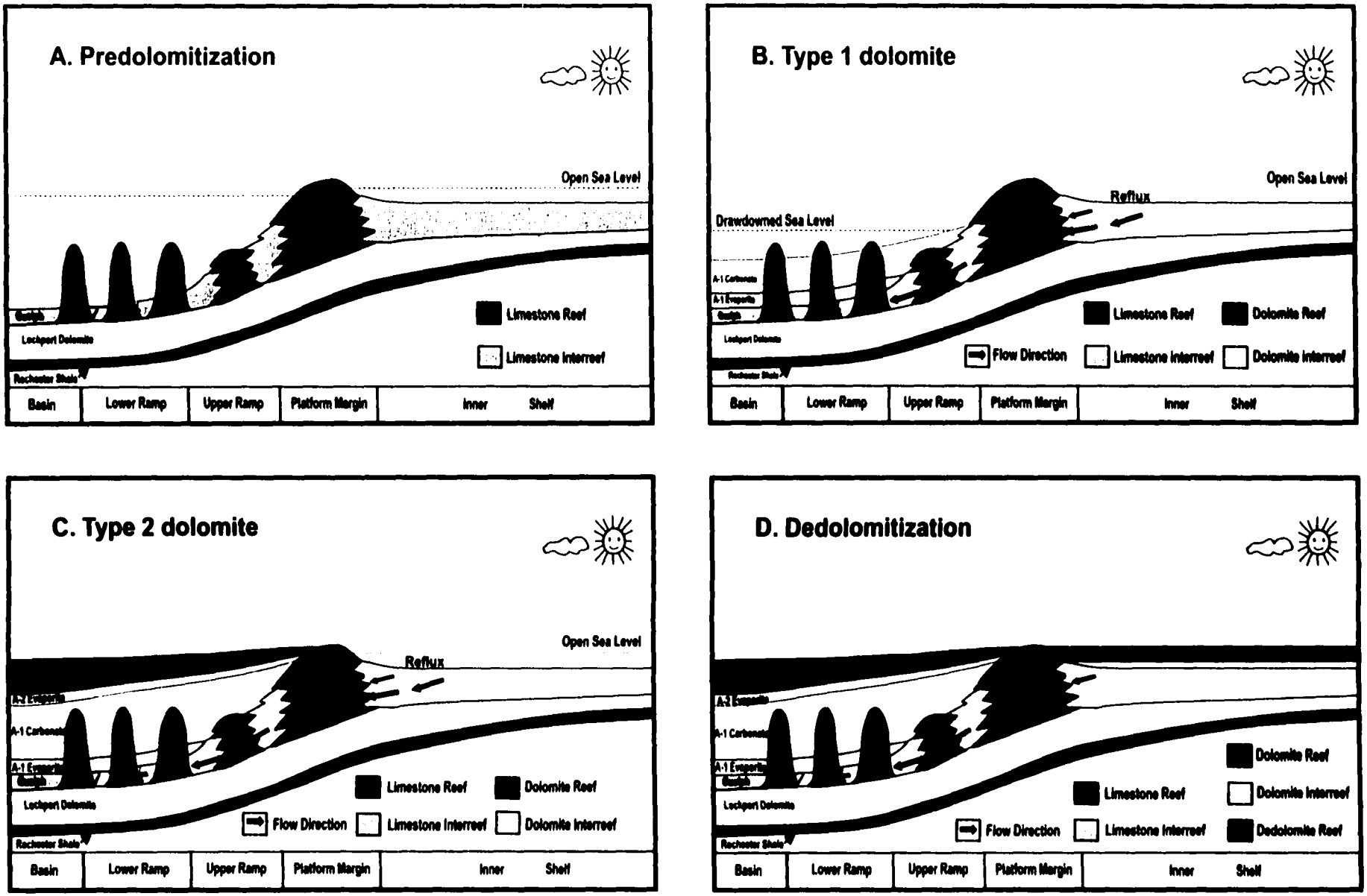



Fig. 5.8 Conceptional model for dolomitization and subsequent dedolomitization, showing early dolomitization resulted from seawater reflux driven by a hydraulic head that was induced by evaporative drawdown during the Late Silurian. Local dedolomitization in basinward pinnacle reefs was caused by limestone dissolution.

reefs. The most likely source of excess $Ca^{2+}$ is from the dissolution of local limestone within a narrow limestone-bearing zone on the lower ramp.

## 5.7 Conclusions

1. Several intervals of dedolomitized rock, ranging from 0.2 to 60 m in thickness, have been recognized in five pinnacle reefs on the lower ramp within a narrow transitional zone (10-20 km) between shelfward dolomite and basinward limestone. The Guelph dedolomite occurs in Type 2 dolomite as a minor replacement to almost complete replacement, with dedolomite contents ranging from 5% to 95%. The lighter colored dolomitized rocks contain variable amounts of darker colored dolomite remains.

2. Guelph dedolomite shows depleted Sr contents, enriched Fe and Mn concentrations, and higher $^{87}Sr/^{86}Sr$ ratios relative to primary limestone, but similar values in comparison with Type 2 dolomite. Based on oxygen isotopic and fluid inclusion data, dedolomitization is interpreted to have occurred at moderate burial conditions that were probably similar to those for Type 2 dolomite formation. This replacement is interpreted to be the product of a one-step replacement of Type 2 dolomite. The relative timing of dedolomitization postdates Type 2 dolomite formation but predates anhydrite cementation.

3. Localized dedolomitization was caused by reaction between Type 2 dolomites and $Ca^{2+}$ -rich or high Ca/Mg ratio fluids. Dedolomitizing fluids most likely evolved from seawater-derived fluids responsible for earlier Type 1 and Type 2 dolomite formation,

and these fluids may have progressively evolved toward being more saturated with respect to calcite, as result of acquiring extra $Ca^{2+}$ from dissolution of local limestone beds in pinnacle reefs.

4. The most likely hydrologic mechanism for the localized dedolomitization in the Guelph Formation is same as the hydrologic system for earlier Type 1 and Type 2 dolomite formation. This hydrologic system is a gravity-driven reflux system initially induced by sea level fall or evaporation drawdown during the Late Silurian. Circulation of modified seawater with local input of extra $Ca^{2+}$ during this period caused local extensive replacement of Type 2 dolomite by calcite in the limestone-bearing pinnacle reefs. This groundwater flow system probably extended until the water supply was reduced when either the recharge area in the inner shelf was sealed by evaporites or the hydraulic head became too low to drive flow.

# Chapter 6 Post-dolomitization diagenesis and porosity

## 6.1 Abstract

Guelph limestones occur as low-porosity and porous intervals. Low-porosity limestones show relatively low porosity (0.1-7.0%) and permeability (0.01-5.4 md), but porous limestones have high and variable porosity (7.7-30.6%) and permeability (20.4-1861.5 md). Most low-porosity limestones were related to extensive early calcite cementation of primary pores, and some resulted from late stage halite plugging. Porous limestones commonly contain abundant moldic and vuggy pores resulting from extensive dissolution. Guelph dolomites exhibit highly variable porosity (0.1-23.6%) and permeability (0.01-10200 md). Type 1 dolomite shows similar low porosity (0.1-6.6%) and permeability (0.01-3.8 md) to associated low-porosity limestones, indicating fabric-preserving dolomitization and early recrystallization are not important processes in changing porosity. Type 2 and Type 3 dolomites exhibit wide ranges of porosity (3.4-35.2%) and permeability (2.5-5128 md). Porosity evolution and reservoir quality in Type 2 and Type 3 dolomites were mainly controlled by dissolution and dolomite alteration. Guelph dedolomites show low porosity (0.2-14.4%) and permeability (0.1-113 md) relative to their precursor Type 2 dolomites, indicating that dedolomitization is a porosity-reducing process.

Intercrystalline pores are the most important porosity in all three dolomite types. Moldic and vuggy pores occur in most porous Type 2 and Type 3 dolomites, but are rare in Type

1 dolomite. Most Type 2 and Type 3 dolomites contain abundant intercrystalline, moldic, and vuggy pores and constitute the best reservoir rocks in the Guelph Formation.

Most Type 2 and Type 3 dolomites occur in close association with fractures and vuggy intervals. Fractures played an important role in reopening low-porosity Type 1 dolomite to allow later diagenetic fluids for dolomite dissolution and formation of Type 2 and Type 3 dolomites. Type 2 dolomites served as a long-lived aquifer and conduit system for late diagenetic fluids that led to further dolomite alteration and porosity evolution. Fractures mainly resulted from tectonic activity and differential compaction that postdated early dolomitization. Major dissolution events that occurred in both dolomites and limestones also postdated Type 1 dolomite formation. Other post-dolomitization diagenesis, especially halite cementation, also played an important role in controlling the final porosity in Guelph carbonates.

## 6.2 Introduction

The origin of porosity in dolomite is commonly attributed to the dolomitization process. To explain the vuggy porosity of approximately 12% in the Triassic dolomites of the Tyrol Alps, De Beaumont (1887) proposed the hypothesis of mole-for-mole replacement of limestone by dolomite. Weyl (1960) supported the mole-for-mole model by assuming that dolomitization was an in situ replacement of $Ca^{2+}$ by $Mg^{2+}$ without major import of $CO_3^{=}$, based on the small amount of $CO_3^{=}$ present in modern day groundwaters. Murray (1960) applied this hypothesis to explain the origin of porosity in porous sucrosic

dolomites but did not explain the origin of associated low-porosity dolomite. However, the validity of this hypothesis has been challenged in a number of studies (e.g., Landes 1946; Purser et al. 1994; Sun 1995). The mole-for-mole replacement hypothesis does not readily explain the coexistence of both porous and low-porosity dolomites in the same rock (Landes 1946; Purser et al. 1994; Sun 1995). Many dolomites have similar or even lower porosities than associated (age-equivalent) limestones in the same strata (Schmoker 1984; Schmoker et al. 1985; Lucia and Major 1994). Purser et al. (1994) pointed out that porosity in dolomites is not necessarily related to dolomitization, nor is it likely a mole-for-mole replacement of Ca by Mg. $CO_3^=$ may also have been transported to the replacement site by large volume of fluid in an open system.

Some recent dolomite studies (e.g., Purser et al. 1994; Negra et al. 1994) have demonstrated that dolomitization could improve, preserve, or destroy the porosity in the limestone precursor, depending on the replacement mode or relative rates of limestone dissolution and dolomite precipitation. Amthor et al. (1994) found that dolomitization in the upper Devonian Leduc Formation of central Alberta mainly redistributed primary limestone porosity to secondary dolomite porosity, with an obvious decrease in porosity but a minor increase in permeability. Lucia and Major (1994) have shown that the porosities in Pliocene-Pleistocene dolomites on Bonaire Island, Netherlands Antilles, were greatly decreased relative to the porosities in precursor limestones as result of early, near-surface dolomitization. Other studies (Amthor and Friedman 1991; Montañez and Stefani 1993; Montañez 1994; Sun 1995) suggested that extensive dolomite alteration through fracturing, dolomite dissolution, dolomite precipitation as overgrowth and

cement, and dolomite recystallization may have promoted the development of significant amounts of intercrystalline and vuggy porosity in many pervasive dolomites. Jameson (1994) concluded that reservoir quality in dolomites of the Pennsylvnian Wahoo Formation at Lisburne field of Prudhoe Bay, Alaska, varies with degree of neomorphic modification. Al Shdidi et al. (1995) reported similar dolomite alteration in controlling porosity evolution in dolomite reservoirs in the Lower Cretaceous Qamchuqa Group of the Zagros Basin in Iraq.

In many ancient dolomites like the Guelph dolomite, especially in fabric-destructive dolomites, primary fabrics and pores were significantly to entirely altered or even destroyed by later diagenesis. Final reservoir quality in Type 2 and Type 3 dolomites in the Guelph Formation was greatly improved by later alteration of early-formed dolomite, including dolomite recrystallization, dedolomitization, compaction, fracturing, dissolution, and other late diagenesis. Dolomite recrystallization is discussed in Chapter 4. Dedolomitization is documented in Chapter 5. This chapter will focus on compaction, fracturing, dissolution, and other late diagenesis including anhydrite cementation, halite cementation, evaporite dissolution, and hydrocarbon emplacement.

The main objectives of this chapter are (1) to demonstrate the porosity and permeability distributions in Guelph carbonates based on core observations, petrographic studies, and available porosity and permeability data; and (2) to examine the role of major post-dolomitization diagenesis in controlling porosity evolution and reservoir quality in the Guelph Formation.

## 6.3 Porosity types

The recognition of porosity types in the Guelph Formation was based on visual examination of cores and thin sections (Appendixes I and III). Using Choquette and Pray's (1970) carbonate porosity classification, the common pore types in Guelph carbonate are interparticle, fenestral, intraskeletal, shelter, intercrystalline, moldic and intracrystalline, vuggy, and fracture porosity (Fig. 6.1). Porosities in Guelph dolomites have multiple origins, including inherited porosity from limestone precursors, modified (enlarged or reduced) precursor porosity, and newly formed porosity.

**6.3.1. Interparticle porosity** - Interparticle pores or intergranular pores commonly occur in limestone and Type 1 dolomite (Fig. 6.2A). These pores were mostly occluded by early fibrous and equant calcite cements in limestones or by dolomitized, early fibrous and equant cements in Type 1 dolomites, and make little contribution to the total porosity in limestone and Type 1 dolomite.

**6.3.2. Fenestral porosity** – Fenestral or stromatactic pores are common in mudstone-wackestones and bafflestones and they are typically filled by fibrous calcite cements and geopetal sediments in limestones. Fenestral pores are preserved in some dolomites, but the fibrous calcite cements were replaced by dolomite. Fenestral porosity may have resulted from gases associated with degradation of organic matter.

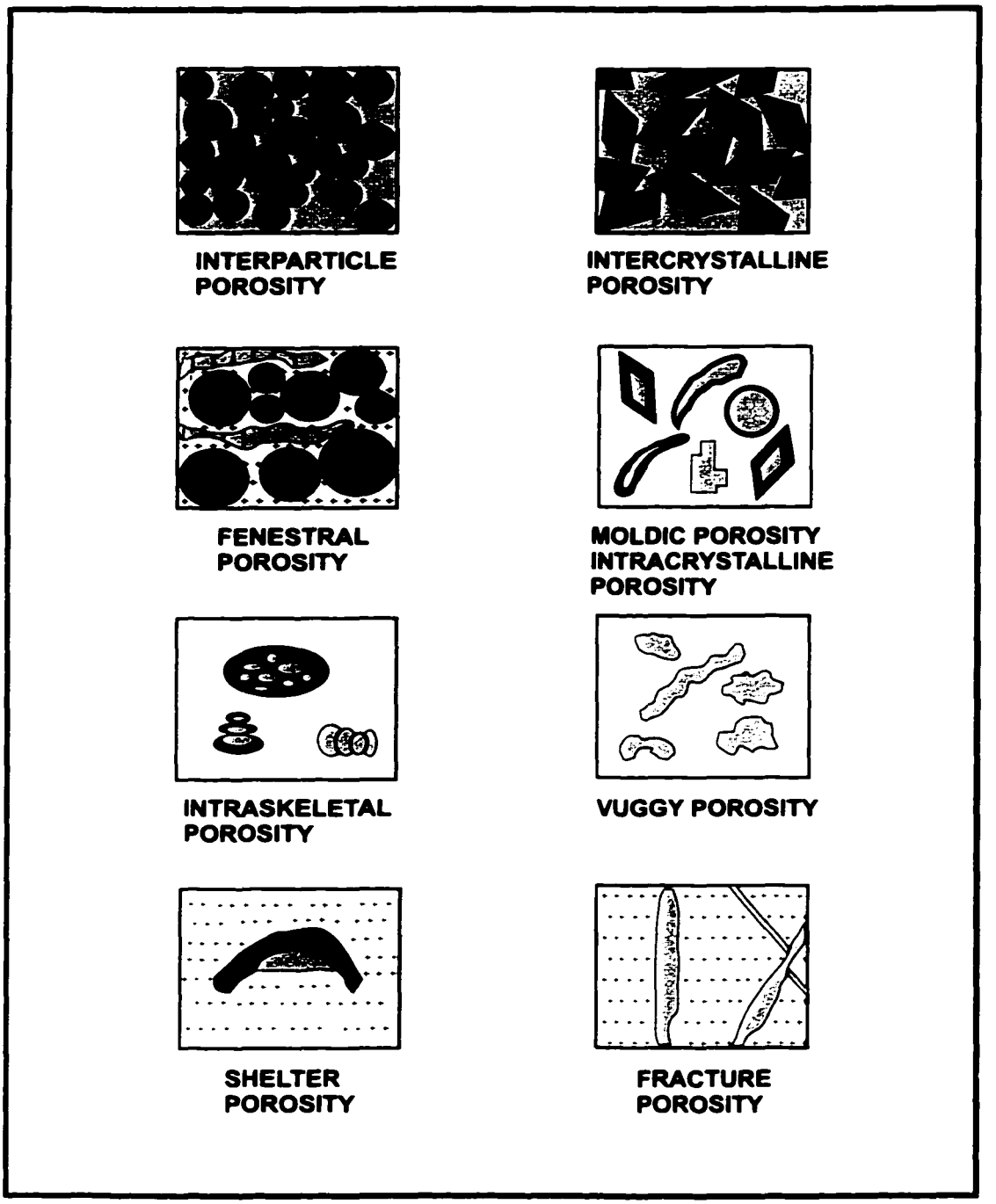



Fig. 6.1 Major porosity types in Guelph carbonates. See text for details.

**6.3.3. Intraskeletal porosity** - Intraskeletal pores occur within fossils such as corals and stromatoporoids (Fig. 6.2B). Intraskeletal porosity commonly occurs in limestone and Type 1 dolomite but is less than 5% of the total porosity.

**6.3.4. Shelter porosity** – Shelter pores occasionally occur beneath some larger fossils such as brachiopods and stromatoporoids in both limestone and dolomite (Fig. 6.2C). This is a minor porosity type.

**6.3.5. Intercrystalline porosity** - Intercrystalline porosity is the most common porosity in all dolomite types. In dolomite, intercrystalline pores were created by dolomite crystallization and modified by subsequent dolomite recrystallization and dissolution (Fig. 6.2D). In Type 1 dolomite, more than 80 to 90% of total porosity consists of intercrystalline porosity. In Type 2 and Type 3 dolomites, more than 50 to 80% of total porosity is intercrystalline porosity and some intercrystalline pores were solution-enlarged due to partial dissolution of crystals.

**6.3.6. Moldic and intracrystalline porosity** - Millimeter to centimeter-sized biomoldic and crystal-moldic pores were formed by selective dissolution of intraclasts such as peloids (Fig. 6.2E), skeletal fragments such as corals, gastropods, bivalves, and crinoids, or millimeter-sized dolomite crystals (Fig. 6.2F). They are rare in Type 1 dolomites but common in porous limestone and Type 2 and Type 3 dolomites. Moldic porosity constitutes approximately 5%-40% of the total porosity in Type 2 and Type 3 dolomites.

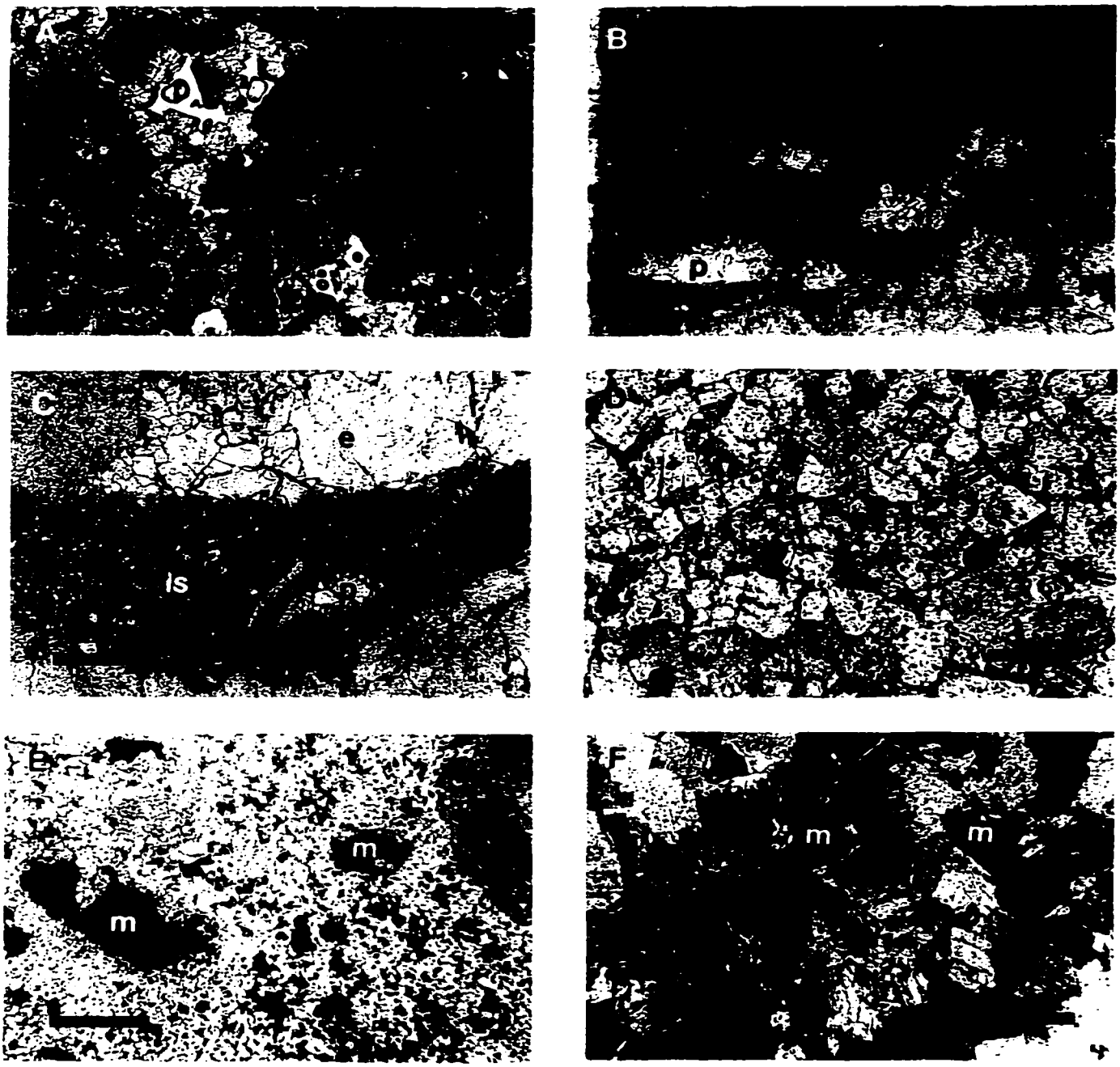



Fig. 6.2 (p.187) Photomicrographs of porosity types in Guelph carbonates. **A.** Interparticle pores (p) in an intraclastic grainstone limestone. Most pores were lined by fibrous calcite cement and later filled by equant calcite cement (red and purple). Sample W157, plane light, scale bar = 1.0 mm. **B.** Intraskeletal pores (p) in a coral clast within a floatstone limestone. All the pores were filled by internal sediments (dark) , fibrous and equant calcite cements (stained red and purple). Sample W31A, stained, plane light, scale bar = 1.0 mm. **C.** A shelter pore (p) beneath a shell (brachiopod?) that occurs in the geopetal sediment (is) which floor a larger intraskeletal pore shown in **B** (p), which was filled by equant calcite cement (e). Sample W31A, stained, plane light, scale bar = 0.2 mm. **D.** Intercrystalline pores (p) in Type 2 dolomite, enlarged by later dissolution. Many dolomite rhombs were corroded. Sample W143, plane light, scale bar = 0.2 mm. **E.** Moldic pores (m) in a porous Type 2 dolomite, resulted from partial to complete dissolution of micritic peloids. Sample W120, crossed-polarized light, scale bar = 1.0 mm. **F.** Moldic pores (m) resulted from partial to complete dissolution of Type 3 dolomite crystals. Sample W155, crossed-polarized light, scale bar = 0.2 mm.

Intracrystalline pores are present in Type 2 and Type 3 dolomites but only constitutes less than 3% of the total porosity.

**6.3.7. Vuggy porosity** - Millimeter to centimeter-sized vuggy cavities were created by selective dissolution (Fig. 6.3A). Vugs commonly have highly irregular shapes and variable sizes. Many vugs could be solution-enlarged moldic pores. They are common in porous limestone and Type 2 and Type 3 dolomites, constituting 10-50% of the total porosity.

**6.3.8. Fracture porosity** - Guelph dolomites were fractured to variable degree by tectonic movement and differential compaction. Fractures are present throughout the formation in different orientations and some intervals contain dense networks of fractures (Fig. 6.3B). Fracture porosity in Guelph dolomites is volumetrically minor (<2%), but may have played an important role in increasing permeability (e.g., Stearns and Friedman 1972) and the formation of porous dolomite reservoirs.

## 6.4 Porosity and permeability distribution

The porosity and permeability ranges of Guelph carbonates from 21 cores in the study area are listed in Appendix V. These porosity and permeability data were compiled from lab analyses conducted by several drilling and production companies. Both limestone and dolomite have highly variable porosity and permeability (Fig. 6.4, Appendix V).

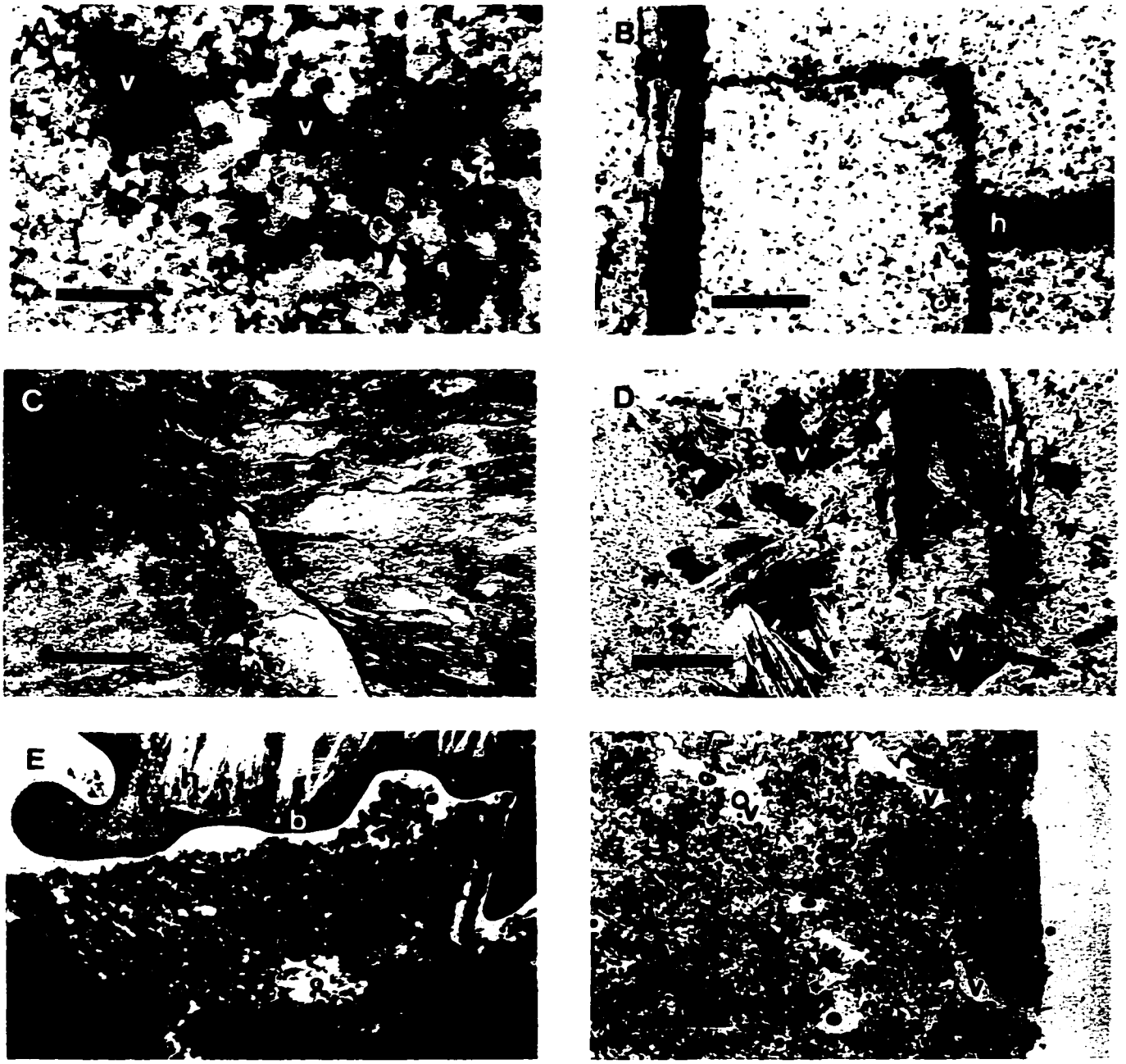



Fig. 6.3 (p.189) Photomicrographs of porosity types and late diagenesis. **A.** Vuggy pores (v) created by selective dissolution in a Type 3 dolomite. Sample W155, crossed-polarized light, scale bar = 1.0 mm. **B.** Fractures in a Type 2 dolomite, partially filled by late anhydrite (a) and halite (h) cements. Sample W74, crossed-polarized light, scale bar = 1.0 mm. **C.** Chemical compaction features including stylolites (st) and seams (sm) in a wackestone dolomite (Type 1). Sample W82, plane light, scale bar = 1.0 mm. **D.** Vuggy pores (v) in a Type 2 dolomite partially filled by bladed to fibrous anhydrite cement (a). Note anhydrite cement was dissolved in places. Sample W93, crossed-polarized light, scale bar = 1.0 mm. **E.** Halite cement (h) in a large vug, partially dissolved and coated by black bitumen or solid hydrocarbon residuals (b). Sample W4, plane light, scale bar = 1.0 mm. F. Vuggy pores (v) in a porous Type 2 dolomite were lined by black bitumen or solid hydrocarbon residuals. Sample W38, plane light, scale bar = 1.0 mm.

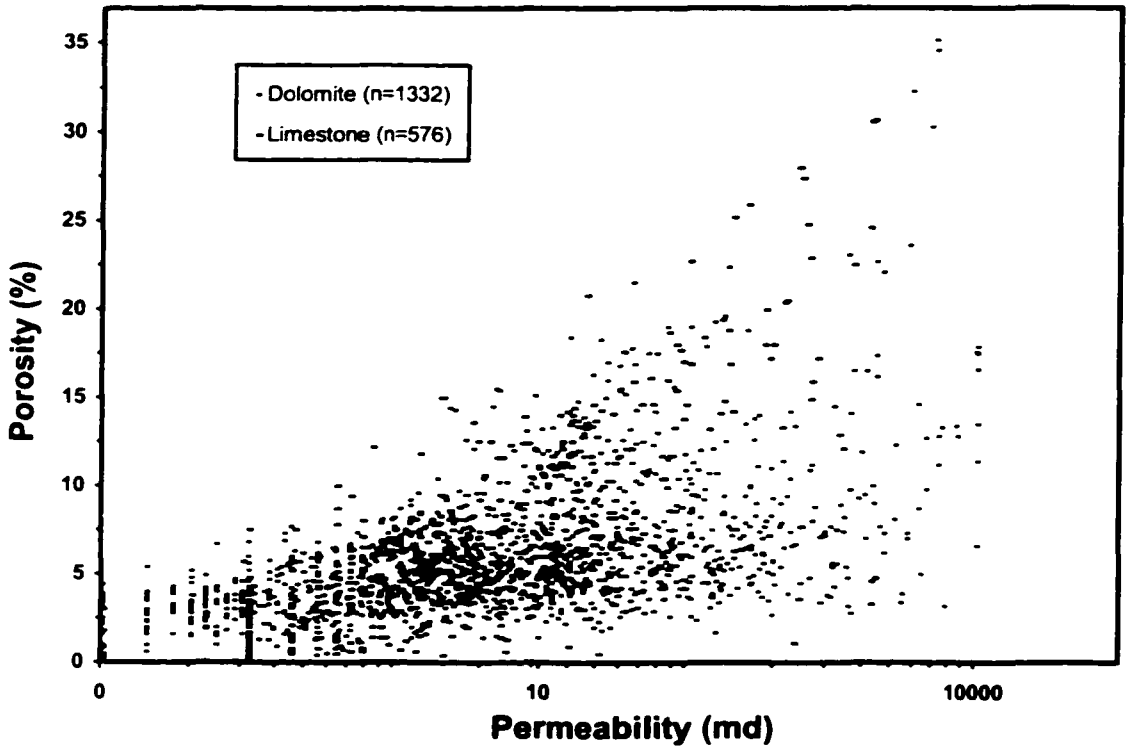



Fig. 6.4 Permeability vs. porosity for Guelph dolomite and limestone in southwestern Ontario.

Core #992 from the partially dolomitized Dow Moore pinnacle reef was chosen to illustrate the porosity and permeability distribution in limestone and dolomite in the same core, because this core penetrates the entire Guelph Formation and contains different types of limestone and dolomite. The limestone samples from core #992 can be readily divided into two separate groups in porosity versus permeability plot (Fig. 6.5). One group (nonporous) shows lower porosity ranging from 0.1 to 7.7% (average 3.9%) and significantly lower permeability varying from approximately 0.01 to 5 md (average 1.5 md) (Appendix VI). The other group exhibits higher porosity varying from approximately 9 to 31% (average 17.7%) and significantly higher permeability ranging from approximately 20 to 1862 md (average 594.7 md). The porosity and permeability of Type 1, Type 2 and Type 3 dolomites in core #992 were determined based on core and thin section observations and were plotted in Fig. 6.6. Type 1 dolomite is dominated by micrometer-sized intercrystalline porosity and is typically a low-porosity, low-permeability rock (0.1%-6.6%, average 2.9%; 0.01-3.8 md, average 0.5 md; Appendix VII). Porosity of Type 1 dolomite is similar to the porosity of interbedded low-porosity limestone (Fig. 6.5 and 6.6). Type 2 and Type 3 dolomites are also dominated by intercrystalline porosity, but commonly contain abundant millimeter-sized intercrystalline pores, as well as many larger moldic and vuggy pores. Type 2 dolomite exhibits moderate to good reservoir quality (3.4%-14.0%, average 6.6%; 2.5-440.6 md, average 63.7 md; Appendix VII), and it is the most common dolomite type and hydrocarbon reservoir in the Guelph Formation. Type 3 dolomite shows the best reservoir quality with the highest porosity and permeability (8.2%-35.2%, average 20%; 686.6-5128 md, average 2443.8 md; Appendix VII), but is volumetrically unimportant.

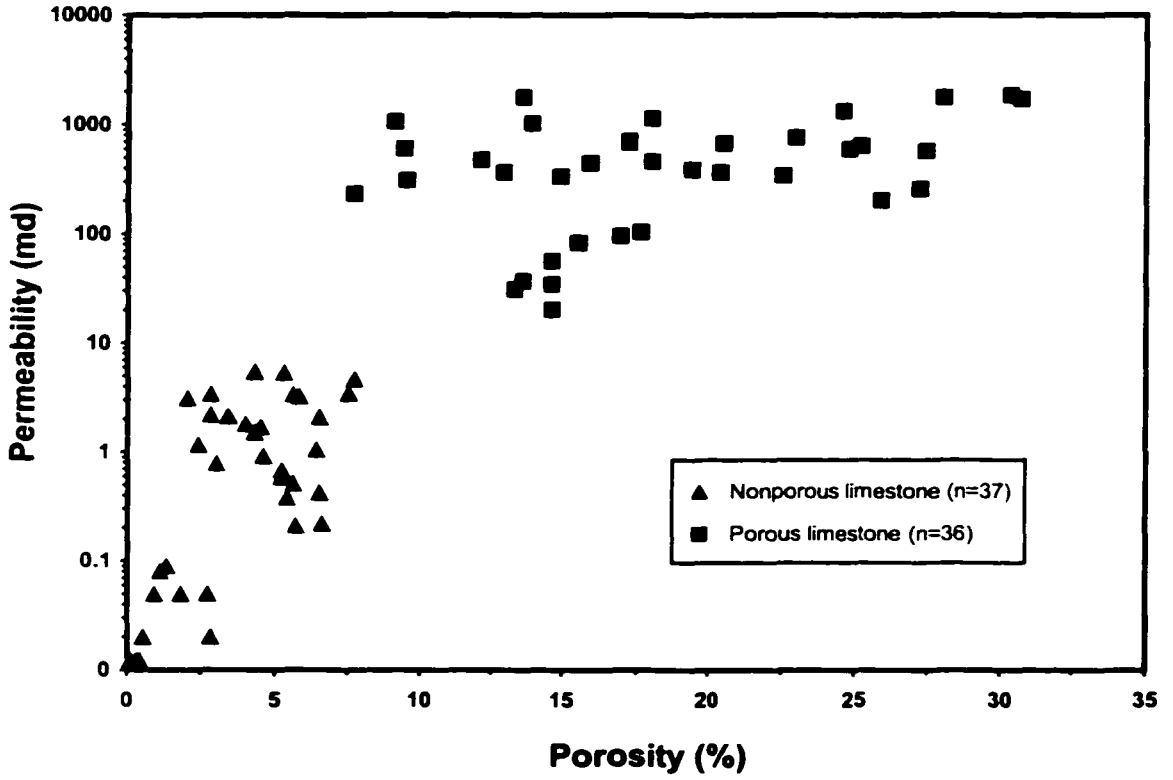



Fig. 6.5 Porosity vs. permeability for nonporous and porous limestones in core 992 from Dow Moore pinnacle reef. The porosity and permeability values were measured from the small column samples taken from core.

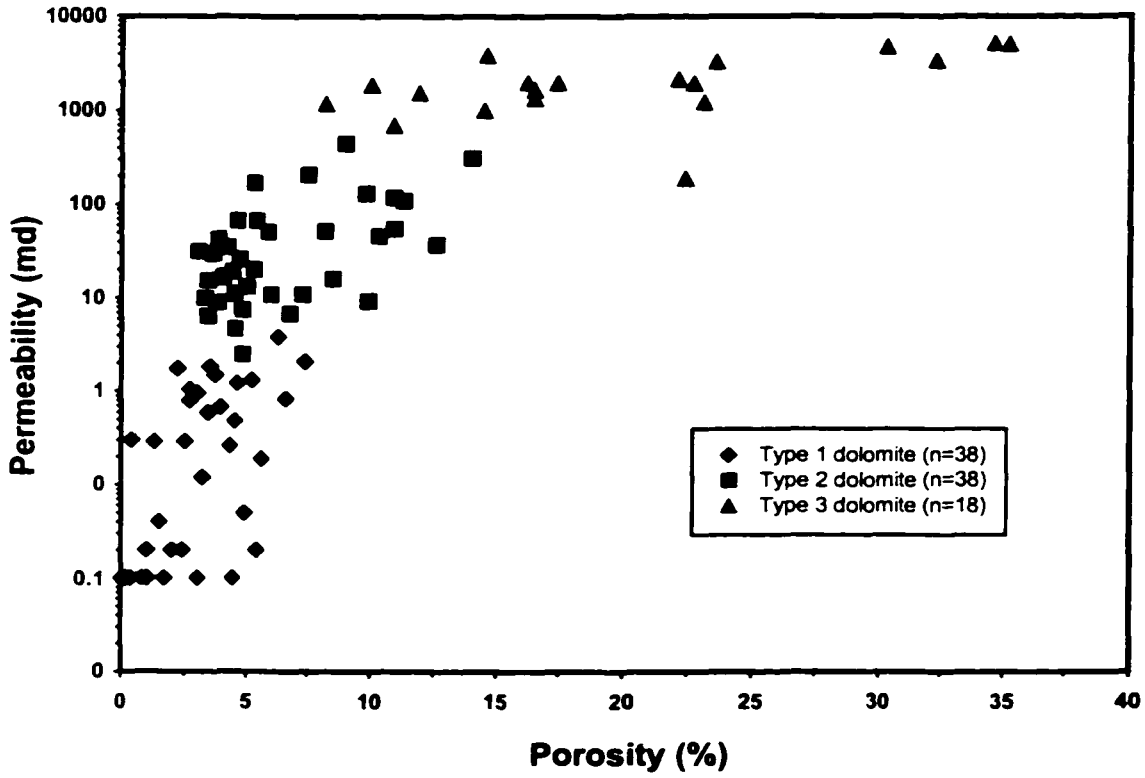



Fig. 6.6 Porosity vs. permeability for Type 1, Type 2 and Type 3 dolomites in core 992 from Dow Moore pinnacle reef. The porosity and permeability values were obtained from measurements of small column samples taken from core.

Dedolomitized Terminus pinnacle reef was chosen to compare porosity and permeability between limestone and dedolomite in the same reef (Fig. 6.7; Appendix V). Dedolomite shows much lower porosity (0.2-14.4%, average 6.6%) and permeability (0.1-113 md, average 12.6 md) than associated limestone (6.5-16.1%, average 11.4%; 2.6-855 md, average 54.9 md).

## 6.5 Post-dolomitization diagenesis

The major post-dolomitization diagenetic events that will be discussed in this chapter include mechanical and chemical compaction, fracturing, carbonate dissolution, anhydrite and halite cementation, evaporite dissolution, and hydrocarbon emplacement. The relative timing of above diagenesis is summarized in Figure 3.5.

### 6.5.1 Mechanical and chemical compaction

Present-day burial depths of the bottom of the Guelph Formation in study area range from approximately 500 to 1000 m. According to previous studies (e.g., Cercone 1984a; Coniglio et al., 1994), the maximum burial depth probably varied from approximately 1400 to 2000 m. There is no obvious mechanical compaction and correlation between porosity or permeability and burial depth in the Guelph Formation.

Chemical compaction fabrics, including stylolites and clay seams are common in both limestone and dolomite. They occur at different levels and generally are parallel to bedding, varying from less than 1 cm to several centimeters in amplitude (Fig. 6.3C).

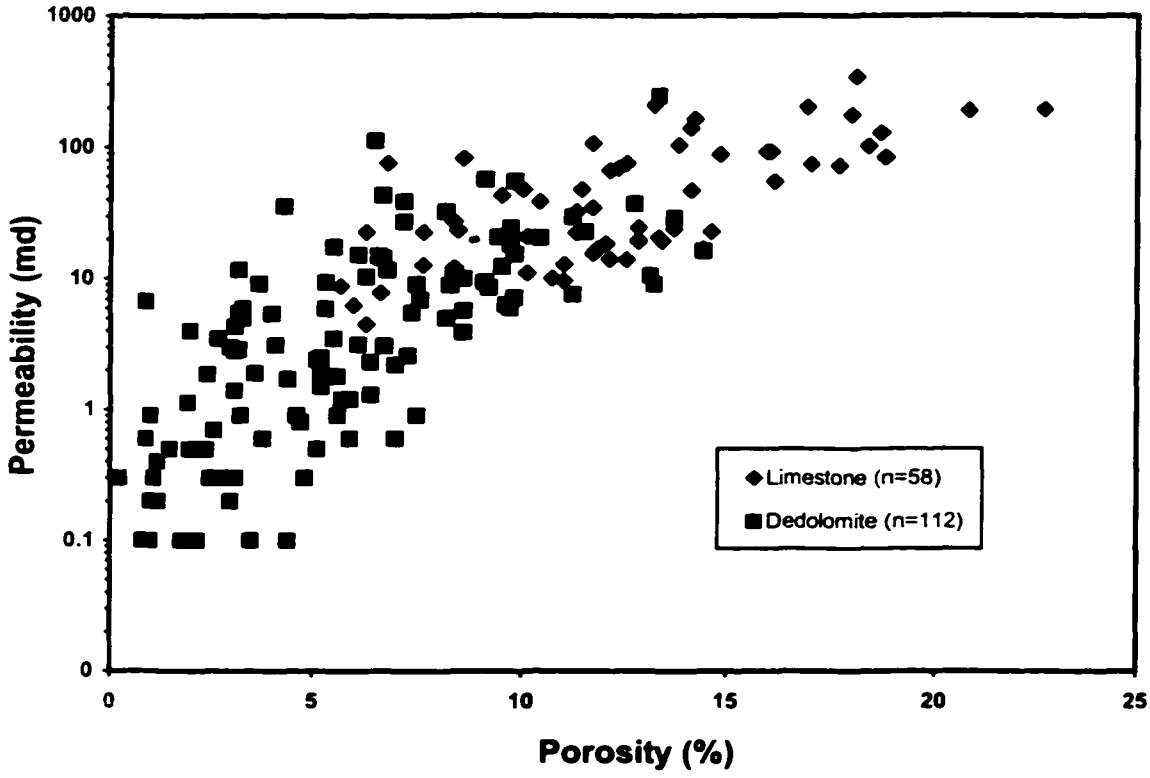



Fig. 6.7 Porosity vs. permeability for Guelph limestone and dedolomite, using the data of cores 198, 381and 604 from Terminus pinnacle reef. The porosity and permeability values were measured from the small column taken from cores.

Stylolites more commonly occur in Type 1 dolomite than in Type 2 dolomite. They are rare in Type 3 dolomite. Some open stylolites connected to pores are lined by limpid dolomite cement.

### 6.5.2 Fracturing

Fractures occur in different orientations and have variable widths ranging from several micrometers to a few millimeters throughout the Guelph Formation. Some intervals contain networks of fractures and some fractures are partially or completely filled by anhydrite and halite cements (Fig. 6.3B). Many fractures crosscut and postdate stylolites and solution seams in both limestone and dolomite.

### 6.5.3 Carbonate dissolution

Carbonate dissolution occurs in close association with fracturing in both limestone and dolomite. Dissolution of fossils such as gastropods, corals, and crinoids resulted in porous intervals containing vugs and abundant biomolds (Figs. 6.2E,F; 6.3A,D). Porous intervals are present at different levels in the Guelph Formation and the abundance of molds and vugs in these intervals is greatly variable. The most extensive leaching occurs in the stromatolitic cap facies in the upper parts of limestone reefs. Some limestone intervals are strongly leached to form extremely porous rocks with visually estimated porosity of 30-35%.

Moldic and vuggy pores are rare in Type 1 dolomite but common in Type 2 and Type 3 dolomites. Some molds and vugs in Type 2 and Type 3 dolomites are lined by variable amounts of limpid dolomite cement and occasionally saddle dolomite cement. Dolomite rhombs with corroded edges indicate partial dissolution in both Type 2 and Type 3 dolomites. The following evidence strongly argues that the major dissolution events occurred late in the diagenetic history of these strata: (1) absence of calcite or mimetically dolomitized fibrous and equant cements in the molds and vugs; (2) presence of later cements including limpid dolomite, saddle dolomite, anhydrite, and halite cements; (3) presence of bitumen or solid hydrocarbon linings in many vugs; and (4) presence of dissolution enlarged fractures and stylolites. Some vugs crosscut fractures and stylolites.

### 6.5.4 Anhydrite and halite cementation

Anhydrite commonly occurs as coarsely crystalline (0.02-1 mm), fibrous, bladed, or blocky cement lining and occasionally filling molds, vugs, and fractures in minor amounts (less than 2% of rock volume) in both porous limestone and porous dolomite (Fig. 6.3D). Many Type 2 dolomite intervals contain minor amount (< 2%) anhydrite cement, but anhydrite cement is commonly absent in nonporous limestone and Type 1 dolomite. Anhydrite cement postdates fibrous and equant calcite cements and limpid dolomite cement in molds and vugs and tends to preferably occupy larger pores (> 2 mm) and fractures (width > 1 mm).

Halite cement occurs as blocky crystals partly to completely filling molds, vugs, and fractures in many vuggy dolomite and limestone intervals and it tends to preferably occupy larger pores (> 2 mm) and wider fractures (width > 1 mm) (Fig. 6.3E). Homogenization temperatures (Th) of primary two-phase fluid inclusions in halite cements range from +89.4 to +94.1°C and final melting temperatures vary from –23.9 to –25.4°C (Appendix IV). Halite occurs as a more widespread and extensive cement than anhydrite in Guelph reefs and some intervals or reefs were completely plugged by halite. Preserved halite cement in cores is highly variable ranging from 2-30%. Halite cement follows anhydrite cement in many cavities and fractures and occurs as a final mineral phase that postdates all other diagenetic mineral phases that are present. Halite is commonly absent in Type 3 dolomite, but many Type 2 dolomite intervals are partially to completely plugged by variable amounts of halite cement (2-30%). Some intervals in the upper part of several pinnacle reef pools were completely plugged by halite to act as seal rocks. Several reefs, such as Bayfield and Wilkesport pinnacle reefs, were extensively plugged by halite. However, other reefs, like the Warwick pinnacle reef, only contain minor amounts of halite cement. Halite cement is much more common in basinward pinnacle reefs than in shelfward patch reefs.

### 6.5.5 Evaporite dissolution

Partially to completely dissolution of evaporite cements, especially halite cement, with variable amounts of corroded relicts are very common in both limestone and dolomite (Fig. 6.3D, E).

### 6.5.6 Hydrocarbon emplacement

Solid hydrocarbons or bitumen that postdate halite cement occur as a final non-mineral phase in many porous reservoirs (Fig. 6.3F). Bitumen coats crystal surfaces and pore walls and reduces porosity and pore throat sizes. It postdates all diagenetic mineral phases in the Guelph Formation.

## 6.6 Interpretation and discussion

Several factors, including paleoclimate (Hird and Tucker 1988; Sun and Esteban 1994), sea level change and sequence stratigraphy (Tucker 1993), precursor limestone facies (Sun 1990; Sun et al. 1992), and intensity of dolomitization (Murray 1960; Powers 1962), have been shown to be important in controlling dolomite porosity. Montañez and Stefani (1993) found that in Knox carbonates of southeastern United States, early dolomitization of mud-rich, regressive sequences resulted in completely dolomitized intervals consisting of nonporous and impermeable rocks. In contrast, grain-rich, transgressive sequences were only partially dolomitized to form more porous and permeable intervals. Other studies (e.g., Sibley and Gregg 1987; Gao and Land 1991) have suggested that grain-rich facies probably were initially replaced by coarser dolomite than the dolomite that replaced mud-rich facies.

The primary porosity in Guelph limestone was greatly reduced by early fibrous calcite cementation and subsequent equant calcite cementation. However, early-lithified

limestone remained sufficiently permeable in order to allow the necessarily large flux of fluid for massive dolomitization. As discussed in Chapter 4, early initial dolomitization in the Guelph Formation occurred during shallow burial and after early lithification of lime sediments. Although early dolomitization and subsequent recrystallization may have caused porosity rearrangement, the similarity between the total porosities of Type 1 dolomite and low-porosity limestone suggests that porosity in primary limestone was essentially preserved in fabric-preserving Type 1 dolomite. Early dolomitization and recrystallization were not important processes in changing porosity.

### 6.6.1 Porosity-creating processes

Porosity enhancement in the Guelph Formation was evidently controlled by post-dolomitization diagenesis, including stylolitization, fracturing, carbonate dissolution, dolomite coarsening, and evaporite dissolution (Fig. 6.8A).

#### 6.6.1.1 Stylolitization

Stylolites and pressure-solution seams have been regarded as a direct result of dissolution in response to stresses during burial (e.g., Wanless 1979). Numerous studies (e.g., Wanless 1979; Braithwaite 1989) have suggested that some stylolites and solution seams also represent former open pathways for diagenetic fluids. Fluid movement must occur during stylolite and seam formation to remove the dissolved minerals. Some stylolites and seams in the Guelph Formation likely acted as fluid conduits for post-dolomitization diagenesis, based on the selective occurrence of Type 2 dolomite and limpid dolomite

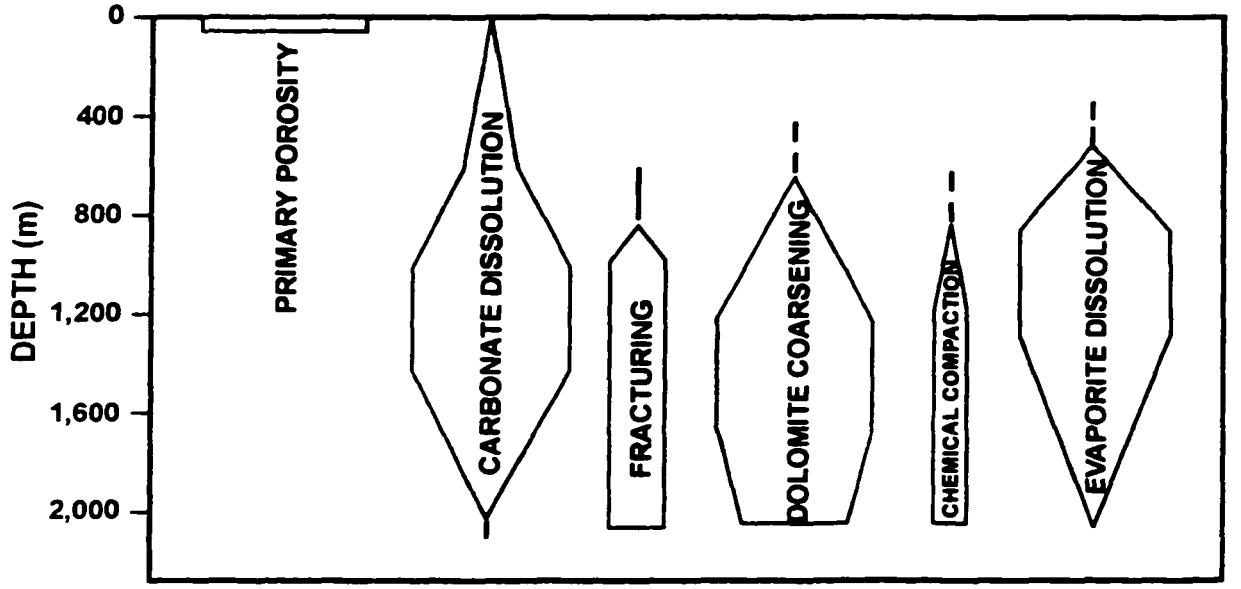



Fig. 6.8A The relationship between depth and major porosity-creating processes for the Guelph Formation in southwestern Ontario. Width of the fields indicates relative importance.

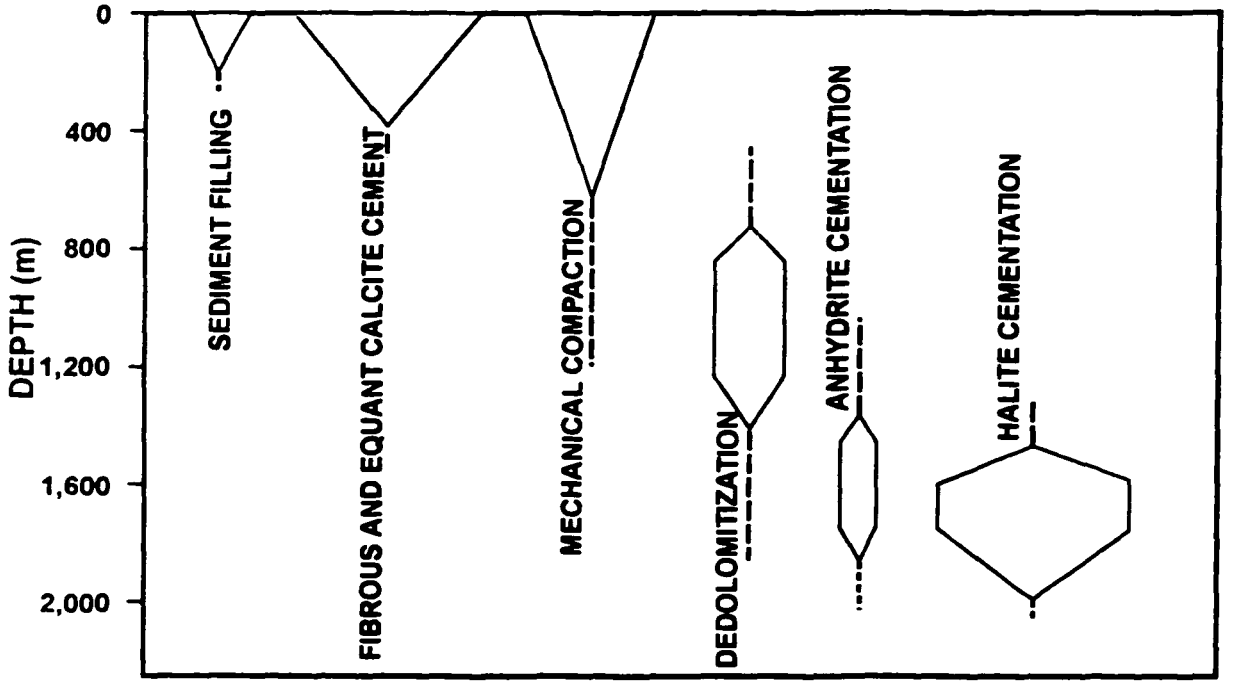



Fig. 6.8B The relationship between depth and major porosity-destroying processes for the Guelph Formation in southwestern Ontario. Width of the fields indicates relative importance.

cement along stylolites and seams. Stylolites and seams could be more effective conduits when connected with fractures.

#### 6.6.1.2 Fracturing and carbonate dissolution

Many Type 2 dolomites and most Type 3 dolomites are related to fractures and probably faults (see Chapter 4). Fracturing and carbonate dissolution are two major and most likely related post-dolomitization processes in controlling porosity in Guelph carbonates.

In southwestern Ontario, a regional fault and fracture framework was generated by differential compaction and basement movement (Brigham 1971; Winder and Sanford 1972), or plate tectonic activity (Sanford et al. 1985). Sanford et al. (1985) suggested that this active fault and fracture network acted as a long-lived conduit system for movement of diagenetic fluids and hydrocarbon migration. Fracture systems at greater depths are more likely to develop and to keep open in dolomites than in limestones since dolomites are more brittle or less ductile and have greater mechanical strength than limestones (Hugman and Friedman 1979). Local dolomitization occurred in the vicinity of faults in the Middle Ordovician carbonate succession in southwestern Ontario (Coniglio and Williams-Jones 1992; Middleton et al. 1993; Coniglio et al. 1994). A similar fault and fracture system could have developed in the Middle Silurian carbonates. Carter (1991) found that some local dolomitization and hydrocarbon accumulation in the A-1 carbonate and halite dissolution in the A-2 and B units are closely associated with faults. The network of fractures and faults, therefore, could have provided conduits to reopen the

early-formed, tightly-packed, nonporous Type 1 dolomite and encouraged subsequent dissolution of Type 1 dolomite and later formation of Type 2 and Type 3 dolomites during burial.

The origin and spatial distribution of porosity in the Guelph Formation was attributed by Smith et. al. (1993) largely to fresh water karsting during sea level fall and subaerial exposure of reef. However, leaching is not necessarily always related to dissolution by fresh water; even hypersaline waters can cause carbonate dissolution (Sun 1992). A major dissolution event occurred after Type 1 dolomite formation and resulted in variable amounts of moldic and vuggy porosity in Type 2 dolomite. Porosity enhancement could also occur under deep burial conditions as the result of carbonate dissolution in fluids charged with organic acids, carbon dioxide, and hydrogen sulfide derived from organic matter maturation and thermochemical sulfate reduction (Moore 1989; Mazzullo and Harris 1992). As discussed in Chapter 4, the primary two-phase fluid inclusions in localized Type 3 dolomite with saddle-like curved faces and sweeping extinction and scattered saddle dolomite cement show exceptional high Th values, implying the involvement of deep hydrothermal fluids. Late dissolution that occurred in Type 3 dolomite is also likely related to deep hydrothermal fluids. Dolomite dissolution would be particularly intense in intervals where hot basinal fluids moved upward along faults and fractures and mixed with cooler formation waters. Such a fluid mixing mechanism has been employed to explain the porous zones in the Trenton and Black River dolomites in Albion-Scipio and Stoney Point fields (Hurley and Budros 1990).

#### 6.6.1.3 Dolomite coarsening

As discussed in Chapter 4, most Type 2 and Type 3 dolomites in the Guelph Formation occur as sucrosic dolomite and they most likely represent the coarsening products of later alteration of early-formed, Type 1 dolomite through dolomite overgrowth or dolomite recrystallization. Negra et. al. (1994) suggested that dolomite textural variations in crystal size, sorting, crystal shape and packing could directly affect porosity and permeability. Reservoir quality in Guelph Type 2 and Type 3 dolomites that are dominated by intercrystalline porosity is obviously controlled by crystal size and other textural features.

#### 6.6.1.4 Evaporite dissolution

Partial to complete dissolution of halite cement allowed previously plugged pores to be used for hydrocarbon migration into the reefs. Many intervals with reopened pores in these reefs became effective oil and/or gas reservoirs. Halite dissolution also played a key role in reopening the halite-plugged pinnacle reefs in northwestern Michigan (Gill 1979).

### 6.6.2 Porosity-destroying processes

Major post-dolomitization processes in destroying porosity in the Guelph Formation include mechanical compaction, dedolomitization, and anhydrite and halite evaporite cementation (Fig. 6.8B). Limpid dolomite cement in Type 2 and Type 3 dolomites and local saddle dolomite cement in porous limestone and dolomite represent important diagenetic events but are unimportant in porosity reduction.

#### 6.6.2.1 Mechanical compaction

Some mechanical compaction must have occurred during burial and reduced porosity in unlithified Guelph sediment.

#### 6.6.2.2 Dedolomitization

Chilingar (1956) discovered that dedolomitization converts porous and permeable dolomite into less porous and practically impermeable rock. In contrast, Al-Hashimi and Hemingway (1973) found that dedolomitization is a process of great potential in converting impermeable dolomite into porous and permeable carbonate. More recently, Purser (1985) suggested that although dedolomites could be important reservoir rocks, dedolomitization could increase, retain, or reduce the porosity, depending on the balance between dolomite dissolution and calcite precipitation rates and the textural changes in the newly-formed rocks. Some dedolomitized intervals in the Terminus pinnacle reef constitute productive hydrocarbon reservoirs (Fig. 5.1), although they have relatively low porosity and permeability compared to Type 2 dolomite reservoirs (Fig. 6.9, Appendix V and VII). As mentioned in Chapter 5, dedolomitization in the Guelph Formation commonly changed a more coarsely crystalline and more porous dolomite into a more finely crystalline and less porous dedolomite. Thus, dedolomitization is basically a porosity-reducing process in the Guelph Formation.

#### 6.6.2.3 Anhydrite cementation

Anhydrite cement is relatively unimportant in occluding porosity due to its limited volume (<2%). However, anhydrite cement is commonly found within vugs, molds, and

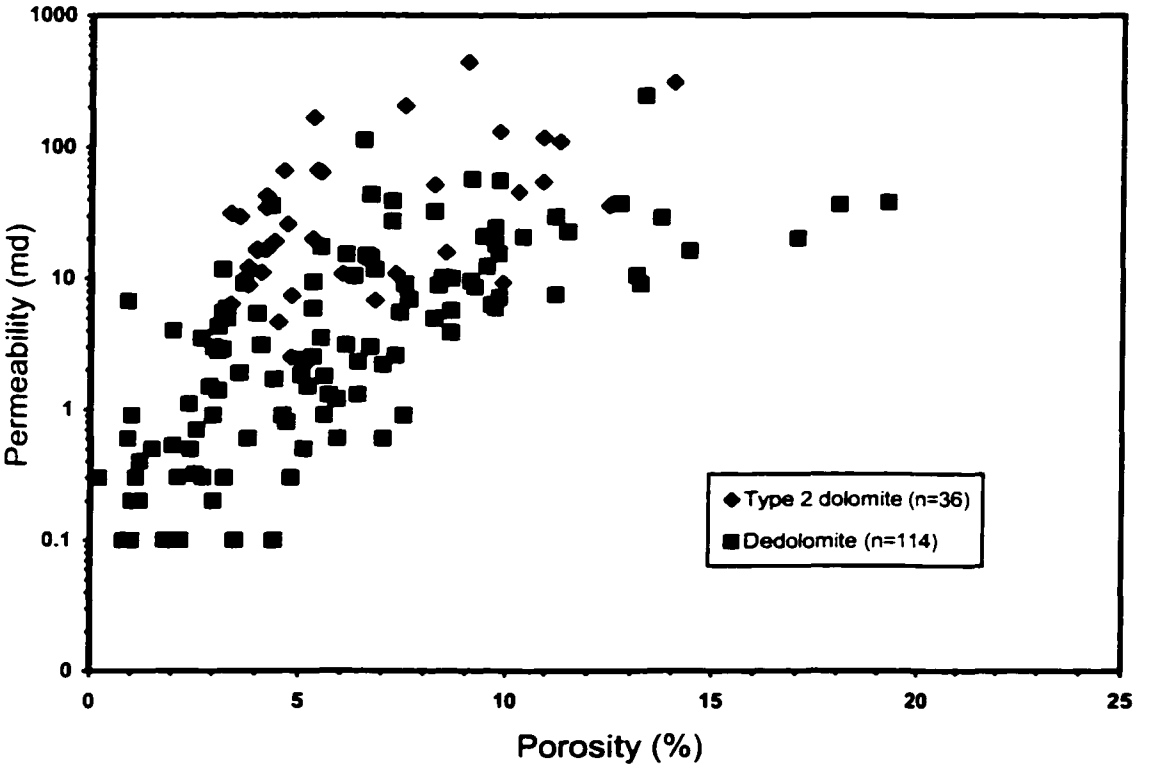



Fig. 6.9 Porosity vs. permeability for Type 2 dolomite in core 992 from Dow Moore pinnacle reef and dedolomite in cores 381, 604 and 918 from Terminus pinnacle reef. The porosity and permeability values were measured from small column samples taken from cores.

fractures that crosscut all dolomite types. This suggests that anhydrite cements are late burial in origin and the brines for anhydrite cement in the Guelph Formation may have shared the same conduit system with the fluids causing dissolution of carbonate.

#### 6.6.2.4 Halite cementation

Halite plugging is the most important single porosity-destroying process in many basinward pinnacle reefs. High homogenization temperatures in halite fluid inclusions ranging from +89.4 to +94.1°C indicate that halite cement is a late diagenetic phase, although former studies (Brigham 1971; Sanford 1969; McMurray 1985) have suggested that halite plugging appears to have undergone several stages of dissolution and reprecipitation. The fluids responsible for halite plugging can be logically related to the same source for anhydrite cement, likely from lateral reflux of evaporitic brines from shelfward lagoon settings during the Late Silurian. The contrast between minor amounts of anhydrite cement and extensive halite plugging may suggest that the fluids in the recharge area evolved quickly from gypsum saturation to halite saturation. Alternatively, halite cement may also have been precipitated from downward fluids from dissolution of A-2 and B halite above the reef crests during the Late Silurian to Early Devonian (McCollough 1975; Sanford et al. 1985; Carter 1991).

## 6.7 Conclusions

1. Porosity and permeability distributions in early-lithified low-porosity limestone precursors were mostly preserved in Type 1 dolomite due to fabric-preserving dolomitization and early recrystallization. Type 1 dolomite, similar to low-porosity

limestone, is a poor reservoir. Early dolomitization and recrystallization were not important processes in creating porosity.

2. The porosity type and final porosity and permeability in Type 1 dolomites were significantly modified by later dolomite alteration during the formation of Type 2 and Type 3 dolomites. The porosity and permeability of many Type 2 and Type 3 dolomite intervals were significantly improved by fracturing, dissolution, and dolomite coarsening through overgrowth and recrystallization. Some Type 2 dolomite intervals were dedolomitized or halite-plugged, thus having lower porosity and permeability. Some halite-plugged Type 2 dolomite intervals or reefs were reopened by dissolution to form porous rocks and prolific reservoirs.

3. The most effective porosity types in Type 2 and Type 3 dolomite reservoirs are secondary in origin, including intercrystalline pores and dissolution-enhanced moldic and vuggy pores. Porosity and permeability distributions in Type 2 and Type 3 dolomites are highly heterogeneous. Type 2 dolomite is the most common and forms important hydrocarbon reservoirs with moderate to high porosity and permeability. Type 3 dolomite is the best reservoir with the highest porosity and permeability, but is unimportant in volume.

# Chapter 7 Summary

## 7.1 Reef facies and diagenesis

The Middle Silurian Guelph Formation in the subsurface of southwestern Ontario is composed of shelfward patch reefs, basinward pinnacle reefs, and interreef facies developed on a gently-sloping carbonate ramp (150-200 km wide) in the southeastern Michigan Basin. The Guelph Formation consists of five major facies, including (1) basal crinoidal mud mound facies; (2) coral-stromatoporoid reef core facies; (3) crinoidal-bryozoan flank facies; (4) stromatolitic cap facies; and (5) interreef mud facies.

The vertical facies and fossil zonation in Guelph reefs indicate three major stages of reef growth, including initial crinoidal mud mound buildup in a relatively low energy subtidal environment, rapid growth of a coral-stromatoporoid organic reef core and accumulation of detrital flank deposits in an agitated normal marine environment, and development of a stromatolite cap in a restricted environment. Basinward pinnacle reefs were initialized on crinoidal mounds whereas more shelfward pinnacle and patch reefs were started as coral-stromatoporoid facies without the crinoidal mound substrate.

Petrographic study shows that Guelph carbonate has undergone a complicated diagenetic history, including (1) pre-dolomitization diagenesis characterized by early fibrous and equant calcite cementation, neomorphism, and limestone dissolution during marine deposition and shallow burial; (2) regional pervasive dolomitization during shallow to moderate burial; and (3) post-dolomitization diagenesis characterized by dolomite

recrystallization, dedolomitization, hydrothermal dolomite formation, halite plugging, and hydrocarbon emplacement under moderate to deep burial conditions. Regional pervasive dolomitization and later dolomite alteration are the most important diagenesis in the Guelph Formation.

## 7.2 Dolomite type and origin

Guelph dolomites mainly consist of three types replacive dolomites: (1) Type 1, microcrystalline (20-50 μm) anhedral dolomite with well preserved precursor textures; (2) Type 2, finely crystalline (50-150 μm) euhedral to subhedral dolomite with partially preserved precursor textures; and (3) Type 3, medium to coarsely crystalline (150-400 μm) euhedral to anhedral dolomite without preserved precursor textures. Type 2 dolomite is the most common type and Type 1 dolomite is the second most abundant type. Type 3 dolomite locally occurs as patches or thin layers within Type 2 or Type 1 dolomite.

Microcrystalline Type 1 dolomite has the best preserved limestone textures, identical $^{87}Sr/^{86}Sr$ ratios (0.70853-0.70864) to both limestone and coeval seawater, and similar low contents of Fe (100-1200 ppm) and Mn (50-150 ppm) to limestone. Type 1 dolomite is interpreted to represent the 'least-altered' dolomite phase that is geochemically the closest to the initial replacive dolomite. The relative timing of Type 1 dolomite formation predates stylolitization but postdates the equant calcite cementation. A general basinward dolomite-decreasing trend in the Guelph Formation, consisting of completely dolomitized patch reefs on the upper ramp, partially dolomitized pinnacle reefs on the lower ramp,

and undolomitized basinal lime mudstone in the basin center, indicates that dolomitizing fluids were derived from shelfward sources. Selectively dolomitized overlying A-1 and A-2 carbonates around dolomitized pinnacle reefs may have been affected by the same dolomitizing fluids for Guelph carbonate. Stratigraphic, petrographic and geochemical data suggest that this initial dolomitization probably resulted from regional subsurface (< 350 m) reflux of normal to near-normal seawater that was induced by evaporative drawdown during the Late Silurian. The driving force for basinward flow was the hydraulic head difference between surrounding open sea level and drawdowned sea level within the isolated Michigan Basin. Regional dolomitization was accomplished by basinward reflux of large volumes of seawater recharged from the back-barrier-reef area connected with the open sea, through the porous barrier reefs and inter-reef facies to the individual patch and pinnacle reefs on the ramp. The duration of this flow system extended from the initial drawdown during the deposition of Salina A-1 Evaporite until the seawater recharge area was completely sealed by evaporites of Salina B and later units.

Early recrystallization likely occurred in Type 1 dolomite, as suggested by its coarser crystal size (20-50 μm) relative to recent dolomite (commonly < 4 μm) and depleted $\delta^{18}O$ values (-4.5‰ to –8.5‰ PDB). Depleted $\delta^{18}O$ values may have resulted from early recrystallization in a fluid similar to that which characterized initial dolomitization but at deeper burial conditions (320-1250 m). The downdip dolomite $\delta^{18}O$-decreasing trend along the dip of ramp, which is not related to dolomite types, is interpreted to have

resulted from downdip increasing burial depths of the Guelph Formation and basinward increasing geothermal gradients along the ramp during early dolomite recrystallization.

The coexistence of three dolomite fabrics with relict textures and their crosscutting relationships indicate that Type 1 dolomite was altered to Type 2 and Type 3 dolomite. The systematic covariance between increasing crystal size with increasing $^{87}Sr/^{86}Sr$ ratios (0.70860-0.70910) and increasing contents of Fe (700-3500 ppm) and Mn (100-300 ppm) reflects an advanced alteration of early-formed dolomite in pore fluids with increasing $^{87}Sr$, Fe and Mn inputs from associated siliciclastics during burial. Type 2 dolomite is interpreted to have formed during moderate to deep burial (approximately 600-1600 m), which is supported by its $\delta^{18}O$ values (-5‰ to -10‰ PDB) and fluid inclusion data (Th: +64.5 to +74.7°C; Tm: -9.9 to -13.5°C). Localized Type 3 dolomite and saddle dolomite cement show the highest Th values and fracture-related occurrences and they are interpreted to have resulted from fracture-conducted hydrothermal fluids during deeper burial.

## 7.3 Dedolomitization

Several partially to nearly completely altered intervals (0.2 to 60 m) from five pinnacle reefs within a narrow zone (10-20 km) on the lower ramp which is between platform dolomites and basinal limestones, previously reported as "paleosols" or marine limestones, are recognized as dedolomitized rocks in this study. These altered rocks contain variable amounts of finely crystalline (20-50 μm) dedolomite (5% to 95%) with dolomite inclusions and Type 2 dolomite crystals with corroded edges. Guelph

dedolomites contrast with their dolomite precursors and associated original limestones by their light color, poor lithification, numerous relict dolomite patches, and poorly preserved precursor textures. Common replacement fabrics, including dolomite rhombs with corroded edges, poikilotopic fabrics with floating dolomite relicts, rhombic calcite pseudomorphs, and micrometer-sized dolomite inclusions within dedolomite, indicate that Guelph dedolomite resulted from replacement of preexisting dolomites.

Guelph dedolomites show depleted Sr contents (40-60 ppm), enriched Fe contents (600-1700 ppm) and Mn concentrations (60-200 ppm), and higher $^{87}Sr/^{86}Sr$ ratios (0.70875 and 0.70885), relative to associated original limestones, but similar values to Type 2 dolomites. Dedolomite $\delta^{18}O$ values (-6 to -9‰ PDB) and $\delta^{13}C$ values (+2.5 to +4‰ PDB) are also similar to the Type 2 dolomite values. Moderate homogenization temperatures (Th: 53.4 to 72.4°C) suggest shallow to moderate burial conditions and low melting temperatures (Tm: -16.8 to –18.4°C) indicate a saline water origin. Combined stratigraphic, petrographic, geochemical, and fluid inclusion data suggest that Guelph dedolomitization was neither controlled by fractures or unconformities nor related to fresh waters, and it likely resulted from subsurface circulation of saline brines with higher Ca/Mg ratio in the same conduit system and under similar burial depth and temperature conditions to those for earlier Type 2 dolomite formation. Dedolomitizing fluids may have acquired extra Ca from the dissolution of local reefal limestones to raise their Ca/Mg ratio and to cause local dedolomitization. This groundwater flow system probably extended until the water supply was reduced when either the recharge area in the inner shelf was sealed by evaporites or the hydraulic head became too low to drive flow. The

relative timing of dedolomitization postdates Type 2 dolomite formation but predates anhydrite cementation.

## 7.4 Porosity type and evolution

Guelph limestones occur as nonporous and porous intervals. Primary limestones occur as nonporous limestones with low porosity (0.1-7.0%) and permeability (0.01-5.4 md). Most nonporous limestones were related to extensive early calcite cementation of primary pores, and some resulted from late stage halite plugging. Some limestones were extensively dissolved to form porous intervals with higher porosity (7.7-30.6%) and permeability (20.4-1861.5 md). These porous limestones commonly contain abundant moldic and vuggy pores. Guelph dolomites also exhibit highly variable porosity (0.1-23.6%) and permeability (0.01-10200 md). Type 1 dolomite shows similar low porosity (0.1-6.6%) and permeability (0.01-3.8 md) to associated nonporous limestone precursors due to fabric-preserving dolomitization and early recrystallization. Compared to Type 1 dolomite, the porosity and permeability in most Type 2 and Type 3 dolomite intervals are highly heterogeneous and significantly improved by fracturing, dissolution, and dolomite coarsening through overgrowth and recrystallization. They exhibit wide ranges of porosity (3.4-35.2%) and permeability (2.5-5128 md). Dedolomitized intervals show low porosity (0.2-14.4%) and permeability (0.1-113 md) relative to their Type 2 dolomite precursors, indicating that dedolomitization is a porosity-reducing process.

Type 1 dolomite occurs in nonporous intervals with low porosity and permeability. Type 2 dolomite is the most common and important hydrocarbon reservoir with moderate to

high porosity and permeability. Type 3 dolomite is the best reservoir with the highest porosity and permeability, although it only occurs as porous patches or thin layers within Type 2 or Type 1 dolomites. Most effective porosity types in Guelph dolomites are secondary in origin, including intercrystalline pores and dissolution-enhanced moldic and vuggy pores. Intercrystalline pores are the most important porosity in all three dolomite types. Moldic and vuggy pores occur in most porous Type 2 and Type 3 dolomites, but are rare in Type 1 dolomite.

The most important factors controlling dolomite reservoir properties are not early dolomitization but later dolomite alteration during burial. Some Type 2 dolomite intervals were dedolomitized or halite-plugged, resulting in their lower porosity and permeability. Some halite-plugged Type 2 dolomite intervals or reefs were reopened by dissolution to form porous rocks and prolific reservoirs.

Fracturing may have played an important role in reopening nonporous Type 1 dolomite to allow the flow of later diagenetic fluids for Type 1 dolomite dissolution and Type 2 dolomite formation. Type 2 dolomite may have served as a conduit thereafter for later diagenetic fluids that led to Type 3 dolomite formation and other diagenesis, such as dedolomitization and halite cementation.

## 7.5 Implications and further studies

The Guelph Formation in southwestern Ontario is a reefal sequence covered by cyclic evaporite and carbonate. This is a common association in the Michigan Basin, in other

basins in the Great Lakes Region, and in many other evaporative basins in the world. The dolomitization model proposed in this study could be applied to other areas of the Michigan Basin and elsewhere.

The general applicability of the dolomite formation and evolution models outlined for Guelph dolomites in this study will require further testing in the Michigan Basin and other similar evaporative basins around the world. Further research in such basins should focus on relating the distribution and geochemistry of platformal dolomites and associated evaporites. To define the scale and duration of the paleohydrologic system related to evaporative drawdown in the study area, a regional investigation of the paleogeographic setting in eastward back-reef-lagoon and in younger strata of the Late Silurian Salina sequence is needed. Further detailed geochemical and especially strontium isotopic study of Salina carbonates and evaporites will be useful in determining the fluid nature and timing for dolomitization relative to evaporative drawdown.

According to this study, the reservoir quality of dolomites in the Guelph Formation is largely controlled by later dolomite alteration instead of earlier dolomitization. Studies on degree and distribution of dolomite alteration will be particularly important for hydrocarbon exploration and production. Local dedolomite occurrence in basinward limestone-bearing pinnacle reefs was firstly discovered in this study and this subsurface dedolomitization may also exist in other areas in the Michigan Basin.

# References


Adams, J.E., and Rhodes, M.L., 1960. Dolomitization by seepage refluxion. American Association of Petroleum Geologists Bulletin, v. 44, p. 1912-1920.

Aharon, P., Socki, R.A., and Chan, L., 1987. Dolomitization of atolls by seawater convection flow: test of a hypothesis at Niue, South Pacific. Journal of Geology, v. 95, p. 187-203.

Al Shdidi, S., Thomas, G., and Delfaud, J., 1995. Sedimentology, diagenesis, and oil habitat of Lower Cretaceous Qamchuqa Group, Northern Iraq. American Association of Petroleum Geologists Bulletin, v. 79, no. 5, p. 763-779.

Al-Hashimi, W.S., and Hemingway, J.E. 1973. Recent dedolomitization and the origin of the rusty crusts of Northumberland. Journal of Sedimentary Petrology, v. 43, p. 82-91.

Allan, J.R., and Matthews, R.K., 1982. Isotope signatures associated with early meteoric diagenesis. Sedimentology, v. 29, p. 797-817.

Allan, J.R., and Wiggins, W.D., 1993. Dolomite reservoirs: geochemical techniques for evaluating origin and distribution. American Association of Petroleum Geologists, Continuing Education Course Note Series no. 36, 129p.

Alling, H.R., and Briggs, L.I., 1961. Stratigraphy of the Upper Silurian Cayugan evaporites. American Association of Petroleum Geologists Bulletin, v. 45, p. 515-547.

Amthor, J.E., and Friedman, G.M., 1991. Dolomite-rock textures and secondary porosity development in Ellenburger Group carbonates (Lower Ordovician), west Texas and southeastern New Mexico. Sedimentology, v. 38, p. 343-362.

Amthor, J.E., Mountjoy, E.W., and Machel, H.G., 1993. Subsurface dolomites in Upper Devonian Leduc Formation buildups, central part of Rimbey-Meadowbrook reef trend, Alberta, Canada. Bulletin of Canadian Petroleum Geology, v. 41, no. 2, p. 164-185.

Amthor, J.E., Mountjoy, E.W., and Machel, H.G., 1994. Regional-scale porosity and permeability variations in Upper Devonian Leduc buildups: Implications for reservoir development and prediction in carbonates. American Association of Petroleum Geologists Bulletin, v. 78, p. 1541-1559.

Anastas, A.S., and Coniglio, M., 1993. Sedimentology of an early Silurian carbonate ramp: the Manitoulin Formation, southern Ontario. Canadian Journal of Earth Science, v.30, p. 2453-2464.

Armstrong, D.K., and Goodman, W.R., 1990. Stratigraphy and depositional environments of Niagaran carbonates, Bruce Peninsula, Ontario. American Association of Petroleum Geologists, 1990 Eastern Section Annual Meeting, Hosted by Ontario Petroleum Institute, Field trip Guide Book no. 4, 59p.

Back, W., Hanshaw, B.B., Plummer, L.N., Rahn, P.H., Righmir, C.T., and Rubin, M., 1983. Process and rate of dedolomitization: mass transfer and $^{14}C$ dating in a regional carbonate aquifer. Geological Society of America, Bulletin, v. 94, p. 1415-1429.

Badiozamani, K., 1973. The dorag dolomitization model–Application to the Middle Ordovician of Wisconsin. Journal of Sedimentary Petrology, v. 43, p. 965-984.

Bailey, S.M.B., 1986. A new look at the development, configuration and trapping mechanisms of the Silurian Guelph reefs of southwestern Ontario. Ontario Petroleum Institute, 25th Annual Conference, Technical Paper no. 14, 28p.

Bailey, S.M.B., and Cochrane, R.O., 1990. Geology of selected oil and gas pools in the Silurian carbonates of southern Ontario. Ontario Geological Survey, Open File Report 5722, 50p.

Baker, P.A., and Burns, S.J., 1985. Occurrence and formation of dolomite in organic-rich continental margin sediments. American Association of Petroleum Geologists Bulletin, v. 69,
p. 1917-1930.

Banner, J.L., 1995. Application of the trace element and isotope geochemistry of strontium to studies of carbonate diagenesis. Sedimentology, v. 42, p. 805-824.

Banner, J.L., Hanson, G.H., and Meyers, W.J., 1988. Water-rock interaction history of regionally extensive dolomites of the Burlington-Keokuk Formation (Mississippian): isotopic evidence. *In* Sedimentology and Geochemistry of Dolostones. *Edited by* Shukla, V. and Baker, P.A., Society of Economic Paleontologists and Mineralogists Special Publications no. 43, p. 97-113.

Barker, C.E., and Reynolds, T.J., 1984. Preparing doubly polished sections of temperature-sensitive sedimentary rocks. Journal of Sedimentary Petrology, v. 54. p. 635-636.

Barnaby, R.J., and Read, J.F., 1992. Dolomitization of a carbonate platform during late burial: Lower to Middle Cambrian shady dolomite, Virginia Appalachians. Journal of Sedimentary Petrology, v. 62, no. 6, p. 1023-1043.

Bay, T.A., 1983. The Silurian of the Northern Michigan Basin. *In* Carbonate Buildups. *Edited by* Harris, P.M., A Core Workshop no. 4, Society of Economic Paleontologists and Mineralogists, p. 53-72.

Behrens, E.W., and Land, L.S., 1972. Subtidal Holocene dolomite, Baffin Bay, Texas. Journal of Sedimentary Petrology, v. 42, p. 155-161.

Bein, A., and Land, L.S., 1983. Carbonate sedimentation and diagenesis associated with Mg-Ca chloride brines: the Permian San Andres Formation in the Texas Panhandle. Journal of Sedimentary Petrology, v. 53, p. 243-260.

Belitz, K., and Bredehoeft, J.D., 1988. Hydrodynamics of the Denver Basin: an explanation of subnormal fluid pressures. American Association of Petroleum Geologists Bulletin, v. 72, p. 1334-1359.

BjØrlykke, K., 1993. Fluid flow in sedimentary basins. Sedimentary Geology, v. 86, p. 137-158.

BjØrlykke, K., Mo, A., and Palm, E., 1988. Modeling of thermal convection in sedimentary basins and its relevance to diagenetic reactions. Marine Petroleum Geology, v. 5, p.338-351.

Bolton, T.E., 1957. Silurian stratigraphy and paleontology of the Niagara Escarpment in Ontario. Geological Survey of Canada, Memoir 289, 145p.

Braithwaite, C.J.R., 1989. Stylolites as open fluid conduits. Marine and Petroleum Geology, v. 6, p. 93-96.

Brand, U., and Veizer, J., 1980. Chemical diagenesis of a multi-component carbonate system-1: Trace elements. Journal of Sedimentary Petrology, v. 50, p. 1219-1236.

Braun, M., and Friedman, G.M., 1970. Dedolomitization fabric in peels: a possible clue to unconformity surfaces. Journal of Sedimentary Petrology, v. 40, p. 417-419.

Brett, C.E., 1983. Sedimentology, facies and depositional environments of the Rochester Shale (Silurian; Wenlockian) in western New York and Ontario. Journal of Sedimentary Petrology, v. 53, p. 947-971.

Brett, C.E., Goodman, W.M., and LoDuca, S.T., 1990. Sequences, cycles, and basin dynamics in the Silurian of the Appalachian foreland basin. Sedimentary Geology, v. 69, p. 191-214.

Briggs, L.I., and Briggs, D., 1974. Niagara-Salina relationships in the Michigan Basin. *In* Silurian Reef-Evaporite Relationships. *Edited by* Kesling, R.V., Michigan Basin Geological Society, Field Guidebook p. 1-30.

Brigham, R.J., 1971 Structural geology of southwestern Ontario and southeastern Michigan. Ontario Department of Mines and Northern Affairs, Petroleum Resources Section, Paper 71-2, 110p.

Brigham, R.J., and Winder, C.G., 1966. Structural geology of Paleozoic sediments in southwestern Ontario. 5th Annual Conference Proceeding, Ontario Petroleum Institute, v. 5, Paper no. 13, p. 22.

Budai, J.M., and Lohmann, K.C., 1984. Burial dedolomite in the Mississippian Madison Limestone, Wyoming and Utah Thrust Belt. Journal of Sedimentary Petrology, v. 54, no. 1, p. 276-288.

Budai, J.M., Lohmann, K.C., and Wilson, J.L., 1987. Dolomitization of the Madison Group, Wyoming and Utah Overthrust Belt. American Association of Petroleum Geologists Bulletin, v. 71, No. 8, p. 909-924.

Budai, J.M., Longman, K.C., and Owen, R.M., 1984. Burial dedolomitization in the Mississippian Madison Limestone, Wyoming and Utah Thrust Belt. Journal of Sedimentary Petrology, v. 54, p. 276-288.

Budros, R., and Briggs, L.I., 1977. Depositional environment of Ruff Formation (Upper Silurian) in southeastern Michigan. *In* Reefs and evaporites, concepts and depositional models. *Edited by* Fisher, J.H., America Association of Petroleum Geologists, Study in Geology no. 5, p. 53-71.

Burgess, R.J., and Benson, A.L., 1969. Exploration for Niagaran reefs in northern Michigan. Ontario Petroleum Institute, v. 8, no. 1, 30p.

Burke, W.H., Denison, R.E., Hetherington, E.A., Koepnick, R.B., Nelson, H.F., and Otto, J.B., 1982. Variation of seawater $^{87}Sr/^{86}Sr$ throughout Phanerozoic time. Geology, v. 10, p. 516-519.

Burns, S.J., Baker, P.A., and Showers, W.J., 1988. The factors controlling the formation and chemistry of dolomite in organic-rich sediments: Miocene Drakes Bay Formation, California. *In* Sedimentology and Geochemistry of Dolostones. *Edited by* Shukla, V., and Baker, P.A., The Society of Economic Paleontologists and Mineralogists, Special Publications no. 43, p. 41-52.

Cander, H.S., Kaufman, J., Daniels, L.D., and Meyers, W.J., 1988, Regional dolomitization of shelf carbonates in the Burlington-Keokuk Formation (Mississippian), Illinois and

Missouri: constraints from cathodoluminescent zonal stratigraphy. *In* Sedimentology and Geochemistry of Dolostones. *Edited by* Shukla, V., and Baker, P.A., Society of Econonmic Paleontologists and Mineralogists Special Publication no. 43, p. 129-144.

Carballo, J.D., Land, L.S., and Miser, D.E., 1987. Holocene dolomitization of supratidal sediments by active tidal pumping, Sugarloaf Key, Florida. Journal of Sedimentary Petrology, v. 57, p. 153-165.

Carpenter, A. B., 1980. The chemistry of dolomite formation I: the stability of dolomite. *In* Concepts and Models of Dolomitization. *Edited by* Zenger, D. H., Dunham, J. B., and Ethington, R. L., The Society Economic Paleontologists and Mineralogists Special Publications no. 28, p. 111-121.

Carter, L.S., Kelley, S.A., Blackwell, D.D., and Naeser, N.D., 1998. Heat flow and thermal history of the Anadarko Basin, Oklahoma. American Association of Petroleum Geologists Bulletin, v. 82, p. 291-316.

Carter, T.R., 1987. A comparison of the Middle Proterozoic Balmat evaporite sequence with Niagaran and Cayugan strata in the Michigan-Appalachian basin. Ontario Petroleum Institute, 26th Annual Conference Proceedings, Technical Paper no. 13, 42p.

Carter, T.R.(ed.), 1990. Subsurface geology of southwestern Ontario: a core workshop. Ontario Petroleum Institute, American Association of Petroleum Geologists, 1990 Eastern Section Meeting, London, Ontario, 146p.

Carter, T.R., 1991. Dolomitization patters in the Salina A-1 and A-2 Carbonate units, Sombra Township, Ontario. Ontario Petroleum Institute, 30th Annual Conference Proceedings, v. 30, Technical Paper no. 4, 35p.

Carter, T.R., 1992. Oil and gas exploration, drilling and production summary, 1988. Ontario Ministry of Natural Resources, Oil and Gas Paper 11, 174p.

Cater, T.R., and Easton, R.M., 1990. Extension of Grenville Basement beneath southwestern Ontario: lithology and tectonic subdivisions. *In* Subsurface Geology of Southwestern Ontario-A Core Workshop. *Edited by* Carter, T.R., American Association of Petroleum Geologists, 1990 Eatern Section Meeting, London, Ontario, Canada, p. 9-28.

Carter, T.R., Trevail, R.A., and Smith, L., 1994. Core workshop: Niagaran reef and inter-reef relationships in the subsurface of southwestern Ontario. Geological Association of Canada, Mineralogical Association of Canada, Joint Annual Meeting, Waterloo 1994, Field Trip A5, Guidebook, 38p.

Cercone, K.R., 1984a. Thermal history of Michigan Basin. American Association of Petroleum Geologists Bulletin, v. 68, p. 130-136.

Cercone, K.R., 1984 b. Diagenesis of Niagaran (Middle Silurian) pinnacle reefs, northwestern Michigan. Unpublished Ph. D thesis, University of Michigan, Ann Arbor, Michigan, U.S.A., 367p.

Cercone, K.R., 1988. Evaporative sea-level drawdown in the Silurian Michigan Basin. Geology, v. 16, p. 387-390.

Cercone, K.R., and Lohmann, K.C., 1985. Early diagenesis of Middle Silurian pinnacle reefs, Northern Michigan. *In* Ordovician and Silurian rocks of the Michigan Basin and its margins. *Edited by* Cercone, K.R., and Budai, J.M., Michigan Basin Geological Society Special Paper 4, p. 109-130.

Cercone, K.R., and Lohmann, K.C., 1987. Late burial diagenesis of Niagaran (Middle Silurian) pinnacle reefs in Michigan Basin. American Association of Petroleum Geologists Bulletin, v. 71, p. 156-166.

Chafetz, H.S., 1972. Surface diagenesis of limestone. Journal of Sedimentary Petrology, v. 42, p. 325-329.

Chafetz, H.S. and Bulter, J.C., 1980. Petrology of recent caliche pisolites, spherulites, and speleothem deposits from central Texas. Sedimentology, v. 27, p. 495-518.

Charbonneau, S.L., 1990. Subaerial exposure and meteoric diagenesis in Middle Silurian Guelph Formation (Niagaran) pinnacle reef bioherms of the Michigan Basin, southwestern Ontario. Unpublished M. Sc. Thesis, Queen's University, Kingston, Ontario, Canada, 215p.

Chilingar, G.V., 1956. Dedolomitization: a review. American Association of Petroleum Geologists, Bulletin, v. 40, p. 762-778.

Choquette, P.W., and Pray, L.C., 1970. Geologic nomenclature and classification of porosity in sedimentary carbonates. American Association of Petroleum Geologists Bulletin, v. 54, no. 2, p. 207-250.

Churnet, H.G., Misra, K.C., and Walker, K.R., 1982. Deposition and dolomitization of Upper Knox carbonate sediments, Copper Ridge district, East Tennessee. Geological Society of America Bulletin, v. 93, p. 76-86.

Cohee, G.V., 1948. Thickness and lithology of Upper Ordovician and Lower and Middle Silurian rocks in the Michigan Basin. United States Geological Survey, oil and Gas Investigations, Preliminary Chart, no. 33.

Coniglio, M., and William-Jones, A.E., 1992. Diagenesis of Ordovician carbonates from the north-east Michigan Basin, Manitoulin Island area, Ontario: evidence from petrography, stable isotopes and fluid inclusions. Sedimentology, v. 39, p. 813-836.

Coniglio, M., James, N.P., and Aissaoui, D.M., 1988. Dolomitization of Miocene carbonates, Gulf of Suez, Egypt. Journal of Sedimentary Petrology, v. 58, p. 100-119.

Coniglio, M., Sherlock, R., William-Jones, A.E., Middleton, K., and Frape, S.K., 1994. Burial and hydrothermal diagenesis of Ordovician carbonates from the Michigan Basin, Ontario, Canada. *In* Dolomites, a volume in honour of Dolomieu. *Edited by* Purser, B., Tucker, M., and Zenger, D., International Association of Sedimentologists, Special Publication no. 21, p. 231-254.

Corbet, T.F., and Bethke, C.M., 1992. Disequilibrium fluid pressures and groundwater flow in the Western Canada Sedimentary Basin. Journal of Geophysical Research, v. 97, p. 7203-7217.

Crawford, M.L., 1981. Phase equilibria in aqueous fluid inclusions. *In* Short course in fluid inclusions: applications to petrology. *Edited by* Hollister, L.S., and Crawford, M.L., Mineralogical Association of Canada, p.75-99.

Crowley, D.J., 1973. Middle Silurian patch reefs in Gasport Member (Lockport Formation), New York. American Association of Petroleum Geologists Bulletin, v. 57, p. 283-300.

Davies, G. R., 1977. Former magnesian calcite and aragonite submarine cements in upper Paleozoic reefs of the Canadian Arctic, a summary. Geology, v. 5, p. 11-15.

Davies, G.R., 1996. Hydrothermal dolomite (HTD) reservoir facies: Global perspectives on the tectonic-structural and temporal linkage between MVT and SEDEX Pb-Zn ore bodies, and subsurface HTD reservoir facies. Canadian Society of Petroleum Geologists, Short Course Notes, Edition 1, 120p.

Davies, S.H., Rosenblat, S., Wood, J.R., and Hewett, T.A., 1985. Convective fluid flow and diagenetic patterns in domed sheets. American Journal of Science, v. 285, p. 207-223.

Dawans, J.M. and Swart, P.K., 1988. Textural and geochemical alteration in late Cenozoic Bahamian dolomites. Sedimentology, v. 35, p. 385-403.

DeBeaumont, E., 1887. Application du calcul à l'hypothèse de la formation par épigénie des anhydites, des gypses et des dolomies. Soc. Geol. France Bull. v. 8, p. 174-177.

Deffeyes, K.S., Lucia, F.J., and Weyl, P.K., 1965. Dolomitization of recent and Plio-Pleistocene sediments by marine evaporite waters on Bonaire, Netherlands Antilles. *In*

Dolomitization and Limestone Diagenesis. *Edited by* Pray, L.C., and Murray, R.C., Society of Economic Paleontologists and Mineralogists, Special Publication no. 13, p. 71-88.

Deike, R.G., 1990. Dolomite dissolution rates and possible Holocene dedolomitization of water-bearing units in the Edwards aquifer, south-central Texas. Journal of Hydrology, v. 112, p. 335-373.

Dickson, J.A.D., and Coleman, M.L., 1980. Changes in carbon and oxygen isotope composition during limestone diagenesis. Sedimentology, v.27, p. 107-108.

Dickson, J.A.D., 1966. Carbonate identification and genesis as revealed by staining. Journal of Sedimentary Petrology, v. 36, p. 491-505.

Dollar, P., Frape, S.K., McNutt, R.H., Fritz, P., and Macqueen, R.W., 1988. Geochemical studies of formation waters, southwestern Ontario, Canada, and southern Michigan, U.S.A. *In*

Geoscience Research Grant Program, Summary of Research 1987-1988. *Edited by* Milne, V.G., Ontario Geological Survey, Miscellaneous Paper 140, p. 14-28.

Dorobek, S.L., and Filby, R.H., 1988. Origin of dolomites in a downslope biostrome, Jefferson Formation (Devonian), Central Idaho: Evidence from reef patterns, stable isotopes, and petrography. Bulletin of Canadian Petroleum Geology, v. 36, no. 2, p. 202-215.

Dorr, J.A., and Eschman, D.F., 1971. Geology of Michigan. University of Michigan Press, Michigan, 476p.

Droste, J.B., and Shaver, R.H., 1977. Synchronization of deposition, Silurian reef-bearing rocks on Wabash Platform with cyclic evaporites of Michigan Basin. *In* Reefs and evaporites, concepts and depositional models. *Edited by* Fisher, J.H., America Association of Petroleum Geologists, Studies in Geology no.5, p. 93-109.

Droste, J.B., and Shaver, R. H., 1982. The Salina Group (Middle and Upper Silurian) of Indiana: Indiana Geological Survey Special Report 24, 41p.

Droste, J.B., and Shaver, R.H., 1983. Atlas of early and middle Paleozoic paleogeography of the southern Great Lakes area. Indiana Geological Survey Special Report 32, 32p.

Droste, J.B., and Shaver, R.H., 1985. Comparative stratigraphic framework for Silurian reefs, Michigan Basin to surrounding platforms. Michigan Basin Geological Society Special Paper, no.4, p. 73-93.

Dunham, J.B., and Olson, E.R., 1980. Shallow subsurface dolomitization of subtidally deposited carbonate sediments in the Hanson Creek Formation (Ordovician-Silurian) of Central Nevada. *In* Concepts and models of dolomitization. *Edited by* Zenger, D.H., Dunham, J.B., and Ethington, R.L., Society of Economic Paleontologists and Mineralogists Special Publications no. 28, p. 139-161.

Dunham, R.J., 1962. Classification of carbonate rocks according to the depositional texture. *In* Classification of carbonate rocks. *Edited by* Ham, W.E., American Association of Petroleum Geologists Memoir 1, p. 108-121.

Durocher, S., and Al-Aasm, I.S., 1998. Dolomitization and neomorphism of Mississipian (Visean) Upper Debolt Formation, Blueberry Field, northeastern British Columbia:

geological, petrologic, and chemical evidence. America Association of Petroleum Geologists Bulletin, v. 81, p. 954-977.

Embry, A.F., and Klovan, J.F., 1971. A late Devonian reef tract on northwestern Banks Island, North West Territories. Bulletin of Canadian Petroleum Geology, v. 19, p. 738-781.

Epstein, S., Buchsbaum, R., Lowenstam, H.A., and Urey, H.C., 1953. Revised carbonate-water isotopic temperature scale. Geological Society of America Bulletin, v. 64, p. 1315-1326.

Evamy, B.D., 1967. Dedolomitization and the development of rhombohedral pores in limestones. Journal of Sedimentary Petrology, v. 37, no. 4, p. 1204-1215.

Evans, C.S., 1950. Underground hunting in the Silurian of southwestern Ontario. Geological Association of Canada Proceedings 3, p. 55-85.

Fairbridge, R.W., 1979. Dedolomitization, *In* The Encyclopedia of Sedimentology. *Edited by* Fairbridge, R.W., and Bourgeois, J., Stroudsburg, Pennsylvania, Dowden, Hutchinson and Ross Incorporated, p. 233-234.

Felber, B.E., 1964. Silurian reefs of southwestern Michigan. Unpublished Ph. D. Thesis, Northwestern University, Evanston, Illiois, U.S.A., 104p.

Fischer, H. J., 1988. Dolomite diagenesis in the Metaline Formation, northeastern Washington State. *In* Sedimentology and Geochemistry of Dolostones. *Edited by* Shukla, V. and Baker P. A., Society of Economic Paleontologists and Mineralogists Special Publications No. 43, p. 178-189.

Fisher, J.H., and Barratt, M.W., 1985. Exploration in Ordovician of the central Michigan Basin. America Association of Petroleum Geologists Bulletin, v. 69, p. 2065-2076.

Fisher, J.H., Barratt, M.W., Droste,J.B., and Shaver, R.H., 1988. Michigan Basin. *In* Sedimentary Cover-North American Craton; U.S. *Edited by* Sloss, L.L., Geological Society of America, The Geology of North America, v. D-2, p. 361-382.

Folk, R.L., 1965. Some aspects of recrystallization in ancient limestones. *In* Dolomitization and limestone diagenesis *Edited by* Zenger, D.H., and Dunham, J.B., The Society of Economic Paleontologists and Mineralogists Special Publications no. 13, p. 13-48.

Folk, R.L., 1974. The natural history of crystalline calcium carbonate: effect of Magnesium content and salinity. Journal of Sedimentary Petrology, v. 44, no. 1, p. 40-53.

Folk, R.L., and Land, L.S., 1975. Mg/Ca ratio and salinity: two controls over crystallization of dolomite. American Association of Petroleum Geologists Bulletin, v. 59, p. 60-68.

Folkman, Y., 1969. Diagenetic dedolomitization in the Albian-Cenomanian Yagur dolomite on Mount Carnel (N. Israel). Journal of Sedimentary Petrology, v. 39, p. 385-390.

Frank, J.R., 1981. Dedolomitization in the Taum Sauk Limestone (Upper Cambrian), southeast Missouri. Journal of Sedimantary Petrology, v. 51, p. 7-18.

Frape, S.K., Fritz, P. and McNutt, R.H., 1984. The role of water-rock interaction in the chemical evolution of groundwaters from the Canadian Shield. Geochimica Cosmochimica Acta, v. 48, p. 1617-1627.

Frape, S.K., Dollar, P.S., Lollar, B.S., and McNutt, R.H., 1989. Mixing of saline basinal fluids in Southern Ontario: Implications of rock-water interaction, hydrocarbon emplacement of Canadian Shield brines. *In* Water-Rock Interaction *Edited by* Miles, A., p. 223-227.

Friedman, G.M., 1975. The making and unmaking of limestones or the downs and ups of porosity. Journal of Sedimentary Petrology, v. 45, no. 2, p. 379-398.

Friedman, G.M., and Sanders, J.E., 1967. Origin and occurrence of dolostones. *In* Developments in Sedimentology; 9B. *Edited by* Chilingar, G.V., Bissel, H.J., and Fairbridge, R.W., Elsevier, Amsterdam, p. 267-348.

Frisia, S., 1994. Mechanisms of complete dolomitization in a carbonate shelf: comparison between the Norian Dolomia Principale (Italy) and the Holocene of Abu Dhabi Sabkha.

*In* Dolomites, A volume in honour of Dolomieu. *Edited by* Purser, B., Tucker, M., and Zenger, D., International Association of Sedimentologists, Special Publication no. 21, p. 55-74.

Fritz, P., 1967. Oxygen and carbon isotope composition of carbonates from the Jura of southern Germany. Canadian Journal of Earth Sciences, v. 4, p. 1247-1267.

Fritz, P., and Katz, A., 1972. The sodium distribution of dolomite crystals. Chemical Geology, v.10, p.237-244.

Gao, G., and Land, L. S., 1991. Early Ordovician Cool Creek Dolomite, Middle Arbuckle Group, Slick Hills, SW Oklahoma, U.S.A.: origin and modification. Journal of Sedimantary Petrology, v. 61, p. 161-173.

Gao, G., 1990. Geochemical and isotopic constraints on the diagenetic history of a massive stratal, late Cambrian (Royer) dolomite, Lower Arbuckle Group, Slick Hills, Southwestern Oklahoma, USA. Geochimica et Cosmochimica Acta, v. 54, p. 1979-1989.

Gardner, W.C., and Bray, E.E., 1985. Oils and source rocks of Niagaran reefs (Silurian) in the Michigan Basin, *In* Petroleum geochemistry and source rock potential of carbonate rocks. *Edited by* Palacas, J.C., American Association of Petroleum Geologists, Study in Geology 18, p. 33-44.

Garven, G., and Freeze, R.A., 1984. Theoretical analysis of the role of groundwater flow in the genesis of stratabound ore deposits; 2, quantitative results. American Journal of Science, v. 284, p. 1125-1174.

Garven, G., 1985. The role of regional fluid flow in the genesis of the Pine Point Deposit, Western Canada Sedimentary Basin. Economic Geology, v. 80, p. 307-324.

Garven, G., 1995. Continental-scale groundwater flow and geological processes. *In* Annual Review of Earth and Planetary Sciences. *Edited by* Wetherill, G.W., Albee, A.L., and Burke, K.C., v. 23, p. 89-118.

Gawthorpe, R.L., 1987. Burial dolomitization and porosity development in a mixed carbonate-clastic sequence: an example from the Bowland Basin, northern England. Sedimentology, v. 34, p. 5333-538.

Gill, D., 1973. Stratigraphy, facies evolution and diagenesis of productive Niagaran-Guelph reefs and Gayugan sabkha deposits, the Belle River Mills gas field, Michigan Basin. Unpublished Ph. D. Thesis, University of Michigan, Ann Arbor, Michigan, U.S.A. 275p.

Gill, D., 1977a. The Belle River Mills Gas Field; Productive Niagaran reefs encased by Sabkha deposits, Michigan Basin. Michigan Basin Geological Society, Special Paper, no. 2, 187p.

Gill, D., 1977b. Salina A-1 sabkha cycles in the late Silurian paleogeography of the Michigan Basin. Journal of Sedimentary Petrography, v. 47, p. 979-1017.

Gill, D., 1979. Differential entrapment of oil and gas in Niagaran Pinnacle-Reef Belt of Northern Michigan. American Association of Petroleum Geologists Bulletin, v. 63; 4, 608-620.

Gill, D., 1985. Depositional facies of Middle Silurian (Niagaran) pinnacle reefs, Belle River Mills gas field, Michigan Basin, southeastern Michigan. *In* Carbonate Petroleum Reservoirs. *Edited by* Roehl, P.O., and Choquette, P.W., Springer Verlag, Berlin, p. 123-139.

Given, R.K., and Wilkinson, B.H., 1987. Perspectives: dolomite abundance and stratigraphic age; constraints on rates and mechanisms of Phanerozoic dolostone formation. Journal of Sedimentary Petrology, v. 57, p. 1068-1078.

Goldberg, M., 1967. Supratidal dolomitization and dedolomitization in Jurassic rocks of Hamakhtesh Hagatan, Israel. Journal of Sedimentary Petrology, v. 37, p. 760-773.

Goldstein, R.H., and Reynolds, T.J., 1994. Systematics of fluid inclusions in diagenetic minerals. Society for Sedimentary Geology, Short Course 31, 199p.

Gould, E., 1976. Oil-The history of Canada's oil and gas industry. Victoria, Handcock House Publishers, 288p.

Grammer, G.M, Ginsburg, R.N., and Harris, P.M., 1995. Timing of deposition, diagenesis, and failure of steep carbonate slopes in response to a high-amplitude/high-frequency fluctuation in sea level, tongue of the ocean, Bahamas. *In* Recent Carbonate Sequence Stratigraphy Developments and Applications. *Edited by* Loucks, R.G., and Sarg, J.F., American Association of Petroleum Geologists, Memoir 57, Chapter 4, p. 107-131.

Gregg, J.M., and Hagni, R.D., 1987. Irregular cathodoluminescent banding in late dolomite cements: Evidence from complex faceting and metalliferous brines. Geological Society of America Bulletin, v. 98, p. 86-91.

Gregg, J.M., and Shelton, K.L., 1990. Dolomitization and dolomite neomorphism in the back reef facies of the Bonneterre and Davis formations (Cambrian), southeastern Missouri. Journal of Sedimantary Petrology, v. 60, no. 4, p. 549-562.

Gregg, J.M., and Sibley, D.F., 1984. Epigenetic dolomitization and the origin of xenotopic dolomite texture. Journal of Sedimentary Petrology, v. 54, no. 3, p. 908-931.

Gregg, J.M., 1983. On the formation and occurrence of saddle dolomite—Discussion. Journal of Sedimantary Petrology, v. 53, no. 3, p. 1025-1033.

Gregg, J.M., Howard, S.A., and Mazzullo, S.J., 1992. Early diagenetic recrystallization of Holocene (<3000 years old) peritidal dolomites, Ambergris Cay, Belize. Sedimentology, v. 39, p. 143-160.

Grimes, D.J., 1987. Depositional models, subaerial facies, and diagenetic histories of the Rosedale and Fletcher reefs, southwestern Ontario. Unpublished M. Sc. Thesis, Queen's University, Kingston, Ontario, Canada, 120p.

Hanor, J.S., 1994. Origin of saline fluids in sedimentary basins. Geological Society of London Special Publication v. 78, p. 151-174.

Hanshaw, B.B., Back, W., and Deike, R.G., 1971. A geochemical hypothesis for dolomitization by ground water. Economic Geology, v. 66, p. 710-724.

Hardie, L.A., 1987. Dolomitization: a critical view of some current views. Journal of Sedimantary Petrology, v. 57, no. 1, p. 166-183.

Harper, D.A., 1993. Secondary K-Feldspar at the Precambrian-Paleozoic boundary, southwestern Ontario. Unpublished M Sc. thesis, University of Western Ontario, London, Ontario, Canada, 140p.

Haxby, W.F., Turcotte, D.L., and Bird, J.M., 1976. Thermal and mechanical evolution of the Michigan basin. Tectonophysics, v. 36, p. 57-75.

Haynes, S.J., 1989. Depositional setting of gypsum deposits, southwestern Ontario: The Domtar Mine. Economic Geology, v. 84, p. 857-870.

Haynes, S.J., and Hughes-Pearl, J., 1990. Gypsum deposits and stratigraphy of the Salina A and B units, Algonquin Arch-Niagara Peninsula, southwestern Ontario. American Association of Petroleum Geologists, 1990 Eastern Section Meeting, Ontario Petroleum Institute, Field Trip Guidebook, no. 4, 31p.

Hein, J.R., Gray, S.C., Richmond, B.M., and White, L. D., 1992. Dolomitization of Quaternary reef limestone, Aitutaki, Cook Islands. Sedimentology, v. 51, p. 1323-1334.

Hill, J.V., 1973. Lithological indicators of reservoir proximity, southwestern Ontario. Ontario Petroleum Institute, 12th Annual Meeting Proceedings, v. 12, Technical Paper no. 14, 9p.

Hird, K. and Tucker, M.E., 1988. Contrasting diagenesis of two Carboniferous oolites from south Wales, a tale of climatic influence. Sedimentology, v. 35, p. 587-602.

Hogarth, C.G., and Sibley, D.F., 1985. Thermal history of the Michigan Basin: evidence from condont coloration index. *In* Ordovician and Silurian Rocks of the Michigan Basin and its Margins. *Edited by* Cercone, K.R., and Budai, J.M., Michigan Basin Geological Society, Special Paper no. 4. p. 45-58.

Holail, H., Lohmann, K.C., and Sanderson, I., 1988. Dolomitization and dedolomitization of Upper Cretaceous carbonates: Bahariya Oasis, Egypt. *In* Sedimentology and Geochemistry of Dolostones. *Edited by* Shukla, V., and Baker,P.A., Society of Economic Paleontologists and Mineralogists, Special Publication no. 43, p. 191-207.

Howell, P.D., and Van der Pluijm, B.A., 1990. Early history of the Michigan basin: Subsidence and Appalachian tectonics. Geology, v. 18, p. 1195-1198.

Hsü, K.J., and Siegenthaler, C., 1969. Preliminary experiments and hydrodynamic movement induced by evaporation and their bearing on the dolomite problem. Sedimentology, v. 12,
p. 11-25.

Hudson, J.D., 1977. Stable isotopes and limestone lithification. Journal of the Geological Society of London, v. 133, p. 637-660.

Hugman, R.H.H., and Friedman, G.M., 1979. Effects of texture and composition on mechanical behaviour of experimentally deformed carbonate rocks. American Association of Petroleum Geologists Bulletin, v. 63, p. 1478-1489.

Huh, J.M., 1973. Geology and diagenesis of the Salina-Niagaran pinnacle reefs in the northern shelf on the Michigan Basin. Unpublished Ph. D. Thesis, University of Michigan, Ann Arbor, Michigan, U.S.A., 253p.

Huh, J.M., Briggs, L.I., and Gill, D., 1977. Depositional environments of pinnacle reefs, Niagara and Salina Groups, northern shelf, Michigan Basin. *In* Reefs and evaporites, Concepts and depositional models. *Edited by* Fisher, J.H., American Association of Petroleum Geologists, Studies in Geology no 5, p. 1-21.

Humphrey, J.D.,1988. Late Pleistocene mixing zone dolomitization, southeastern Barbados, West Indies. Sedimentology, v. 35, p. 327-348.

Hurley, N.F., and Budros, R., 1990. Albion-Scipio and Stoney Point fields-U.S.A. Michigan basin. *In* Stratigraphic traps 1. *Edited by* Beaumont, E.A., and Foster, N.H.,

American Association of Petroleum Geologists. Treatise of Petroleum Geology. Atlas of Oil and Gas Fields, p. 1-33.

Irving, E., 1979. Paleopoles and paleolatitudes of North America and speculations about displaced terrains. Canadian Journal of Earth Sciences, v. 16, p. 669-694.

Irwin, H., Curtis, C., and Coleman, M., 1977. Isotopic evidence for source of diagenetic carbonates formed during burial of organic-rich sediments. Nature, v. 269, p. 209-213.

Jacobso., R.L., and Usdowski, H.E.,1976. Partitioning of strotium between calcite, dolomite and liquids: an experimental study under higher temperature diagenetic conditions and the model for prediction of mineral pairs for geothermometry. Contribution to minerology and Petrology, v. 59, p. 171-185.

James, N.P., and Bourque, P.A., 1992. Reefs and Mounds. *In* Facies models: response to sea level change. *Edited by* Walker, R.G., and James, N.P., Geological Association of Canada, p. 323-347.

James, N.P., Bone, Y., and Kyser, T. K., 1993. Shallow burial dolomitization and dedolomitization of Mid-Cenozoic, cool-water, calcitic, deep shelf limestones, southern Australia. Journal of Sedimentary Petrology, v. 63, no. 3, p. 528-538.

James, N.P., Ginsburg, R.N., Marszalek, D.S., and Choquette, P. W., 1976. Facies and fabric specificity of early subsea cements in shallow Belize (British Honduras) reefs. Journal of Sedimentary Petrology, v. 46, p. 523-544.

James, N.P., Bone, Y., and Kyser, T.K., 1993. Shallow burial dolomitization and dedolomitization of Mid-Cenozoic, cool-water, calcitic, deep-shelf limestones, southern Australia. Journal of Sedimentary Petrology, v. 63, p. 528-538.

Jameson, J., 1994. Models of porosity formation and their impact on reservoir description, Lisburne Field, Prudhoe Bay, Alaska. American Association of Petroleum Geologists Bulletin, v. 78, p. 1651-1678.

Jodry, R.L., 1969. Growth and dolomitization of Silurian Reefs, St. Clair County, Michigan. American Association of Petroleum Geologists Bulletin, v. 52, p. 957-981.

Johnson, M.D., Armstrong, D.K., Sanford, B.V., Telford, P.G., and Rutka, M.A., 1992. Paleozoic and Mesozoic Geology of Ontario. In Geology of Ontario. Edited by Thurston, P.C., Williams, H.R., Sutchiffe, R.H., and Stott, G.M., Ontario Geological Survey, Special Volume 4, part 2, Chapter 20, p. 907-1008.

Jones, B., Pleydell, S.M., Ng, K.C., and Longstaffe, F.J., 1989. Formation of poikilotopic calcite-dolomite fabrics in the Oligocene-Miocene Bluff Formation of Grand Cayman, British West Indies. Bulletin of Canadian Petroleum Geology, v. 37, no. 3, p. 255-265.

Jones, H.D., and Kesler, S.E., 1992. Fluid inclusion gas chemistry in east Tennessee Mississippi Valley-type districts: evidence for immiscibility and implications for depositional mechanisms. Geochimica et Cosmochimica Acta, v. 56, p. 137-154.

Kaleem, S.M., 1994. Role of carbonate diagenesis and halite plugging on the reservoir quality of Middle Silurian reefal dolomites. Unpublished M. Sc. Thesis, University of waterloo, Waterloo, Ontario, Canada, 167p.

Kastner, M., 1982. When does dolomitization occur and what controls it. 11 th International Congress of Sedimentology (Abstract), Hamilton, Ontario, Canada, p. 124.

Katz, A., 1971. Zoned dolomite crystals. Journal of Geology, v. 79, p. 38-51.

Katz, A., 1968. Calcian dolomite and dedolomitization. Nature, v. 217, p. 439-440.

Katz, A. and Matthews. A. 1977. The dolomitization of CaCo3: An experimental study at 252-295 °C. Geochimica et Cosmochimica Acta, v.41, p.297-308.

Kaufman, J., 1989. Sedimentology and diagenesis of the Swan Hill Formation (Middle-Upper Devonian) Rosevear Field. Unpublished Ph. D. Thesis, State University of New York, Stony Brook, New York, U.S.A., 412p.

Kaufman, J., 1994. Numerical models of fluid flow in carbonate platforms: implication for dolomitization. Journal of Sedimentary Research, v. A64, p. 128-139.

Kelts, K., and McKenzie, J., 1984. A comparison of anoxic dolomite from deep sea sediments: Quaternary Gulf of California and Messinian Tripoli Formation of Sicily. *In* Dolomites of the Monterey Formation and other Organic-rich units. *Edited by* Garrison, R.E., Kastner, M., Zenger, D.H., Special. Publication, Society of Economic Paleontologists and Mineralogists, Pac sect. 41, p. 119-140.

Kendall, A.C., 1989. Brine mixing in the Middle Devonian of western Canada and its possible significance to regional dolomitization. Sedimentary Geology, v. 64, p. 271-285.

Kenny, R., 1992. Origin of disconformity dedolomite in the Martin Formation (Late Devonian, northern Arizona). Sedmentary Geology, v. 78, p. 137-146.

Klein, G.D., 1995. Intracratonic Basins. *In* Tectonics of Sedimentary Basins. *Edited by* Busby, C.J., and Ingersoll, R.V., Blackwell Science, Chapter 13, p. 459-477.

Koepke, W.E., and Sanford, B.V., 1966. The Silurian oil and gas fields of southern Ontario. Geological Survey of Canada, Paper 65-30, 137p.

Kohout, F.A., 1967. Groundwater flow and the geothermal regime of the Floridian plateau. Trans. Gulf Coast Association Geological Societies, v. 17, p. 339-354.

Krouse, H.R., Viau, C.A., Eliuk, L.S., Ueda, A., and Halas, S., 1988. Chemical and isotopic evidence of thermochemical sulphate reduction by light hydrocarbon gases in deep carbonate reservoirs. Nature, v. 333, p. 415-419.

Kupecz, J.A. and Land, L.S., 1991. Late-stage dolomitization of the Lower Ordovician Ellenburger Group, West Texas. Journal of Sedimentary Petrology, v. 61, no. 4, p. 551-574.

Kupecz, J.A., and Land, L.S., 1994. Progressive recrystallization and stabilization of early-stage dolomite: Lower Ordovician Ellenburger Group, west Texas. *In* Dolomites, A volume in honour of Dolomieu. *Edited by* Purser, B., Tucker, M., and Zenger, D., International Association of Sedimentologists, Special Publication no. 21, p. 155-166.

Kupecz, J.A., Montañez, I.P., and Gao, G., 1993. Recrystallization with time. *In* Carbonate Microfabrics: Frontiers in Sedimentology. *Edited by* Rezak, R., and Lavoie, D., Springer-Verlag, New York, p.256-267.

Land, L.S., 1973. Contemporaneous dolomitization of Middle Pleistocene reefs by meteoric water, North Jamaica. Bulletin of Marine Science, v. 23, p. 64-92.

Land, L.S., 1980. The isotopic and trace element geochemistry of dolomite: the state of the art. *In* Concepts and models of dolomitization. *Edited by* Zenger, D.H., Dunham, J.B., and Ethington, R.L., Society Economic Paleontologists and Mineralogists, Special Publication no. 28, p. 87-110.

Land, L.S., 1983. Dolomitization: Education Course Note Series no. 24. American Association of Petroleum Geologist Education Conference, Denver, Colorado, 34p.

Land, L.S., 1985. The origin of massive dolomite. Journal of Geological Education, v. 33, p. 112-125.

Land, L.S., 1986. The carbon and oxygen isotopic chemistry of surficial Holocene shallow marine carbonate sediment and Quaternary limestone and dolomite. *In* Handbook of Environmental Isotope Geochemistry. *Edited by* Fritz, P., and Fontes, J.C.H., v. 3, p. 191-217.

Land, L.S., 1991. Dolomitization of the Hope Gate Formation (north Jamaica) by seawater: Reassessment of mixing-zone dolomite. *In* Stable isotope geochemistry: a tribute to Samuel

Epstein. *Edited by* Taylor, Jr., H.P., O'Neil, J.R., and Kaplan, I.R., Geochemical Society, Special Publication no. 3, p. 121-134.

Land, L.S., 1992. The dolomite problem: stable and radiogenic isotope clues. *In* Lecture notes in Earth Sciences, no. 43 *Edited by* Clauer, N., and Chaudhuri, S., Springer-Verlag, p. 49-65.

Land, L.S., and Prezbindowski, D.R., 1981. The origin and evolution of saline formation water in Lower Cretaceous carbonates, south-central Texas. Journal of Hydrology, v. 54, p. 51-74.

Land, L.S., and Hoops, G.K., 1973. Sodium in carbonate sediments and rocks: A possible index to the salinity of diagenetic solutions. Journal of Sedimentary Petrology, v. 43, p. 614-617.

Landes, K.K., 1945. Salina and Bass Island rocks in Michigan Basin. United States Geological Survey Oil and Gas Investigation, Preliminary Map 40.

Landes, K.K., 1946. Porosity through dolomitization. American Association of Petroleum Geologists Bulletin, v. 30, p. 305-318.

Lavoie, D., 1993. Early Devonian marine isotopic signatures: brachiopods from the Upper Gaspe Limestones, Gaspe Peninsula, Quebec, Canada. Journal of Sedimentary Petrology,
v. 63, no. 4, p. 620-627.

Lawrence, M.J.F., 1991. Early diagenetic dolomite concretions in the late Cretaceous Herring Formation, eastern Marlborough, New Zealand. Sedimentary Geology, v. 75, p. 125-140.

Leach, D. L., Plumlee, G. S., Hofstra, A. H., Landis, G. P, Rowan, E. L., and Viets, J. G., 1991. Origin of late dolomite cement by $CO_2$–saturated deep basin brines: evidence from the Ozark region, central United States. Geology, v. 19, p. 348-351.

Lee, Y.I., and Friedman, G.M., 1987. Deep-Burial dolomitization in the Ordovician Ellenburger Group Carbonates, west Texas and southeastern New Mexico. Journal of Sedimentary Petrology, v. 57, p. 544-557.

Legall, F.D, Barnes, C.R.,and Macqueen, R.W., 1981. Thermal maturation, burial history and hot spot development, Paleozoic strata of southern Ontario – Quebec, from conodont and acritarch colour alteration studies. Bulletin of Canadian Petroleum Geology, v. 29, p. 493-539.

Liberty, B.A., and Bolton, T.E, 1971. Paleozoic geology of the Bruce Peninsula area, Ontario. Geological Survey of Canada, Memoir 360, 163p.

Lippman, F., 1973. Sedimentary carbonate minerals. Springer-Verlag/Berlin, New York, 228p.

Logan, B.W., 1987. The MacLeod evaporite basin, western Australia. American Association of Petroleum Geologists Memoir 44, 140p.

Lohmann, K.C., and Walker, J.C.C., 1989. The record of Phanerozoic abiotic marine calcite cements. Geophysical Research Letters, v. 16, no. 4, p. 319-322.

Lohmann,K.C., 1988. Geochemical patterns of meteoric diagenesis system and their application to studies of paleokarst. *In* Paleokarst. *Edited by* James, N.P., and Choquette, P.W., Springer-Verlag, New York, p. 58-80.

Logan, W.E., 1863. Geology of Canada. Canada Geological Survey Progress Report, 125p.

Longman, M.W., 1980. Carbonate diagenetic textures from nearsurface diagenetic environments. American Association of Petroleum Geologists Bulletin, v. 64, p. 461-487.

Longman, M.W., and Mench, P.A., 1978. Diagenesis of Cretaceous limestones in the Edwards acquifer system of south-central Texas: a scanning electron microscope study. Sedimentary Geology, v. 21, p.241-276.

Lopatin, N.V., 1971. Temperature and geological time as factors in coalication. Akademiya Nauk SSR Izvestiya Seriya Geologicheskikh, no. 3, p.95-106.

Lorens, R.B., 1981, Sr, Cd, Mn and Co distribution coefficients in calcite as a function of calcite precipitation rate. Geochimica Cosmochimica Acta, v. 45, p. 553-561.

Lu, F.H., and Meyers, W.J., 1998. Massive dolomitization of a late Miocene carbonate platform: a case of mixed evaporative brines with meteoric water, Nijar, Spain. Sedimentology, v. 45, p. 263-277.

Lucia, F.J., 1961. Dedolomitization in the Tansill (Permian) Formation. Geological Society of America, Bulletin, v. 72, p. 1107-1110.

Lucia, F.J., and Major, R.P., 1994. Porosity evolution through hypersaline reflux dolomitization. *In* Dolomites: a volume in honour of Dolomieu. *Edited by* Purser, B.H., Tucker, M.E., Zenger, D.H., Special publication of the International Association Sedimentologists, 21, p. 325-341.

Lumsden, D. N. and Chimahusky, J. S., 1980. Relationship between dolomite nonstoichiometry and carbonate facies parameters. *In* Concepts and models of dolomitization. *Edited by* Zenger, D. H., Dunham, J. B., and Ethington, R. L., Society Economic Paleontologists and Mineralogists Special Publications No. 28, p. 123-137.

Lumsden, D.N., 1988. Characteristics of deep-marine dolomite. Journal of Sedimentary Petrology, v. 58, no. 6, p. 1023-1031.

Machel, H.G., 1987. Saddle dolomite as a by-product of chemical compaction and thermochemical sulphate reduction. Geology, v. 15, p. 936-940.

Machel, H.G., 1988. Fluid flow direction during dolomite formation as deduced from trace-element trends. *In* Sedimentology and Geochemistry of Dolostones. *Edited by* Shukla, V., and Baker, P.A., Society of Economic Paleontologists and Mineralogists Special Publications no. 43, p. 115-125.

Machel, H.G., 1998. Recrystallization versus neomorphism, and the concept of "significant recrystallization" in dolomite research. Sedimentary Geology, v. 113; 3-4, p. 161-168.

Machel, H.G., and Anderson, J.H., 1989. Pervasive subsurface dolomitization of the Nisku Formation in the central Alberta. Journal of Sedimentary Petrology, v. 59, no. 6, p. 891-911.

Machel, H.G., and Mountjoy, E.W., 1986. Chemistry and environments of dolomitization: a reappraisal. Earth Science Reviews, v. 23, p. 175-222.

Machel, H.G., and Mountjoy, E.W., 1987. General constraints of extensive pervasive dolomitization and their application to the Devonian carbonates of western Canada. Bulletin of Canadian Petroleum Geology, v. 35, no. 2, p. 143-158.

Machel, H.G., Mountjoy, E.W., and Amthor, J.E., 1996. Mass balance and fluid flow constraints on regional-scale dolomitization, Late Devonian, Western Canada Sedimentary Basin – Discussion. Bulletin of Canadian Petroleum Geology, v. 44, p. 566-571.

Magaritz, M., and Kafri, U., 1981. Stable isotope and $Sr^{2+}/Ca^{2+}$ evidence of diagenetic dedolomitization in a schizohaline environment: Cenomanian of northern Israel. Sedimentary Geology, v. 28, p. 29-41.

Maiklem, W.R., 1971. Evaporative drawdown-a mechanism for water-level lowering and diagenesis in the Elk Point basin. Bulletin of Canadian Petroleum Geology, v. 19, p. 487-503.

Malone, M.J., Barker, P.A., and Burns, S., 1996. Recrystallization of dolomite: An experimental study from 50 to 200 °C. Geochimica Cosmochimica Acta, v. 60, p. 2189-2207.

Mantek, W., 1973. Niagaran pinnacle reefs in Michigan. Michigan Basin Geological Society Guidebook, p.35-46.

Mareschal, J.C., 1987. Subsidence and heat flow in intracontinental basins and passive margins. *In* Sedimentary basins and basin-forming mechanisms. *Edited by* Beaumont, C., and Tankard, A.J., Canadian Scoiety of Petroleum Geologists, Memoir 12, p. 519-527.

Mattavelli, L., Chilingarian, G.V., and Storer, D., 1969. Petrography and diagenesis of the Taormina Formation, Gela Oil Field, Sicily (Italy). Sedimentary Geology, v. 3, p. 59-86.

Mattes, B.W., and Mountjoy, E.W., 1980. Burial dolomitization of the Upper Devonian Miette buildup, Jasper National Park, Alberta. *In* Concepts and models of dolomitization. *Edited by* Zenger, D.H., Dunham, J.B., and Ethington, R.L., Society of Economic Paleontologists and Mineralogists Special Publication no. 28, p. 259-297.

Mazzullo, S.J., and Harris, P.M., 1992. Mesogenetic dissolution: Its role in porosity development in carbonate reservoirs. American Association of Petroleum Geologists Bulletin, v. 76, no. 5, p. 607-620.

Mazzullo, S.J., 1992. Geochemical and neomorphic alteration of dolomite: a review. Carbonates and Evaporites, v. 7, no. 1, p. 21-37.

McCaffrey, M.A., Lazar, B. and Holland, H.D., 1987. The evaporation path of seawater and the coprecipitation of Br and K with halite. Journal of Sedimentary Petrology, v. 57, p. 928-937.

McCollough, C.N., Jr., 1975. Origin of pore-filling salts in the Niagaran reefs of northern Michigan. Abstract, American Association of Petroleum Geologists Bulletin, v. 59, p. 1737.

McCrea, J.M., 1950. On the isotopic chemistry of carbonates and a paleotemperature scale. Journal of Chemical Physics, v. 18, p. 849-857.

McKenzie, J.A., Hsü, K.J., and Schneider, J.F., 1980. Movement of subsurface waters under the sabkha, Abu Dhabi, UAE, and its relation to evaporative dolomite genesis. *In* Concepts and Models of Dolomitization *Edited by* Zenger, D.H., Dunham, J.B., and Ethington, R.L., Society of Economic Paleontologists and Mineralogists Special Publication no. 28, p. 11-30.

McMurray, M., 1985. Geology and organic geochemistry of Salina A-1 Carbonate oil source-rock lithofacies (Upper Silurian), southwestern Ontario. Unpublished M. Sc. Thesis, University of Waterloo, Waterloo,Ontario, Canada, 236p.

McNutt, R.H., Frape, S.K., and Dollar, P., 1987. A strontium, oxygen and hydrogen isotopic composition of brines, Michigan and Appalachian Basins, Ontario and Michigan. Applied Geochemistry, v. 2, p. 495-505.

Mesolella, K.J., Robinson, J.D., McCormick, L.M., and Ormiston, A.R., 1974. Cyclic deposition of Silurian carbonates and evaporites in Michigan Basin. American Association of Petroleum Geologists Bulletin, v. 58, p. 34-62.

Mesolella, K.J., 1978. Paleogeography of some Silurian and Devonian reef trends, central Appalachian Basin. American Association of Petroleum Geologists Bulletin, v. 62, p. 1607-1644.

Middleton, K., Coniglio, M., Sherlock, R., Frape, S. K., 1993. Dolomitization of Middle Ordovician carbonate reservoirs, southwestern Ontario. Bulletin of Canadian Petroleum Geology, v. 41, p. 150-163.

Milliman, J.D., 1974. Marine carbonates. Springer-Verlag/Berlin, New York, 375p.

Mitchell, J.T., Land, L.S., and Miser, D.E., 1987. Modern marine dolomite cement in a north Jamaican fringing reef. Geology, v. 15, p. 557-560.

Montañez, I.P., and Read, J.F., 1992. Fluid-rock interaction history during stabilization of early dolomites, Upper Knox Group (Lower Ordovician), U.S. Appalachians. Journal of Sedimentary Petrology, v. 62, no. 5, p. 753-778.

Montañez, I.P., and Stefani, A.B., 1993. An overview of the factors contributing to the evolution and spatial distribution of reservoir properties in Knox cyclic carbonates. *In* Paleokarst, karst-related diagenesis, reservoir development, and exploration concepts: examples from the Paleozoic section of the southern mid-continent. *Edited by* Keller, D.R., and Reed, C.L., 1993 Annual Permian Basin Section- SEPM, Arbuckle Mountains, Oklahoma. Permian Basin Section, Society of Economic Paleontologists and Mineralogists Publication no. 93-34, p. 67-83.

Montañez, I.P., 1994. Late diagenetic dolomitization of Lower Ordovician, Upper Knox carbonates: A record of the hydrodynamic evolution of the Southern Appalachian Basin. American Association of Petroleum Geologists Bulletin, v. 78, no. 8, p. 1210-1239.

Moore, C.H., 1989. Carbonate diagenesis and porosity. Developments in Sedimentology; 46, p. 61-68.

Morrow, D.W., 1990. Dolomite part II: Dolomitization models and ancient dolostones. *In* Diagenesis. *Edited by* McIreath, I.A., and Morrow, D.W, Geoscience Canada Reprint Series no. 4, p. 125-139.

Morrow, D.W., 1998. Regional subsurface dolomitization: models and constraints. Geoscience Canada, v. 25, p. 57-70.

Mountjoy, E.W., Amthor, J. E., and Mache, H. G., 1994. Has burial dolomitization come of age? Some answers from the Western Canada Sedimentary Basin. *In* Dolomites, A volume in honour of Dolomieu. *Edited by* Purser, B., Tucker, M., and Zenger, D., International Association of Sedimentologists, Special Publication no. 21, p. 203-231.

Muchez, P., and Viaene, W., 1994. Dolomitization caused by water circulation near the mixing zone: an example from the Lower Visean of the Campine Basin (northern Belgium). *In* Dolomites, A volume in honour of Dolomieu. *Edited by* Purser, B., Tucker, M., and Zenger, D., International Association of Sedimentologists, Special Publication no. 21,
p. 155-166.

Murray, R.C.,1960. Origin of porosity in carbonate rocks. Journal of Sedimentary Petrology, v. 30, p. 59-84.

Murray, R.C., 1969. Hydrology of south Bonaire, Netherlands Antilles-a rock selective dolomitization model. Journal of Sedimentary Petrology, v. 39, p. 1007-1013.

Mutti, M., and Simo, J. A., 1994. Distribution, petrography and geochemistry of early dolomite in cyclic shelf facies, Yates Formation (Guadalupian), Capital Reef Complex, USA. *In* Dolomites, A volume in honour of Dolomieu. *Edited by* Purser, B., Tucker, M., and Zenger, D., International Association of Sedimentologists, Special Publications no. 21, p. 91-107.

Negra, M.H., Purser, B.H., and M'Rabet, A., 1994. Permeability and porosity evolution in dolomitized Upper Cretaceous pellagic limestones of Central Tunisia. *In* Dolomites, A volume in honour of Dolomieu. *Edited by* Purser, B., Tucker, M., and Zenger, D., International Association of Sedimentologists, Special Publications no. 21, p. 309-323.

Noor, I., 1989. Lithostratigraphy, environment interpretation, and paleogeography of the Middle Ordovician Shadow Lake, Gull River, and Bobcaygeon formations in parts of southern Ontario. Unpublished Ph D thesis, University of Toronto, Ontario, Canada, 262p.

Nunn, J.A., 1986. Subsidence and thermal history of the Michigan Basin, *In* Thermal modeling in sedimentary basins. *Edited by* Burrus, J., Editions Technip, Paris, p. 417-436.

Nunn, J.A., Sleep, N.H., and Moore, W.E., 1984. Thermal subsidence and generation of hydrocarbons in the Michigan basin. American Association of Petroleum Geologists Bulletin, v. 68, p. 296-315.

Nurmi, R.D., and Friedman, G.M., 1977. Sedimentology and depositional environments of basin-center evaporites, Lower Salina Group (Upper Silurian), Michigan Basin. *In* Reefs and Evaporites; Concepts and Depositional Models. *Edited by* Fisher, J.H., American Association of Petroleum Geologists, Studies in Geology no. 5, p. 23-52.

O'Shea, K. J., Miles, M. C., Fritz, P., Frape, S. K., and Lawson, D. E., 1988. Oxygen-18 and Carbon-13 in the carbonates of the Salina Formation of southwestern Ontario. Canadian Journal of Earth Sciences, v. 25, p. 182-194.

Pearson, E.M., 1980. Sedimentology and diagenesis of the Warwick reef (Silurian), Lambton County, southwestern Ontario. Unpublished M. Sc. Thesis, University of Waterloo, Waterloo, Ontario, Canada, 250p.

Perkins, R.D., Dwyer, G.S., Rosoff, D.B., Fuller, Baker, P.A., and Lloyd, R.M., 1994. Salina sedimentation and diagenesis: West Caicos Island, British West Indies. *In* Dolomites, A volume in honour of Dolomieu. *Edited by* Purser, B., Tucker, M., and Zenger, D., International Association of Sedimentologists, Special Publication no. 21, p. 37-54.

Petta, T. J., 1980. Silurian pinnacle reef diagenesis, northern Michigan: Effects of evaporites on pore space distribution. Society Economic Paleontologists and Mineralogists, Carbonate Reservoir Rocks, Core Workshop no. 2, p. 32-42 .

Pingitore, N.E. Jr., 1976. Vadose and phreatic diagenesis: processes, products and their recognition in corals. Journal of Sedimentary Petrology, v. 46, p. 985-1006.

Popp, B.N., Anderson, T.F., and Sandberg, P.A., 1986a. Brachiopods as indicators of original isotopic compositions in some Paleozoic limestones. Geological Society of America Bulletin, v. 97, p. 1262-1269.

Popp, B.N., Anderson, T.F., and Sandberg, P.A., 1986 b. Textural, elemental, and isotopic variations among constituents in Middle Devonian limestones, North America. Journal of Sedimentary Petrology, v. 56, no. 5, p. 715-727.

Pounder, J.A., 1962, Guelph-Lockport Formation of southwestern Ontario. Ontario Petroleum Institute, First Annual Meeting Proceedings, v. 1, Technical Paper no. 5, 19p.

Powell, T.G., Macqueen, R.W., Barker, J.F., and Bree, D.G., 1984. Geochemical character and origin of Ontario oils. Bulletin of Canadian Society of Petroleum Geologists, v. 32, p. 289-312.

Powers, R. W., 1962. The Arabian Upper Jurassic carbonate reservoir rock. *In* Classification of Carbonate Rocks – a symposium. *Edited by* Ham, W. E., American Association of Petroleum Geology Mem., 1, p. 122-192.

Prezbindowski, D.R., and Larese, R.E., 1987. Experimental stretching of fluid inclusion in calcite-implications of diagenetic studies. Geology, v. 15, p. 333-336.

Purser, B.H., Brown, A., and Aissaoui, D.M., 1994. Nature, origins and evolution of porosity in dolomites. *In* Dolomites, A volume in honour of Dolomieu. *Edited by* Purser, B., Tucker, M., and Zenger, D., International Association of Sedimentologists, Special Publication no. 21, p. 283-308.

Purser, B.H., 1985. Dedolomite porosity and reservoir properties of Middle Jurassic Cabonates in the Paris Basin, France. *In* Carbonate Petroleum Reservoirs. *Edited by* Roehl, P.O., and Choquette, P.W., p. 343-355.

Qing, H. and Mountjoy, E. W., 1989. Multistage dolomitization in rainbow buildups, Middle Devonian Keg River Formation, Alberta, Canada. Journal of Sedimentary Petrology, v. 56, 2, p. 237-247.

Qing, H., and Mountjoy, E.W., 1994. Formation of coarsely crystalline, hydrothermal dolomite reservoirs in the Presqu'ile Barrier, Western Canada Sedimentary Basin. American Association of Petroleum Geologists Bulletin, v. 78, no. 1, p. 55-77.

Quinlan, G., 1987. Models of subsidence mechanisms in intracratonic basins, and their applicability to North American examples. In Sedimentary Basins and Basin-forming Mechanisms. Edited by Beaumont, C., and Tankard, A.J., Canadian Society of Petroleum Geologists, Memoir 12, p. 463-481.

Quinlan, G.M., and Beaumont, C., 1984. Appalachian thrusting, lithospheric flexure, and the Paleozoic stratigraphy of the eastern interior of North America. Canadian Journal of Earth Science, v. 21, p. 973-996.

Radke, B.M., and Mathis, R.L., 1980. On the formation and occurrence of saddle dolomite. Journal of Sedimentary Petrology, v. 50, p. 1149-1168.

Read, J.F., 1985. Carbonate platform facies models. American Association of Petroleum Geologists Bulletin, v. 69, p. 1-21.

Richard, L.V., 1969. Stratigraphy of the Upper Silurian Salina Group, New York, Pennsylvania, Ohio, Ontario. New York State Museum and Science Service, Map and Chart Series 12.

Ricken, W., 1987. The carbonate compaction law: a new tool. Sedimentology, v. 34, p. 571-584.

Robinson, P., 1980. Determination of calcium, magnesium, manganese, strontium, sodium and iron in the carbonate fraction of limestones and dolomites. Chemical Geology, v. 28, p. 135-146.

Roedder, E., 1984. Fluid inclusions. Reviews in Mineralogy, Mineralogical Society of America, v. 12, 646p.

Roy, J.L., Opdyke, N.D., and Irving, D., 1967. Further paleomagnetic results from the Bloomsbug Formation. Journal of Geophysical Research, v. 72, p. 5075-5086.

Rybansky, R., and Trevail, R.A., 1983. Oil and gas exploration, drilling and production summary, 1983. Ontario Ministry of Natural Resources, Toronto, Oil and Gas Paper 4, 174p.

Saller, A.H., and Yaremko, K., 1994. Dolomitization and porosity development in the Middle and Upper Wabamun Group, southeast Peace River Arch, Alberta, Canada. American Association of Petroleum Geologists Bulletin, v. 78, no. 9, p. 1406-1430.

Saller, A.H., 1984. Petrologic and geochemical constraints on the origin of subsurface dolomite, Enewetak Atoll: an example of dolomitization by normal seawater. Geology, v. 12, p. 217-220.

Sanford, B.V., 1962. Sources and occurrences of oil and gas in the sedimentary basins of Ontario. Proceedings of the Geological Association of Canada, v. 14, p. 59-89.

Sanford, B.V., 1969. Silurian of southwestern Ontario. Ontario Petroleum Institute, 8th Annual Conference Proceedings, v. 8, Technical Paper no.5, 44p.

Sanford, B.V., Thompson, F.J. and Mcfall, G.H., 1985. Plate tectonics- a possible controlling mechanism in the development of hydrocarbon traps in Southwestern Ontario. Bulletin of Canadian Petroleum Geology, v. 33, p. 52-71.

Sarg, J.F., 1982. Off-reef Salina deposition (Silurian), southern Michigan Basin-implications for reef genesis. *In* Depositional and diagenetic spectra of evaporites -a core workshop. *Edited by* Robertson, H.C., Loucks, R.G., and Davies, G.R., Society of Economic Paleontologists and Mineralogists, Core Workshop no. 3, p. 354 395.

Sass, E., and Bein, A., 1988. Dolomites and salinity: a comparative geochemical study, *In* Sedimentology and Geochemistry of Dolostones. *Edited by* Shukla, V., and Baker P.A., Society of Economic Paleontologists and Mineralogists Special Publication no. 43, p. 223-233.

Sass, E., and Katz, A., 1982. The origin of platform dolomites. American Journal of Science, v. 282, p. 1184-1213.

Sass, E., Bein, A., and Almogi-Labin, A., 1991. Oxygen-isotope composition of diagenetic calcite in organic-rich rocks: evidence for $^{18}O$ depletion in marine anaerobic pore water. Geology, v. 19, p. 839-842.

Schmidt, V., 1965. Facies, diagenesis, and related reservoir properties in the Gigas Beds (Upper Jurassic), northwestern Germany. *In* Dolomitization and Limestone Diagenesis. *Edited by* Pray, L.C., and Murray, R.C., Society of Economic Paleontologists and Mineralogists Special Publication no. 13, p. 124-168.

Schmoker, J.W., 1984. Empirical relation between carbonate porosity and thermal maturity: an approach to regional porosity prediction. American Association of Petroleum Geologists Bulletin, v. 68, 1697-1703.

Schmoker, J.W., Krystink, K.B., and Halley R.B., 1985. Selected characteristics of limestone and dolomite reservoirs in the United States. American Association of Petroleum Geologists Bulletin, v. 69, p. 733-741.

Schofield, K., and Adams, A.E., 1986. Burial dolomitization of the Woo Dale Limestones Formation (Lower Carboniferous), Derbyshire, England. Sedimentology, v. 33, p. 207-219.

Searl, A., 1991. Early Dinatian dolomites from East Fife: hydrothermal overprinting of early diagenetic fabrics? Journal of Geological Society, London, v. 148, p. 737-747.

Searl, A., 1994. Discontinuous solid solution in Ca-rich dolomites: the evidence and implications for the interpretation of dolomite petrographic and geochemical data. *In* Dolomites, A volume in honour of Dolomieu. *Edited by* Purser, B., Tucker, M., and Zenger, D., International Association of Sedimentologists, Special Publication no. 21, p. 361-376.

Searl, A., 1988. Mixing-zone dolomites in the Gully Oolite, Lower Carboniferous, South Wales. Journal of Geological Society, London, v. 145, p. 891-899.

Sears, S.O., and Lucia, F.J., 1979. Reef growth model for Silurian pinnacle reefs, northern Michigan reef trend. Geology, v. 7, p. 299-302.

Sears, S.O., and Lucia, F.J., 1980. Dolomitization of northern Michigan Niagara reefs by brine refluxion and freshwater/seawater mixing. *In* Concepts and Models of Dolomitization. *Edited by* Zenger, D.H., Dunham, J.B., and Ethington, R.L., Society of Economic Paleontologists and Mineralogists, Special Publications no. 28, p. 215-236.

Sellwood, B.W., Shepard, T.J., Evans, M.R., and James, B. 1989. Origin of late cements in oolitic reservoir facies: a fluid inclusion and isotopic study (Mid-Jurassic, southern England). Sedimentary Geology, v. 61, p. 223-237.

Sharma, G.D., 1966. Geology of Peters Reef, St. Clair County, Michigan. American Association of Petroleum Geologists Bulletin, v. 50, p. 327-350.

Sharma, T., and Clayton, R.N., 1965. Measurement of $^{18}O/^{16}O$ ratios of total oxygen of carbonates. Geochimica et Cosmochimica Acta, v. 29, p. 1347-1353.

Shaver, R.H., 1991. A history of study of Silurian reefs in the Michigan Basin environs. *In* Early Sedimentary Evolution of the Michigan Basin. *Edited by* Catacosinos, P.A., and Daniels, P.A., Jr., Geological Society of America Special Paper no. 256, p. 101-138.

Shaver, R.H., Edwards, D.J., Droste, J.B., Lazor, D.J., Orr, W.R., Pollock, C.A., and Rexroad, C.B., 1971. Silurian and Middle Devonian stratigraphy of the Michigan Basin; A view from the southwestern flank. *In* Geology of the Lake Erie islands and adjacent shores. *Edited by* Forsyth, J.L., Michigan Basin Geological Society Guidebook, p. 37-59.

Shaver, R.H., Ault, C.H., Ausich, W.I., Droste, J.B., Horowitz, A.S., James, W.C., Okla, S.M., Rexroad, C.B., Suchomel, D.M., and Welch, J.R., 1978. The search for a Silurian reef model, Great Lakes area. Department of Natural Resources, Geological Survey Special Report 15, 36p.

Shearman, D.J., and Shirmohammadi, N.H. 1969. Distribution of strontium in dedolomites from the French Jura. Nature, v. 223, p. 606-608.

Shearman, D.J., Khouri, J., and Tahas, S., 1961. On the replacement of dolomite by calcite in some Mesozoic limestones from the French Jura. Proceedings of the Geological Association of London, v. 12, p. 1-12.

Shi, Y., and Wang, C.Y., 1986. Pore pressure generation in sedimentary basins: overloading versus aquathermal. Journal of Geophysical Research, v. 91, no. B2, p. 2135-2162.

Shields, M.J., and Brady, P.V., 1995. Mass balance and fluid flow constraints on regional-scale dolomitization, Late Devonian, Western Canada Sedimentary Basin. Bulletin of Canadian Petroleum Geology, v. 43, no. 4, p. 371-392.

Shinn, E. A., Ginsburg, R.N., and Lloyd, R.M., 1965. Recent supratidal dolomite from Andros Island, Bahamas. *In* Dolomitization and Limestone Diagenesis. *Edited by* Pray, L.C., and Murray, R.C., Society of Economic Paleontologists and Mineralogists Special Publication no.13, p. 112-123.

Shinn, E.A., Halley, R.B., Hudson, J.H., and Lidz, B.H., 1977. Limestone compaction: An enigma. Geology, v. 5, p. 21-24.

Shukla, V., and Friedman, G.M., 1983. Dolomitization and diagenesis in a shallowing-upward sequence: the Lockport Formation (Middle Silurian), New York State. Journal of Sedimentary Petrology, v. 53, p. 703-717.

Sibley, D.F., 1980. Climatic control of dolomitization, Seroe Domi Formation (Pliocene), Bonaire, N.A. *In* Concepts and models od dolomitization. *Edited by* Zenger, D.H., Dunham, J.B., and Ethington, R.L., Society Economic Paleontologists and Mineralogists, Special Publication no. 28, p. 247-258.

Sibley, D.F., 1991. Secular changes in the amount and texture of dolomite. Geology, v. 19, p. 151-154.

Sibley, D.F., 1982. The origin of common dolomite fabrics, clues from the Pliocene. Journal of Sedimentary Petrology, v. 52, p. 1087-1100.

Sibley, D.F., 1990. Unstable to stable transformations during dolomitization. Journal of Geology, v. 98, p. 739-748.

Sibley, D.F., and Gregg, G.M., 1987. Classification of dolomite rock textures. Journal of Sedimentary Petrology, v. 57, p. 967-975.

Sibley, D.F., Gregg, G.M., Brown, R.G., and Laudon, P.R., 1993. Dolomite crystal size distribution. *In* Carbonate Microfabrics, frontiers in Sedimentology. *Edited by* Rezak, R., and Lavoie, D.L., Springer-Verlag, New York, p. 195-204.

Simms, M., 1984. Dolomitization by groundwater-flow systems in carbonate platforms: Gulf Coast. Association of Geological Societies, Transactions, v. XXXIV, p. 411-421.

Sleep, N.H., and Sloss, L.L., 1978. A deep borehole in the Michigan Basin. Journal of Geophysical Research, v. 83, p. 5815-5819.

Sleep, N.H., and Snell, N.S., 1976. Thermal contraction and flexure of midcontinent and Atlantic marginal basins. Geophisical Journal of the Royal Astronomical Society, v. 45, p. 125-154.

Sloss, L.L., 1988. Tectonic evolution of the Craton in Phanerozoic time. *In* Sedimentary Cover-North American Craton, U.S. *Edited by* Sloss, L.L., Geological Society of America, The Geology of North America, v. D-2, p. 25-51.

Smith, A.L., and Legault, J.A., 1985. Preferred orientations of Middle Silurian Guelph-Amabel reefs of southern Ontario. Bulletin of Canadian Petroleum Geology, v. 33, p. 421-426.

Smith, D.E., and Swett, K., 1968. Devaluation of "Dedolomitization". Journal of Sedimentary Petrology, v. 39, p. 379-380.

Smith, L, Charbonneau, S.L., and Grimes, D.J., 1993. Karst episodes and permeability development, Silurian reef reservoirs, southwestern Ontario. Ontario Geoscience Research Grant Program, Grant no. 295, Ontario Geological Survey, Open File Report 5850, 240p.

Smith, L., 1990. Karst episodes during cyclic development of Silurian reef reservoirs, southwestern Ontario. *In* Subsurface geology of southwestern Ontario; a core workshop. *Edited by* Carter, T.R., Ontario Petroleum Institute, American Association of Petroleum Geologists, 1990 Eastern Section Meeting, p. 69-88.

Smith, L., and Chapman, D.S., 1983. On the thermal effects of groundwater flow, 1 regional scale systems. Journal of Geophysical Research, v. 88, p. 593-608.

Smith, L., 1992. The Salina Group; salt solution and the Algonquin Arch: reservoir porosity, salt caverns, and industrial minerals. Ontario Petroleum Institute, v.32, Paper no. 12, 20p.

Smith, T.M., and Dorobek, S.L., 1989. Dolomitization of the Devonian Jefferson Formation, South-Central Montana. The Mountain Geologist, v. 26, no. 3, p. 81-96.

Smosna, R., 1984. Diagenesis of a stromatporoid patch reef. Journal of Sedimentary Petrology, v. 54, p. 1000-1011.

Sonnenfeld, P., 1985. Flow regimes in the Silurian of the Michigan Basin. *In* Ordovician and Silurian rocks of the Michigan Basin and its margins. *Edited by* Cercone, K.R., and Budai, J.M., Michigan Basin Geological Society Special Paper 4, p. 157-171.

Sonnenfeld, P., and Al-Aasm, I., 1991. The Salina evaporites in the Michigan Basin. *In* Early sedimentary evolution of the Michigan Basin. *Edited by* Catacosinos, P.A., and Daniels, P.A., Jr., Geological Society of America, Special Paper 256, p. 139-153.

Soussi, M., and M'Rabet, A., 1994. Burial dolomitization of organic-rich and organic-poor carbonates, Jurassic of Central Tunisia. *In* Dolomites ; A volume in honour of Dolomieu. *Edited by* Purser, B., Tucker, M., and Zenger, D., International Association of Sedimentologists, Special Publication no. 21, p. 429-445.

Sperber, C.M., Wilkinson, B.H., and Peacor, D.R., 1984. Rock composition, dolomite stoichiometry, and rock/water reactions in dolomitic carbonate rocks. Journal of Geology, v. 92, p. 609-622.

Stearns, D.W., and Friedman, M., 1972. Reservoirs in fractured rock. American Association Petroleum Geologists Memoir 17, p. 82.

Stoessell, R.K., Klimentidis, R.E., and Prezbindowski, D.R., 1987. Dedolomitization in Na-Ca-Cl brines from 100° to 200 °C at 300 bars. Geochimica et Cosmochimica Acta, v. 51, p. 847-855.

Stueber, A.M., Saller, A.H., and Ishida, H., 1998. Origin, migration, and mixing of brines in the Permian Basin: geochemical evidence from the eastern central basin platform, Texas. American Association of Petroleum Geologists Bulletin, v. 82, p. 1652-1672.

Sun, S.Q., and Esteban, M., 1994. Paleoclimatic controls on sedimentation, diagenesis, and reservoir quality: lessons from Miocene carbonates. American Association of Petroleum Geologists Bulletin, v. 78, no. 4, p. 519-543.

Sun, S.Q., 1990. Facies-related diagenesis in a cyclic shallow marine sequence: the Corallian Group (Upper Jurassic) of the Dorset coast, southern England. Journal of Sedimentary Petrology, v. 60, no. 1, p. 42-52.

Sun, S.Q., 1992. Skeletal aragonite dissolution from hypersaline seawater: a hypothesis. Sedimentary Geology, v. 77, p. 249-257.

Sun, S.Q., 1994. A reappraisal of dolomite abundance and occurrence in the Phanerozoic. Journal of Sedimentary Research, v. A64, p. 396-404.

Sun, S.Q., 1995. Dolomite reservoirs: porosity evolution and reservoir characteristics. American Association of Petroleum Geologists Bulletin, v. 79, p. 186-204.

Sun, S.Q., Fallick, A.E., and Williams, B.P.J., 1992. Influence of original fabric on subsequent porosity evolution: an example from the Corallian (Upper Jurassic) reefal limestones, the Weald Basin, southern England. Sedimentary Geology, v. 79, p. 139-160.

Theriault, F., and Hutcheon, I., 1987. Dolomitization and calcitization of the Devonian Grosmont Formation, northern Alberta. Journal of Sedimentary Petrology, v. 57, p. 955-966.

Tucker, M.E., and Wright, V.P., 1990. Carbonate Sedimentology. Blackwell, Oxford, 482p.

Tucker, M.E., 1993. Carbonate diagenesis and sequence stratigraphy. *In* Sedimentary Review / 1. *Edited* by Wright, V.P, Blackwell Scientific Publications, chapter 4, p. 51-72.

Vahrenkamp, V. C. and Swart, P. K., 1990. New distribution coefficient for the incorporation of strontium into dolomite and its implications for the formation of ancient dolomites. Geology, v. 18, p. 387-391.

Vahrenkamp, V.C., and Swart, P.K., 1994. Late Cenozoic dolomites of the Bahamas: metastable analogues for the genesis of ancient platform dolomites. *In* Dolomites, A volume in honour of Dolomieu. *Edited by* Purser, B., Tucker, M., and Zenger, D., International Association of Sedimentologists, Special Publication no. 21, p. 133-153.

Van der Voo, R., 1982. Pre-Mesozoic paleomagnetism and plate tectonics. Annual Review of Earth and Planetary Science, v. 10, p. 191-220.

Van der Voo, R., 1988. Paleozoic paleogeography of North America, Gondwana, and intervening displaced terranes; Comparison of paleomagnetism with paleoclimatology and biogeographic patterns. Geological Society of America Bulletin, v. 100, p. 311-324.

Veizer, J., 1992. Depositional and diagenetic history of limestones: stable and radiogenic isotopes. *In* Isotopic Signatures and Sedimentary Records. *Edited by* Clauer, N., and Chaudhuri, S., Lecture Notes in Earth Sciences, Sringer-Verlag, p. 13-48.

Veizer, J., 1983. Chemical diagenesis of carbonates: theory and application of trace element technique. *In* Stable Isotopes in Sedimentary Petrology. *Edited by* Arthur, M.A., Anderson, T.F., Kaplan, I.R., Veizer, J., and Land, L.S., Society of Economic Paleontologists and Mineralogists Short Course no. 10, p. 3-1 to 3-100.

Veizer, J., Fritz, P., and Jones, B., 1986. Geochemistry of brachiopods: Oxygen and carbon isotopic records of Paleozoic oceans. Geochimica et Cosmochimica Acta, v. 50, p. 1679-1696.

Veizer, J., Lemieux, J., Jones, B., Gibling, M.R.. and Savelle, J., 1978. Paleosalinity and dolomitization of a Lower Paleozoic carbonate sequence, Somerset and Prince of Wales Islands, Arctic Canada. Canadian Journal of Earth Science, v. 15, p. 1448-1461.

Von Morlot, A., 1847. Ueber Dolomit und seine kuenstliche Darstellung aus Kaalstein. Haidinger Naturwiss Abhanlinger, v. 1, p. 305-315.

Vugrinovich, R.G., 1988. Shale compaction in the Michigan Basin: estimates of former depth of burial and implications for paleogeothermal gradients. Bulletin of Canadian Petroleum Geologists, v. 36, p. 1-8.

Vugrinovich, R.G., 1989. Subsurface temperatures and surface heat flow in the Michigan Basin and their relationships to regional subsurface fluid movement. Marine and Petroleum Geology, v. 6, p. 60-70.

Walker, J.C.C., and Lohmann, K.C., 1989. Why the oxygen isotopic composition of sea water changes with time. Geophysical Research Letters, v. 16, no. 4, p. 323-326.

Wallace, M.W., Kerans, C., Playford, P.E., and McManus, A., 1991. Burial diagenesis in the Upper Devonian reef complexes of the Geikie Gorge region, Canning Basin, western Australia. American Association of Petroleum Geologists Bulletin, v. 75, p. 1018-1038.

Wanless, H.R., 1979. Limestone response to stress: pressure-solution and dolomitization. Journal of Sedimentary Petrology, v. 49, p. 437-462.

Ward, W.C.,and Halley, R.B., 1985. Dolomitization in a mixing zone of near-seawater composition, Late Pleistocene, northeastern Yucatan Peninsula. Journal of Sedimentary Petrology, v. 55, p. 407-420.

Wendte, J., Qing, H., Dravis, J.J., Moore, S.L.O., Stasiuk, L.D., and Ward, G., 1998. High-temperature saline (thermoflux) dolomitization of Devonian Swan Hills platform and bank carbonates, Wild River area, west-central Alberta. Bulletin of Canadian Petroleum Geology, v. 46, p. 210-265.

Weyl, P.K., 1960. Porosity through dolomitization: conservation of mass requirements. Journal of Sedimentary Petrology, v. 30, no. 1, p. 85-90.

Wilson, T.P., and Long, D.T., 1992. Evolution of $CaCl_2$ brine in Silurian aged formations of the Michigan bsin, USA: The role of mineralogic reactions and evaporite diagenesis. *In* Water-Rock Interaction. *Edited* by Kharaka, Y.K., and Maest, A.S., v. 2, p. 1213-1216.

Winder, C.G., and Sanford B.V., 1972. Stratigraphy and paleontology of the Paleozoic rocks of southern Ontario. 24th International Geological Congress, Montreal, Quebec, Guidebook, Excursion A45-C45, 74p.

Yanat'eva, O.K., 1955. Effect of aqueous solutions of gypsum on dolomite in the presence of carbon dioxide. Akademiia Nauk SSSR Doklady, v. 101, p. 911-912.

Ye, Q., and Mazzullo, S.J., 1993. Dolomitization of Lower Permian platform facies, Wichita Formation, North Platform, Midland Basin, Texas. Carbonates and Evaporites, v. 8, no. 1, p. 55-70.

Zenger, D.H., 1973. Syntaxial calcite borders on dolomite crystals, Little Falls Formation (Upper Cambrian), New York. Journal of Sedimentary Petrology, v. 43, p. 118-124.

Zenger, D.H., 1983. Burial dolomitization in the Lost Burro Formation (Devonian), east-central California, and the significance of the late diagenetic dolomitization. Geology, v. 11, p. 519-522.

Zenger, D.H., and Dunham, J.B., 1988. Dolomitization of Siluro-Devonian limestones in a deep core (5,350 m), southeastern New Mexico. *In* Sedimentology and Geochemistry of Dolostones. *Edited by* Shukla, V., and Baker, P.A., Society of Economic Paleontologists and Mineralogists Special Publication, no. 43, p. 161-173.

Ziegler, A.M., Hansen, K.S., Johnson, M.E., Kelly, M.A., Scotese, C.R., and Van der Voo, R., 1977. Silurian continental distributions, paleogeography, climatology, and biogeography. Tectonophysics, v. 40, 1-2, p. 13-51.

## Appendix I. List of subsurface cores described in this study (to be continued)

| Reefs and Pools | Core No. | Intervals | Guelph Lithology* |
|---|---|---|---|
| Bayfield Pinnacle | 300 | Guelph-Goat Island | Dolomite |
| Bentpath Pinnacle | 138 | Guelph | Dolomite |
| | 344 | A2-Guelph | Dolomite |
| Bickford Pinnacle | 539 | A2-Gasport | Dolo,Dedo |
| | 581 | A1-Rochester | Dolomite |
| Clay Creek Pinnacle | 542 | A1-Gasport | Dolomite |
| Colinville Pinnacle | 142 | Guelph | Dolomite |
| | 608 | A1-Guelph | Dolomite |
| | 874 | A1-Guelph | Lime,Dolo |
| Corden Pinnacle | 241 | A1-Goat Island | Dolomite |
| | 382 | A1-Goat Island | Dolomite |
| | 582 | A1-Goat Island | Dolomite |
| | 587 | A1-Guelph | Dolomite |
| | 599 | A1-Goat Island | Dolomite |
| Corey East Pinnacle | 1014 | A1-Guelph | Dolomite |
| Corunna Pinnacle | 217 | A2-Guelph | Dolomite |
| | 522 | A1-Goat Island | Dolomite |
| | 557 | A1-Guelph | Dolomite |
| Dawn 47-49 Pinnacle | 873 | Guelph | Dolomite |
| Dawn 156 Pinnacle | 591 | Guelph | Dolomite |
| | 596 | A1-Goat Island | Dolomite |
| Dow Moore 3-21-XII Pinnacle | 967 | A1-Guelph | Lime,Dolo |
| | 992 | A2-Guelph | Lime,Dolo |
| | 996 | A2-Rochester | Lime,Dolo |
| Duthill Pinnacle | 139 | A1-Rochester | Dolomite |
| Edys Mills Pinnacle | 1026 | A2-Guelph | Dolomite |
| Enniskillen 28 Pinnacle | 1003 | A2-Guelph | Dolomite |
| | 1004 | Guelph | Dolomite |
| | 1005 | A2-Guelph | Dolomite |
| Fletcher Patch | 750 | Guelph | Dolomite |
| | 751 | A2-Rochester | Dolomite |
| | 752 | A2-Guelph | Dolomite |
| | 759 | A2-Guelph | Dolomite |
| | 760 | A2-Guelph | Dolomite |
| | 772 | A2-Guelph | Dolomite |
| | 937 | A1-Guelph | Dolomite |
| | 938 | A1-Guelph | Dolomite |
| | 939 | A1-Guelph | Dolomite |
| Grand Bend Pinnacle | 329 | A2-Guelph | Dolomite |
| Kimball Pinnacle | 530 | A1-Guelph | Dolomite |

Appendix I (continued-1)

| Well Name | County/Township | Depth (m) | Year | Reservoir |
|---|---|---|---|---|
| Bluewater O&G Porter | Huron/Stanley | 527.6-584.8 | 1956 | Gas |
| Union Bentpath 3 | Lambton/Dawn | 568.1-604.1 | 1970 | Oil/Gas |
| Union Bentpath 2 | Lambton/Dawn | 492.3-547.1 | 1970 | Oil/Gas |
| Imperial 433 | Lambton/Sombra | 550.2-691.0 | 1954 | Oil/Gas |
| Imperial 702 Young 4 | Lambton/Sombra | 649.2-719.5 | 1959 | Oil/Gas |
| Imperial 576 | Lambton/Plympton | 663.9-719.4 | 1956 | Oil |
| Imperial 430 | Lambton/Moore | 620.1-737.5 | 1954 | Oil/Gas |
| Imperial 420 | Lambton/Moore | 669.0-739.6 | 1954 | Oil/Gas |
| TEC Kimball 38 | Lambton/Moore | 617.5-629.4 | 1972 | Oil/Gas |
| Corden ET AL. 1 | Lambton/Sombra | 618.7-631.9 | 1969 | Gas |
| Corden ET AL. 2 | Lambton/Moore | 643.1-658.4 | 1969 | Gas |
| Corden ET AL. 3 | Lambton/Sombra | 614.2-629.4 | 1969 | Gas |
| Corden | Lambton/Sarnia | 652.6-670.9 | 1968 | Gas |
| Corden ET AL. 4 | Lambton/Moore | 646.2-663.2 | 1971 | Gas |
| RAM 101 | Lambton/Enniski. | 564.0-610.5 | 1990 | Oil |
| Imperial 607 | Lambton/Moore | 696.5-749.8 | 1957 | Oil/Gas |
| Imperial 591 | Lambton/Moore | 699.5-758.0 | 1957 | Oil/Gas |
| Imperial 419 | Lambton/Moore | 701.8-746.7 | 1953 | Oil/Gas |
| Union 247 | Lambton/Dawn | 483.7-544.3 | 1984 | Oil/Gas |
| Union Dawn 230 | Lambton/Dawn | 605.0-645.3 | 1959 | Oil/Gas |
| Union Dawn 185 | Lambton/Dawn | 542.2-661.1 | 1954 | Oil/Gas |
| TEC Dow 14 | Lambton/Moore | 725.5-742.0 | 1988 | Gas |
| TEC Dow 7 | Lambton/Moore | 84.0-774.4 | 1988 | Gas |
| TEC Dow 4 | Lambton/Moore | 750.0-833.0 | 1988 | Gas |
| Imperial 889 | Lambton/Sombra | 511.5-691.9 | 1965 | Gas |
| Edys Mills 1 | Lambton/Dawn | 481.3-526.1 | 1991 | Oil |
| Union Enniskillen 60 | Lambton/Enniski. | 548.8-616.5 | 1989 | Gas |
| Union Enniskillen 54 | Lambton/Enniski. | 624.0-641.5 | 1989 | Gas |
| Union Enniskillen 55 | Lambton/Enniski. | 556.0-643.2 | 1989 | Gas |
| Consumers'33323 | Kent/Tilbury E. | 413.4-440.9 | 1981 | Oil |
| Consumers'33409 | Kent/Tilbury E. | 373.0-549.0 | 1982 | Oil |
| Consumers'33406 | Kent/Raleigh | 418.8-446.0 | 1981 | Oil |
| Consumers'33407 | Kent/Tilbury E. | 410.0-445.3 | 1982 | Oil |
| Consumers'33411 | Kent/Tilbury E. | 404.0-459.0 | 1982 | Oil |
| Consumers'33408A | Kent/Tilbury E. | 376.0-460.0 | 1983 | Oil |
| Consumers'40000 | Kent/Tilbury E. | 412.2-437.2 | 1983 | Oil |
| Consumers'40001 | Kent/Tilbury E. | 407.0-438.0 | 1983 | Oil |
| Consumers'40003 | Kent/Tilbury E. | 408.0-437.8 | 1983 | Oil |
| Imperial 525 | Huron/Stephen | 517.0-645.0 | 1955 | Oil |
| Imperial 387 | Lambton/Moore | 618.0-734.9 | 1953 | Oil/Gas |

Appendix I (continued-2)

| Reefs and Pools | Core No. | Intervals | Guelph Lithology* |
|---|---|---|---|
| | 984 | A2-Gasport | Dolomite |
| | 991 | A1-Guelph | Limestone |
| Ladysmith Pinnacle | 594 | A1-Guelph | Dolomite |
| Oil Spring East Pinnacle | 1007 | Guelph | Dolomite |
| Payne Pinnacle | 198 | A1-Rochester | Lime,Dolo |
| | 598 | Guelph-Rochester | Lime,Dolo |
| Petrola East Pinnacl | 671 | Guelph | Dolomite |
| Rosedale Pinnacle | 578 | A2-Rochester | Lime,Dolo |
| Samia 1-8-A Pinnacale | 1025 | A2-Guelph | Lime,Dolo,Dedo |
| Seckerton Pinnacle | 152 | Guelph-Rochester | Dolomite |
| | 523 | A2-Rochester | Dolomite |
| | 524 | A1-Guelph | Dolomite |
| | 584 | Guelph-Goat Island | Dolomite |
| | 592 | Guelph | Dolomite |
| Sombra Pinnacle | 1006 | A2-Guelph | Dolomite |
| Terminus Pinnacle | 381 | A1-Goat Island | Lime,Dolo,Dedo |
| | 570 | Guelph | Lime,Dolo |
| | 604 | A2-Goat Island | Lime,Dolo,Dedo |
| | 611 | A1-Guelph | Dolomite |
| | 918 | A1-Guelph | Lime,Dolo,Dedo |
| Terminus North Pinnacle | 227 | Guelph-Goat Island | Dolomite |
| | 265 | A1-Goat Island | Dolomite |
| | 668 | Guelph-Goat Island | Dolomite |
| Warwick Pinnacle | 140 | A2-Guelph | Dolomite |
| | 410 | Guelph | Dolomite |
| | 526 | A2-Guelph | Dolomite |
| Waubuno Pinnacle | 424 | A2-Guelph | Lime,Dolo,Dedo |
| | 525 | A2-Rochester | Lime,Dolo,Dedo |
| | 556 | Guelph-Goat Island | Dolomite |
| Wilkesport Pinnacle | 412 | A2-Goat Island | Lime,Dolo,Dedo |
| | 637 | A1-Guelph | Dolomite |
| Patch reefs in Lake Erie | 965 | Guelph | Dolomite |
| | 966 | A1-Guelph | Dolomite |
| Regional Interreef | 840 | A2-Gasport | Dolomite |
| | 860 | Devonian-Cambrian | Dolomite |
| | 994 | Devonian-Cambrian | Dolomite |
| Total 76 cores, including 73 cores from 32 reefs and 3 cores from interreef areas | | | |

* Lime-limestome, Dolo-dolomite, Dedo-dedolomite

Appendix I (continued-3)

| Well Name | County/Township | Depth (m) | Year | Reservoir |
|---|---|---|---|---|
| TEC Kimball-Colin 54 | Lambton/Moore | 652.5-725.5 | 1988 | Oil/Gas |
| TEC Kimball-Colin 55 | Lambton/Moore | 645.0-680.5 | 1988 | Oil/Gas |
| Mcclure | Lambton/Moore | 662.3-694.9 | 1969 | Oil/Gas |
| ICG 2 | Lambton/Enniski. | 503.0-525.0 | 1990 | Oil/Gas |
| Imperial 242 Payne 4 | Lambton/Moore | 611.4-763.5 | 1953 | Gas |
| Imperial 405 Payne 8 | Lambton/Moore | 691.3-760.2 | 1953 | Gas |
| Ram 38 | Lambton/Enniski. | 566.9-632.2 | 1976 | Oil |
| Union Enniskillen | Lambton/Enniski. | 494.1-666.6 | 1970 | Gas |
| Dow Sarnia 3 | ambton/Sarnia | 670.0-758.7 | 1991 | Oil |
| Imperial 344 Murray | Lambton/Moore | 655.3-794.0 | 1953 | Oil/Gas |
| Imperial 376 | Lambton/Moore | 702.9-793.4 | 1953 | Oil/Gas |
| Tecumseh Seckerton 7 | Lambton/Moore | 696.1-741.0 | 1953 | Oil/Gas |
| Imperial 706 | Lambton/Moore | 733.0-785.2 | 1959 | Oil/Gas |
| Imperial 656 | Lambton/Moore | 723.6-760.8 | 1958 | Oil/Gas |
| Union Sombra 11 | Lambton/Sombra | 540.0-592.2 | 1989 | Gas |
| RAM 4 | Lambton/Sombra | 551.6-599.2 | 1968 | Gas |
| RAM 2 | Lambton/Sombra | 488.3-498.7 | 1968 | Gas |
| RAM 5 | Lambton/Sombra | 497.4-592.5 | 1968 | Gas |
| Mcclure-Union | Lambton/Sombra | 580.6-611.1 | 1970 | Gas |
| RAM 3 | Lambton/Sombra | 501.1-602.0 | 1968 | Gas |
| RAM Baslen 3 | Lambton/Sombra | 614.8-630.0 | 1969 | Oil/Gas |
| RAM Baslen 2 | Lambton/Sombra | 613.3-631.5 | 1969 | Oil/Gas |
| RAM Baslen 1 | Lambton/Sombra | 604.7-620.0 | 1968 | Oil/Gas |
| Imperial 407 | Lambton/Warwick | 535.5-622.1 | 1953 | Oil |
| Imperial 619 | Lambton/Warwick | 553.8-588.6 | 1953 | Oil |
| Imperial 399 | Lambton/Warwick | 495.3-685.8 | 1953 | Oil |
| Imperial 410 | Lambton/Moore | 552.0-682.9 | 1954 | Gas |
| Imperial 431 | Lambton/Moore | 558.4-729.4 | 1954 | Gas |
| Imperial 712 | Lambton/Moore | 656.8-687.3 | 1954 | Gas |
| I.O.E. | Lambton/Sombra | 554.1-665.1 | 1966 | Gas |
| I.O.E. BP | Lambton/Sombra | 677.4-689.7 | 1966 | Gas |
| Consumers'An.13104 | Lake Erie | 410.0-428.2 | 1969 | Gas |
| Consumers'An.13311 | Lake Erie | 359.7-395.6 | 1974 | Gas |
| Consumers'16285 | Lambton/Moore | 639.8-698.3 | 1968 | Gas |
| OGS 82-2 | Kent/Chatham | 20.8-1180.8 | 1982 | |
| OGS 82-1 | Lambton/Moore | 62.2-1380.7 | 1982 | |

## Appendix II. List of rock samples for this study (to be continued)

| Core No. | Reef Name | Litho. unit | Depth Feet | Depth Meters | Description |
|---|---|---|---|---|---|
| 300 | Bayfield | Guelph | 1767.0 | 538.6 | Coral floatstone dolomite, fine crystalline |
| 300 | Bayfield | Guelph | 1780.0 | 542.5 | Bryozon bafflestone dolomite, fine crystalline |
| 300 | Bayfield | Guelph | 1843.0 | 561.7 | Branching coral bafflestone dolomite, fine crystalline |
| 381 | Bayfield | Guelph | 1901.5 | 579.6 | Fine crystalline dolomite |
| 412 | Wikesport | Guelph | 1894.0 | 577.3 | Wackestone or bafflestone limestone |
| 412 | Wikesport | Guelph | 1962.0 | 598.0 | Wackestone or bafflestone limestone |
| 412 | Wikesport | Guelph | 2032.0 | 619.4 | Wackestone or bafflestone, fine crystalline |
| 412 | Wikesport | Guelph | 2032.0 | 619.4 | Dedolomite, fine crystalline |
| 412 | Wikesport | Guelph | 2056.0 | 626.7 | Dedolomite, fine crystalline |
| 525 | Waubun | A-1 Carb. | 1847.0 | 563.0 | Dedolomite, fine crystalline |
| 525 | Waubun | A-1 Carb. | 1871.0 | 570.3 | Medium crystalline dolomite |
| 525 | Waubun | Guelph | 1920.0 | 585.2 | Microcrystalline dolomite |
| 525 | Waubun | Guelph | 1964.0 | 598.6 | Microcrystalline dolomite |
| 525 | Waubun | Guelph | 1902.0 | 579.7 | Fine crystalline dolomite |
| 525 | Waubun | Guelph | 1984.0 | 604.7 | Dedolomite, fine crystalline |
| 525 | Waubun | Guelph | 2059.0 | 627.6 | Dedolomite, fine crystalline |
| 525 | Waubun | Guelph | 2085.0 | 635.5 | Brown dolomite with dedolomite patches |
| 525 | Waubun | Guelph | 2123.5 | 647.2 | Dedolomite, fine crystalline |
| 526 | Wawick | A-1 Carb. | 1675.0 | 510.5 | Stromatolitic dolomite, fine crystalline |
| 526 | Wawick | Guelph | 1734.0 | 528.5 | Stromatolite limestone with fibrous calcite |
| 526 | Wawick | Guelph | 1828.0 | 557.2 | Bryozon bafflestone limestone with calcite |
| 526 | Wawick | Guelph | 1884.0 | 574.2 | Dedolomite with oil staining, fine crystalline |
| 526 | Wawick | Guelph | 2190.0 | 667.5 | Strom bindstone limestone with saddle dolomite |
| 542 | Clay Creek | Guelph | 2189.0 | 667.2 | Fine Crystalline dolomite, porous. |
| 542 | Clay Creek | Guelph | 2228.0 | 679.1 | Microcrystalline dolomite with fine crystalline patches |
| 542 | Clay Creek | Guelph | 2285.0 | 696.5 | Mudstone-Wackstone,microcrystalline-fine crystalline |
| 542 | Clay Creek | Guelph | 2332.0 | 710.8 | Wackestone-packstone, fine crystalline |
| 578 | Rosedale | A-1 Carb. | 1660.0 | 506.0 | Stromatolitic limestone, porous |
| 578 | Rosedale | A-1 Carb. | 1670.0 | 509.0 | Limestone with large cavitities filled calcite cements |
| 578 | Rosedale | Guelph | 1934.0 | 589.5 | Bafflestone limestone with large cavity and geopetal |
| 578 | Rosedale | Guelph | 1720.0 | 524.3 | Nonporous limestone |
| 578 | Rosedale | Guelph | 1837.0 | 559.9 | Wackstone limestone with cavities and geopetal |
| 578 | Rosedale | Guelph | 1945.0 | 592.8 | Wackestone or bafflestone limestone |
| 578 | Rosedale | Guelph | 2056.0 | 626.7 | Strom framestone limestone |
| 671 | Petrola E. | Guelph | 1915.0 | 583.7 | Wackestone-packstone, microcrystalline |
| 671 | Petrola E. | Guelph | 1993.0 | 607.5 | Fine crystalline dolomite |
| 671 | Petrola E. | Guelph | 2070.0 | 630.9 | Fine crystalline dolomite |
| 751 | Fletcher | Guelph | 1415.8 | 431.5 | Stromatolitic dolomite with geopetal and dolomite silt |
| 751 | Fletcher | Guelph | 1453.8 | 443.1 | Strom floatstone, microcrystalline to fine crystalline |
| 751 | Fletcher | Guelph | 1461.0 | 445.3 | Fine crystalline dolomite |
| 751 | Fletcher | Guelph | 1659.5 | 505.8 | Crinoidal Wackstone, microcrystalline-fine crystalline |
| 751 | Fletcher | Guelph | 1696.3 | 517.0 | Crinoidal Wackstone, fine crystalline |
| 759 | Fletcher | A-1 Carb. | 1355.1 | 413.0 | Microcrystalline stromatolitic dolomite |
| 759 | Fletcher | A-1 Carb. | 1358.0 | 413.9 | Fine crystalline stromatolitic dolomite |
| 759 | Fletcher | Guelph | 1440.4 | 439.0 | Fine crystalline dolomite |
| 759 | Fletcher | Guelph | 1460.7 | 445.2 | Coral-strom floatstone, fine crystalline dolomite |
| 772 | Fletcher | A-1 Carb. | 1282.5 | 390.9 | Dolomite mudstone with random anhydrite needles |
| 772 | Fletcher | A-1 Carb. | 1322.2 | 403.0 | Dolomite with anhydrite lamina and fractuer |
| 772 | Fletcher | Guelph | 1355.7 | 413.2 | Fine crystalline dolomite with local coarsening |
| 772 | Fletcher | Guelph | 1370.5 | 417.7 | Medium to coarsely crystalline dolomite |

Appendix II (continued-1)

| Core No. | Reef Name | Litho. unit | Depth Feet | Depth Meters | Description |
|---|---|---|---|---|---|
| 772 | Fletcher | Guelph | 1370.8 | 417.8 | Medium crystalline dolomite and dolomite cement |
| 772 | Fletcher | Guelph | 1383.3 | 421.6 | Bryzon bafflestone, fine crystalline dolomite |
| 772 | Fletcher | Guelph | 1465.0 | 446.5 | Stroms floatstone with large vugs, fine crystalline |
| 772 | Fletcher | Guelph | 1608.0 | 490.1 | Microcrystalline dolomite |
| 873 | Dawn 47-49 | Guelph | 1589.0 | 484.3 | Microcrystalline dolomite |
| 873 | Dawn 47-49 | Guelph | 1611.0 | 491.0 | Microcrystalline stromatolitic dolomite |
| 873 | Dawn 47-49 | Guelph | 1689.7 | 515.0 | Strom floatstone with mimetic fibrous cement |
| 873 | Dawn 47-49 | Guelph | 1735.6 | 529.0 | Microcrystalline dolomite |
| 873 | Dawn 47-49 | Guelph | 1776.7 | 541.5 | Baffle-floatstone, fine crystalline |
| 918 | Terminus | A-1 Carb. | 1677.0 | 511.1 | Stromatolitic dolomite, fine crystalline |
| 918 | Terminus | Guelph | 1701.5 | 518.6 | Fine crystalline dolomite |
| 918 | Terminus | Guelph | 1719.5 | 524.1 | Stromatolitic limestone |
| 918 | Terminus | Guelph | 1724.0 | 525.5 | Medium to coarsely crystalline dolomite |
| 918 | Terminus | Guelph | 1746.0 | 532.2 | Wackstone limestone with scattered dolomite |
| 918 | Terminus | Guelph | 1762.0 | 537.1 | Dedolomite, fine crystalline |
| 918 | Terminus | Guelph | 1775.0 | 541.0 | Wackestone limestone with scattered dolomite |
| 918 | Terminus | Guelph | 1781.5 | 543.0 | Coral floatstone limestone |
| 918 | Terminus | Guelph | 1802.0 | 549.2 | Bryzoan bafflestone limestone with coral clasts |
| 918 | Terminus | Guelph | 1821.0 | 555.0 | Dedolomite, replaced bryzoan bafflestone |
| 918 | Terminus | Guelph | 1848.0 | 563.3 | Algal bafflestone with large cavity & fibrous calcite |
| 918 | Terminus | Guelph | 1858.0 | 566.3 | Stroms bindstone with minor dolomite rhombs |
| 948 | Terminus | Guelph | 2141.2 | 652.6 | Dedolomite, fine crystalline |
| 948 | Terminus | Guelph | 2154.0 | 656.5 | Microcrystalline dolomite with anhydrite and halite |
| 948 | Terminus | Guelph | 2162.2 | 659.0 | Microcrystalline mimetic dolomite |
| 948 | Terminus | Guelph | 2226.5 | 678.6 | Laminated dolomite, fine crystalline |
| 948 | Terminus | Guelph | 2232.7 | 680.5 | Limestone with black shale seams |
| 948 | Terminus | Guelph | 2374.1 | 723.6 | Crinoidal wackstone with vugs, fine crystalline |
| 948 | Terminus | A-1 Carb. | 2290.1 | 698.0 | Fine crystalline dolomite |
| 1005 | Ennisk.28 | Guelph | 1972.9 | 601.3 | Coral floatstone, dedolomite, fine crystalline |
| 1005 | Ennisk.28 | Guelph | 2029.0 | 618.4 | Bryzoan bafflestone, medium-coarsely crystalline |
| 1006 | Sombra | A-1 Carb. | 1790.3 | 545.7 | Microcrystalline dolomite with bioturbation |
| 1006 | Sombra | A-1 Carb. | 1836.2 | 559.7 | Stromatolitic dolomite with fractuers, fine crystalline |
| 1006 | Sombra | A-1 Carb. | 1851.3 | 564.3 | Stromatolitic dolomite, fine crystalline |
| 1006 | Sombra | Guelph | 1880.8 | 573.2 | Bafflestone with fractuer and pyrite cement |
| 1006 | Sombra | Guelph | 1956.8 | 596.4 | Bafflestone, fine crystalline |
| 1014 | Corey E. | Guelph | 1852.5 | 564.6 | Bafflestone-wackstone, fine crystalline |
| 1014 | Corey E. | Guelph | 1899.0 | 578.8 | Bafflestone, microcrystalline with mimetic texture |
| 1014 | Corey E. | Guelph | 1932.5 | 589.0 | Bafflestone, microcrystalline with mimetic texture |
| 1025 | Sarnia 1-8-A | Guelph | 2199.9 | 670.5 | Stromatolitic limestone |
| 1025 | Sarnia 1-8-A | Guelph | 2246.5 | 684.7 | Fine crystalline dolomite, porous |
| 1025 | Sarnia 1-8-A | Guelph | 2277.8 | 694.3 | Stromatolitic limestone |
| 1025 | Sarnia 1-8-A | Guelph | 2277.8 | 694.3 | Stromatolitic limestone |
| 1025 | Sarnia 1-8-A | Guelph | 2286.2 | 696.8 | Stromatolitic limestone |
| 1025 | Sarnia 1-8-A | Guelph | 2295.1 | 699.5 | Stromatolitic limestone |
| 1025 | Sarnia 1-8-A | Guelph | 2302.9 | 701.9 | Dedolomite, fine crystalline |
| 1025 | Sarnia 1-8-A | Guelph | 2316.4 | 706.0 | Stromatolitic limestone |
| 1025 | Sarnia 1-8-A | Guelph | 2322.9 | 708.0 | Stromatolitic limestone |
| 1025 | Sarnia 1-8-A | Guelph | 2385.9 | 727.2 | coral-bryzoan bafflestone limestone |
| 1025 | Sarnia 1-8-A | Guelph | 2473.9 | 754.0 | bryzoan-bafflestone dedolomite, fine crystalline |
| 138 | Bentpath | Guelph | 1945.0 | 592.8 | Crinoid wack-packstone, medium crystalline |
| 138 | Bentpath | Guelph | 1956.0 | 596.2 | Crinoid packstone, fine crystalline |

Appendix II (continued-2)

| Core No. | Reef Name | Litho. unit | Depth Feet | Depth Meters | Description |
|---|---|---|---|---|---|
| 140 | Wawick | Guelph | 1786.0 | 544.4 | Microcrystalline dolomite |
| 140 | Wawick | Guelph | 1864.0 | 568.1 | Stroms floatstone limestone |
| 140 | Wawick | Guelph | 1930.0 | 588.3 | Crinoid packstone, fine crystalline and porous |
| 227 | Terminus N. | Guelph | 2018.0 | 615.1 | Fine crystalline dolomite |
| 328 | Terminus N. | Guelph | 2127.0 | 648.3 | Medium crystalline dolomite |
| 344 | Bentpath | Guelph | 1744.0 | 531.6 | Fine crystalline dolomite |
| 522 | Corunna | Guelph | 2396.0 | 730.3 | Medium-coarsely crystalline dolomite |
| 523 | Seckerton | Guelph | 2566.0 | 782.1 | Crinoid packstone, medium crystalline |
| 523 | Seckerton | Guelph | 2583.0 | 787.3 | Crinoid packstone, fine crystalline |
| 524 | Seckerton | Guelph | 2354.0 | 717.5 | Crinoid packstone, microcrystalline |
| 530 | Col-kim | Guelph | 2150.0 | 655.3 | Crinoid packstone, medium crystalline |
| 530 | Col-kim | Guelph | 2230.0 | 679.7 | Crinoid packstone, fine crystalline dolomite |
| 530 | Col-kim | Guelph | 2314.0 | 705.3 | Crinoid packstone dolomite, fine crystalline |
| 530 | Col-kim | Guelph | 2396.0 | 730.3 | Crinoid packstone, fine crystalline dolomite |
| 539 | Bickford | Guelph | 1912.0 | 582.8 | Stromatolitic dolomite, microcrystalline |
| 539 | Bickford | Guelph | 1967.0 | 599.5 | Dedolomite, fine crystalline |
| 557 | Corunna | A-1 Carb. | 2312.0 | 704.7 | Pelloid wacke-packstone dolomite, microcrystalline |
| 557 | Corunna | Guelph | 2421.0 | 737.9 | Fine crystalline crystalline dolomite |
| 584 | Seckerton | Guelph | 2464.5 | 751.2 | Baffiestone, fine crystalline |
| 584 | Seckerton | Guelph | 2419.5 | 737.5 | Crystalline dolomite with grain coarsening |
| 591 | Dawn 156 | Guelph | 1986.0 | 605.3 | Fine crystalline dolomite with dedolomite patches |
| 596 | Dawn 156 | Guelph | 1820.0 | 554.7 | Fine crystalline dolomite |
| 671 | Petrola E. | Guelph | 1946.0 | 593.1 | Microcrystalline dolomite |
| 939 | Fletcher | Guelph | 1425.6 | 434.5 | Stroms framestone, fine crystalline dolomite |
| 984 | Kimball | Guelph | 2154.3 | 656.6 | Stromatolitic dolomite, microcrystalline |
| 1005 | Ennisk. 28 | A-1 Carb. | 1868.5 | 569.5 | Stromatolitic dolomite, fine crystalline |
| 1005 | Ennisk. 28 | Guelph | 1910.2 | 582.2 | Stromatolitic dolomite, fine to medium crystalline |
| 604 | Terminus | Guelph | 1658.0 | 505.4 | Stromatolitic dolomite, microcrystalline |
| 604 | Terminus | Guelph | 1682.0 | 512.7 | Stromatolitic dolomite, fine crystalline |
| 604 | Terminus | Guelph | 1866.0 | 568.8 | Limestone with fibrous calcite cement |
| 604 | Terminus | Guelph | 1871.0 | 570.3 | Bryzoan baffiestone limestone |
| 604 | Terminus | Guelph | 1880.0 | 573.0 | Bryzoan baffiestone limestone with fibrous cement |
| 604 | Terminus | Guelph | 1884.0 | 574.2 | Baffiestone limestone |
| 604 | Terminus | Guelph | 1896.0 | 577.9 | Dedolomite, fine crystalline |
| 604 | Terminus | Guelph | 1902.0 | 579.7 | Bryzoan baffiestone limestone |
| 604 | Terminus | Guelph | 1904.0 | 580.3 | Bryzoan baffiestone limestone |
| 604 | Terminus | Guelph | 1941.0 | 591.6 | Microcrystalline-fine crystalline dolomite |
| 939 | Fletcher | Guelph | 1388.2 | 423.1 | Medium-coarsely crystalline dolomite, surcosic |
| 938 | Fletcher | Guelph | 1434.5 | 437.2 | Medium-coarsely crystalline dolomite, surcosic |
| 938 | Fletcher | Guelph | 1378.0 | 420.0 | Medium-coarsely crystalline dolomite, surcosic |
| 1007 | Oil Spring E. | Guelph | 1704.5 | 519.5 | Microcrystalline crystalline dolomite |
| 1007 | Oil Spring E. | Guelph | 1717.9 | 523.6 | Microcrystalline to fine crystalline dolomite |
| 1003 | Ennisk.28 | Guelph | 2001.4 | 610.0 | Microcrystalline dolomite |
| 598 | Payne | Guelph | 2301.0 | 701.3 | Fine crystalline dolomite, surcosic |
| 138 | Bentpath | Guelph | 1950.0 | 594.4 | Fine crystalline dolomite, surcosic |
| 539 | Bickford | Guelph | 2029.0 | 618.4 | Strom-coral floatstone with fibrous dolomite cement |
| 139 | Duthill | Guelph | 2111.0 | 643.4 | Crinoid grainstone, fine crystalline |
| 591 | Dawn 156 | Guelph | 2083.0 | 634.9 | Medium-coarsely crystalline dolomite |
| 873 | Dawn 47-49 | Guelph | 1637.9 | 499.2 | Fine crystalline with stylolites |
| 581 | Bickford | Guelph | 2273.0 | 692.8 | Strom framestone with fibrous dolomite cement |
| 198 | Payne | Guelph | 2298.0 | 700.4 | Medium-coarsely crystalline dolomite |
| 873 | Dawn 47-49 | Guelph | 1743.2 | 531.3 | Crinoid pack-grainstone |

Appendix II (continued-3)

| Core No. | Reef Name | Litho. unit | Depth Feet | Depth Meters | Description |
|---|---|---|---|---|---|
| 578 | Rosedale | Guelph | 1656.9 | 505.0 | Alagal fragment grainstone |
| 1007 | Oil Spring E. | Guelph | 1710.7 | 521.4 | Stromatolitic dolomite |
| 1004 | Ennisk.28 | Guelph | 2091.3 | 637.4 | Stromatolitic dolomite |
| 424 | Waubun | Guelph | 2240.5 | 682.9 | Medium-coarsely crystalline dolomite |
| 424 | Waubun | Guelph | 1908.0 | 581.6 | Fine crystalline dolomite |
| 751 | Fletcher | Guelph | 1528.0 | 465.7 | Coral floatstone |
| 751 | Fletcher | Guelph | 1528.0 | 465.7 | Coral floatstone |
| 760 | Fletcher | Guelph | 1475.5 | 449.7 | Coral floatstone |
| 772 | Fletcher | Guelph | 1445.3 | 440.5 | Coral floatstone |
| 772 | Fletcher | A-1 Carb. | 1291.7 | 393.7 | Stromatolitic dolomite |
| 860 | Inter-reef | Guelph | 1874.8 | 571.4 | Medium crystalline dolomite |
| 918 | Terminus | A-1 Carb. | 1667.0 | 508.1 | Fine crystalline dolomite, porous |
| 918 | Terminus | Guelph | 1863.0 | 567.8 | Coral floatstone limestone |
| 918 | Terminus | Guelph | 1868.0 | 420.0 | Dedolomite, fine crystalline |
| 938 | Fletcher | Guelph | 1387.9 | 423.0 | Dolomite cement in large cavity |
| 938 | Fletcher | Guelph | 1399.3 | 426.5 | Fine crystalline dolomite |
| 938 | Fletcher | Guelph | 1424.0 | 434.0 | Medium-coarsely crystalline dolomite |
| 938 | Fletcher | Guelph | 1434.5 | 437.2 | Medium crystalline dolomite. |
| 939 | Fletcher | Guelph | 1404.3 | 428.0 | Medium-coarsely crystalline dolomite |
| 939 | Fletcher | Guelph | 1417.4 | 432.0 | Medium-coarsely crystalline dolomite cement |
| 939 | Fletcher | Guelph | 1428.7 | 435.2 | Microcrystalline dolomite |
| 939 | Fletcher | Guelph | 1432.5 | 436.6 | Fine crystalline dolomite |
| 991 | Kimbell | A-1 Carb. | 2144.1 | 653.5 | Fine crystalline dolomite |
| 1004 | Ennisk. 28 | Guelph | 2091.3 | 637.4 | Fine crystalline dolomite, porous |
| 1007 | Oil Spring E. | A-1 Carb. | 1704.5 | 519.5 | Stromatolitic dolomite, fine crystalline |
| 1025 | Sarnia 1-8-A | Guelph | 2389.2 | 728.2 | Stromatolitic limestone |
| 1025 | Sarnia 1-8-A | Guelph | 2441.7 | 744.2 | Bryzoan bafflestone, fine crystalline |
| 1025 | Sarnia 1-8-A | Guelph | 2455.5 | 748.4 | Medium-coarsely crystalline dolomite cement |

## Appendix III. Elemental and isotopic analyses of Guelph and A-1 carbonates (to be contonued)

| No. | Thin Section | Core No. | Reef Name | Unit | Depth Feet | Meter | Sample type for Geochemical Analysis | Major Elements Ca (%) | Mg (%) | Trace Elements Fe(ppm) | Mn(ppm) | Sr(ppm) | Na(ppm) | Analysis Method | Stable Isotopes 13C(PDB) | Duplicate | 18O (PDB | Duplicate | Sr Isotope 87Sr/86Sr |
|---|---|---|---|---|---|---|---|---|---|---|---|---|---|---|---|---|---|---|---|
| 1 | W2 | 300 | Bayfield | Guelph | 1767 | 538.6 | Type 1 dolomite | 20.6 | 11.5 | 859.6 | 118.0 | 67.1 | 651.7 | AAS | 4.42 | | -8.47 | | |
| 2 | W3 | 300 | Bayfield | Guelph | 1780 | 542.5 | Type 2 dolomite | 20.0 | 11.8 | 718.9 | 132.1 | 54.8 | 606.8 | AAS | 4.71 | | -7.92 | | |
| 3 | W4 | 300 | Bayfield | Guelph | 1843 | 561.7 | Type 2 dolomite with halite | 19.0 | 10.4 | 959.4 | 107.9 | 62.3 | 6121.9 | AAS | 2.12 | | -7.86 | | 0.70872 |
| 4 | W6 | 412 | Wilkesport | Guelph | 1894 | 577.3 | Nonporous limestone | 37.1 | 0.3 | 234.9 | 43.7 | 138.0 | 496.5 | AAS | 2.25 | | -9.13 | | |
| 5 | W7 | 412 | Wilkesport | Guelph | 1962 | 598.0 | Fibrous calcite cement | 38.4 | 2.8 | 160.7 | 33.1 | 170.5 | 641.3 | AAS | 3.67 | | -8.51 | | |
| 6 | W8A | 412 | Wilkesport | Guelph | 2032 | 619.4 | Fibrous dolomite cement | 20.7 | 12.1 | 1165.2 | 91.3 | 52.4 | 574.6 | AAS | 4.11 | | -8.30 | | |
| 7 | W8B-1 | 412 | Wilkesport | Guelph | 2032 | 619.4 | Dedolomite | 20.7 | 12.4 | 1464.6 | 91.8 | 54.9 | 452.1 | AAS | 4.06 | | -8.06 | | |
| 8 | W8B-2 | 412 | Wilkesport | Guelph | 2032 | 619.4 | Dedolomite | 15.9 | 9.9 | 1424.0 | 129.5 | 113.1 | 645.5 | AAS | 4.05 | | -8.38 | | 0.70885 |
| 9 | W11 | 525 | Waubun | A-1 Carb. | 1871 | 570.3 | Type 2 dolomite | 22.9 | 11.0 | 2197.6 | 168.2 | 1286.7 | 358.6 | AAS | 2.99 | | -7.77 | | |
| 10 | W12 | 525 | Waubuno | Guelph | 1920 | 585.2 | Equant dolomite cement | 20.0 | 11.7 | 162.9 | 153.7 | 64.6 | 296.9 | AAS | 2.52 | 2.72 | -7.79 | -7.60 | |
| 11 | W13 | 525 | Waubuno | Guelph | 1964 | 598.6 | Type 1 dolomite | 21.0 | 12.6 | 1746.4 | 232.9 | 32.2 | 372.8 | AAS | 3.14 | | -8.46 | | 0.70854 |
| 12 | W14-1 | 525 | Waubuno | Guelph | 1902 | 579.7 | Limpid dolomite cement | 20.3 | 10.1 | 2879.3 | 313.6 | 72.5 | 367.1 | AAS | 2.52 | | -8.85 | | |
| 13 | W14-2 | 525 | Waubuno | Guelph | 1902 | 579.7 | Limpid dolomite cement | 20.6 | 10.9 | 3123.5 | 283.1 | 84.6 | 367.2 | AAS | 2.59 | 2.53 | -8.63 | -8.68 | |
| 14 | W15 | 525 | Waubuno | Guelph | 1984 | 604.7 | Dedolomite | 24.8 | 7.3 | 1612.7 | 150.0 | 39.9 | 368.5 | AAS | 3.47 | | -7.98 | | |
| 15 | W16 | 525 | Waubuno | Guelph | 2059 | 627.6 | Dedolomite | 20.1 | 8.9 | 1744.0 | 183.9 | 62.2 | 486.1 | AAS | 3.52 | | -7.95 | | |
| 16 | W18 | 525 | Waubuno | Guelph | 2124 | 647.2 | Dedolomite | 21.4 | 8.5 | 1231.9 | 58.9 | 57.4 | 771.6 | AAS | 2.62 | | -8.74 | | |
| 17 | W20 | 526 | Warwick | A-1 Carb. | 1675 | 510.5 | Type 2 dolomite with halite | 19.4 | 9.0 | 526.3 | 49.9 | 633.0 | 51629.9 | AAS | 3.37 | | -5.59 | | |
| 18 | W21 | 526 | Warwick | Guelph | 1734 | 528.5 | Strom lm limestone with halite | 34.8 | 0.5 | 214.6 | 21.2 | 1167.7 | 6155.2 | AAS | 3.58 | 3.55 | -7.05 | -6.92 | |
| 19 | W22 | 526 | Warwick | Guelph | 1828 | 557.2 | Fossil ln limestone with halite | 33.3 | 0.7 | 322.9 | 68.5 | 287.6 | 55424.7 | AAS | 3.77 | | -7.49 | | 0.70847 |
| 20 | W24 | 526 | Warwick | Guelph | 2190 | 667.5 | Strom in limestone | 31.8 | 0.6 | 312.0 | 64.9 | 174.7 | 387.2 | AAS | 1.46 | | -4.99 | | |
| 21 | W28 | 542 | Clay Creek | Guelph | 2332 | 710.8 | Type 2 dolomite | 20.9 | 12.5 | 2453.8 | 265.9 | 78.6 | 298.4 | AAS | 4.97 | | -8.72 | | |
| 22 | W30 | 578 | Rosedale | A-1 Carb. | 1670 | 509.0 | Nonporous limestone | 38.9 | 1.2 | 187.2 | 16.7 | 1140.8 | 500.2 | AAS | 3.41 | | -4.27 | | |
| 23 | W31 | 578 | Rosedale | Guelph | 1934 | 589.5 | Fibrous calcite cement | 42.5 | 0.6 | 262.9 | 30.5 | 308.3 | 432.4 | ICP | 3.62 | | -5.16 | | 0.70855 |
| 24 | W32 | 578 | Rosedale | Guelph | 1720 | 524.3 | Porous limestone | 37.5 | 0.5 | 594.7 | 38.5 | 292.1 | 683.0 | AAS | 2.44 | | -9.28 | | |
| 25 | W34C | 578 | Rosedale | Guelph | 1945 | 592.8 | Nonporous lime matrix | 33.2 | 0.4 | 455.6 | 30.5 | 185.7 | 265.4 | AAS | 1.53 | | -4.84 | | |
| 26 | W37A-1 | 671 | Petrolia E | Guelph | 1993 | 607.5 | Type 2 dolomite | 17.6 | 11.2 | 870.9 | 131.6 | 59.0 | 440.1 | AAS | 4.34 | | -7.00 | | |
| 27 | W37A-2 | 671 | Petrolia E | Guelph | 1993 | 607.5 | Type 2 dolomite | 19.1 | 10.7 | 839.3 | 128.7 | 69.9 | 432.2 | AAS | | | | | |
| 28 | W38 | 671 | Petrolia E. | Guelph | 2070 | 630.9 | Type 1 dolomite | 17.0 | 11.6 | 504.5 | 60.2 | 59.9 | 631.4 | AAS | 1.93 | | -6.95 | | |
| 29 | W44 | 759 | Fletcher | A-1 Carb. | 1355 | 413.0 | Type 2 dolomite | 21.3 | 11.9 | 326.5 | 59.6 | 59.7 | 511.7 | AAS | 2.45 | | -5.66 | | |
| 30 | W52 | 772 | Fletcher | Guelph | 1371 | 417.8 | Type 2 dolomite | 19.6 | 12.6 | 923.9 | 95.8 | 47.2 | 627.4 | AAS | 1.81 | | -6.80 | | 0.70874 |
| 31 | W60-1 | 873 | Dawn 47-49 | Guelph | 1777 | 541.5 | Type 2 dolomite | 22.1 | 11.4 | 901.2 | 106.3 | 52.1 | 440.9 | AAS | 4.65 | | -7.32 | | |
| 32 | W60-2 | 873 | Dawn 47-49 | Guelph | 1777 | 541.5 | Type 2 dolomite | 19.6 | 11.9 | 853.1 | 108.5 | 56.5 | 465.0 | AAS | | | | | |
| 33 | W61 | 918 | Terminus | A-1 Carb. | 1677 | 511.1 | Type 2 dolomite | 19.7 | 10.6 | 1055.7 | 88.3 | 72.4 | 625.9 | AAS | 3.55 | 3.75 | -4.67 | -4.35 | |
| 34 | W62 | 918 | Terminus | Guelph | 1702 | 518.6 | Type 2 dolomite | 20.6 | 12.4 | 1182.7 | 87.5 | 44.6 | 437.4 | AAS | 3.38 | | -4.96 | | 0.70877 |
| 35 | W63 | 918 | Terminus | Guelph | 1720 | 524.1 | Nonporous limestone | 36.5 | 0.2 | 184.7 | 30.0 | 716.3 | 195.7 | AAS | 3.62 | 3.54 | -7.28 | -7.48 | |
| 36 | W64 | 918 | Terminus | Guelph | 1724 | 525.5 | Type 3 dolomite | 20.7 | 10.6 | 1911.9 | 172.8 | 77.2 | 412.7 | AAS | 4.04 | | -6.49 | | |
| 37 | W65-1 | 918 | Terminus | Guelph | 1746 | 532.2 | Nonporous limestone | 35.0 | 0.8 | 321.2 | 55.0 | 144.4 | 271.9 | AAS | 3.67 | | -7.25 | | |
| 38 | W65-2 | 918 | Terminus | Guelph | 1746 | 532.2 | Nonporous limestone | 35.2 | 0.9 | 323.5 | 57.2 | 139.3 | 286.1 | AAS | | | | | |
| 39 | W67 | 918 | Terminus | Guelph | 1775 | 541.0 | Nonporous limestone | 35.8 | 0.4 | 172.0 | 50.4 | 129.6 | 431.8 | AAS | 4.10 | | -7.52 | | |
| 40 | W72 | 918 | Terminus | Guelph | 1858 | 566.3 | Nonporous limestone | 34.9 | 0.2 | 164.6 | 50.4 | 319.7 | 563.1 | AAS | 4.02 | | -6.78 | | |
| 41 | W75-1 | 948 | Terminus | Guelph | 2162 | 659.0 | Type 1dolomite | 19.2 | 11.4 | 662.5 | 77.4 | 39.7 | 396.0 | AAS | 1.93 | | -5.90 | | |
| 42 | W75-2 | 948 | Terminus | Guelph | 2162 | 659.0 | Type 1 dolomite | 19.8 | 13.4 | 643.1 | 72.4 | 40.2 | 386.9 | AAS | | | | | |
| 43 | W78 | 948 | Terminus | Guelph | 2374 | 723.6 | Type 2 dolomite with halite | 18.4 | 9.6 | 3608.2 | 218.4 | 77.5 | 24220.1 | AAS | 2.30 | | -8.08 | | |
| 44 | W79 | 948 | Terminus | A-1 Carb. | 2290 | 698.0 | Type 1 dolomite | 20.6 | 10.7 | 1409.4 | 116.4 | 79.4 | 503.0 | AAS | 3.59 | | -6.99 | | |
| 45 | W80 | 1005 | Enniskillen 28 | Guelph | 1973 | 601.3 | Dedolomite with halite | 13.4 | 8.7 | 643.6 | 129.5 | 49.9 | 11776.0 | AAS | 3.95 | | -6.06 | | |
| 46 | W81 | 1005 | Enniskillen 28 | Guelph | 2029 | 618.4 | Type 3 dolomite with halite | 19.9 | 11.0 | 2731.0 | 166.1 | 79.9 | 25595.6 | ICP | 2.63 | | -9.01 | | 0.70910 |

## Appendix III (continued-1)

| No. Thin Section | Core No. | Reef Name | Unit | Depth Feet | Depth Meter | Sample type for Geochemical Analysis | Major Elements Ca (%) | Mg (%) | Fe(ppm) | Trace Elements Mn(ppm) | Sr(ppm) | Na(ppm) | Analysis Method | Stable Isotopes 13C(PDB) | Duplicate | 18O (PDB | Duplicate | Sr Isotope 87Sr/86Sr |
|---|---|---|---|---|---|---|---|---|---|---|---|---|---|---|---|---|---|---|
| 48 W86 | 1006 | Sombra | Guelph | 1957 | 596 4 | Type 3 dolomite | 20 4 | 11 2 | 1366 6 | 152 7 | 78 4 | 453 9 | ICP | 4 63 | | -7.75 | | 0 70879 |
| 49 W87 | 1014 | Corey E | Guelph | 1852 | 564 6 | Type 2 dolomite | 20 6 | 11 8 | 1325 0 | 108 3 | 61 8 | 450 2 | AAS | 1 98 | | -7.78 | | |
| 50 W88 | 1014 | Corey E | Guelph | 1899 | 578 8 | Type 2 dolomite | 20 3 | 10 2 | 507 5 | 91 3 | 69 6 | 493 5 | AAS | 4 13 | | -6 53 | | |
| 51 W89 | 1014 | Corey E | Guelph | 1933 | 589 0 | Type 2 dolomite | 19 8 | 10 9 | 622 3 | 80 0 | 75 0 | 505 9 | AAS | 4 24 | 4 32 | -6 55 | -6.46 | |
| 52 W90 | 1025 | Sarnia 1-8-A | Guelph | 2200 | 670 5 | Porous limestone with halite | 27 7 | 0 6 | 710 5 | 32 4 | 2049 4 | 46705 6 | AAS | 2 50 | | -6 21 | | |
| 53 W92A-1 | 1025 | Sarnia 1-8-A | Guelph | 2278 | 694 3 | Porous limestone | 36 3 | 0 2 | 285 9 | 37 5 | 144 2 | 278 7 | AAS | 2 62 | | -8 65 | | |
| 54 W92A-2 | 1025 | Sarnia 1-8-A | Guelph | 2278 | 694 3 | Porous limestone | 36 5 | 0 2 | 267 4 | 35 4 | 144 9 | 410 3 | AAS | | | | | |
| 55 W92B | 1025 | Sarnia 1-8-A | Guelph | 2278 | 694.3 | Nonporous limestone | 35 8 | 0 3 | 756 0 | 57 5 | 129 7 | 216 3 | AAS | 2 82 | | -8 35 | | |
| 56 W95 | 1025 | Sarnia 1-8-A | Guelph | 2303 | 701.9 | Dedolomite | 29 1 | 3 8 | 1097.9 | 182 8 | 72 0 | 733 7 | AAS | 2 56 | | -6.83 | | |
| 57 W96A | 1025 | Sarnia 1-8-A | Guelph | 2316 | 706.0 | Strom in nonporous limestone | 42 6 | 0 3 | 177 7 | 61 0 | 211 5 | 126 1 | ICP | 2 82 | | -7.11 | | 0 70847 |
| 58 W96B-1 | 1025 | Sarnia 1-8-A | Guelph | 2323 | 708 0 | Strom in nonporous limestone | 37.2 | 0 2 | 104 7 | 65 8 | 1052 4 | 644 9 | AAS | 3 13 | | -6.64 | | |
| 59 W96B-2 | 1025 | Sarnia 1-8-A | Guelph | 2323 | 708.0 | Strom in nonporous limestone | 36 7 | 0 2 | 120 0 | 64 9 | 1037.8 | 308 7 | AAS | | | | | |
| 60 W97 | 1025 | Sarnia 1-8-A | Guelph | 2386 | 727.2 | Nonporous lime matrix | 35 7 | 0 2 | 274 9 | 73 6 | 294 1 | 381 4 | AAS | 4 13 | | -7 00 | | |
| 61 W98 | 1025 | Sarnia 1-8-A | Guelph | 2474 | 754.0 | Dedolomite | 33 5 | 2 0 | 1065 6 | 153 8 | 52 2 | 201 9 | AAS | 3 50 | | -8 66 | | |
| 62 W125 | 596 | Dawn 156 | Guelph | 1820 | 554.7 | Type 2 dolomite | 21 3 | 11 1 | 1002 2 | 102 9 | 83.7 | 384.3 | ICP | 2 19 | | -6 45 | | 0.70865 |
| 63 W143 | 938 | Fletcher | Guelph | 1378 | 420 0 | Type 3 dolomite | 20 1 | 10 8 | 2422 9 | 197.0 | 42.3 | 432 6 | ICP | 1.74 | | -5.70 | | 0.70901 |
| 64 W145 | 1007 | Oil Spring E. | Guelph | 1704 | 519.5 | Type 1 dolomite | 21 9 | 11.7 | 1311.4 | 65 2 | 46.2 | 372 3 | ICP | 1.50 | | -7.86 | | 0.70845 |
| 65 W146 | 1007 | Oil Spring E. | Guelph | 1718 | 523.6 | Equant dolomite cement | 20 6 | 11 3 | 2033 6 | 159 3 | 56 3 | 442 9 | ICP | 2 66 | | -6.51 | | 0.70847 |
| 66 W147 | 1003 | Enniskillen 2 | Guelph | 2001 | 610.0 | Coral in Type 1 dolomite | 21.8 | 11 6 | 2259 3 | 240 4 | 64.7 | 405 5 | ICP | 2 36 | | -7.96 | | 0.70861 |
| 67 W148 | 598 | Payne | Guelph | 2301 | 701.3 | Type 2 dolomite | 21 9 | 11.4 | 1363 7 | 200 8 | 80.8 | 563.1 | ICP | 3 86 | | -8.46 | | 0.70861 |
| 68 W149 | 138 | Bentpath | Guelph | 1950 | 594.4 | Type 2 dolomite | 21.4 | 11.0 | 2511.2 | 179 5 | 62.3 | 1459.5 | ICP | 3 84 | | -8 63 | | 0.70873 |
| 69 W150 | 539 | Bickford | Guelph | 2029 | 618.4 | Type 2 dolomite | 21.0 | 11.6 | 1848 5 | 85 6 | 72 8 | 639 2 | ICP | 3.38 | | -9.03 | | 0.70868 |
| 70 W151 | 139 | Duthill | Guelph | 2111 | 643.4 | Type 2 dolomite | 22 7 | 12 2 | 1121.6 | 124 6 | 85 5 | 1166 5 | ICP | 1.38 | | -8 58 | | 0.70865 |
| 71 W152 | 591 | Dawn 156 | Guelph | 2083 | 634.9 | Type 3 dolomite | 22 7 | 11.5 | 3219 4 | 163 0 | 76 0 | 1102 0 | ICP | 2 86 | | -7.68 | | 0.70887 |
| 72 W153 | 873 | Dawn 47-49 | Guelph | 1638 | 499.2 | Type 2 dolomite | 20.5 | 11 6 | 1314.1 | 134 6 | 67.9 | 818 2 | ICP | 2.46 | | -7.90 | | 0.70866 |
| 73 W154 | 581 | Bickford | Guelph | 2273 | 692.8 | Strom in Type 2 dolomite | 20 8 | 11 8 | 902.7 | 65 8 | 69 8 | 1558 6 | ICP | 1.28 | | -8.29 | | 0 70875 |
| 74 W155 | 198 | Payne | Guelph | 2298 | 700.4 | Type 3 dolomite | 21 0 | 11 1 | 2852 9 | 213 7 | 66 4 | 585 3 | ICP | 4 42 | 4 01 | -9 72 | -9 67 | 0.70879 |
| 75 751A | 751 | Fletcher | Guelph | 1528 | 465 7 | Type 1 dolomite matrix | 18 9 | 11.4 | 504 6 | 49 5 | 42.1 | 400.4 | AAS | 1.27 | | -6.15 | | |
| 76 751B | 751 | Fletcher | Guelph | 1528 | 465.7 | Brachopoid in Type 1 dolomite | 19 3 | 10 1 | 448 6 | 68 0 | 32 0 | 447.8 | AAS | 1 49 | | -5.98 | | |
| 77 760 | 760 | Fletcher | Guelph | 1475 | 449.7 | Type 3 dolomite | 10 5 | 12 3 | 1234.7 | 58 9 | 32 5 | 888 7 | AAS | 1.52 | | -5.28 | | |
| 78 772A | 772 | Fletcher | Guelph | 1445 | 440.5 | Type 2 dolomite | 16.7 | 12 5 | 1267.9 | 58 5 | 75 0 | 416.2 | AAS | 1.58 | | -5 40 | | 0.70872 |
| 79 772B | 772 | Fletcher | A-1 Carb. | 1292 | 393 7 | Type 2 dolomite | 18 0 | 13 0 | 1379.3 | 43 2 | 32.4 | 410 8 | AAS | 1.66 | | -4 69 | | |
| 80 860-1 | 860 | Interreef | Guelph | 1875 | 571.4 | Type 3 dolomite | 22 0 | 13 1 | 1575 8 | 183 1 | 42 1 | 792.4 | AAS | 2 77 | | -6.33 | | |
| 81 860-2 | 860 | Interreef | Guelph | 1875 | 571.4 | Type 3 dolomite | 19 2 | 12 1 | 1571.9 | 184 1 | 44 9 | 817.6 | AAS | | | | | |
| 82 918B-1 | 918 | Terminus | A-1 Carb. | 1667 | 508.1 | Type 2 dolomite with halite | 20 9 | 8 9 | 954 1 | 51.4 | 289.3 | 5920 5 | AAS | 4.44 | | -3.86 | | |
| 83 918B-2 | 918 | Terminus | A-1 Carb. | 1667 | 508.1 | Type 2 dolomite with halite | 19.8 | 8 5 | 922 8 | 49 7 | 300 9 | 6395 4 | AAS | | | | | |
| 84 918C-1 | 918 | Terminus | Guelph | 1863 | 567.8 | Coral in nonporous limestone | 35 6 | 0 2 | 174 5 | 46 5 | 164.0 | 753.9 | AAS | 4.44 | | -5.46 | | 0.70870 |
| 85 918C-2 | 918 | Terminus | Guelph | 1863 | 567.8 | Coral in nonporous limestone | 35.7 | 0 2 | 155 9 | 45 0 | 143 5 | 354 5 | AAS | | | | | |
| 86 918D | 918 | Terminus | Guelph | 1868 | 420 0 | Dedolomite | 28 2 | 3 7 | 1240 1 | 130 7 | 52.0 | 1964 1 | AAS | 3.58 | 3 65 | -7.96 | -7.96 | 0.70876 |
| 87 938A | 938 | Fletcher | Guelph | 1388 | 423.0 | Saddle dolomite cement | 19 3 | 11 4 | 1962 8 | 140 7 | 57.1 | 578.7 | AAS | 1.97 | 1.92 | -5 24 | -5.17 | |
| 88 938B | 938 | Fletcher | Guelph | 1399 | 426 5 | Porous Type 2 dolomite | 18 4 | 9 9 | 1232.3 | 73 7 | 64 9 | 645 9 | AAS | 1.08 | | -5 54 | | |
| 89 938C-1 | 938 | Fletcher | Guelph | 1424 | 434.0 | Type 3 dolomite | 18 9 | 10 0 | 1693 6 | 125 3 | 27.4 | 759 0 | AAS | 1.37 | | -6 65 | | |
| 90 938C-2 | 938 | Fletcher | Guelph | 1424 | 434.0 | Type 3 dolomite | 18 8 | 10 2 | 1588 7 | 113 8 | 32 3 | 538 0 | AAS | 1.53 | | -6 02 | | |
| 91 938D | 938 | Fletcher | Guelph | 1434 | 437.2 | Type 3 dolomite | 18 8 | 10.2 | 1468 7 | 93 9 | 47.2 | 412 8 | AAS | 1.48 | | -6 66 | | 0 70887 |
| 92 939B-1 | 939 | Fletcher | Guelph | 1404 | 428 0 | Type 3 dolomite | 19 6 | 10 4 | 1531.7 | 94 4 | 37 4 | 743 9 | AAS | 1 56 | 1.50 | -6 65 | -6 79 | |
| 93 939B-2 | 939 | Fletcher | Guelph | 1404 | 428 0 | Type 3 dolomite | 19 4 | 11 4 | 1447 1 | 93 7 | 39 7 | 808 8 | AAS | | | | | |
| 94 939D-1 | 939 | Fletcher | Guelph | 1417 | 432 0 | Saddle dolomite cement | 18 3 | 10 2 | 1694 1 | 104 8 | 47.1 | 628 6 | AAS | 1.64 | | -6.06 | | |
| 95 939D-2 | 939 | Fletcher | Guelph | 1417 | 432.0 | Type 2 dolomite matrix | 19 4 | 11 2 | 514 5 | 116 1 | 32 5 | 445 6 | AAS | 1.62 | | -6.04 | | |

## Appendix III (continued-2)

| No. | Thin Section | Core No. | Reef Name | Unit | Depth Feet | Depth Meter | Sample type for Geochemical Analysis | Major Elements Ca (%) | Mg (%) | Trace Elements Fe(ppm) | Mn(ppm) | Sr(ppm) | Na(ppm) | Analysis Method | Stable isotopes 13C(PDB | Duplicate | 8O (PDB | Duplicate | Sr isotope 87Sr/86Sr |
|---|---|---|---|---|---|---|---|---|---|---|---|---|---|---|---|---|---|---|---|
| 96 | 939F-1 | 939 | Fletcher | Guelph | 1429 | 435.2 | Type 1 dolomite on strom | 20.0 | 10.1 | 336.3 | 67.3 | 47.3 | 634.0 | AAS | 1.17 | | -6.40 | | |
| 97 | 939F-2 | 939 | Fletcher | Guelph | 1429 | 435.2 | Type 1 dolomite on strom | 21.7 | 10.8 | 241.8 | 64.6 | 57.3 | 681.9 | AAS | | | | | |
| 98 | 939G-1 | 939 | Fletcher | Guelph | 1433 | 436.6 | Type 3 dolomite on strom | 20.0 | 10.7 | 1580.8 | 86.5 | 45.0 | 555.5 | AAS | 1.44 | | -6.46 | | |
| 99 | 939G-2 | 939 | Fletcher | Guelph | 1433 | 436.6 | Type 3 dolomite on strom | 19.9 | 10.9 | 1578.8 | 82.3 | 64.9 | 567.4 | AAS | | | | | |
| 100 | 991 | 991 | Kimball | A-1 Carb. | 2144 | 653.5 | Type 2 dolomite | 20.5 | 12.6 | 1468.8 | 85.8 | 62.3 | 453.4 | AAS | | | | | |
| 101 | 1004-1 | 1004 | Enniskillen 28 | Guelph | 2091 | 637.4 | Type 2 dolomite | 19.1 | 11.8 | 1203.1 | 216.2 | 51.9 | 983.7 | AAS | 4.02 | | -7.14 | | |
| 102 | 1004-2 | 1004 | Enniskillen 28 | Guelph | 2091 | 637.4 | Type 2 dolomite | 21.2 | 11.6 | 1237.4 | 230.4 | 61.9 | 939.5 | AAS | | | | | |
| 103 | 1007 | 1007 | Oil Spring E. | A-1 Carb. | 1704 | 519.5 | Type 2 dolomite | 19.3 | 11.0 | 1266.2 | 63.5 | 32.4 | 387.2 | AAS | 3.05 | 2.99 | -6.00 | -6.10 | |
| 104 | 1025-19-1 | 1025 | Sarnia 1-8-A | Guelph | 2389 | 728.2 | Strom in nonporous limestone | 36.2 | 0.2 | 311.6 | 51.1 | 488.7 | 221.4 | AAS | 3.55 | | -6.39 | | |
| 105 | 1025-19-2 | 1025 | Sarnia 1-8-A | Guelph | 2389 | 728.2 | Porous limestone | 36.0 | 0.2 | 181.6 | 94.3 | 289.6 | 234.1 | AAS | 3.66 | | -7.21 | | |
| 106 | 1025-25 | 1025 | Sarnia 1-8-A | Guelph | 2442 | 744.2 | Type 2 dolomite | 19.7 | 10.5 | 1379.0 | 360.8 | 54.2 | 385.9 | AAS | 4.74 | | -8.82 | | |
| 107 | 1025-27 | 1025 | Sarnia 1-8-A | Guelph | 2456 | 748.4 | Limpid dolomite cement | 20.7 | 12.6 | 1695.3 | 300.1 | 29.8 | 382.5 | AAS | 4.04 | | -9.27 | | |

## Appendix IV. Fluid inclusion data from the diagenetic minerals in the Guelph Formation (Means and numbers of analyses are given in parentheses)

| Sample Number | Diagenetic minerals | Te (°C) | Tm (°C) | Th (°C) | Estimated salinity* (wt.%NaCl equi.) |
|---|---|---|---|---|---|
| 1 | Equant calcite cement | -27.6 to -29.8 (-28.7, 2) | -6.2 to -8.4 (-7.3, 2) | +53.0 to +61.2 (+57.1, 3) | 9.5 to 12.2 (10.9) |
| 2 | Type 2 dolomite | ------ | -10.8 to -12.3 (-11.5, 3) | +67.0 to +74.3 (+69.9, 3) | 14.8 to 16.3 (10.9) |
| 3 | Type 2 dolomite | -29.7 to -32.6 (-31.2, 2) | -9.9 to -11.5 (-10.7, 3) | +70.5 to +74.7 (+72.6, 2) | 13.9 to 15.5 (14.7) |
| 4 | Type 2 dolomite | -30.7 to -34.5 (-32.9, 3) | -11.7 to -13.5 (-12.6, 2) | +64.5 to +73.4 (+68.9, 3) | 15.7 to 17.5 (16.6) |
| 5 | Dedolomite | -29.2 to -31.4 (-30.2, 3) | -16.8 to -17.6 (-17.2, 2) | +53.4 to +67.3 (+59.7, 3) | 20.2 to 20.9 (20.5) |
| 6 | Dedolomite | -28.0 to -30.3 (-29.2, 2) | -17.3 to -18.4 (-17.9, 2) | +57.6 to +72.4 (+65.5, 3) | 20.6 to 21.5 (21.1) |
| 7 | Type 3 dolomite | -39.6 to -47.5 (-43.6, 2) | -24.7 to -27.8 (-25.9, 3) | +95.8 to +108.2 (+101.2, 4) | 25.8 to 27.7 (26.6) |
| 8 | Type 3 dolomite | ------ | -28.7 to -31.2 (-30.0, 2) | +102.0 to +109.3 (+105.7, 2) | 28.4 to 30.0 (29.2) |
| 9 | Type 3 dolomite | -42.2 to -44.9 (-43.6, 2) | -27.9 to -30.7 (-29.2, 3) | +99.6 to +116.7 (+108.5, 4) | 27.8 to 29.7 (28.7) |
| 10 | Saddle dolomite cement | -46.2 to -47.6 (-46.9, 2) | -29.2 to -32.4 (-30.7, 3) | +98.7 to 12[illegible].4 (+112.9, 3) | 28.7 to 30.7 (29.7) |
| 11 | Saddle dolomite cement | ------ | -27.6 to -30.5 (-29.1, 2) | +105.6 to +128.2 (+117.1, 5) | 27.5 to 30.3 (28.9) |
| 12 | Megaquartz cement | -48.2 to -52.3 (-50.6, 3) | -27.9 to -28.6 (-28.3, 2) | +97.2 to +102.3 (+99.7, 3) | 27.8 to 28.3 (28.1) |
| 13 | Halite cement | ------ | -23.9 to -25.4 (-24.7, 3) | +89.4 to +94.1 (+91.2, 4) | 25.3 to 26.3 (25.8) |

* The estimated salinity values (wt.% NaCl equivalent) were calculated from fluid inclusion Tm values using Potter et al.'s (1978) equation.

# Appendix V. Porosity and permeability data from Guelph carbonates

| Core No. | Reef Name | Interval (m) | Lithology* | No. of sample | Porosity (%)** | Permeability (md)** |
|---|---|---|---|---|---|---|
| Patch Reef | | | | | | |
| 939 | Fletcher | 411-438 | D | 95 | 1.9 – 23.6 (5.0) | 0.01-340 (13.7) |
| 759 | Fletcher | 420-445 | D | 75 | 1.4 – 8.8 (4.6) | 0.1-1847 (119.9) |
| 750 | Fletcher | 428-442 | D | 24 | 2.2 – 10.4 (4.5) | 0.04-5380 (259.1) |
| 938 | Fletcher | 407-438 | D | 115 | 1.0 – 14.1 (4.5) | 0.01-1260 (30.0) |
| 772 | Fletcher | 413-457 | D | 131 | 1.8 – 14.2 (5.6) | <0.1-3893 (298.4) |
| 752 | Fletcher | 433-446 | D | 40 | 1.7 – 12.5 (6.3) | 0.1-1174 (151.2) |
| 940 | Fletcher | 410-438 | D | 106 | 0.5 – 8.0 (3.8) | 0.01-2230 (89.3) |
| 760 | Fletcher | 414-454 | D | 90 | 1.7 – 12.6 (6.3) | <0.1-450 (65.6) |
| Pinnacle Reef | | | | | | |
| 1. Limestone Pinnacle Reef | | | | | | |
| 578 | Rosedale | 554-687 | L | 402 | 0.2 – 14.3 (5.0) | <0.1-145 (8.1) |
| 2. Completely Dolomitized Pinnacle Reef | | | | | | |
| 873 | Dawn 47-49 | 484-544 | D | 182 | 0.3 – 19.7 (6.5) | 0.1-1242 (10.3) |
| 1014 | Corey East | 568-611 | D | 36 | 4.3 – 17.1 (9.5) | 0.37-5641 (413.9) |
| 1003 | Enniskillen 28 | 564-617 | D | 89 | 1.6 – 12.8 (7.0) | 0.02-10200 (595.1) |
| 1004 | Enniskillen 28 | 624-642 | D | 41 | 1.4 – 17.9 (6.3) | 0.13-10200(1250.9) |
| 1006 | Sombra | 556-592 | D | 79 | 1.6 – 13.5 (4.6) | 0.01-10200 (161.6) |
| 522 | Corunna | 708-788 | D | 27 | 6.9 – 29.5 (14.4) | 0.18-104 (23.7) |
| 557 | Corunna | 776-803 | D | 76 | 1.3 – 19.3 (8.9) | <0.1-5355 (104.1) |
| 3. Partially Dolomitized Pinnacle Reef | | | | | | |
| 992 | Dow Moore | 686-774 | L, D | 215 | 0.1 – 35.2 (15.9) | 0.01-5128 (338.5) |
| 992 | Dow Moore | 686-695,705-732 | L | 115 | 0.1 – 30.6 (8.9) | 0.01-1861 (232.5) |
| 992 | Dow Moore | 695-705,732-774 | D | 100 | 0.1 – 35.2 (7.9) | 0.1-5128 (474.5) |
| 996 | Dow Moore | 796-806 | D | 26 | 2.4 – 12.1 ( 6.5) | 0.01-12.2 (2.6) |
| 4. Partially Dedolomitized Pinnacle Reef | | | | | | |
| 381 | Terminus | 600-612 | L, DD | 34 | 1.0 – 16.1 (10.0) | 0.1-855 (44.2) |
| 381 | Terminus | 600-603,606-612 | L | 27 | 6.5 – 16.1 (11.4) | 2.6-855 (54.9) |
| 381 | Terminus | 603-606 | DD | 7 | 1.0 – 9.1 (4.7) | 0.1-9.4 (3.0) |
| 604 | Terminus | 559-630 | DD | 57 | 2.5 – 14.4 (9.0) | 0.2-113 (18.9) |
| 918 | Terminus | 563-577 | DD | 43 | 0.2 – 11.5 (3.7) | 0.1-43.2 (5.7) |
| 5. Average Values | | | | | | |
| All Reef Limestone | | 554-732 | L | 544 | 0.1 – 30.6 (6.1) | 0.01-1861 (57.8) |
| All Reef Dolomite | | 407-806 | D | 1332 | 0.1 – 35.2 (6.1) | 0.01-10200 (206.6) |
| All Patch Reef | | 407-457 | D | 676 | 0.5 – 23.6 (5.0) | 0.01-5380 (121.6) |
| All Pinnacle Reef | | 484-806 | D | 656 | 0.1 – 35.2 (7.4) | 0.01-10200 (289.0) |
| All Reef Dedolomite | | 559-606 | DD | 107 | 0.2 – 14.4 (6.6) | 0.1-113 (12.6) |

* L- limestone, D- dolomite, DD- dedolomite

** Ranges and means of porosity and permeability

# Appendix VI. Porosity and permeability of Guelph limestone (core #992)

| Depth (m) | Low Porosity Limestone P (%) | K (md) | Depth (m) | Porous Limestone P (%) | K (md) |
|---|---|---|---|---|---|
| Sample values | | | | | |
| 685.93 | 6.5 | 0.42 | 686.23 | 14.6 | 20.4 |
| 705.40 | 0.5 | 0.02 | 686.53 | 14.6 | 56.9 |
| 705.80 | 0.4 | 0.01 | 687.13 | 15.5 | 83.3 |
| 706.20 | 2.8 | 2.19 | 687.48 | 14.6 | 34.8 |
| 706.54 | 4.2 | 1.46 | 687.83 | 16.9 | 95.8 |
| 706.54 | 2.8 | 3.41 | 688.20 | 17.6 | 104.5 |
| 708.16 | 1.8 | 0.05 | 688.60 | 13.6 | 37.1 |
| 708.46 | 0.3 | 0.01 | 689.23 | 13.3 | 31.2 |
| 708.76 | 0.1 | 0.01 | 689.48 | 15.9 | 446.9 |
| 709.06 | 0.9 | 0.05 | 689.73 | 17.2 | 708.3 |
| 709.89 | 5.3 | 5.36 | 689.98 | 22.9 | 764.9 |
| 711.38 | 2.0 | 3.12 | 690.28 | 20.5 | 675.4 |
| 711.55 | 2.7 | 0.05 | 690.58 | 12.1 | 477.3 |
| 711.95 | 5.6 | 3.34 | 690.88 | 18.0 | 1143.8 |
| 712.85 | 4.0 | 1.80 | 691.15 | 14.9 | 337.0 |
| 713.40 | 4.6 | 0.92 | 691.41 | 17.2 | 684.6 |
| 713.80 | 3.0 | 0.79 | 691.72 | 20.4 | 366.5 |
| 715.00 | 1.1 | 0.08 | 692.12 | 18.0 | 459.9 |
| 715.35 | 5.2 | 0.58 | 692.40 | 20.0 | 171.7 |
| 716.03 | 7.5 | 3.44 | 692.90 | 22.5 | 342.7 |
| 716.38 | 5.7 | 0.21 | 693.20 | 24.6 | 1331.7 |
| 716.78 | 6.6 | 0.22 | 693.50 | 30.7 | 1733.7 |
| 717.58 | 2.8 | 0.02 | 693.80 | 30.6 | 1861.5 |
| 718.20 | 2.4 | 1.16 | 694.05 | 28.0 | 1762.1 |
| 718.52 | 5.7 | 2.20 | 694.28 | 27.4 | 576.2 |
| 718.84 | 1.3 | 0.09 | 694.55 | 24.8 | 601.0 |
| 719.60 | 5.2 | 0.67 | 694.80 | 25.2 | 647.9 |
| 719.90 | 3.4 | 2.13 | 695.01 | 25.9 | 204.0 |
| 720.70 | 5.7 | 3.20 | 695.50 | 27.2 | 258.7 |
| 721.10 | 4.4 | 1.58 | 707.31 | 13.9 | 1019.8 |
| 722.53 | 6.5 | 2.08 | 707.59 | 13.6 | 1784.1 |
| 722.88 | 5.4 | 0.38 | 722.15 | 9.5 | 311.8 |
| 723.18 | 6.4 | 1.05 | 723.48 | 7.7 | 234.5 |
| 725.27 | 7.7 | 4.67 | 724.53 | 12.9 | 367.4 |
| 726.00 | 5.6 | 0.51 | 724.83 | 9.1 | 1068.4 |
| 726.30 | 4.3 | 5.43 | 725.62 | 9.4 | 603.8 |
| 726.90 | 7.1 | 2.79 | | | |

Average values

| Limestone type | Interval (m) | No. of sample | P (%) | K (md) |
|---|---|---|---|---|
| Low Porosity | 685.93 - 726.30 | 37 | 0.1 - 7.7 (3.9) | 0.01 - 5.4 (1.5) |
| Porous | 686.23 - 726.90 | 36 | 7.7 - 30.7 (17.7) | 20.4 - 1861.5 (594.7) |

P- porosity , K-permeability, and P, K means shown in parentheses.

# Appendix VII. Porosity and permeability of Guelph dolomite (core #992)

| Type | Depth(m) | P(%) | K(md) | Type | Depth(m) | P(%) | K(md) | Type | Depth(m) | P(%) | K (md) |
|---|---|---|---|---|---|---|---|---|---|---|---|
| Sample values | | | | | | | | | | | |
| T1 | 705.00 | 6.6 | 0.83 | T1 | 767.60 | 3.5 | 1.8 | T2 | 771.30 | 9.9 | 9.2 |
| T1 | 732.95 | 2.4 | 0.02 | T1 | 767.90 | 2.2 | 1.7 | T2 | 771.60 | 3.4 | 6.4 |
| T1 | 733.80 | 5.2 | 1.31 | T1 | 768.30 | 1.3 | 0.3 | T2 | 771.85 | 3.8 | 12.1 |
| T1 | 734.84 | 7.4 | 2.08 | T1 | 768.80 | 2.5 | 0.3 | T2 | 772.14 | 4.0 | 16.3 |
| T1 | 736.03 | 2.7 | 0.79 | T1 | 770.00 | 3.7 | 1.5 | T2 | 772.40 | 4.5 | 4.7 |
| T1 | 736.90 | 1.7 | 0.01 | T1 | 770.30 | 3.0 | 1.0 | T2 | 772.95 | 4.8 | 7.4 |
| T1 | 737.28 | 4.6 | 1.22 | T2 | 697.26 | 12.4 | 188.0 | T2 | 773.15 | 4.2 | 42.5 |
| T1 | 738.00 | 4.9 | 0.05 | T2 | 698.48 | 6.0 | 10.8 | T2 | 773.48 | 4.4 | 19.1 |
| T1 | 738.30 | 1.0 | 0.02 | T2 | 698.68 | 8.2 | 51.4 | T2 | 773.70 | 4.8 | 2.5 |
| T1 | 738.62 | 4.4 | 0.01 | T2 | 702.64 | 9.8 | 130.7 | T2 | 773.99 | 4.2 | 16.5 |
| T1 | 738.94 | 5.4 | 0.02 | T2 | 703.55 | 11.3 | 109.3 | T2 | 774.15 | 4.2 | 34.4 |
| T1 | 739.45 | 6.3 | 3.83 | T2 | 703.75 | 14.0 | 309.6 | T2 | 774.40 | 4.1 | 11.1 |
| T1 | 739.80 | 4.5 | 0.48 | T2 | 704.05 | 12.6 | 36.7 | T3 | 695.80 | 32.3 | 3409.1 |
| T1 | 740.10 | 1.5 | 0.04 | T2 | 704.35 | 4.0 | 16.7 | T3 | 696.00 | 35.2 | 5061.9 |
| T1 | 740.76 | 2.7 | 1.04 | T2 | 704.68 | 8.5 | 15.9 | T3 | 696.18 | 34.6 | 5128.1 |
| T1 | 760.28 | 5.6 | 0.19 | T2 | 733.40 | 6.8 | 6.8 | T3 | 696.34 | 30.3 | 4707.0 |
| T1 | 760.68 | 0.1 | 0.01 | T2 | 734.21 | 5.5 | 63.7 | T3 | 696.64 | 10.9 | 686.6 |
| T1 | 761.08 | 0.1 | 0.01 | T2 | 735.21 | 7.3 | 10.9 | T3 | 697.57 | 22.1 | 2155.0 |
| T1 | 761.58 | 0.3 | 0.01 | T2 | 735.58 | 9.0 | 440.6 | T3 | 698.18 | 10.0 | 1856.1 |
| T1 | 762.00 | 0.2 | 0.01 | T2 | 737.65 | 5.4 | 66.1 | T3 | 699.30 | 16.2 | 1974.8 |
| T1 | 762.40 | 0.8 | 0.01 | T2 | 740.40 | 4.6 | 65.9 | T3 | 699.80 | 23.6 | 3289.2 |
| T1 | 762.76 | 1.0 | 0.01 | T2 | 759.26 | 10.3 | 45.3 | T3 | 700.05 | 14.6 | 3843.8 |
| T1 | 763.10 | 3.0 | 0.01 | T2 | 759.53 | 10.9 | 117.6 | T3 | 700.28 | 8.2 | 1177.1 |
| T1 | 763.43 | 2.0 | 0.02 | T2 | 759.91 | 10.9 | 54.7 | T3 | 700.69 | 11.9 | 1533.9 |
| T1 | 763.98 | 0.2 | 0.01 | T2 | 764.90 | 5.3 | 167.0 | T3 | 700.99 | 16.5 | 1666.6 |
| T1 | 764.30 | 1.0 | 0.01 | T2 | 765.20 | 7.5 | 204.8 | T3 | 701.29 | 14.5 | 999.6 |
| T1 | 764.60 | 4.3 | 0.26 | T2 | 766.00 | 3.4 | 31.4 | T3 | 701.64 | 17.4 | 1959.7 |
| T1 | 765.60 | 3.2 | 0.12 | T2 | 768.53 | 5.3 | 20.1 | T3 | 701.99 | 16.5 | 1363.1 |
| T1 | 766.30 | 3.9 | 0.69 | T2 | 769.10 | 3.8 | 8.9 | T3 | 702.97 | 22.7 | 1946.9 |
| T1 | 766.60 | 3.4 | 0.59 | T2 | 769.40 | 3.6 | 29.4 | T3 | 703.30 | 23.1 | 1230.4 |
| T1 | 766.90 | 0.4 | 0.30 | T2 | 769.70 | 3.7 | 10.0 | | | | |
| T1 | 767.20 | 1.7 | 0.01 | T2 | 770.95 | 4.7 | 25.9 | | | | |

Average values

| Type | Interval (m) | No. of sample | P (%) | K (md) |
|---|---|---|---|---|
| T 1 | 705.00-770.30 | 38 | 0.1 – 6.6 (2.9) | 0.01 – 3.8 (0.5) |
| T 2 | 697.26-774.40 | 38 | 3.4 – 14.0 (6.6) | 2.49 – 440.6 (63.7) |
| T 3 | 695.80-703.30 | 18 | 8.2 – 35.2 (20.0 ) | 686.6 –5128.0 (2443.8) |

P- porosity , K-permeability, and P, K means shown in parentheses.

Note: Type-replacive dolomite type, T1-Type 1 dolomite, T2-type 2 dolomite, and T3-Type 3 dolomite.